Modelling the spread of disease on networks

Dorey, Matthew

Award date:
2008

Awarding institution:
University of Bath

Modelling the spread of disease on networks

submitted by

Matthew Dorey

for the degree of Doctor of Philosophy

of the

University of Bath

Department of Mathematical Sciences

June 2008

For Mum and Dad.

But even with donkey, water and soil
there wasn't enough to level the hole
after what was washed away
or turned to clay
or trodden in, so we opened the earth
and started in on a second trench for dirt
to fill the first.
Which left a taste
of starting something that wouldn't finish:
a covered grave with a donkey in it,
a donkey-sized hole
within a stone's throw
and not a single bone to drop in it
or a handful of dust to toss on top of it.

From "Parable of the Dead Donkey"
by Simon Armitage.

Acknowledgments

I would like to thank my supervisor Jane White for the guidance and encouragement given to me throughout the my period of study. Without her patience and support, writing this thesis would have been much more difficult.

Many thanks are also due to Dushyant Mital, for his time and ideas that ultimately helped me to focus on where to apply these models. The enthusiasm and knowledge he imparted in our conversations provided me with a great deal of motivation to carry out this work.

Discussions of mathematical matters with Nick Britton, Dick James, Ivana Gudelj and Hartmut Schwetlick were of great importance throughout my time working on this project.

The PhD students that have worked on mathematical biology projects at Bath in my time here have also significantly improved my understanding and enthusiasm for the subject: Steven White, James Stewart-Cox, Peter Hancock, Loukia Lili, Zoe Ward, Vicki Brown and Farida Chamchod.

As with any major undertaking in life, the love and support of family and friends throughout my time on this project has been crucial. I wish to thank the following people for all they have added to my life in the past few years: Barrie and Rachel Cooper, James and Helen Coughlan, Ana Cristina Cruz (*Deus dá nozes a quem não tem dentes!*), Duncan and Claire Lee, Jon Feldman and Marina Jaumouillé, James and Jo Stewart-Cox, Damien and Petra Harwin, Chris and Zoe Ward, Vicki Brown and James Kent, Jason Cook, Khat Rahmat, Nicola Newman, Eugen and Lorina Varvaruca, Kwabena Doku-Amponsah, John Harris, Alix Blockley, Nick Lambert, Gemma Nicholson, Nikki Ayriss, Phil Balmond, Dominique Holland, Mahlet Tsigé-Getachew and James Edwards.

Finally, an emphatic dedication to my family who are the reason why I did this, and why I was able to: My parents, Marion and David Dorey. My sisters, Helen and Tilly. My Grandparents, Bertram and Patricia Barker.

Summary

This thesis is concerned with providing an overview of mathematical and computational techniques used to investigate the spread of sexually transmitted infections throughout heterogeneous populations. These techniques are then applied to issues arising in healthcare provision for a major UK city.

Chapter 1 discusses the nature of sexually transmitted infections (STIs) and some healthcare issues arising as a consequence of their treatment and management, together with a discussion of the role of mathematical modelling in answering critical questions about such diseases.

In Chapter 2, we show how the population can be considered as a network (or graph) consisting of sites, representing individuals, and the connections between them. From this viewpoint, we can formulate a deterministic mathematical model - pair approximation - or use stochastic simulations on computer generated networks to study the spread of infection within the population.

Many populations also consist of several subgroups which are particularly at risk to sexually transmitted infection. Management of infection within these groups and the prevention of transmission to other groups or the wider population is crucial. Chapters 3 and 4 provide modifications to the pair approximation model to incorporate the effects of one sub-population on others and compares the results to similarly extended simulations.

In Chapter 5 we use simulations to estimate the parameters of a nonlinear incidence model, where the homogeneous mixing assumption is replaced by an incidence function that incorporates the build-up of infection. We also demonstrate the effects of certain network properties, such as clustering and variation in degree, on the nonlinear incidence parameters.

Chapters 6 and 7 respectively apply the nonlinear incidence model to the interaction of core groups and the spread of STI co-infection. These models are the entry point to more sophisticated and practical models for the spread and subsequent management of these infections.

Contents

List of Figures

List of Tables

Part I

Incorporating contact structure

Chapter 1

Introduction

1.1 Background

1.1.1 Sexually Transmitted Infections

A sexually transmitted infection (STI) is a bacterial or viral infection characterised by its presence in and transmission between the tissues and fluids of the sexual organs. The range of symptoms can vary between largely asymptomatic to severe neurological damage or death. Though most can be treated with antibiotics, many go untreated due to social taboo or the lack of symptoms present. Untreated sexually transmitted infections can produce a number of grave sequelae, including cancer and infertility.

Whilst many STIs conform to these archetypes, one the most infamous STIs of recent history sits very much outside them. Human Immunodeficiency Virus (HIV) is a viral infection that eventually causes the onset of Acquired Immune Deficiency Syndrome (AIDS), a condition that suppresses immune system function, and ultimately leads to death from attendant opportunistic infections. Whilst anti-retroviral treatment can prolong the lifetime of individuals with HIV, the onset of AIDS is inevitable so that the infection is ultimately fatal.

HIV/AIDS is now a pandemic of global proportions, though sub-Saharan Africa is worst affected by the disease. UNAIDS estimated that there were 33.2 million individuals living with the disease by 2007 and that an estimated 2.1 million people had died from the disease in that same year, [47]. Since there is currently no vaccine and no cure, the most important concern for health workers is that of prevention of onward transmission.

Returning to other sexually transmitted infections, one of the most prevalent infections worldwide is Chlamydia, with an estimated 2.8 million cases a year in the USA

a) HIV

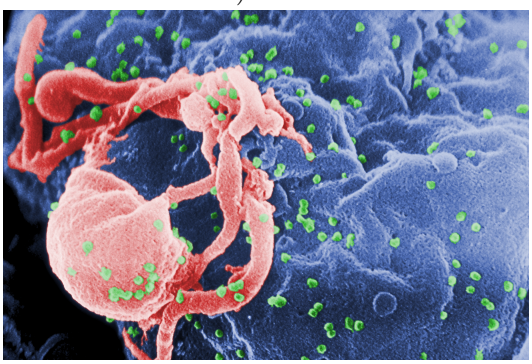

b) Chlamydia

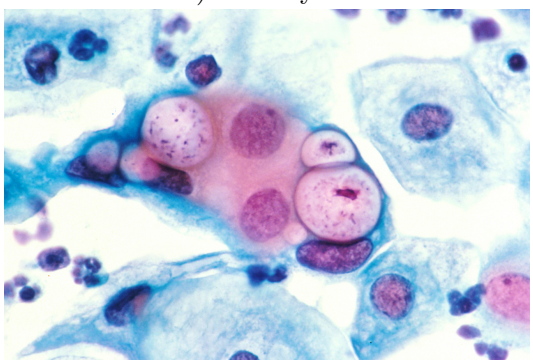

Figure 1-1: *Pictures of sexually transmitted infections at the microscopic level. a) Scanning electron micrograph of HIV-1 budding from cultured lymphocyte. Photo by C. Goldsmith. Source: CDC, public domain. b) Human pap smear showing Chlamydia in the vacuoles. Photographer unknown. Source: Public domain.*

alone, [8]. In the UK, 10% of individuals between 16 and 24 years of age screened for the disease were found to be infected, [36]. The endemic status of Chlamydia infection is largely due to its asymptomatic nature, around 50-75% of all women with the infection will exhibit no symptoms and will not be aware that they are infected. Unfortunately, this masks a great deal of traumatic sequelae, over half of women undiagnosed will go on to develop an inflammation of the uterus, ovaries or Fallopian tubes, a collection of symptoms gathered under the name Pelvic Inflammatory Disease (PID). This condition is a significant contributory factor in difficulties in conceiving a child, in ectopic pregnancy and in complications during pregnancy.

According to the Centers for Disease Control, a woman with Chlamydia is five times more likely to acquire HIV, if exposed, [8]. Clearly, with Chlamydia endemic throughout the world, this is a worrying effect and yet another motivating factor for the prevention and control of this infection. As well as an obvious moral duty to the human rights of its citizens, governments and health care services have compelling economic arguments for the prevention of these infections, since the cost of providing condoms or antibiotics is far smaller than that of assisted conception or retroviral drugs. Unfortunately in the UK it is often the case that GUM clinics are underfunded and over subscribed, [38]. The Health Protection Agency reported in 2006 that the workload at GUM clinics had increased by 268% between 1996 and 2005, [15].

As a consequence of this, prevention and testing measures are aimed at particular sectors of the population deemed to be the most vulnerable for behavioural or biological reasons. These are often referred to as 'core groups'. In the UK, the following are

Table 1.1: *Estimated per act risk for acquisition of HIV by exposure route, reproduced from [45], highlighting the differences in transmission rates for different sexual roles.*

Exposure route[a]	Estimated infections per 10,000 exposures to infection source
Blood transfusion	9,000
Needle sharing	67
Receptive anal intercourse	50
Needle stick injury	30
Receptive penile-vaginal intercourse	10
Insertive anal intercourse	6.5
Insertive penile-vaginal intercourse	5

[a]Assumes no condom use

regarded as the key groups to be targeted, with additional information from [15] unless otherwise cited:

Men who have sex with men Men who have sex with men (MSM) are the group most likely to be infected with HIV. This is due to the increased transmission rate for anal sex (see Table 1.1, as reproduced from [45]) and the greater tendency among these individuals for high risk sexual behaviour. Gonorrhoea incidence is also high within this group, along with a more aggressive strain of Chlamydia known as LGV that originated in the Caribbean. Co-infection with multiple STIs is also a significant problem within this group, increasing the severity of symptoms and causing difficulties in treatment.

Black and minority ethnic populations Due to the fact that the HIV/AIDS pandemic has affected Africa most severely, [47], a large number of immigrating individuals are also infected with the disease, particularly from sub-Saharan regions. Many black and minority ethnic (BME) individuals with HIV from this core group are diagnosed late, presenting problems with treatment and increasing the need for contact tracing.

Pregnant women Women who are pregnant are screened routinely for sexually transmitted infections as an early diagnosis can prevent vertical transmission of HIV. Other STIs can be the cause of serious congenital defects, so an early prognosis is desirable. Though not entirely representative, the incidence levels for infections within this core group are a good indicator for the non-core elements of the population.

Young people Individuals aged between 16 and 24 are disproportionately afflicted by STIs, a fact generally due to a larger number of partners, a larger number of concurrent partners and a higher turnover of partners than in older people, [20]. In this sector of the population the number of diagnoses of most major STIs has increased in recent years, with the exception of Gonorrhoea.

Injecting Drug Users Needle sharing significantly increases the risk of contracting HIV, as seen in Table 1.1. The practice of needle sharing continues with more than half of injecting drug users (IDUs) reporting sharing injecting equipment. As a result diagnoses of HIV among IDUs has remained constant. Within this group there are strong geographical links to the spread of HIV infection, with the majority of cases occurring in London.

1.1.2 Mathematical Modelling

Perhaps the simplest mathematical model for the spread of disease within a population is the SIR adapted from the work of Kermack and McKendrick, [23]. The following is a pedagogical variant used as a starting point for many such models, such as in [5], [16] and [35]:

$$\begin{aligned} \frac{\mathrm{d}S}{\mathrm{d}t} &= -\beta SI, \\ \frac{\mathrm{d}I}{\mathrm{d}t} &= \beta SI - \gamma I, \\ \frac{\mathrm{d}R}{\mathrm{d}t} &= \gamma I. \end{aligned} \tag{1.1}$$

Here β denotes the transmission rate, γ the recovery rate per unit time, $S(t)$ is the number of susceptibles, $I(t)$ the number of infective individuals and $R(t)$ the number of recovered individuals. The sum total of individuals within the population comprises all such individuals, thus

$$N(t) = S(t) + I(t) + R(t). \tag{1.2}$$

Here $N(t)$ can be held fixed, or given its own ODE to describe how the population evolves in the absence of disease. In such cases (1.1) will require modifications so that reasonable assumptions such as all newborn individuals being susceptible, or more complex ones like vertical transmission from mother to child, can also be modelled.

The most important quantity for any disease is the basic reproductive ratio R_0, defined to be the average number of infections caused by a single infective in a wholly susceptible population. The principal results that can be obtained from analysis of (1.1) are the existence of a threshold for the basic reproductive ratio R_0, above which an epidemic

will occur; and an expression for the number of individuals that remain uninfected after the epidemic has passed through the population and died out. This quantity is often denoted by S_∞.

In order to obtain R_0 for the system (1.1), we first consider the reduced system

$$\begin{aligned} \frac{\mathrm{d}I}{\mathrm{d}t} &= \beta(N-I-R)I - \gamma I \\ \frac{\mathrm{d}R}{\mathrm{d}t} &= \gamma I. \end{aligned} \tag{1.3}$$

There will be an epidemic if the trivial equilibrium is unstable. The Jacobian of (1.3) is given by

$$\mathcal{J} = \begin{pmatrix} \beta(N-I-R) - \beta I - \gamma & -\beta I \\ \gamma & 0 \end{pmatrix}, \tag{1.4}$$

which evaluated at $(0,0)$ is

$$\mathcal{J}(0,0) = \begin{pmatrix} \beta N - \gamma & 0 \\ \gamma & 0 \end{pmatrix} \tag{1.5}$$

and has eigenvalues

$$\begin{aligned} \lambda_1 &= 0 \\ \lambda_2 &= \beta N - \gamma. \end{aligned} \tag{1.6}$$

Thus, if

$$R_0 := \frac{\beta N}{\gamma} > 1 \tag{1.7}$$

both eigenvalues are non-negative, and the trivial equilibrium is unstable. Thus above this threshold an epidemic will occur within the population, and below it the disease will fail to establish itself and die out. Obviously (1.1) is a very simplistic model of an infection and considerable effort has been applied to determine or infer similar thresholds for more realistic models of infection. A review of models for infectious diseases is given in [16] and the challenges presented by modelling diseases of humans are described at length in [2].

S_∞, the number of susceptibles remaining after the epidemic, will be derived for (1.1) and another model in Chapter 3.

In terms of modelling disease spread, the crucial component of (1.1) is the use of the bilinear term

$$\beta SI, \tag{1.8}$$

to model transmission events. This assumes that all members of the population mix

freely and equally. The very existence of core groups for STIs suggests that in order to model these infections, this assumption must be modified.

One approach is to further subdivide the population into compartments according to core groups and to assume free and equal mixing within these subpopulations, as proposed by [27] and discussed in [18]. However, this is also problematic since there is evidence that the contact structure of these subpopulations is too heterogeneous to be amenable to the homogeneous mixing assumption, as discovered in [29] and modelled in [34]. Moreover, the underlying contact structure may vary from one subgroup to another, as discussed in [44], where the sexual networks of MSM and BME populations are compared.

As a result, this thesis concerns itself with modelling the contact structure of core groups and the integration of core groups into models of the overall population.

1.2 Thesis Outline

The thesis is divided into two parts. In part one we seek to incorporate contact structure directly into models. In the second part, we look for means with which to infer contact structure within mathematical models. Throughout the central problem is of incorporating core groups into models for the entire population is discussed.

We begin Part 1 by taking a general view of how the underlying contact structure of the population affects the spread of the considered disease. This takes the form of an extended literature review in Chapter 2, in which the pairwise equation models of Keeling and Eames, [22] and [11] are studied for lattices, together with a number of other models for more heterogeneous networks such as scale-free networks, as proposed in [34].

Chapter 3 discusses the effect of an external population on a core group, thus beginning the process of modelling the interaction between core groups and their host populations. We discuss mean field, pairwise and simulation models in this context.

This process continues in Chapter 4, which presents the interactions of multiple core groups in these settings. Particular attention is paid to how systems evolve away from states achieved in isolation and the consequences of interaction for the groups.

The central model of Part 2 is that proposed by Liu et al in [32] and [31]. The model features a nonlinear equivalent to (1.8) parameterised in such a way that no mechanistic derivation has yet been achieved. Chapter 5 discusses the models proposed by these authors and then proceeds to demonstrate the estimation of the parameters for their

incidence function through the use of data from computer simulations. This allows us to infer a connection between contact structure and the parameters of these models.

In Chapters 6 and 7, we utilise the techniques and results of Chapter 5 to produce new models for the interaction of multiple core groups and the spread of co-infections. In Chapter 6, we also seek to investigate the nature of the interaction between groups, given a particular model for the construction of physical between subgroups in simulations. Chapter 7 addresses a problem commonly observed in STIs but rarely modelled, that of co-infection. As with the previous chapter, the models are a combination of variants of the nonlinear incidence model and computer simulations.

Chapter 8 then provides a discussion of the results and suggests ways in which they may be improved in future work.

Chapter 2

Network Structure

2.1 Motivation and Background

2.1.1 Chapter outline

The assumption of homogeneous mixing within a population is not necessarily accurate for many populations, especially for human populations where the contact necessary for the transmission of disease is often socially based and non-random. In the case of sexually transmitted infections, contacts are with a very particular subset of these social interactions and the resulting contact structure will be complicated, with a great variation between individuals.

This chapter presents computer simulations and mathematical models that attempt to incorporate directly the contact structure of the individuals within a population, in the hope of improving the predictions made by models centred on the homogeneous mixing assumption.

This chapter combines a literature review with the results of our own computer simulations, which allows a novel discussion of how various topological features of contact networks impact on the spread of disease.

2.1.2 Network terminology

We will frequently use the terminology of networks throughout this and subsequent chapters as we seek to describe the contact structure of populations. A network or graph, $\mathcal{G}$, consists of N nodes (or vertices, or sites) and E edges (or links) between the nodes. The nodes will represent individuals within our population and the edges

social interactions between individuals sufficient for the transmission of disease. For the time being we make no assumption about the quality of links, nor do we impose any time order upon their existence. That is to say, all edges centred on a given node are deemed to be equal, concurrent and active.

The number of nodes in the population connected to an individual i is called the degree of i and is denoted k_i. We consider only undirected edges, so that if node i is connected to node j, then j is also connected to i. A network is called simple if only one edge can exist between two nodes i and j. Because of this, the maximum degree of any node is $N-1$ and the maximum number of edges in a network is $\frac{1}{2}N(N-1)$. A network that consists of all possible edges between nodes is said to be complete. The degree distribution of a network is the probability that a randomly selected node is of degree k,denoted $\mathbb{P}(k)$. Similarly, the degree-degree distribution $\mathbb{P}(k,k')$ is defined to be the probability that a randomly selected edge consists a node of degree k connected to one of degree k'.

2.1.3 The roles of mathematical modelling and computer simulation

The problem of describing the spread of disease within a structured population can lead to increasingly complicated models. Two mechanisms by which this can occur are via the amount of complexity in the network (i.e. the extent to which variability between individuals is measured) and the generalisations required to take account of inaccuracies within real world data.

The complexity of the contact structure increases rapidly with the attention paid to detail in the modelling process. It is possible with computer simulations to model many facets of the behaviour of individuals within the population, giving a precise picture of the number and nature of contacts over time. In such a situation a mathematical model would consist of so many variables and compartments as to obviate any meaningful analysis. Given the speed with which computer simulations can be formulated and performed, mathematical models can often be relegated to the task of validating simple test cases.

The modelling process nevertheless needs to remain centred on real world data, with a view to capturing as much of the necessary detail of the observed behaviour as possible. However, such data can often be hard to come by or be restricted by various factors, such as inaccuracy or restricted sample size. For example, Wylie and Jolly collected data from a large number of individuals entered into a Chlamydia screening program in Manitoba, Canada, [48]. They found three main structures within the population:

doubletons, representing monogamous couples; hubs that consisted of one individual and many partners; and linear components, consisting of several small hubs connected together. It is likely that the larger components are present not merely for behavioural reasons, but also due to the contact tracing process itself. In such a situation, computer simulations are useful for evaluating alternative hypotheses about the data quickly and accurately.

2.2 Lattices

We begin by performing computer simulations for the spread of a disease on a lattice. The lattice is a simple structure which is easy to characterise for the purpose of simulations and straightforward to consider for mathematical models. The lattices we consider are given in Figure 2-1. We identify the edges of the lattice, effectively producing a torus, in order to ensure that all nodes are identical and to mitigate against any edge effects that would otherwise arise.

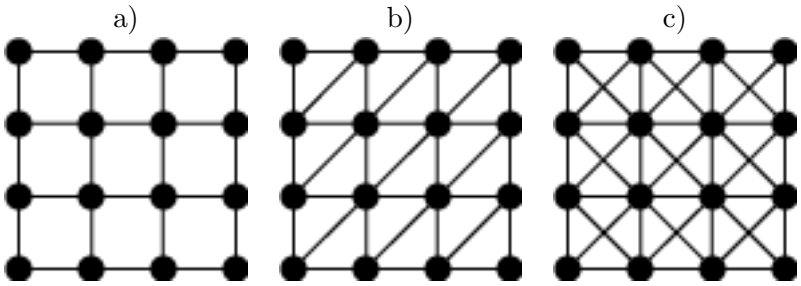

Figure 2-1: *Lattices used include a) Square Lattice, b) Hexagonal Lattice and c) the square lattice with Moore neighbourhood.*

We describe the algorithms used to describe the spread of a disease for the SIR and $SIRS$ models and the results of these processes occurring on the lattices of Figure 2-1. We then discuss a mathematical model that captures the spread of disease by concentrating on the local description of events occurring on the lattice and compare the results to both the traditional mean field model and the results of simulations.

2.2.1 The SIR process

For simulation purposes, we use the following algorithmic formulation of the SIR process.

Algorithm 2.1.

- Within each time step, each infective site contacts its susceptible neighbours and successfully infects each one with probability β.
- Each infection attempt is considered to be independent of all others.
- Each infected node also recovers with fixed probability γ per unit time. Once recovered, a node enters a separate class, where it has no further interactions with its neighbours.

Figure 2-2 shows the progress of this disease process on a hexagonal lattice at various points in time for the case where β exceeds γ. Starting from a few initial infectives, the disease spreads to each of the six neighbours of these sites and continues to spread in the six directions away from each of the initial points of infection. As infectives begin to recover, this has the effect of producing a front of infectives that expands throughout the network with susceptibles ahead and recovered nodes behind. In some regimes with a low transmission probability or a high recovery rate, this may lead to susceptibles around this front not being infected before their infected neighbours recover. Once all the neighbours of a susceptible node have recovered, it is safe from infection and as a result some nodes may never actually be infected.

Figure 2-3 below shows the number of infected nodes versus time step for the three different types of lattice, averaged over 100 realisations. It is to be noted that as the number of neighbours increases, the speed at which the infection travels increases and the number infected at any given time is higher.

2.2.2 The SIRS process

As not all diseases confer permanent immunity, we also consider the SIRS process on the lattice. In this situation the mean field model predicts an equilibrium. However, on a lattice the situation is made more complicated by the network structure.

The SIRS process is a slight modification of Algorithm 2.1.

Algorithm 2.2.

- Within each time step, each infective site contacts its susceptible neighbours and successfully infects each one with probability β.
- Each infection attempt is considered to be independent of all others.
- Each infected node also recovers with fixed probability γ per unit time. Once recovered, a node enters a separate class, where it has no further interactions with its neighbours.

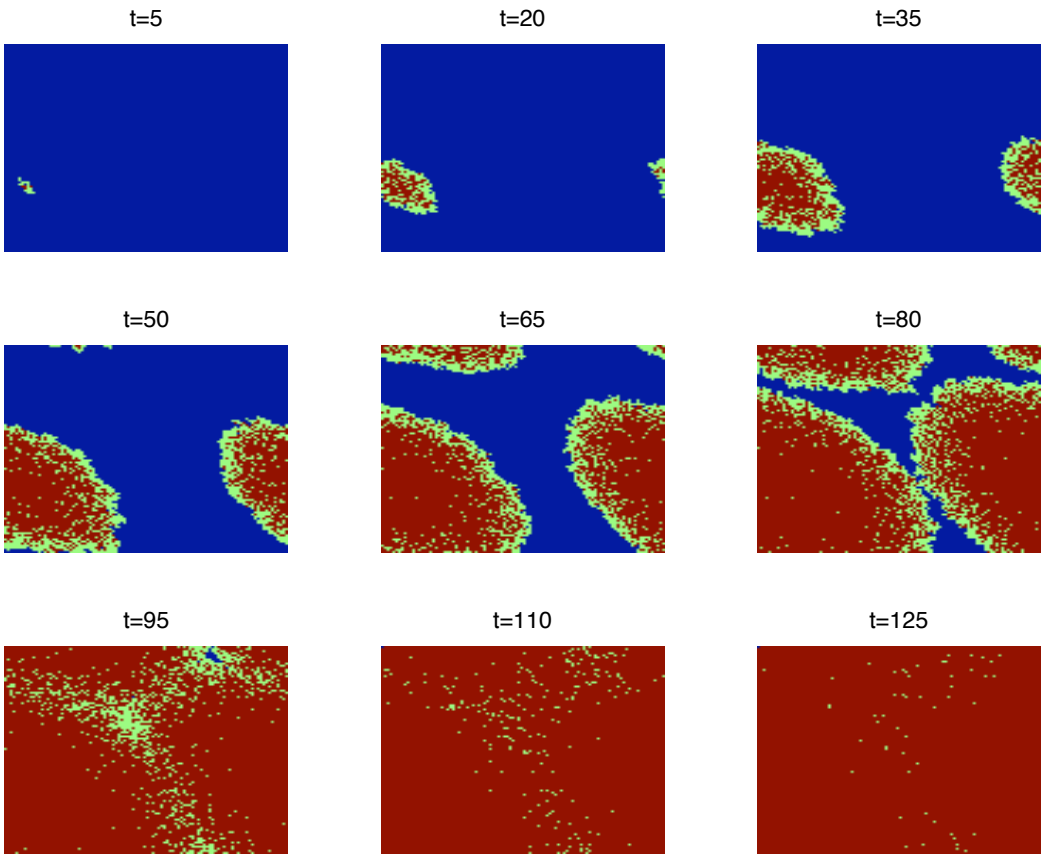

Figure 2-2: *Snapshots of a* 100×100 *hexagonal lattice under the disease process (2.1) with* $\beta = 0.3$ *and* $\gamma = 0.1$. *Susceptible nodes are coloured blue, infected nodes are green and recovered nodes red.*

- Each recovered node returns to the susceptible class with probability ν.

Figure 2-4 shows a computer simulation of the progress of the SIRS process given by Algorithm 2.2 on a hexagonal lattice. We can see that initially the disease proceeds similarly to the SIR model shown in Figure 2-3 but that eventually individuals behind the front of infection are returned to a susceptible state. Provided that the loss of immunity rate is sufficiently high for contiguous regions of susceptibles to be produced, the infection can be sustained. As the process of both recovery and loss of immunity are random, there will be small variations in the level of infection about what can be considered as an equilibrium. Figure 2-5 shows the effect of increasing the loss of immunity rate on the proportion infected at equilibrium. We see that at $\nu = 0$, which corresponds to the SIR case the equilibrium is zero. As ν increases, the level of infection at equilibrium increases, albeit at a decreasing rate due to saturation effects.

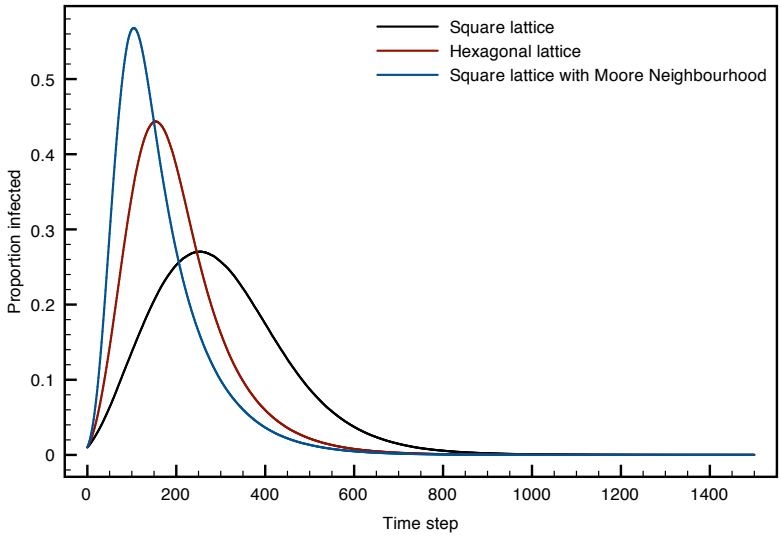

Figure 2-3: *The number of infectives versus time, averaged over 100 realisations, for the spread of an SIR process on lattices with 10000 sites and 4, 6 and 8 neighbours per site. The spreading rate β was 0.02 and the recovery rate γ was 0.01. 100 nodes were initially infected, corresponding to 1% of each lattice.*

2.2.3 Pairwise equations

In a mathematical model for the spread of disease on a discrete structure incorporating population heterogeneity, it is perhaps natural to move beyond considering the individual, in order to better utilise the network topology. With the underlying contact structure in mind, we can instead focus upon the edges or connections between individuals, characterising each such edge in terms of the states of its endpoints. Using conservation considerations, ordinary differential equations can then be formulated, to take account of the changes in the number of edges in different combinations of endpoint states.

Models such as these are also necessary to approximate the kinds of stochastic processes that are used in simulations, examples of which abound throughout this thesis. There is an obvious need to validate simulations in order to ensure that erroneous conclusions are not drawn from the complex, complicated scenarios that modern computers are so adept at exploring. For this purpose, an intuitive mathematical model that explores a simple case at a reasonable level of tractability is essential.

We begin by discussing some notation. Following Keeling [22] and others, we use the notation $[A]$ to denote the number of individuals in state A and $[AB]$ to denote the

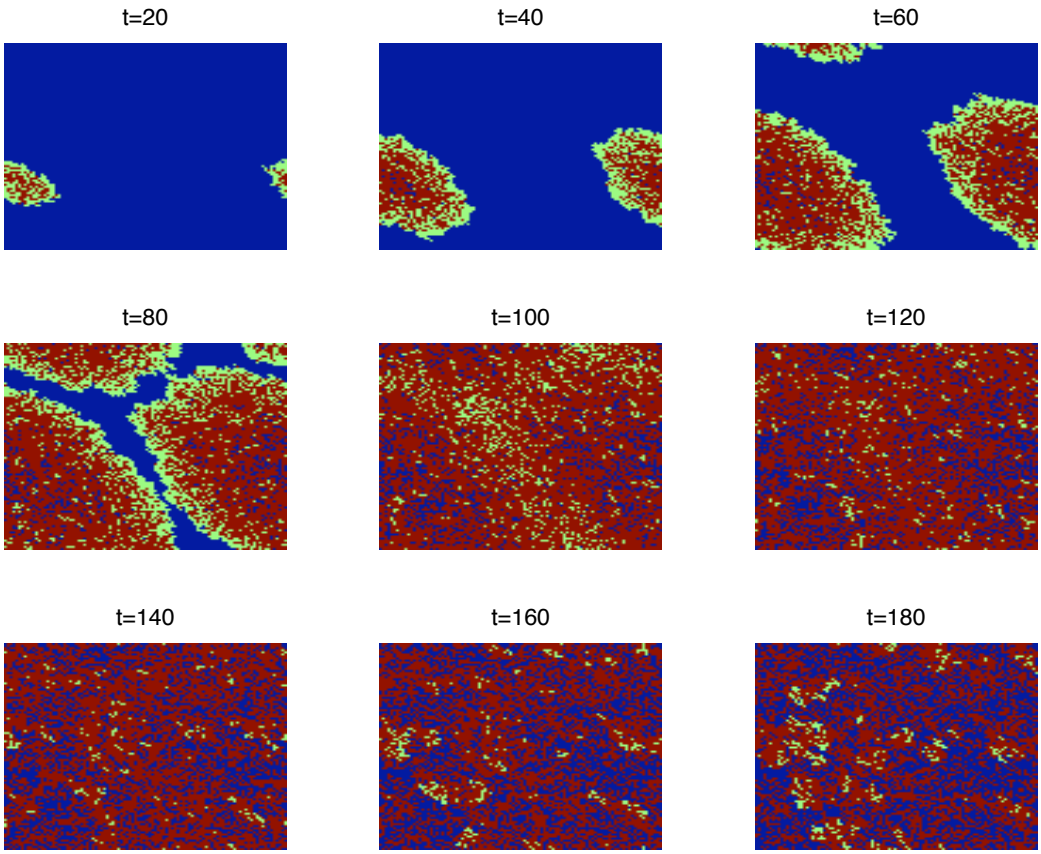

Figure 2-4: *Snapshots of a* 100×100 *hexagonal lattice under the disease process (2.2) with* $\beta = 0.3$, $\gamma = 0.1$ *and* $\nu = 0.01$. *Susceptible nodes are coloured blue, infected nodes are green and recovered nodes red.*

number of edges whose endpoints are respectively in states A and B. Since each edge is to represent the potential for the state of one node to influence the state of the other, it has to be thought of as a directed link and hence, from this point of view, $[AB]$ is very much different from $[BA]$.

By extension, it is no surprise to learn that $[ABC]$ denotes a triple in which nodes in states A, B and C are connected. Again it is necessary to clarify the notation in terms of disease transmission pathways. The potential to confer changes of state is to be read from right to left. For an $[ABC]$ triple this means that if the central node (in state B) is able to confer a change of state upon its neighbours, then it can only affect the node

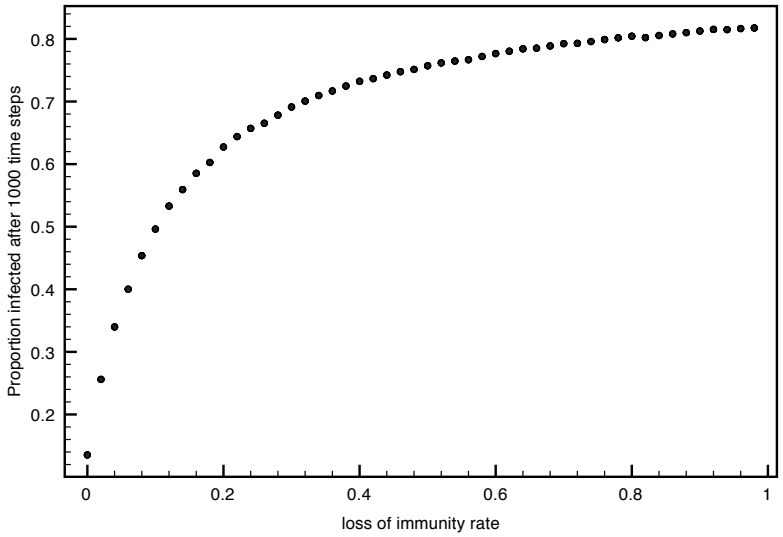

Figure 2-5: *Effect of increasing the loss of immunity parameter ν on the SIRS process on a lattice. The SIRS process with fixed infection rate* 0.3 *and recovery rate* 0.1 *was simulated 10 times for 1000 time steps on a hexagonal lattice with the loss of immunity rate ν varied between* 0 *and* 1*. The average of the proportion infected at the final time step is plotted against the corresponding value of ν.*

to the left of it in state A. Pictorially, the situation is:

$$[AB] \quad : \quad A \leftarrow B \tag{2.1}$$

$$[ABC] \quad : \quad A \leftarrow B \leftarrow C, \tag{2.2}$$

where the arrow denotes possible influence. We shall also think of triples in the following manner:

$$[ABC] = [[AB]C] : (A \leftarrow B) \leftarrow C \tag{2.3}$$

which will be of use when describing transmission events outside of pairs. Whilst these are clarifying thoughts for modelling purposes, it should also be noted that, structurally, the network is undirected and that therefore there are always the same number of $[BA]$ links as there are $[AB]$ ones. This leads to the following expressions that recover the number of individuals in a given state from the numbers in pair states:

$$[A] = \tfrac{1}{z} \textstyle\sum_{\text{all states}} [A\bullet]. \tag{2.4}$$

Here z is the number of neighbours per site in the lattice.

Next we formulate pairwise equations for the SIR model. Whilst this particular model

does not match a typical sexually transmitted infection, the purpose of this construction is to demonstrate the similarities and differences of the disease dynamics when compared to both the mean field model discussed in Chapter 1 and the simulations presented earlier in this chapter.

The probability that contact between a susceptible and an infective results in the transmission of infection is τ. The rate at which infectives recover per unit time is given by γ. Equations for the individual level events take a familiar form:

$$\begin{aligned} [\dot{S}] &= -\tau[SI] \\ [\dot{I}] &= \tau[SI] - \gamma[I] \\ [\dot{R}] &= \gamma[I]. \end{aligned} \tag{2.5}$$

However, in this case susceptibles are lost at the rate at which infectives connected to them successfully transmit the disease and hence the inclusion of the terms explicitly involving S-I links. The system is now no longer closed and we must write down further equations for how the number of such pairs changes with time. An example of a closure of this system is the mean-field model, whereby $[SI]$ is approximated by $[S]\frac{[I]}{N}$ - tantamount to assuming that the proportion of infected neighbours of a particular susceptible is the same as the proportion of infected individuals within the entire population. Clearly we can see from the computer simulations of the SIR process on a lattice as shown in Figure 2-2 that this is not the case here, due to the localised initial spread of the infection.

It is clear therefore that the processes by which susceptibles acquire infected neighbours have an important role to play in describing the spread of infection through the population. The following equation describes the changes in the number of $[SI]$ pairs over time:

$$[\dot{SI}] = -\tau[SI] - \gamma[SI] - \tau[ISI] + \tau[SSI]. \tag{2.6}$$

The first term accounts for the infection of the susceptible half of the $[SI]$ pair by its infected partner, which will produce an $[II]$ pair. The infection rate is τ, the infection rate across a single partnership per time step. The second term corresponds to the recovery of the infected half of the pair, resulting in an $[SR]$ pair. The third term corresponds to the loss of $[SI]$ pairs due to the susceptible half having at least one other infected partner. The final term describes how $[SI]$ pairs are formed from the infection of one half of an $[SS]$ pair.

The full set of equations for the SIR model is derived from similar considerations:

$$\begin{aligned}
[\dot{SS}] &= -2\tau[SSI] \\
[\dot{SI}] &= \tau[SSI] - \tau[ISI] - (\tau+\gamma)[SI] \\
[\dot{SR}] &= \gamma[SI] - \tau[ISR] \\
[\dot{II}] &= 2\tau[SI] + 2\tau[ISI] - 2\gamma[II] \\
[\dot{IR}] &= \tau[ISR] + \gamma[II] - \gamma[IR] \\
[\dot{RR}] &= 2\gamma[IR]
\end{aligned} \tag{2.7}$$

Note that, by adapting equation (2.4) accordingly, the above equations fully characterise the system. We can recover the number of individuals in a given state from the following equations:

$$\begin{aligned}
[S] &= \tfrac{1}{z}([SS] + [SI] + [SR]) \\
[I] &= \tfrac{1}{z}([SI] + [II] + [IR]) \\
[R] &= \tfrac{1}{z}([SR] + [IR] + [RR]).
\end{aligned} \tag{2.8}$$

The system can be closed using the following pair approximation, which assumes that the likelihood of an $[AB]$ pair being connected to a node in state C is simply the likelihood that a node in state B has a neighbour in state C multiplied by the number of $[AB]$ pairs:

$$[ABC] \approx \frac{z-1}{z}\frac{[AB][BC]}{[B]}. \tag{2.9}$$

However in networks that contain triangles, there is a chance that the node in state A may also be connected to the node in state C. In this case, we must also consider the proportion of nodes in state A that are connected to a node in state C and we use the multiplicative correlation,

$$\mathcal{C}_{AC} = \frac{Q(C|A)}{Q(C|\bullet)} = \frac{N}{z}\frac{[AC]}{[A][C]}, \tag{2.10}$$

as a measure of the likelihood of this occurring. This gives the following clustered triple approximation:

$$[ABC] \approx \frac{z-1}{z}\frac{[AB][BC]}{[B]}((1-\phi) + \phi\mathcal{C}_{AC}). \tag{2.11}$$

The parameter ϕ is the clustering coefficient of the network and is calculated per site as the proportion of all possible edges between the neighbours of a given node that actually exist in the network. This is described in Figure 2-6.

The incorporation of edges into the description of the population allows us to explore

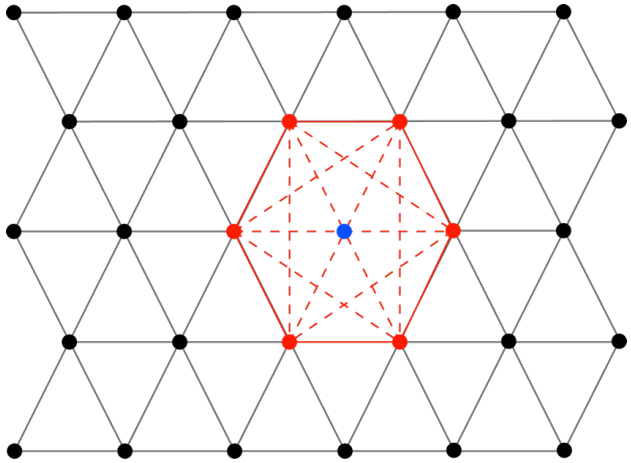

Figure 2-6: *The clustering coefficient ϕ for the hexagonal lattice. Of the 15 possible edges between the neighbours of a site, as shown in red, the six in solid lines are actually present in the network. This gives a clustering coefficient of $6/15 = 0.4$ per site and thus for the hexagonal lattice as a whole.*

the effects of contact structure. The principal criticism of the mean field closure is that it assumes that the proportion of infected neighbours surrounding a given susceptible is the same as that in the population generally. To demonstrate that this is not necessarily the case, one can define the susceptible-infective correlation as in (2.10):

$$\mathcal{C}_{SI} = \frac{N}{z}\frac{[SI]}{[S][I]}, \tag{2.12}$$

which takes the value one if the proportion of infected neighbours around the average susceptible is the same as the level of infection in the population as a whole. When $\mathcal{C}_{SI}$ is less than one, there is a weaker correlation between susceptibles and infectives than predicted by the mean field closure; that is to say, there are proportionally fewer infectives in the neighbourhood of the average susceptible than in the population as a whole.

Solving the pairwise equations (2.7) using the ordinary pair approximation closure (2.9), we can demonstrate how $\mathcal{C}_{SI}$ changes with time in response to events at the individual and pair level. Figure 2-7 compares the time profiles of the number of infectives, the number of $[SI]$ pairs and the susceptible-infective correlation.

Examining the time profile of the susceptible-infective correlation we see that starting from one, the correlation initially decreases as the disease spreads throughout the network. This is because at the start of an outbreak, it is actually the infected nodes that are most likely to have infected neighbours. These are nodes that they have infected

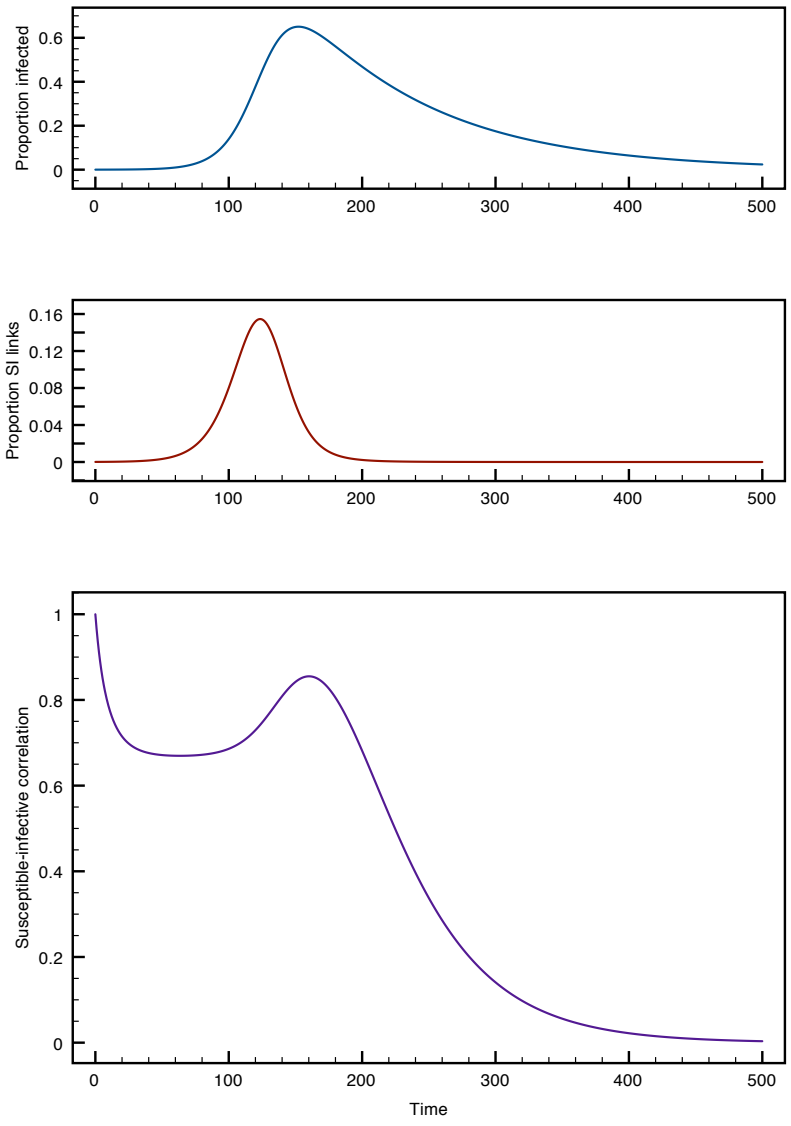

Figure 2-7: *Solution of (2.7) using ordinary pair approximation closure (2.9), with parameter values* $N = 10000$, $z = 6$, $\tau = 0.02$, $\gamma = 0.01$. *Top: Proportion infected versus time. Middle: Proportion of edges containing a susceptible and an infective. Bottom: Susceptible-Infective correlation versus time.*

before they themselves recover. At the point at which $\mathcal{C}_{SI}$ enters its local minimum, we can see that $[SI]$ is increasing at a constant rate and that this point represents a stage in the course of the epidemic where the disease has established itself within in the population. This is indicated by both the slight increase in the rate of new infections and the increase in $\mathcal{C}_{SI}$, the turning point occurring where infected nodes are not only beginning to recover but are also sufficient in number for the mean-field approximation to be more accurate. From this point, the epidemic proceeds as we might expect: the increased rate of infection leads to a shortage of susceptibles and as a consequence infection begins to slow and the process of recovery begins to take hold. This leads to a decline in the number of infectives, which is slower than the declines of both $[SI]$ and $\mathcal{C}_{SI}$ due to the presence of $[IR]$ links.

In Figure 2-8, we see that by solving system (2.7) together with the clustered pair approximation (2.11) it is possible to demonstrate that the local minimum in the susceptible-infective correlation towards the beginning of the epidemic is indeed due to the build up of clusters of infection. If the initially infected nodes are more likely to be clustered together, then the number of $[II]$ links produced is greater and the acquisition of new infectives from susceptibles is much less than the mean field. As the clustering parameter ϕ is increased in Figure 2-8, we see that the initial local minimum is deeper and occurs later in time. At around $\phi = 0.78$, the level of clustering prevents an outbreak from occurring at all, in which case the local minimum does not occur and the correlation monotonically decreases to zero.

The basic reproduction rate of a disease, denoted R_0, is perhaps the single most important quantity in epidemiological modelling. It is defined as the average number of secondary infections produced by a single infective in an otherwise entirely susceptible population. If R_0 exceeds one, an epidemic ensues. We now use the pairwise equation model to demonstrate the additional effects of network structure on the value of R_0.

To find R_0 for the SIR pair approximation model (2.7), we consider the individual level equations (2.5) and consider the conditions under which $[\dot{I}] > 0$:

$$\tau[SI] - \gamma[I] > 0$$

After some rearrangement and the use of equation (2.12), we have that

$$\frac{\tau z}{N}\mathcal{C}_{SI}[S][I] > \gamma[I]. \tag{2.13}$$

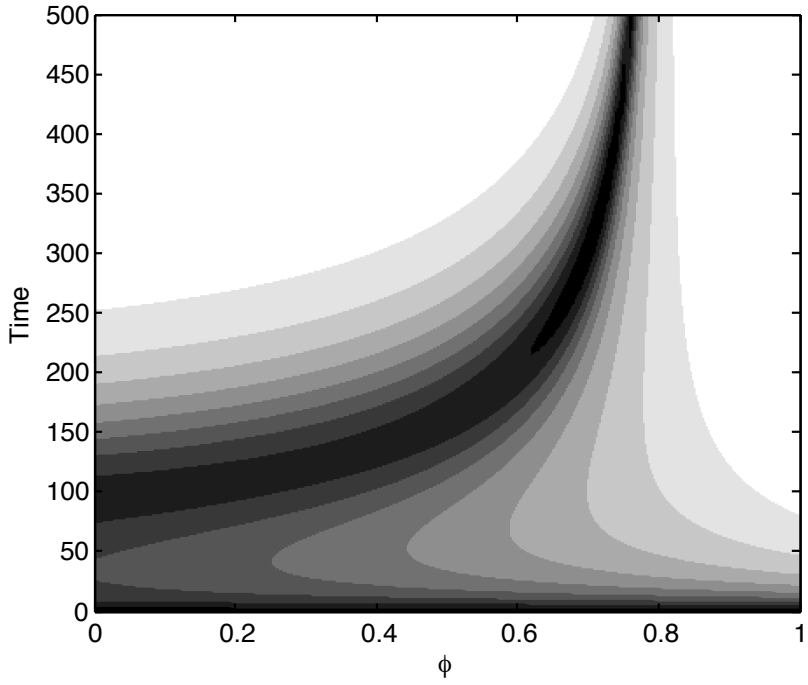

Figure 2-8: *The susceptible-infective correlation is computed from the solution of (2.7) using clustered pair approximation closure (2.11), with parameter values* $N = 10000$, $z = 6$, $\tau = 0.02$, $\gamma = 0.01$ *and values of the clustering coefficient* ϕ *ranging between zero and one. Each time profile is presented chromatically for varying* ϕ *along the y-axis, with black corresponding to a value of one and white to zero. The leftmost such sequence corresponds to the third plot of Figure 2-7.*

Initially, $[S] \approx N$ and $[I] \neq 0$, so we have that $[\dot{I}] > 0$ provided that

$$\frac{\tau z}{\gamma} \mathcal{C}_{SI} > 1. \tag{2.14}$$

Hence

$$R_0 \propto \frac{\tau z}{\gamma} \mathcal{C}_{SI}. \tag{2.15}$$

Whilst initially, the correlation takes a value of one (which would yield an estimate of R_0 identical to that of the mean field model, as discussed in Chapter 1 (1.7)), we have seen from Figures 2-7 and 2-8 that the correlation decreases initially and that for a substantial period after the initial outbreak $\mathcal{C}_{SI} < 1$ due to the fact that infection is grouped in clusters around the initially infected node(s). Keeling [22] argues that R_0 should therefore incorporate some aspect of this initial behaviour of $\mathcal{C}_{SI}$, suggesting that the local minimum attained represents the point at which the structure of the network has most impact on the spread of the disease. This then allows for the effect

of network topology (parameters N, ϕ and z are all involved in the calculation of $\mathcal{C}_{SI}$) on the value of R_0, as well as the impact of the epidemiological parameters β and γ.

For this choice of R_0, as we see from Figure 2-8, the effect of increasing the clustering ϕ (for fixed z and N) is to decrease R_0. This produces scenarios in which an epidemic cannot occur, even though it may be predicted for the given epidemiological parameters by the mean field model.

Of course, situations where the difference between the two predictions for R_0 is really that dramatic are rare, since the parameter values may suggest either networks that cannot by physically constructed or those that represent pathological cases.

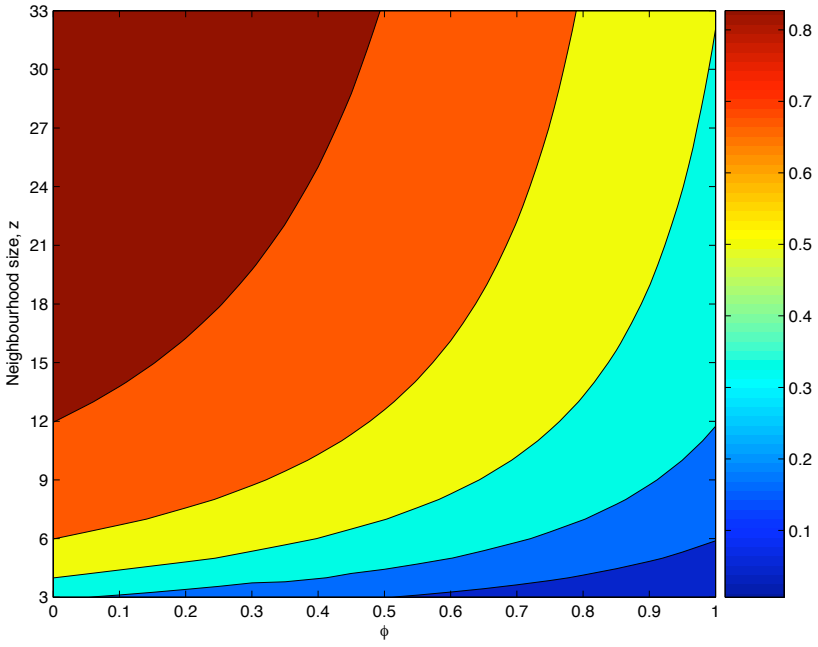

Figure 2-9: *The minimum of the susceptible-infective correlation (2.12) is calculated for different neighbourhood sizes and values of the clustering coefficient, ϕ. The epidemiological parameters are fixed at $\beta = 0.3$ ($\tau = 0.05$) and $\gamma = 0.1$. The network size was 10000 nodes. We see that for small neighbourhood sizes and large values of the clustering coefficient, R_0 as defined in (2.15) will be less than one and an epidemic will not occur.*

Figure 2-9 shows the effect of neighbourhood size and clustering coefficient ϕ on the local minimum of the susceptible-infective correlation. This is essentially a plot of the "discount" that should be given to the mean field prediction for R_0 given the structure of the underlying network.

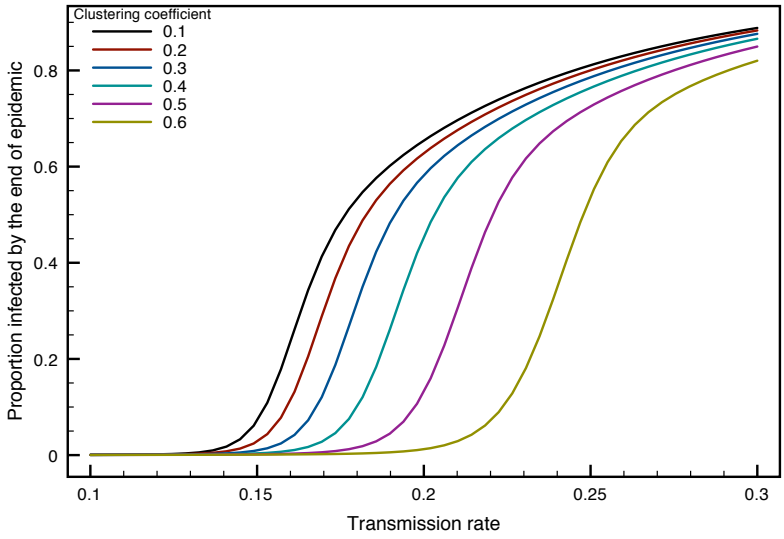

Figure 2-10: *Final number proportion infected at the end of the epidemic against the infection rate β for different values of the clustering coefficient ϕ. Model parameters used were γ=0.1, $N = 10000$, $z = 10$.*

2.2.4 Discussion

Extensions to pair approximation models in the literature tend to focus on three aspects from the point of view of our application. The first is to incorporate additional aspects of the contact structure in order to better capture the effects of various topological features and processes occurring. [21] incorporates empty sites in order to better capture demography in the context of an SIRS process. In two other papers, Eames and Keeling apply the technique to sexually transmitted infections. In the first, [12], the authors consider the degrees of end points as well as their states. This introduces many more pair types and therefore many more equations to solve, but their results compare favourably with simulations. In [13], the same authors look at the effect of restricting the spread of infection to a subset of the contact structure, deemed to be the active partnerships required for transmission of this nature to occur. As discussed in Chapter 1, the level of concurrency in partnerships is a major factor in whether an STI can persist within a population, and such a parameter is introduced in this particular model. The authors find that for polygamous relationships, a smaller value of the infection rate is required for an outbreak to occur. Moreover, as the level of concurrency is increased, the proportion infected increases in all behaviour types of the population, especially within the non-monogamous population.

Another motivation to extend pair approximation is to incorporate more epidemiological detail into the model. Sharkey et al [43] incorporate directional links to model the spread of disease in fish farms, looking specifically to model the consequences of directional flow in rivers and the impact of restricting the movement of fish on the spread of infection. Whilst not directly engaged with our application, the act of qualitatively labelling links is a natural step forwards from [22]. More natural would be some method of weighting links, since many contact structures are built upon contemporaneous 'casual' and 'steady' relationships, as discussed in [44].

Equally important is the modelling of contact tracing, whereby the partners of infected individuals are tracked with the intention of preventing onward transmission. This has been explored in a pair approximation setting in [11] and [24]. The effect of a vaccination program is discussed in [22].

2.3 Scale-free networks

In investigating the network of lifetime sexual partners of 2180 members of the Swedish population, Liljeros et al [30] discovered that the degree distribution of the network was scale-free, taking the form $\mathbb{P}(k) = k^{-\gamma}$. The exponent γ in this case was found to be 2.31 for $k > 5$ and is often found to be in the range $(2, 3)$ for networks generated by social processes, see [37] or [1] for examples. Networks such as these are dominated by nodes of small degree and characterised by the presence of a few extremely well-connected sites, often referred to as hubs. The existence of hubs in sexual networks has often been observed, be it in a historical setting [6] or more recently with identification of 'core groups' by Hethcote and Yorke, [18], who attribute 80% of infections to 20% of the population.

In this section we shall discuss the preferential attachment mechanism and review how this process leads to a scale-free degree distribution. We proceed to demonstrate various topological features of networks with such degree distributions and the consequences for the spread of diseases upon them.

We then present two mathematical models that incorporate these heterogeneous networks structures to validate our computer simulations.

2.3.1 Preferential attachment

One way to generate a scale-free network is by using a preferential attachment algorithm, such as the one described by Barabasi and Albert in [1]. It is described as

Figure 2-11: *The initial configuration of the network is a doubly connected pair of nodes, chosen to simplify the calculations.*

follows:

Algorithm 2.3 (**Barabasi-Albert process).** Let $\mathcal{N}$ be a network of N nodes. Allow the first $c \ll N$ nodes to form a complete clique. For each of the subsequent $N - c$ nodes, allow each to make m connections to the extant network, one at a time. These connections are to be made preferentially, with nodes of higher degree preferred to those of lower degree. For the i th node to be added, the probability of each of its m links being added to node j with degree k_j is:

$$\mathbb{P}(i \text{ connects to } j) = \frac{k_j}{\sum_s k_s}, j < i.$$

We note that in this version of preferential attachment multiple links between nodes are permitted, that is to say that if $m > 1$, the same node could be selected multiple times. Also, the use of an initial clique is not important and is mentioned here for consistency, since all computer simulations of the preferential attachment process presented here will use an initial clique with $c = m$, unless otherwise stated.

It is shown in [37] that this process generates a network with a scale-free distribution. As an illustrative example, following [10], we show that this is the case for $m = 1$. The first two nodes each contribute one edge to the network, so each is linked to the other. This creates a multiple edge between the first two nodes, we allow this in order to simplify some calculations later on. The arrangement is show below in Figure 2-11. Each node subsequent to these two contributes one edge to the network in turn. The source of the edge in question is the contributing node and the destination is chosen from the pre-existing nodes by linear preferential attachment. The following figure shows one possibility for how events may occur: Note that under the labelling shown in Figure 2-12 the network has the same number of edges as nodes, which is the reason for choice of the initial configuration. At the addition of the $(t+1)^{\text{th}}$ node, we are also contributing the $(t+1)^{\text{th}}$ edge. Furthermore the total degree of the existing component

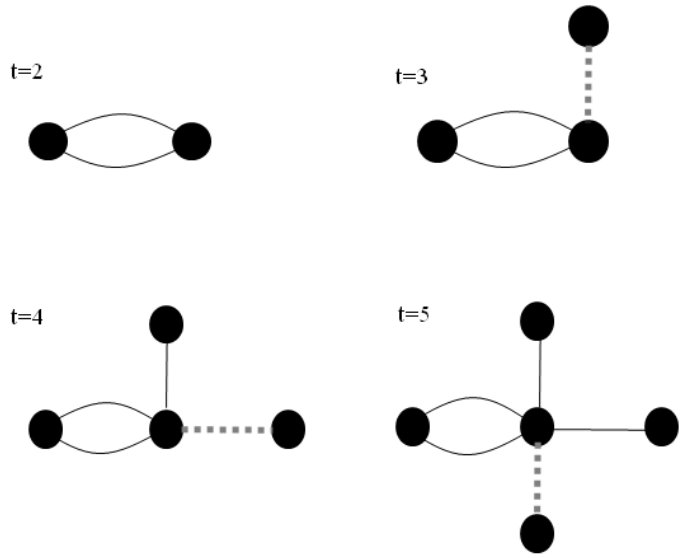

Figure 2-12: *The graph is grown from the initial configuration seen in Figure 2-11. The additional nodes are added using linear preferential attachment, whereby nodes of higher degree are added to with higher probability. The most recently added link is shown as a dashed line. Note that after the addition of t nodes, there are also t edges and the total degree of the network is $2t$.*

at this point is $2t$. Thus the probability of choosing node i of degree k_i is

$$\mathbb{P}(t+1 \to i) = \frac{k_i}{\sum_s k_s} = \frac{k_i}{2t}. \tag{2.16}$$

Let us now denote by $p(k, s, t)$ the probability that the node s is of degree k at the addition of the t^{th} node. If we consider how this quantity changes as further nodes are added, we find that there are two possibilities:

(i) The node s is chosen by preferential attachment and its degree is increased by one.

(ii) The node s is not chosen and its degree remains the same.

Thus we have

$$p(k, s, t+1) = \frac{k-1}{2t} p(k-1, s, t) + \left(1 - \frac{k}{2t}\right) p(k, s, t) \tag{2.17}$$

for $s \leq t$. Obviously, $p(k, t+1, t+1) = \delta_{k,1}$ for the new node, as it cannot yet be selected for preferential attachment. The initial condition described above is given by

$p(k, s = 1, 2, 2) = \delta_{k,2}$. Let $P(k,t)$ be the probability that a randomly selected node is of degree k after the addition of the t^{th} node. This is found by averaging $p(k,s,t)$ over all nodes s:

$$P(k,t) = \frac{1}{t}\sum_{s=1}^{t} p(k,s,t). \tag{2.18}$$

Summing (2.17) in this fashion and rearranging a little, we have

$$(t+1)P(k,t+1) - tP(k,t) = \frac{k-1}{2}P(k-1,t) - \frac{k}{2}P(k,t) + \delta_{k,1}. \tag{2.19}$$

Noting that the average number of vertices of degree k after the addition of t vertices (which we denote by $M(k,t)$) is given by

$$M(k,t) = tP(k,t), \tag{2.20}$$

we see that (2.19) can be written as

$$M(k,t+1) - M(k,t) = \frac{k-1}{2t}M(k-1,t) - \frac{k}{2t}M(k,t) + \delta_{k,1}. \tag{2.21}$$

Therefore, in taking the continuum approximation, we have

$$\frac{\partial}{\partial t}M(k,t) = \frac{k-1}{2t}M(k-1,t) - \frac{k}{2t}M(k,t) + \delta_{k,1}, \tag{2.22}$$

or

$$\frac{\partial}{\partial t}\left[tP(k,t)\right] = \frac{1}{2}\left[(k-1)P(k-1,t) - kP(k,t)\right] + \delta_{k,1}. \tag{2.23}$$

The corresponding stationary equation is

$$P(k) + \frac{1}{2}[kP(k) - (k-1)P(k-1)] = \delta_{k,1} \tag{2.24}$$

which has solution

$$P(k) = \frac{4}{k(k+1)(k+2)} \tag{2.25}$$

as can be verified by substitution. This is the degree distribution, and as we see $P(k) \approx k^{-3}$ and is scale-free.

Figure 2-13 shows the degree distribution for $k < 30$ and an estimate of -2.7 for the scaling exponent of a 10000 node network generated by Algorithm 2.3, with $m = 3$.

Figure 2-14 shows the effect of population size N on various topological features of the networks generated by Algorithm 2.3. Whilst the maximum degree of such a network will always be of order N, the variance of the degree distribution increases at a slower

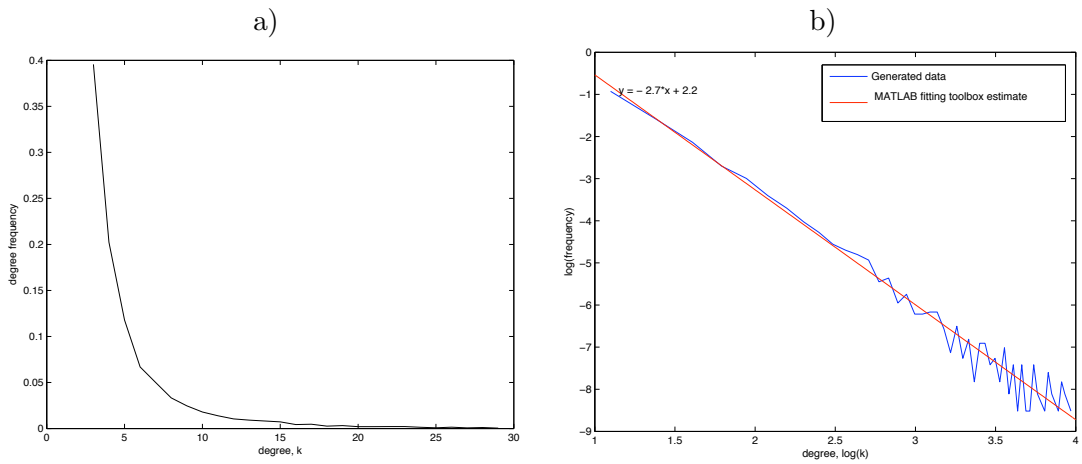

Figure 2-13: *The degree distribution for $k < 30$ and an estimate of the scaling exponent γ for a 10000 node network with $m = 3$ produced by Algorithm 2.3.*

rate. This is evidence of the topology of the network, a tree-like structure dominated by the well-connected hubs, with the dominance increasing with system size.

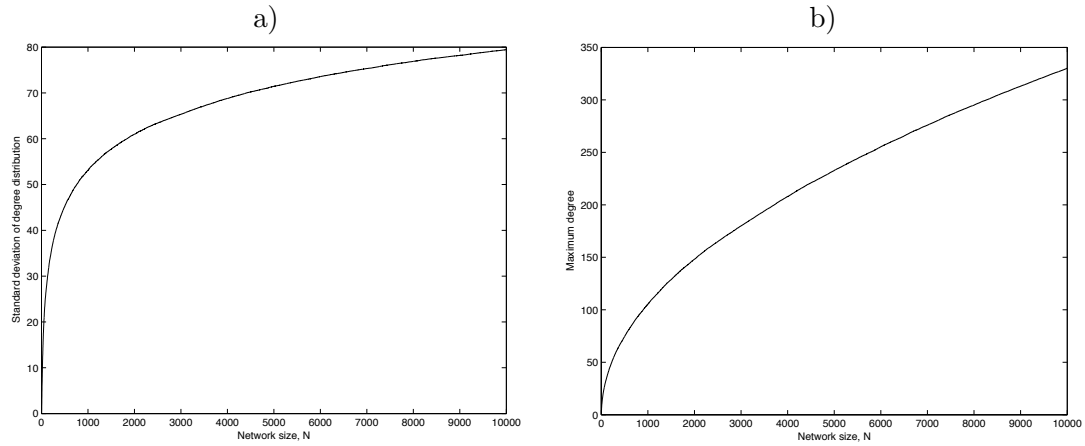

Figure 2-14: *The effect of network size N on the networks produced by Algorithm 2.3, a) shows the increasing variability in the degree distribution and b) shows how the maximum degree is affected by network size.*

2.3.2 Computer simulation

As before, simulating the SIR process on networks that have been generated using Algorithm 2.3 gives a similar shape to that predicted by a mean field model but occurring on a much faster time scale. To compare between the lattice and the scale-free network, we use Algorithm 2.3 to generate a scale-free network with an average of 6 connections

per node, on which the average of 100 outcomes is compared to the same average on a hexagonal lattice. Table 2.1 displays basic information about these networks and Figure 2-15 shows the difference in the cumulative infection rate.

Table 2.1: *Comparison of summary statistics for a hexagonal lattice and a scale-free network generated by the preferential attachment mechanism of Algorithm 2.3.*

Type	Lattice	Scale-free
Number of nodes	10000	10000
Number of edges	30000	29994
Average degree	6	5.9988
σ_k^2	0	73.69
$\max_k$	6	289
$\min_k$	6	3

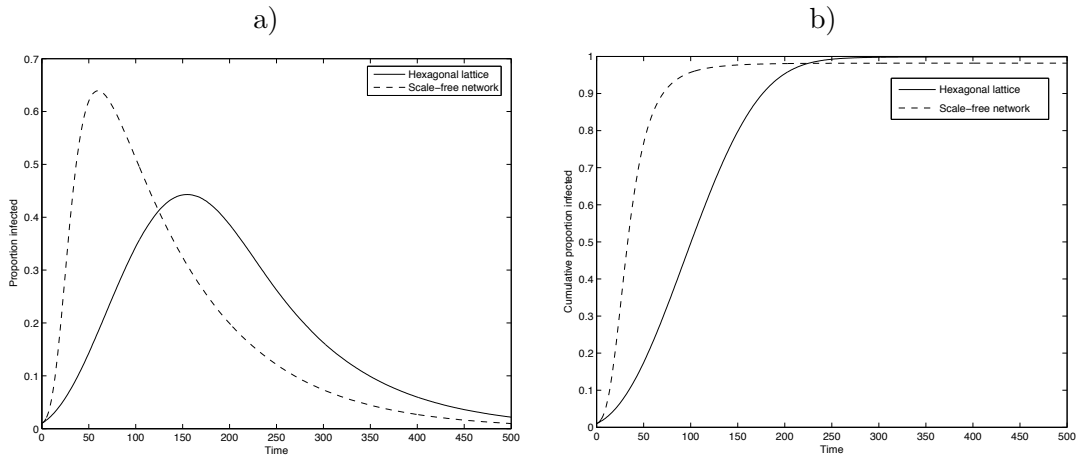

Figure 2-15: *Infection profiles from the average of 100 realisations of the SIR process (Algorithm 2.1) on the hexagonal lattice and the scale-free network, each comprising 10000 nodes. The latter was generated using Algorithm 2.3. Initially 100 nodes were infected with the infection rate* $\beta = 0.02$ *and recovery rate* $\gamma = 0.01$*. a) shows the proportion infected and b) the cumulative level of infection per time step.*

On a network, the interactions between susceptibles and infectives are what drive the epidemic. In the case of the lattice there is a clearly defined interface between susceptibles and infectives, which has a profound influence on the outbreak profile and the overall time scale of the disease. This interface obviously takes the form of the number of links between susceptible nodes and infected ones. This can be modelled mathematically using pairwise models and pair approximation, as we shall discuss later. Figure 2-16 shows the difference in the growth of the number of such edges for lattices and scale-free networks.

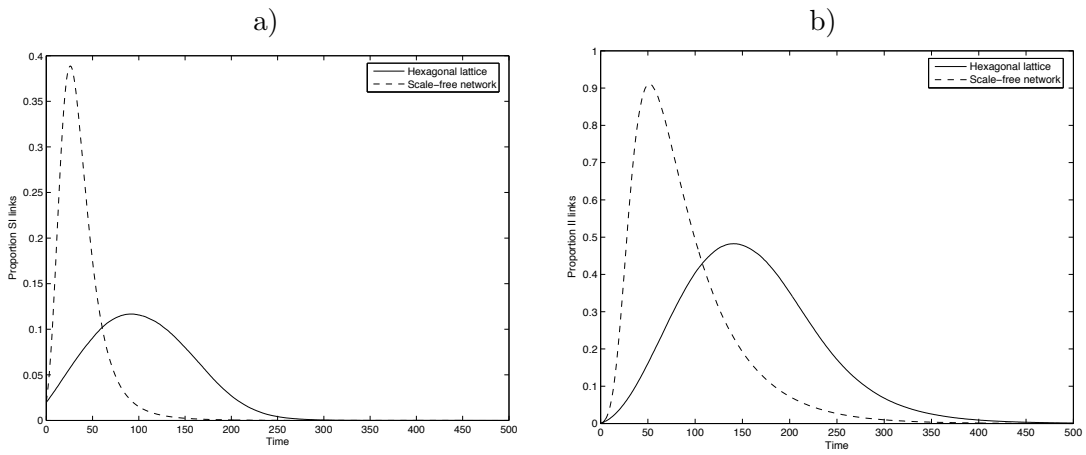

Figure 2-16: *a) Proportion of links comprising one susceptible and one infective and b) proportion of links comprising two infectives; from the average of 100 simulations of the SIR process on a hexagonal lattice and a scale-free network, each comprising 10000 nodes. The latter was generated using Algorithm 2.3. Initially 100 nodes were infected with the infection rate* $\beta = 0.02$ *and recovery rate* $\gamma = 0.01$.

The effect of this on the susceptible-infective correlation is quite pronounced. Figure 2-17 shows how the correlation on the scale-free network initially peaks above one, suggesting a high concentration of infection around susceptible nodes. This is no doubt due to the presence of the hubs, which once infected have connections to large parts of the network. Once the peak has occurred, we see the correlation decline to zero. Once the hubs and their neighbours have recovered, the few remaining susceptible nodes are unlikely to be connected to an infective as the short paths through the network will have been removed.

2.3.3 A compartmental model

Pastor-Satorras et al [34] considered an SIR type infection on a fixed network with degree distribution $\mathbb{P}(k)$ and finite average degree $\langle k \rangle$. Their model considers the proportions susceptible, infected and recovered within each connectivity class, so that $S_k(t) + I_k(t) + R_k(t) = 1$, whilst from these quantities, figures such as the total number of infectives $I(t)$ can be calculated, $I(t) = \sum_k \mathbb{P}(k) I_k(t)$. The spreading rate is given by λ and time is scaled so that the recovery rate can be assumed to be one. The densities

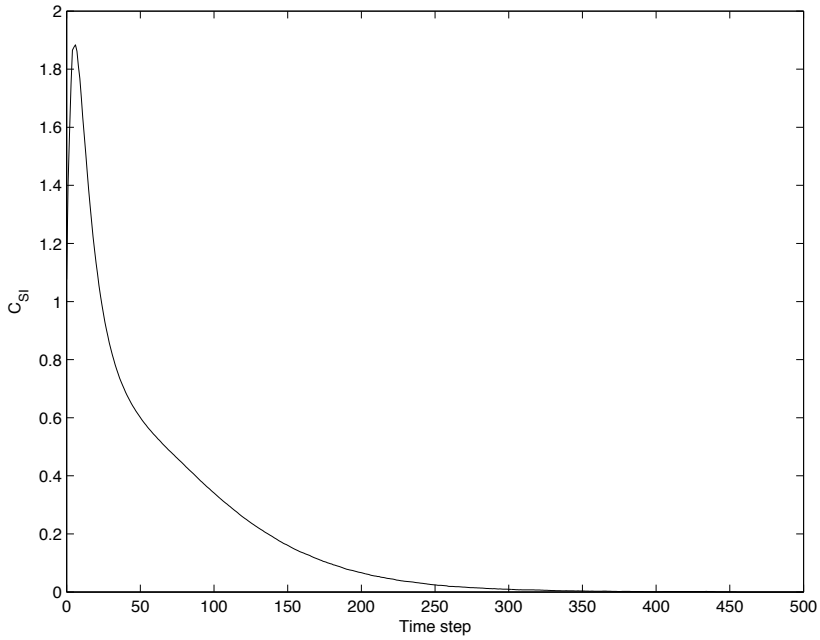

Figure 2-17: *The susceptible-infective correlation is calculated using (2.12) for the average of 100 SIR processes performed on a 10000 node scale-free network generated by Algorithm 2.3 with* $m = 3$. *The epidemiological parameters were* $\beta = 0.02$ *and* $\gamma = 0.01$. 1% *of the network was initially infected.*

in each connectivity class satisfy the set of coupled differential equations:

$$\dot{S}_k(t) = -\lambda k S_k(t)\theta(t) \tag{2.26}$$

$$\dot{I}_k(t) = \lambda k S_k(t)\theta(t) - I_k(t) \tag{2.27}$$

$$\dot{R}_k(t) = I_k(t) \tag{2.28}$$

where $\theta(t)$ is the probability that any given susceptible is connected to an infective. Since the probability of any given node pointing to one of degree s is given by $s\mathbb{P}(s)$, it follows that

$$\theta(t) = \frac{1}{\langle k \rangle} \sum_k k\mathbb{P}(k) I_k(t). \tag{2.29}$$

This expression for $\theta(t)$ obviously neglects the effect of degree-degree correlations, which could play an important role. For example, consider a network where node degree is assortative and high-degree nodes are more likely to be connected to one another. In this case, if the initially infected nodes comprise those that are high-degree, the infection will tend to aggregate among high-degree nodes and the value of $\theta(t)$ will be inaccurate. The effects of degree-degree correlations are discussed in [4].

An initially homogeneous distribution of infected nodes is assumed, ie $I_k(0) = I_0$ for all k. As $I_0 \to 0$, the fact that (2.26) is separable can be used to obtain:

$$S_k(t) = \mathrm{e}^{-\lambda k \phi(t)} \tag{2.30}$$

where

$$\phi(t) = \int_0^t \theta(s)\,\mathrm{d}s = \frac{1}{\langle k \rangle} \sum_k k\mathbb{P}(k) R_k(t) \tag{2.31}$$

making use of (2.29) and (2.28).

To obtain a closed relation for the total density of infected individuals, the time evolution of $\phi(t)$ is examined:

$$\begin{aligned} \frac{\mathrm{d}\phi(t)}{\mathrm{d}t} = \theta(t) &= \frac{1}{\langle k \rangle} \sum_k k\mathbb{P}(k) I_k(t) && (2.32) \\ &= \frac{1}{\langle k \rangle} \sum_k k\mathbb{P}(k)(1 - S_k(t) - R_k(t)) && (2.33) \\ &= 1 - \phi(t) - \frac{1}{\langle k \rangle} \sum_k k\mathbb{P}(k) S_k(t) && (2.34) \end{aligned}$$

A complete ODE for $\phi(t)$ is then obtained by substituting in (2.30):

$$\frac{\mathrm{d}\phi(t)}{\mathrm{d}t} = 1 - \phi(t) - \frac{1}{\langle k \rangle} \sum_k k\mathbb{P}(k) \mathrm{e}^{-\lambda k \phi(t)} \tag{2.35}$$

This equation cannot be solved in a closed form for general $\mathbb{P}(k)$. However, the final epidemic size R_∞ can be derived as a function of $\phi_\infty = \lim_{t\to\infty} \phi(t)$. Since R_∞ is reached at a point in time when no infectives remain, we have $R_k(\infty) = 1 - S_k(\infty)$ and so

$$R_\infty = \sum_k k\mathbb{P}(k)(1 - \mathrm{e}^{-\lambda k \phi_\infty}) \tag{2.36}$$

The two equations (2.35) and (2.36) form an alternative characterisation of the model presented in equations (2.26-2.28), from which an epidemic threshold can be derived. Recalling that $I_k(\infty) = 0$, we proceed as follows:

$$\lim_{t\to\infty} \frac{\mathrm{d}\phi}{\mathrm{d}t} = 0 = 1 - \phi_\infty - \frac{1}{\langle k \rangle} \sum_k k\mathbb{P}(k) \mathrm{e}^{-\lambda k \phi_\infty} \tag{2.37}$$

This gives the relationship

$$\phi_\infty = 1 - \frac{1}{\langle k \rangle} \sum_k k\mathbb{P}(k)\mathrm{e}^{-\lambda k \phi_\infty} \tag{2.38}$$

from which ϕ_∞ can be found using an iterative method. It is easy to see that $\phi_\infty = 0$ is always a solution. A non-zero solution requires fulfillment of the criterion:

$$\frac{\mathrm{d}}{\mathrm{d}\phi_\infty}\left(1 - \frac{1}{\langle k \rangle} \sum_k k\mathbb{P}(k)\mathrm{e}^{-\lambda k \phi_\infty}\right)|_{\phi_\infty = 0} > 1. \tag{2.39}$$

This leads to

$$\lambda \frac{\langle k^2 \rangle}{\langle k \rangle} < 1, \tag{2.40}$$

which defines the following epidemic threshold

$$\lambda_c = \frac{\langle k \rangle}{\langle k^2 \rangle}. \tag{2.41}$$

For values of λ below this threshold, $\phi_\infty = 0$ is the only solution of (2.38) and therefore $R_\infty = 0$, with no outbreak occurring on the network. Conversely, values of λ above λ_c yield a non-zero value of ϕ_∞ - giving a finite value for the total epidemic prevalence R_∞.

Therefore, networks with a high variance in the degree distribution will produce lower values of the threshold λ_c. As we can see from Figure 2-14, $\langle k^2 \rangle$ becomes large as N becomes large. In the limit of large N, the threshold is effectively zero, the presence of highly connected nodes ensuring that the disease always has a chance to persist.

2.3.4 A pairwise equation model

Figure 2-18 shows the difference between the average of several simulations of the SIR process on a scale-free network with average degree $z = 6$ and the solutions of equation (2.7) for the same parameter values. The differences between the simulation and the solutions of the pairwise equations are apparent. The solutions of the pairwise equations are delayed in time and the size of the epidemic peak is over-estimated. Another means to discuss analytically the spread of disease on a heterogeneous network is to extend the pair approximation formulation as discussed in 2.2.3. We again model the edges of the network and include variables for the degrees of nodes at each end of an edge, as well as their disease state. This presentation follows the work of Eames and Keeling in [12].

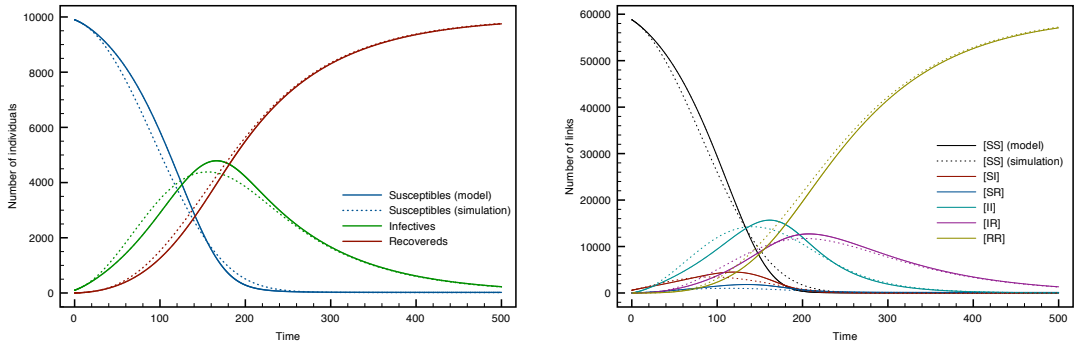

Figure 2-18: *Comparison of solutions of the pairwise equations (2.7) to the output of the average of 100 simulations on a scale-free network. Left: Individual states. Right: Pair states. The epidemiological parameters were* $\tau = 0.05$ *and* $\gamma = 0.1$*. Both networks comprised 10000 nodes and had an average degree* $z = 6$*.*

We shall denote by $[mn]$ the matrix that has entries $[mn]_{ij}$ corresponding the number of edges beginning in a node of degree m and terminating in a node of degree n. Obviously for an undirected graph, this matrix is symmetric. The notation $[A^m B^n]$ denotes an edge where the node of degree m is in state A and the node of degree n is in state B. The notation extends in a similar fashion to $[A^n]$ for the number of individuals nodes in state A and of degree n, and to triples $[A^n B^m C^p]$.

For recovering individual states, we have the following relationships:

$$\begin{aligned} \sum_{\text{states } A} \sum_{\text{states } B} [A^n B^m] &= [nm] \\ \sum_{m} \sum_{\text{states } B} [A^n B^m] &= n[A^n] \\ \sum_{n} [A^n] &= [A] \end{aligned} \tag{2.42}$$

Eames and Keeling, [12] present the equations for the SIS model, which necessitates the consideration of four pair types. Rather than use the relationships above, the individual level equations can be presented as differential equations as follows:

$$\begin{aligned} \frac{\mathrm{d}[S^n]}{\mathrm{d}t} &= -\tau \sum_m [S^n I^m] + \gamma [I^n] \\ \frac{\mathrm{d}[I^n]}{\mathrm{d}t} &= \tau \sum_m [S^n I^m] - \gamma [I^n] \end{aligned} \tag{2.43}$$

However, since all pair types are required for the approximation of triples by pairs,

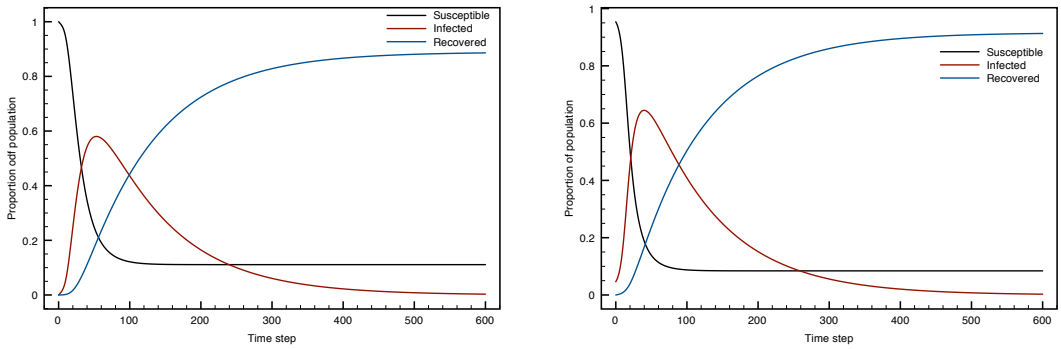

Figure 2-19: *Solutions of (2.44) for: Left, the random graph; and Right, the scale-free network. Each network has average degree $z = 6$. The other epidemiological parameters were $\tau = 0.05$, $\gamma = 0.1$. Two nodes were initially infected.*

we develop equations for all pair types and 'rebuild' the individual level results using the relationships in (2.42). For the SIR and $SIRS$ model, this means a set of nine equations per n, m pair, since for $m \neq n$, we no longer have symmetry of the links $[SI]$ and $[IS]$ as in the case of the homogeneous equations.

For the SIR model, they are as follows for $m \leq n$:

$$
\begin{aligned}
\frac{\mathrm{d}[S^n S^m]}{\mathrm{d}t} &= -\tau \sum_p [S^n S^m I^p] - \tau \sum_p [I^p S^n S^m] \\
\frac{\mathrm{d}[S^n I^m]}{\mathrm{d}t} &= \tau \sum_p [S^n S^m I^p] - \tau \sum_p [I^p S^n I^m] - (\tau + \gamma)[S^n I^m] \\
\frac{\mathrm{d}[I^n S^m]}{\mathrm{d}t} &= \tau \sum_p [I^p S^n S^m] - \tau \sum_p [I^n S^m I^p] - (\tau + \gamma)[I^n S^m] \\
\frac{\mathrm{d}[S^n R^m]}{\mathrm{d}t} &= -\tau \sum_p [I^p S^n R^m] + \gamma [S^n I^m] \\
\frac{\mathrm{d}[R^n S^m]}{\mathrm{d}t} &= -\tau \sum_p [R^n S^m I^p] + \gamma [I^n S^m] \\
\frac{\mathrm{d}[I^n I^m]}{\mathrm{d}t} &= \tau \sum_p [I^p S^n I^m] + \tau \sum_p [I^n S^m I^p] + \tau [S^n I^m] + \tau [I^n S^m] - 2\gamma [I^n I^m] \\
\frac{\mathrm{d}[I^n R^m]}{\mathrm{d}t} &= \gamma([I^n I^m] - [R^n I^m]) + \tau \sum_p [I^p S^n R^m] \\
\frac{\mathrm{d}[R^n I^m]}{\mathrm{d}t} &= \gamma([I^n I^m] - [I^n R^m]) + \tau \sum_p [R^n S^m I^p] \\
\frac{\mathrm{d}[R^n R^m]}{\mathrm{d}t} &= \gamma [R^n I^m] + \gamma [I^n R^m]
\end{aligned}
\tag{2.44}
$$

Again τ represents the probability of infection being transmitted along an edge and γ the recovery rate. The triples have to be summed over all possible (m, n, p) connections in the network. For particular values of m, n and p, we have the following approximation of triples:

$$[A^m B^n C^p] \approx \frac{(n-1)}{n} \frac{[A^m B^n]}{[B^n]} [B^n C^p] \tag{2.45}$$

Since the clustering coefficient for a heterogeneous network is a local measure, this approximation makes no assumptions about the presence of triangles. Due to our interest in scale-free networks, which are largely tree-like and contain few such triangles, we do not pursue this matter further.

If the network has a large range of degrees, the number of equations produced by the set of equations (2.44) will be very large. A computer program calculates the equations for each non-zero entry below the diagonal of the matrix $[mn]$, together with a vector of initial conditions and a list of rules for summing the variables, akin to those of (2.42). These can be solved for reasonably sized networks using MATLAB. The results are shown below.

Figure 2-19 shows the number of susceptible, infected and recovered nodes on a scale-free network and a random graph of the same size and average degree. The pairwise equations are generated from a representation of each network. The initial conditions are determined from randomly infecting an initial number of sites and directly enumerating the links present. Perhaps the most striking feature of the profiles is how similar they are. This may be due to the fact that we are restricted to networks comprising around 100 nodes due to the large number of equations generated from the matrix $[mn]$. In these cases, there are not enough nodes in each network to truly tell them apart.

Figure 2-20 further investigates these difficulties, showing how the number of nonzero entries of $[mn]$, and their density, increase with the size of the network.

We can see that the number of non-zero entries of $[mn]$ increases much faster for the scale-free network than for the random graph, so that the systems we have to solve become very large as population size increases. We also calculate the density of non-zero entries in the matrix $[mn]$ in order to explain why the systems also become impractically slow to solve for random graphs. We can see that the proportion of non-zero elements of $[mn]$ is higher for the random graphs and increasing with population size, while the same quantity decreases with population size for the scale-free network. A larger such density for these sets of equations will lead to more complicated expressions for the triples, which also increases the complexity of the system to be solved.

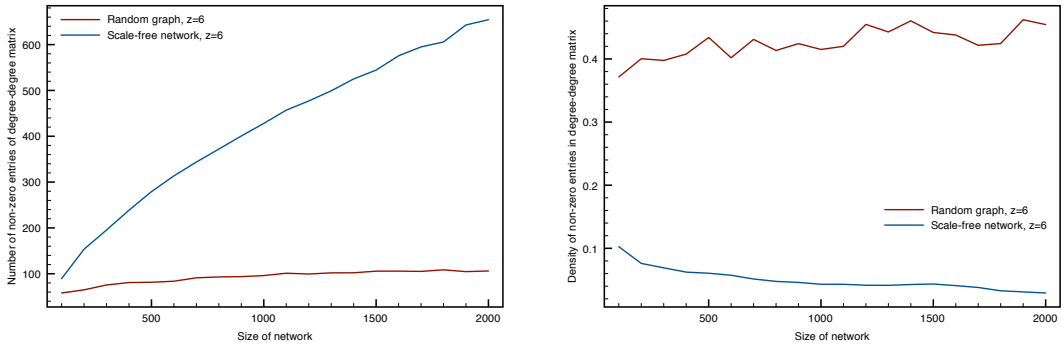

Figure 2-20: *Data concerning the computational difficulties of solving (2.44). Left: The number of non-entries in the degree-degree matrix* $[mn]$ *is plotted for random graphs and scale-free networks of different sizes and average degree* $z = 6$*. Right: The proportion of non-zero entries in the matrix* $[mn]$ *calculated for the same networks.*

Despite the computational limitations imposed, the solutions to (2.44) are of value. Figure 2-21 shows the proportion infected for some degree classes as compared to the overall population. For both networks, we see that the profiles for those degrees smaller than the average tend to be proportionally less infected than the overall population and vice versa. Though there are few well connected individuals in each network, those individuals are more likely to be infected than any given individual with fewer connections.

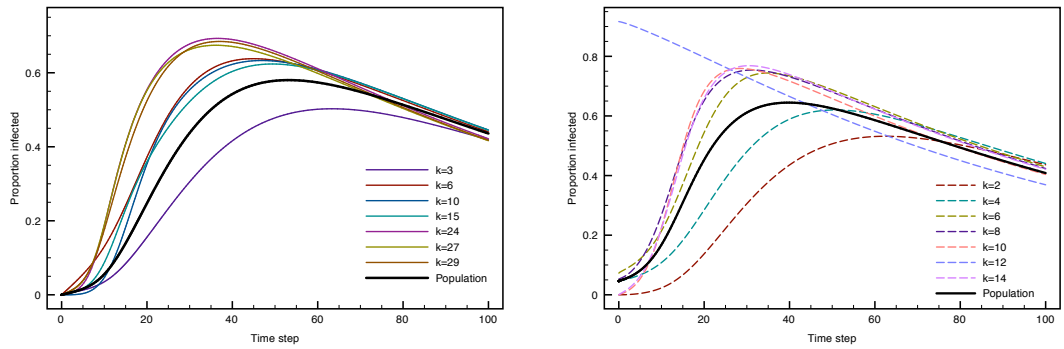

Figure 2-21: *Solutions of (2.44) on heterogeneous networks, with proportion infected by degree. Not all degrees are shown. Left: A scale-free network. Right: A random graph. Both networks have average degree,* $z = 6$*. The other epidemiological parameters were* $\tau = 0.05$*,* $\gamma = 0.1$*. Two nodes were initially infected.*

We note that not only is this method very protracted and difficult to obtain solutions from, it is also the case that the results are no more accurate than the homogeneous pairwise equations. As such, we concentrate our attention in future chapters solely on

the homogeneous pairwise equations.

2.4 Discussion

In this chapter, we have modelled the spread of disease on various contact structures, exploring the effects of this structure on various epidemiological features such as the basic reproduction number.

The effect of contact structure on disease dynamics is obvious on even the simplest networks. The effect of neighbourhood size is seen for lattices, a feature which can be reproduced in mean field models through incorporation of the number of contacts per individual into the transmission rate. However, it is not possible to capture the effects of the interconnections of neighbours within a mean field model and it is the inability to effectively describe the 'wasted' connections between infective individuals that lead to inaccuracies in this case.

The inherent variability in the number of contacts across a population of individuals also presents problems. The concentration of infection amongst a few highly connected individuals or aggregation of infection within a cluster of poorly connected individuals will mean that the infection will not grow at a rate proportional to those infected. Scale-free networks have been presented in this chapter as an example of such a contact structure and the effects of its topology on the spread of infection.

Population size is also important in assessing the impact of contact structure. For smaller populations, the deterministic mean field model will not account well for the discrete, stochastic nature of transmission and recovery events within small populations. Deterministic models with their continuous approximations are dependent only on initial conditions and parameters, and will not be susceptible to random extinction events in the way that computer simulations are.

The lattice and the scale-free network have therefore revealed a number of areas in which epidemiological results predicted by the mean field model should be evaluated again using models that explicitly incorporate contact structure.

For the lattice we find that the interconnection of neighbourhoods can be expressed in pairwise equations by modelling the states of nodes at the ends of each edge, with events occurring outside of the pair also taken into consideration as triples and expressed in terms of the original pairs in order to produce a closed system. The overlap of neighbourhoods which can appear in structures such as the hexagonal lattice, where an individual can be the neighbour of a neighbour, is dealt with by further refining this

approximation.

This leads to an expression for R_0 that expresses this threshold value in terms of the susceptible-infective correlation, a quantity that augments the traditional formulation involving the epidemiological parameters and the network structure. We have been able to verify the work of Keeling [22] and demonstrate the effect of clustering on the basic reproduction ratio of the disease. We have also reported the result of [34] that the threshold for an outbreak to occur in a network with the properties of a scale-free network can vanish as the population size increases. This shows the contrasting effects of clustering and degree heterogeneity, the former restricts the spread of infection, the latter enhances it. This 'sliding scale' of response to infection is a manifestation of the modularity property of complex networks as discussed in [39], whereby the more clustered a network is, the less variation appears in the degree distribution. This also appears to exist in real life, Smith et al report [44] that among men who have sex with men, those that have fewer sexual partners are also more likely to share those partners with others. In contrast, those that have many partners tend not have partners in common.

The primary method for dealing with contact structure has been the use of computer simulation, using algorithms to simulate the spread of disease on representations of networks within the computer. These can be repeated many times and from varying initial conditions, so that average behaviour may be deduced. Large networks can be used and more complicated processes than those demonstrated here can run quickly and accurately. Experiments can devised for determining the effects of both structural and epidemiological parameters. Large amounts of data can be generated as the full state of the system is known at each time step.

However, we do require the means to validate whether in running a simulation we are seeing the expected behaviour of the system in question. Committing oneself to performing a large scale simulation can consume large amounts of time and resources, so it is desirable to have an analytical and deterministic model to compare with the outcome of simulations. One such method is pairwise equations, which for lattices and other networks with constant degree distribution, provide an intuitive formulation of the infection process. The results agree well with simulation data and can be solved quickly numerically, then used to explore the dependence of models on parameters in a faster and more efficient fashion than with simulations. In fact, the pairwise equations give us access to parameters that are very difficult to access via simulations, for example, it is very difficult to construct a network with a given level of clustering at each node. This makes the pairwise equations a useful predictor of the effects of

network structure in this regard.

Nevertheless, in comparison to simulations on a scale-free network of a given average degree, the pairwise equations do not compare as favourably. In order to take account of heterogeneous degree distribution, we can construct a degree-based pair approximation that also takes account of the degrees of nodes at the end of edges, as well as their infection states. Whilst this increases the number of equations to be solved to an impractical extent, to the point where the original simulations are faster, it allows for differences in infection level for different connectivity strata of the population to be plotted and compared with data from simulations.

The restrictions imposed on network size by the sheer number of equations in the degree based pairwise equation model is unfortunate, since simulations on smaller networks are more subject to the drastic stochastic events that compare unfavourably with deterministic models. Eames and Keeling [11] propose further reductions in the number of equations using the summation criteria to create new variables, and a more sophisticated approximation of triples in terms of these variables. For a broader approach and comparison with larger networks, the extension of the mean field model as suggested by Moreno et. al. [34] to incorporate some aspects of the degree distribution gives some idea of what happens in general for very large networks, namely the disappearance of the epidemic threshold.

From this point we proceed to develop models for the interaction of core groups using the techniques developed in this chapter. In Chapter 3 we consider a population subject to infection from an external source, modelling the relationship between a core group and the wider population. In Chapter 4 we expand this to encompass multiple groups and their relationships to one another. For both chapters, we continue to use pairwise equations and simulations - alongside existing mathematical models that assume homogeneous mixing, which are presented for comparative purposes.

Chapter 3

A Single Core Group

3.1 Motivation and Background

3.1.1 Chapter outline

This chapter is concerned with the spread of a disease within a subset of a larger population. The effect of the wider population on the subgroup is discussed with the aid of mathematical models and computer simulations. We consider two mathematical models: firstly a mean field model used for its analytical tractability and then a pair approximation model which allows for some discussion of contact structure. Thereafter, we examine the results of computer simulations in order to discuss more heterogeneous contact structures and to validate results obtained from the mathematical models previously discussed.

3.1.2 Motivation

In the modelling of sexually transmitted infections, particular mention is often made of the fact that core groups of highly active individuals are crucial in maintaining infections within a wider less active population [18]. In more general populations, attention turns to frequent travellers who will often come into contact with more people as a result [48]. However, whilst models will often divide the population into compartments along these lines, it is often the case that there is no account for the difference in contact structure within these subpopulations.

In subsequent chapters, we shall present models that overcome this and incorporate contact structures within populations subdivided according to activity, location or be-

haviour. This chapter provides the basis for these models by considering a single population influenced by another external to it.

3.2 A mean-field model

We consider the case where contacts with an external population can result in additional transmission of infection. We compartmentalise the population into those who are susceptible, those infected by the disease and those that are recovered from it. These are denoted by $S(t)$, $I(t)$ and $R(t)$ respectively. All individuals in the population fall into exactly one of these categories, so that $S(t) + I(t) + R(t) = N$.

Transmission of the disease within the population from infectives to susceptibles occurs according to the law of mass action. The infectious contact rate is denoted by β. Each susceptible can also become infected due to contact with members of another group. We assume that this infection rate takes the form $\delta f(S, I)$ where δ is the maximum rate of external infection and f describes the influence of the level of infection within the group on the likelihood that an external infection may occur. We shall discuss the likely form of f below. For modelling purposes, we impose the following constraints on f:

(i) $f \in C^1$;

(ii) $0 \leq f(S, I) \leq 1$ for all $S + I \leq N$.

We assume that the disease is qualitatively the same for all individuals irrespective of how it was acquired, whether from within the group or externally. Therefore the recovery rate γ is constant for all individuals. We assume that individuals are immune for a short period once recovered and that when this immunity is lost individuals return to the susceptible class at a constant rate ν. We assume that there is no disease induced mortality but that individuals may die of other causes at a rate μ, irrespective of their disease status. We consider the population to be in equilibrium so that all such deaths are replaced by corresponding births into the susceptible class.

This gives us the following system:

$$\begin{aligned}
\frac{\mathrm{d}S}{\mathrm{d}t} &= -\beta S\frac{I}{N} + \mu(N-S) + \nu R - \delta f(S,I)S \\
\frac{\mathrm{d}I}{\mathrm{d}t} &= \beta S\frac{I}{N} - (\gamma+\mu)I + \delta f(S,I)S \\
\frac{\mathrm{d}R}{\mathrm{d}t} &= \gamma I - (\mu+\nu)R \\
S(t) + I(t) + R(t) &= N
\end{aligned} \tag{3.1}$$

3.2.1 The form of the external function

The function f describes the magnitude of the external infection in terms of the number of susceptibles and infectives within the observed group. This allows us to model the external infection as a response of the observed population to the perceived level of infection within the group. For example, if the observed population is composed of people who meet in a given location to acquire sexual partners, then the perception that a large proportion of their potential partners may be infected may cause contacts to be sought elsewhere.

Here we shall principally concern ourselves with the cases of constant external infection

$$f(S,I) = 1, \tag{3.2}$$

and that of linear dependence on the number of infectives,

$$f(S,I) = cI. \tag{3.3}$$

The form of f could also depend on the number of susceptibles, essentially by a converse argument to the one given above for dependence on infection levels. The more susceptibles there are, the more external contacts are made, which could plausibly be explained by a perception of safety within the group or increased attractiveness to external contacts.

This mechanism obviously assumes that individuals within the external population all have identical behaviour and that the same proportion of individuals interfacing with the observed group remains infected for the duration of the spread of the disease. We shall develop beyond this assumption in the sequel, allowing several groups to mutually influence one another.

Since it is the the underlying behaviour of exposure to external infections that motivates this work - the form of f is not known from any direct experiments - we use these

caricatures to explore the potential effects.

3.2.2 SIRS model

We reduce system 3.1 to the (I, R) plane. At a equilibrium positive equilibrium (I^*, R^*), we have

$$\begin{aligned} 0 &= \beta(N - I^* - R^*)I^* + \delta f(I^*)(N - I^* - R^*) - \gamma I^* \\ 0 &= \gamma I^* - \nu R^* \end{aligned} \tag{3.4}$$

Hence we have

$$R^* = \frac{\gamma}{\nu} I^* \tag{3.5}$$

and I^* is any feasible root of

$$\beta(N - (1 + \frac{\gamma}{\nu})I^*)I^* + \delta f(I^*)(N - (1 + \frac{\gamma}{\nu})I^*) - \gamma I^* = 0. \tag{3.6}$$

Constant external infection, $f = 1$ In this case (3.6) takes the form

$$-\beta(1 + \frac{\gamma}{\nu})I^{*2} + ((\beta N - \gamma) - \delta(1 + \frac{\gamma}{\nu})I^* + \delta N = 0, \tag{3.7}$$

which has solutions

$$I^* = \frac{\delta(1 + \frac{\gamma}{\nu}) - (\beta N - \gamma) \pm \sqrt{((\beta N - \gamma) - \delta(1 + \frac{\gamma}{\nu}))^2 + 4\beta(1 + \frac{\gamma}{\nu}}}{-2(1 + \frac{\gamma}{\nu}\delta N}. \tag{3.8}$$

Setting $\delta = 0$ in (3.8) recovers the two expected equilibria, the trivial equilibrium $I^* = 0$ and the positive equilibrium $I^* = \frac{\beta N - \gamma}{\beta(1 + \frac{\gamma}{\nu}}$. For $\delta > 0$, we can see that the discriminant is always positive and always ensures that a positive equilibrium exists. This can also be seen from (3.4), for which $(0, 0)$ is not an equilibrium. Figure 3-1 shows how I^* varies as δ is increased.

Having shown that for a constant external infection at least one positive equilibrium exists, we proceed to show that this equilibrium is unique and globally asymptotically stable in the region $\Omega := \{(S^*, I^*) \ : \ S^* + I* \leq N\}$. We use the framework developed in [5], which is summarised in Appendix A.

We have the system

$$\begin{aligned} \frac{\mathrm{d}S}{\mathrm{d}t} &= -\beta SI + \nu(N - S - I) - \delta S \\ \frac{\mathrm{d}I}{\mathrm{d}t} &= \beta SI - \gamma I + \delta S, \end{aligned} \tag{3.9}$$

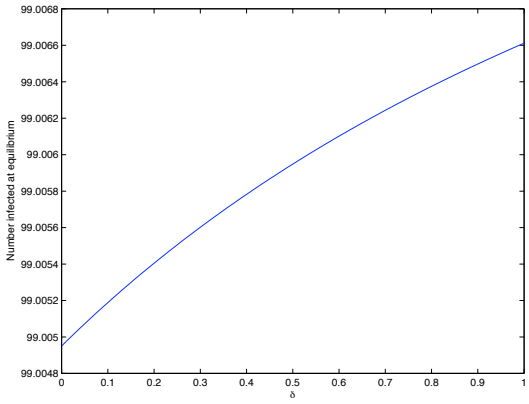

Figure 3-1: *The size of the positive equilibrium of (3.1) as δ is increased for $f(I) = 1$.*

which, with the substitution

$$\bar{S} = S + \frac{\nu}{\beta}, \tag{3.10}$$

can be rewritten as:

$$\begin{aligned} \frac{\mathrm{d}S}{\mathrm{d}t} &= -\beta SI + \nu(N - S) - \delta S + \frac{\nu}{\beta}(\delta + \nu) \\ \frac{\mathrm{d}I}{\mathrm{d}t} &= \beta SI - (\gamma + \nu)I + \delta S - \frac{\delta\nu}{\beta}. \end{aligned} \tag{3.11}$$

This can now be put into the form

$$\frac{\mathrm{d}z}{\mathrm{d}t} = \mathrm{diag}(z)(e + Az) + b(z) \tag{3.12}$$

with

$$z = (S, I)^{\mathrm{T}}, \tag{3.13}$$

$$A = \begin{pmatrix} 0 & -\beta \\ \beta & 0 \end{pmatrix}, \tag{3.14}$$

$$B = \begin{pmatrix} 0 & 0 \\ \delta & 0 \end{pmatrix}, \tag{3.15}$$

$$c = (\mu + \frac{\nu}{\beta}(\delta + \nu + \beta), -\frac{\delta\nu}{\beta})^{\mathrm{T}}, \tag{3.16}$$

$$e = (-\delta - \nu, -\nu - \gamma)^{\mathrm{T}}, \tag{3.17}$$

where we have defined $b(z) = Bz + c$. Assuming a strictly positive equilibrium z^* of the system (3.12), its uniqueness and global asymptotic stability are assured by

Theorem A.3 if

- the matrix $\tilde{A} := A + \mathrm{diag}(z^{*-1})B$ is skew-symmetrisible;
- a graph can be constructed from $\tilde{A}$ and $b(z)$ that satisfies the conditions of Lemma A.2.

A matrix U is skew-symmetric if $U^{\mathrm{T}} = -U$ and is skew-symmetrisable if there exists a positive diagonal matrix W such that WU is skew-symmetric. The matrix

$$\tilde{A} = \begin{pmatrix} 0 & -\beta \\ \beta + \frac{\delta}{I^*} & 0 \end{pmatrix} \tag{3.18}$$

is skew-symmetrisable, using the matrix $W = \mathrm{diag}(\frac{1}{\beta}, \frac{1}{\beta + \frac{\delta}{I^*}})$.

The graph which we construct to identify the stability of the equilibrium z^* consists of n vertices corresponding to the number of components of z. The edges of the graph are determined by the entries of $\tilde{A}$, a connection exists between vertex i and vertex j if $\tilde{A}_{ij}\tilde{A}_{ji} < 0$.

In the case of the two vertex graph corresponding to system (3.11), we have that $\tilde{A}_{12}\tilde{A}_{21} < 0$, yielding the simple graph on two vertices.

The function $b(z)$ is then used to label the vertices $\circ$ or $\bullet$, and the presence of certain configurations of $\bullet$-labelled vertices provide the stability result. Due to the simplicity of the graph, Lemma A.2 only requires that both vertices be connected and $\bullet$-labelled. A vertex is $\circ$-labelled if $b_i(z) = 0$ for all $z \in \Omega$, and $\bullet$-labelled otherwise.

For the system of interest,

$$b_1(z) = \mu + \frac{\nu}{\beta}(\beta + \delta + \mu + \nu) > 0, \tag{3.19}$$

ensuring that the first vertex is $\bullet$-labelled. For the second vertex, we have

$$b_2(z) = \delta z_1 - \frac{\delta\nu}{\beta} = \delta S - \frac{\delta\nu}{\beta}, \tag{3.20}$$

which, for $\delta > 0$, is positive provided $S > \frac{\nu}{\beta}$, or for all $S > 0$ prior to the transformation made in (3.10). Hence the second vertex is also $\bullet$-labelled and Lemma A.2 assures us that the equilibrium $z^* = (S^*, I^*)$ is unique and globally asymptotically stable.

External infection depending on the number of infectives In the case where $f(I) = I$, (3.6) takes the form

$$-(\beta+\delta)(1+\frac{\gamma}{\nu})I^{*2} + ((\beta+\delta)N-\gamma)I^* = 0, \tag{3.21}$$

which has solutions

$$I^* = 0 \quad \text{and} \quad \frac{(\beta+\delta)N-\gamma}{(\beta+\delta)(1+\frac{\gamma}{\nu})}. \tag{3.22}$$

The nontrivial equilibrium is only feasible if $(\beta+\delta)N > \gamma$. When it exists, the nontrivial equilibrium is always stable. To see this, we calculate the eigenvalues of the Jacobian for system (3.1) evaluated at the nontrivial equilibrium I^*. The Jacobian is given by

$$\mathcal{J} = \begin{pmatrix} (\beta+\delta)(N-I-R) - (\beta+\delta)I - \gamma & -(\beta+\delta)I \\ \gamma & \nu \end{pmatrix}, \tag{3.23}$$

which evaluated at I^* as given in (3.22) is

$$\mathcal{J}_{(I^*,R^*)} = \begin{pmatrix} \frac{(\beta+\delta)N-\gamma}{(1+\frac{\gamma}{\nu})} & \frac{(\beta+\delta)N-\gamma}{(1+\frac{\gamma}{\nu})} \\ \gamma & \nu \end{pmatrix}. \tag{3.24}$$

The eigenvalues of (3.24) are given by

$$\lambda_{1,2} = \frac{-(\nu + \frac{(\beta+\delta)N-\gamma}{(1+\frac{\gamma}{\nu})}) \pm \sqrt{(\nu - \frac{\beta N-\gamma}{(1+\frac{\gamma}{\nu})})^2 + 4\gamma\frac{(\beta+\delta)N-\gamma}{(1+\frac{\gamma}{\nu})}}}{2}. \tag{3.25}$$

The expression within the surd is always positive, but never of sufficient magnitude for either eigenvalue to be positive. Hence the nontrivial equilibrium, when it exists, is stable.

Other forms of f For other forms of f, numerical calculations again show a single equilibrium that is globally attractive. Figure 3-2 shows the nullclines for the same parameter values for different forms of f including the two cases considered above. We can see that the positive equilibrium also exists for each of the additional forms of f. The directions of trajectories within the quadrants of the phase plane formed by the two nullclines are the same for each f. Thus for each f the stability of the positive equilibrium remains the same. This constitutes a qualitative description of the stability results for these non-constant forms of f, to accompany the analytical derivation of the stability results for the positive equilibrium in the case of constant f.

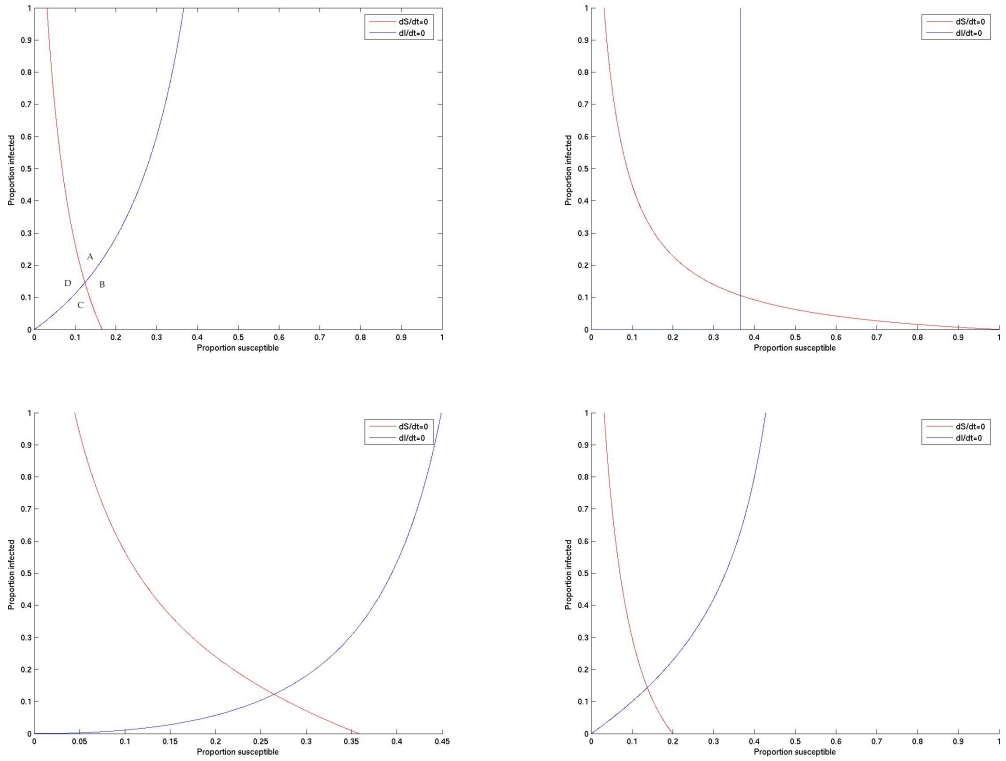

Figure 3-2: *Nullclines of system (3.1) for (clockwise from top left)* $f = 1$, $f = I$, $f = 1 - S$ *and* $f = S$. *For the top left figure, the regions marked A, B, C and D correspond to the following trajectories: A:* $\dot{I} < 0$, $\dot{S} < 0$; *B:* $\dot{I} > 0$, $\dot{S} < 0$; *C:* $\dot{I} > 0$, $\dot{S} > 0$; *and D:* $\dot{I} < 0$, $\dot{S} > 0$. *The same pattern persists for each of the analogous regions on the remaining three plots. The intersection of the nullclines therefore corresponds to a stable equilibrium in each case. The parameters used were* $\beta = 0.2$, $\gamma = 0.1$, $\delta = 0.1$, $\mu = 0.01$ *and* $\nu = 0.01$.

3.2.3 SIR model

If $\nu = 0$ in equation (3.1) we have an SIR model. Considering the (I, R) components of the system as before, the Jacobian is:

$$\mathcal{J} = \begin{pmatrix} \beta(N - I - R) - \beta I + \delta \frac{\partial f}{\partial I}(N - I_R) & \beta I - \delta f(I) \\ \gamma & 0 \end{pmatrix}. \tag{3.26}$$

By considering the stability of the trivial equilibrium $(0, 0)$ we can determine a threshold for an epidemic to occur. First consider the case of $f(I) = 1$, whereupon the Jacobian

simplifies to

$$\mathcal{J}_{(0,0)} = \begin{pmatrix} \beta N - \delta - \gamma & -\delta \\ \gamma & 0 \end{pmatrix}, \tag{3.27}$$

which has eigenvalues

$$\lambda_{1,2} = \frac{(\beta N - \delta - \gamma) \pm \sqrt{(\beta N - \delta - \gamma)^2 - 4\delta\gamma}}{2}. \tag{3.28}$$

Note that if $\delta = 0$, the eigenvalues are $\lambda_1 = 0$ and $\lambda = \beta N - \gamma$ so that the trivial equilibrium is unstable if $\beta N > \gamma$, so that $(0, 0)$ is unstable if βN exceeds γ. However, if $\delta > 0$, at least one of the eigenvalues will be positive. This ensures the instability of the trivial equilibrium for all $\delta > 0$. This is to be expected as a constant external infection will always force the population away from the disease free steady state.

The more interesting case is that of $f(I) = I$, for which the Jacobian is

$$J_{(0,0)} = \begin{pmatrix} (\beta + \delta)N - \gamma & 0 \\ \gamma & 0 \end{pmatrix}, \tag{3.29}$$

which has eigenvalues

$$\begin{aligned} \lambda_1 &= 0 \\ \lambda_2 &= (\beta + \delta)N - \gamma \end{aligned} \tag{3.30}$$

so that the disease free steady state is unstable if $(\beta + \delta)N > \gamma$. Thus for this choice of external infection, there will be an epidemic if the threshold

$$\frac{(\beta + \delta)N}{\gamma} > 1 \tag{3.31}$$

is exceeded.

In conclusion, for the SIR model and constant external infection there is no threshold that needs to be exceeded for the disease to become established as the trivial equilibrium is unstable for all positive values of δ. For the case of an external infection proportional to the number of infectives within the population, the threshold derived demonstrates the manner in which the external infection augments the internal infection.

3.3 A pairwise equation model

In Chapter 2 a pairwise equation model was presented that described the spread of a disease within a population with a distinct contact structure. For the case where each

individual has a fixed number of contacts far smaller than the overall population size, this model constitutes an improvement upon a mean field model. We adapt this model to incorporate an external infection, similar to that introduced for the mean field model above. We shall demonstrate how the structure of the network, characterised by the number of neighbours per site z and the clustering coefficient ϕ, affects the impact of the external infection.

For simplicity we concentrate on a constant external infection δ which has the effect of spontaneously converting susceptibles into infectives, regardless of the composition of the surrounding neighbourhood. Therefore all terms of the form $[S\bullet]$ become $[I\bullet]$ with probability δ.

3.3.1 The SIR model

The pairwise model for an SIR infection as seen in Chapter 2 can be converted to include an external infection as follows:

$$\begin{aligned}
[\dot{SS}] &= -2\tau[SSI] - 2\delta[SS] \\
[\dot{SI}] &= \tau[SSI] + \delta[SS] - \tau[ISI] - (\tau+\gamma+\delta)[SI] \\
[\dot{SR}] &= \gamma[SI] - \delta[SR] - \tau[ISR] \\
[\dot{II}] &= 2\tau[SI] + 2\tau[ISI] + 2\delta[SI] - 2\gamma[II] \\
[\dot{IR}] &= \delta[SR] + \tau[ISR] + \gamma[II] - \gamma[IR] \\
[\dot{RR}] &= 2\gamma[IR]
\end{aligned} \tag{3.32}$$

Triples are closed using the closure (2.11) discussed in Chapter 2. Because the approximation of triples results in approximation by the number of pairs, we ignore the impact that the external infection might have on triples, as these effects are manifested in the pairwise equations.

As discussed in Chapter 2, the external infection free system has similar properties to the mean-field model: there is a threshold value of R_0 above which an epidemic occurs; and there will always be susceptibles remaining at the end of an outbreak, [22].

From Figure 3-3 we can see that, as before, the susceptible-infective correlation can be used to examine the spread of disease throughout the population and to assess the impact of the external infection. We see that for small values of δ the characteristic shape of the correlation seen previously in Figure 2-7 is preserved, but that the local minimum achieved in the outbreak phase increases with δ. This is due to the fact that with random external infections occurring, we would expect to see the effects of

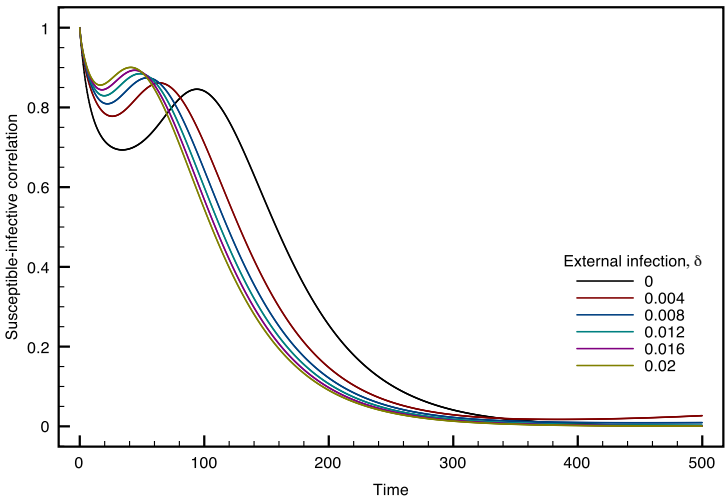

Figure 3-3: *The effect of an external infection on the solutions of (3.32) using the closure (2.11). The model parameters used are* $N = 10000$*,* $z = 6$*,* $\phi = 0$*,* $\tau = 0.02$*,* $\gamma = 0.01$*.*

clustering somewhat diminished.

Figure 3-4 shows that the long term behaviour of the correlation when $\delta > 0$ is also interesting. We see that for $0 < \delta < \gamma$ the correlation returns to a value greater than one after a long period of time. For $\delta > \gamma$, we see that the correlation tends to zero, as in the $\delta = 0$ case.

When $\delta > 0$, the external infection can continue to infect the remaining susceptibles after the epidemic has passed through the observed population. However, while $\delta < \gamma$ fewer infectives are produced than recover per time step and so the process takes a long time. Meanwhile, the value of the correlation will continue to increase because the number of susceptible-infective pairs $[SI]$ will be much larger than the number of infectives. When $\delta > \gamma$, the external infection will clear the remaining susceptibles sufficiently quickly and the number of $[SI]$ links will go to zero faster than the number of infected individuals, and so the correlation eventually tends to zero as in the external infection free case.

This effect of continued disease spread after the epidemic has passed also manifests itself when $\beta = \tau z$ is smaller than the recovery rate γ. Figure 3-5 shows the susceptible-infected correlation when $\delta = \frac{\gamma - \tau z}{N}$, with the external infection close to the threshold for infection to persist within the population. We see the characteristic formation of the local minimum (best seen in the inset for early time steps), as discussed in Chapter 2,

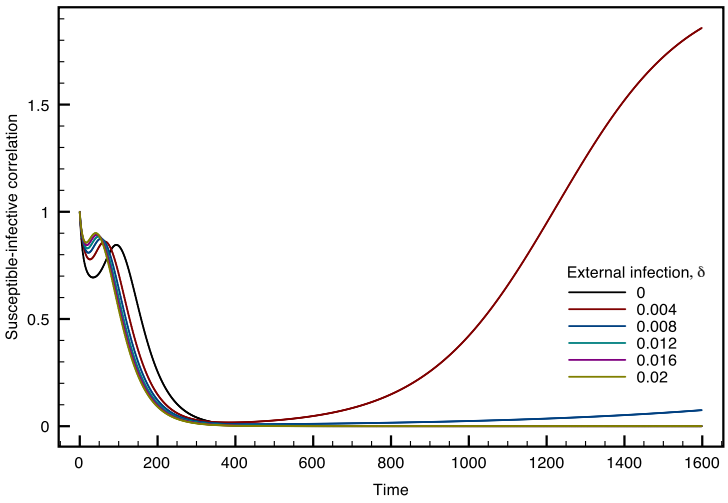

Figure 3-4: *Long term behaviour of the susceptible-infective correlation, where the effect of continued infection can clearly be seen for the two values of* δ *satisfying* $0 < \delta < \gamma$. *The model parameters are the same as in Figure 3-3.*

before the correlation tends to a value greater than one as we have seen for small δ in the $\beta > \gamma$ case above. Inset, we plot the cumulative number of individuals infected to show how although the number of infectives is small, the network is gradually infected.

We note that $\mathcal{C}_{SI}$ is no longer a genuine correlation when it exceeeds one, but instead appeals to the description given together with its definition in Chapter 2. This was that $\mathcal{C}_{SI}$ is a comparison between the level of infection in the neighbourhoods of susceptibles, and that in the population as a whole. At the point where $\mathcal{C}_{SI}$ becomes very large, the number of $[SI]$ pairs far exceeds that predicted from the number of susceptibles and infectives, $[S]$ and $[I]$. This is because the external infection forces the existence of $[SI]$ pairs, even when the main phase of the epidemic is over. We shall see later that this effect can be seen when calculated from computer simulations of the same process.

Figure 3-6 shows the effect of increasing the clustering coefficient and the external infection on the total proportion of the population that is infected after fifty time steps. As the level of external infection is increased, we see that a larger proportion of the population have been infected by this time for any given ϕ. Likewise, as seen for the case of no external infection in Figure 2-8, the slowing down of epidemics consequent of increased clustering is present over all levels of external infection. However as δ increases, the variation in the size of the epidemic (at fifty time steps) decreases over the rage of ϕ. This is indicative of the fact that as δ increases, the effect of increasing ϕ is reduced due to the fact that the external infections can bypass any clustering present

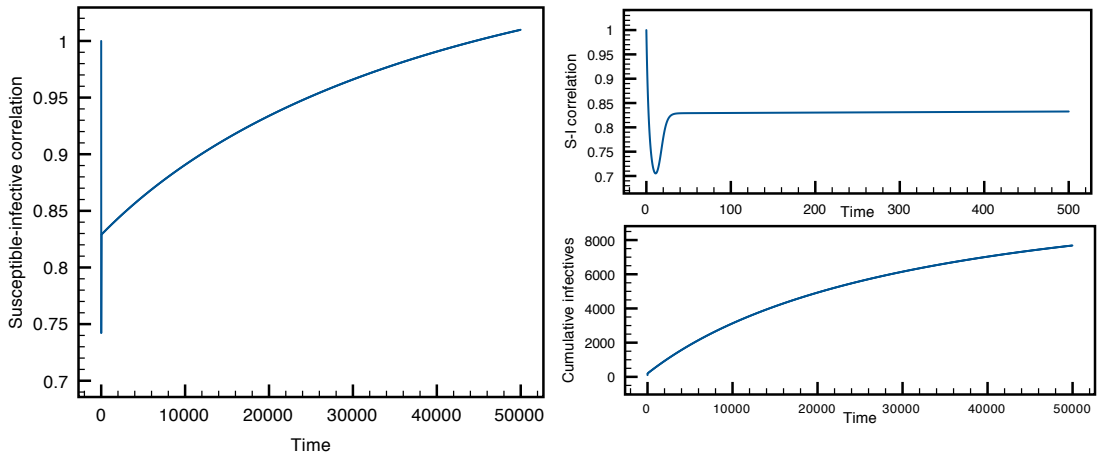

Figure 3-5: *The SIR pairwise equations are solved for $\gamma > \beta$ with the external infection δ sufficiently large to ensure the spread of the disease. Main figure: The long term effect of constant external infection on the susceptible-infective correlation, C_{SI}. Inset, top: The first 500 time steps of the susceptible-infective correlation plotted for insight into the initial behaviour. Inset, lower: The cumulative number of individuals infected throughout the course of the infection. Parameter values: $\beta = 0.3$ ($\tau = 0.05$), $\gamma = 0.5$, $\delta = 2 \times 10^{-5}$, $N = 10000$, $z = 6$, $\phi = 0$.*

in the observed population.

As in the case of the mean field model, solutions of (3.32) are not expected to have a finite fraction of susceptibles remaining once the epidemic is over, since the constant external infection δ will continue to remove any remaining susceptibles after the major wave of infection has finished. Keeling [22] demonstrated that as ϕ was increased the final proportion infected over the course of the epidemic was decreased, as seen in Figure 2-10. In the case of external infection, every individual is infected eventually, so an analogue of Figure 2-10 would show constant value 1, independent of values of τ, ϕ and δ.

3.3.2 The SIRS model

To extend to a scenario where we can evaluate the effect of external infection on disease persistence, we now turn our attention to a set of pairwise equations for an SIRS model. The disease dynamics we consider are analogous to the mean field model (3.1) except we do not incorporate the demographic turnover (deaths unrelated to the infection) represented by the parameter μ in those equations. The incorporation of demographic structure into pairwise equations is rather fraught and not entirely satisfying, for more details the reader is referred to Keeling's paper [21].

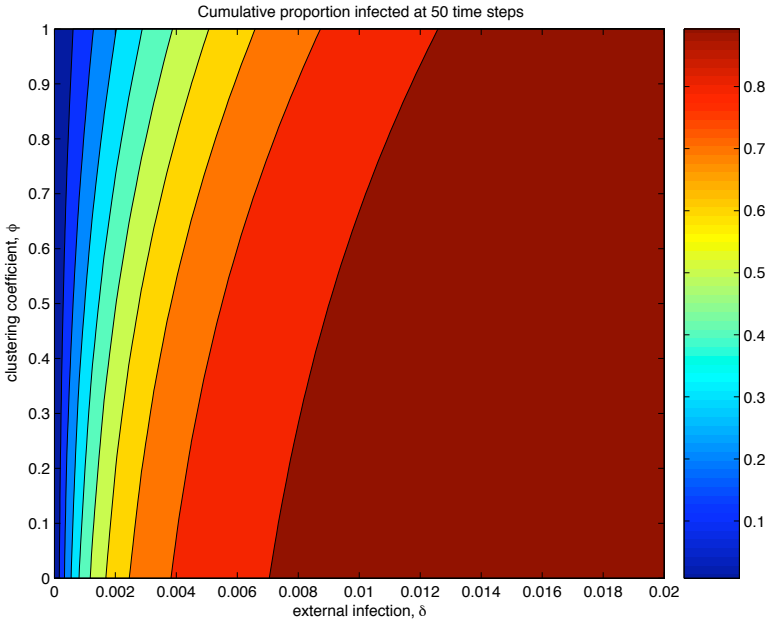

Figure 3-6: *The effect of increasing the clustering coefficient and the external infection on the total proportion of the population that has been infected after fifty time steps. The model parameters used are* $N = 10000$, $z = 6$, $\phi = 0$, $\tau = 0.02$, $\gamma = 0.01$.

With the addition of terms that restore the susceptibility of recovered nodes with probability ν to (3.32), we have the following system of ordinary differential equations for a pairwise SIRS model that incorporates external infection:

$$\begin{aligned}
[\dot{SS}] &= -2\tau[SSI] - 2\delta[SS] + 2\nu[SR] \\
[\dot{SI}] &= \tau[SSI] + \delta[SS] - \tau[ISI] - (\tau + \gamma + \delta)[SI] + \nu[IR] \\
[\dot{SR}] &= \gamma[SI] - \delta[SR] - \tau[ISR] + \nu[RR] \\
[\dot{II}] &= 2\tau[SI] + 2\tau[ISI] + 2\delta[SI] - 2\gamma[II] \\
[\dot{IR}] &= \delta[SR] + \tau[ISR] + \gamma[II] - (\nu + \gamma)[IR] \\
[\dot{RR}] &= 2\gamma[IR] - 2\nu[RR]
\end{aligned} \tag{3.33}$$

Triples are approximated in terms of pairs and the clustering coefficient ϕ as given in equation (2.11). As with the SIR model, we include a constant external infection that converts susceptible halves of pairs to the infective state at a rate δ.

As in the mean field case, solutions approach an equilibrium with a non-zero proportion of the population infected if $\delta > 0$. Figure 3-7 shows the effect of the clustering coefficient ϕ and external infection δ on the proportion infected at equilibrium. As we

have reported in Chapter 2, the nontrivial equilibrium is lost for a critical value of ϕ when there is no external infection. For all values of δ however, some infection remains across all values of ϕ and the nontrivial equilibrium persists. For smaller values of δ, the additional structure imposed by increasing ϕ produces a similar decrease in the proportion infected at equilibrium as when the external infection is absent, whereas for larger values of δ this level is independent of ϕ. This demonstrates once again how the external infection bypasses any imposition of contact structure for large enough values of δ.

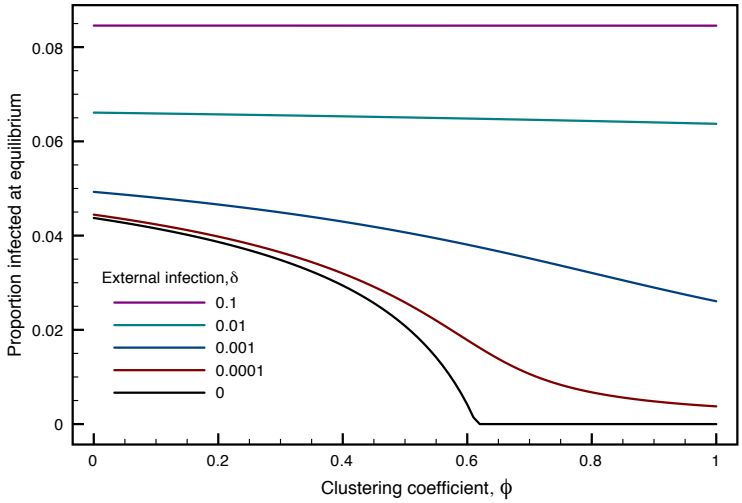

Figure 3-7: *The proportion infected at equilibrium from solutions of (3.33) is plotted against ϕ for various values of the external infection δ as shown in the legend. The model parameters used were $\tau = 0.05$, $\gamma = 0.1$, $\nu = 0.01$, $N = 10000$ and $z = 6$.*

Figure 3-8 shows that the difference between the infected equilibria of the mean field and pairwise equations decreases as δ increases. In fact, as the external infection bypasses contact structure we see that the proportion infected at equilibrium predicted by the pairwise equation model approaches that predicted by the mean field model.

3.4 Computer simulations

We now present computer simulations of the models discussed so far. These allow us to do two things. First we can compare whether the interaction between contact structure and external infection is as predicted by our models. Second, we can continue to investigate the effects of external infection on more heterogeneous structures that

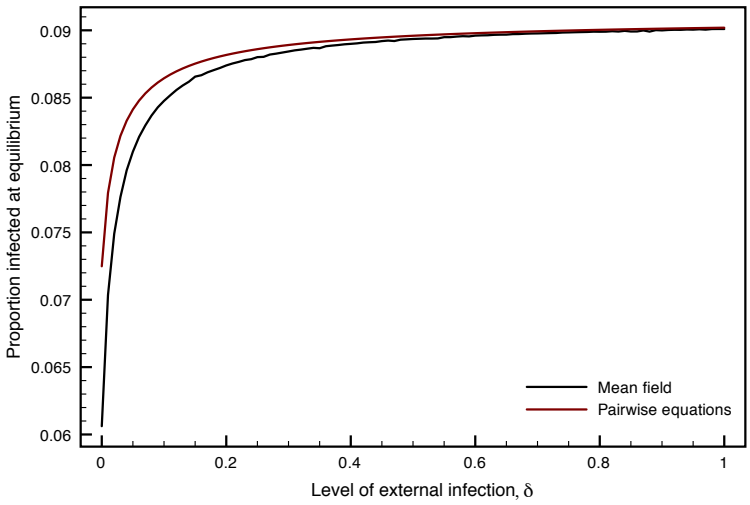

Figure 3-8: *Comparison between the solutions of mean field model (3.1) and those of the pairwise equation model (3.33). The proportion infected at equilibrium is plotted against the level of external infection, δ. As δ increases and the network structure is circumvented by the external infection, the two models predict similar equilibrium values. Model parameters used were $\tau = 0.05$ ($\beta = 0.3$), $\gamma = 0.1$, $\nu = 0.01$ and $\mu = 0$. For the pairwise equations, $N = 10000$, $z = 6$ and $\phi = 0.4$.*

prove difficult to analyse with mathematical models.

3.4.1 Simulations on lattices

In order to compare with the solutions of both mean field models and pairwise equation models we simulate the spread of an SIR infection on a hexagonal lattice consisting of 10000 nodes with a constant external infection δ. In the simulations this is implemented in the following manner: in any given time step, any given susceptible has probability δ of spontaneously changing its state to infective, regardless of the state of its neighbours.

Figure 3-9 shows the effect of increasing δ on the average of fifty repetitions. In the case of no external infection epidemics are very small when the initial number of infectives is small, whereas with the external infection present the epidemics are much larger. As δ is increased, the severity and speed of the epidemic are increased. These features are predicted by both the mean field and pairwise approximation models.

Figure 3-10 compares the solutions of the mean field equations, the pairwise equations and the output of simulations (once again, the average of 50 repetitions) for $\delta = 0.01$. We can see that the simulations and the pairwise equations are extremely close. As we

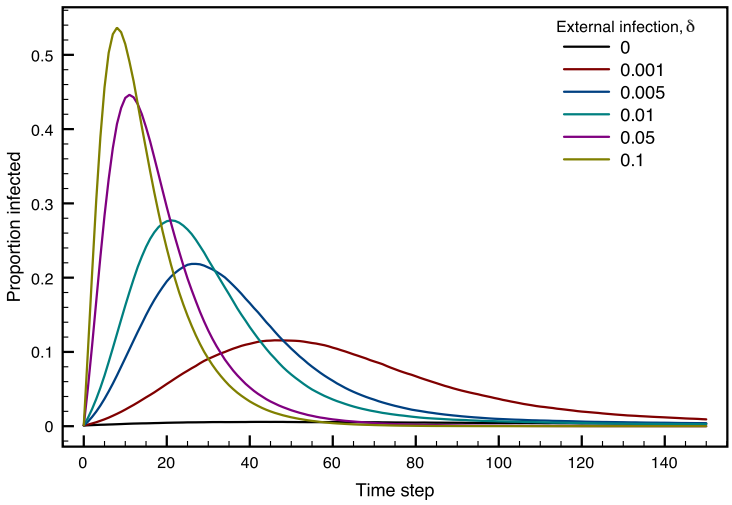

Figure 3-9: *The effect of increasing δ on an SIR process simulated on a hexagonal lattice. The simulations were run for 150 time steps on a lattice comprising 10000 nodes. The parameters used were $\tau = 0.05$ and $\gamma = 0.1$. The results presented are the mean of 50 repetitions.*

have seen previously in the external infection free case, the mean field overestimates the height of the epidemic. This is due to the fact that contact structure is not adequately represented and so the number of infective to susceptible contacts is over-estimated. However, as we have seen in Figure 3-3, the effect of contact structure is diminished as δ increases.

This is also true of the simulations, as we see in Figure 3-11, where the susceptible-infective correlation is calculated from the simulation output. As in Figure 3-4 we see that as δ approaches γ, the correlation tends to zero as time progresses but also that while γ exceeds δ, the correlation tends to a value exceeding one.

Figure 3-12 shows the results of realisations of the $SIRS$ process on a hexagonal lattice, in particular how the proportion infected at equilibrium I^* varies with the loss of immunity rate ν for different magnitudes of external infection. Whilst the effect of increasing δ increases the final proportion infected, the difference between the values of I^* at each value of ν does not appear to change, particularly for larger values of ν.

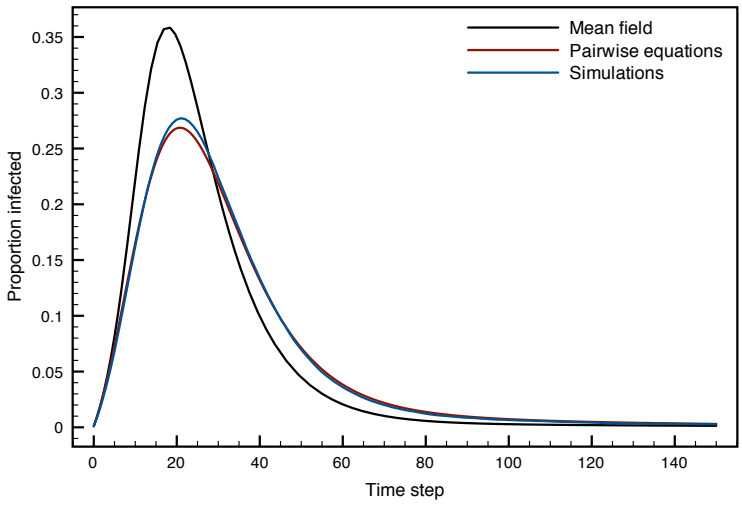

Figure 3-10: *Comparison of solutions of (3.1) with* $\nu = 0$*, (3.32) and computer simulations of an SIR process on a hexagonal lattice with constant external infection* $\delta = 0.01$*. Model and simulation parameters were* $\tau = 0.05(\beta = 0.3)$*,* $\gamma = 0.1$*,* $N = 10000$*,* $z = 6$*,* $\phi = 0.4$*. 10 nodes were initially infected and simulations are averaged over 50 realisations.*

3.4.2 Heterogeneous networks

SIR model Figure 3-13 shows the effect of increasing δ on the average of fifty realisations of an SIR process on a scale-free network with average degree 6. Again, as we might expect, the epidemic has a higher peak as δ increases and passes through the population in fewer time steps. In reference to figure 3-9, the effect is not as dramatic as for the hexagonal lattice, where a small increase in δ has a large impact upon the overall outcome of the epidemic, particularly for $\delta \approx 0$. In terms of the scale-free network, internal infections (that is those involving direct transmission between sites) will often lead to the 'hubs' becoming infected early on. Once these sites have recovered, they disconnect the more poorly connected sites that have yet to become infected from one another. As a result, the infection of poorly connected nodes and a few subsequent infections is the manifestation of the external infection in this case. However, for the hexagonal lattice, all sites are equal and as the disease spreads slowly in clusters, the external infections that occur can initiate new internal epidemics in clusters of susceptibles

Figure 3-14 shows the effect of δ on the susceptible-infective correlation $\mathcal{C}_{SI}$ for one realisation of the SIR process on a scale-free network with average degree $z = 6$. The

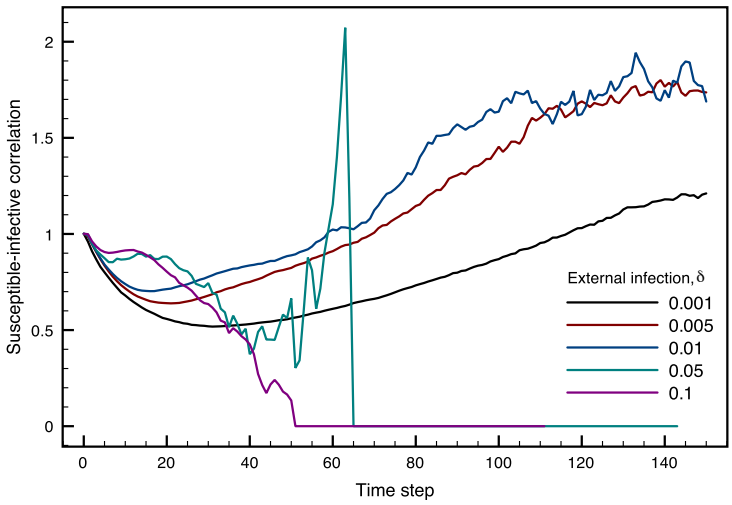

Figure 3-11: *The susceptible-infection correlation plotted from simulation output for different values of δ. Model parameters are the same as for Figure 3-9.*

early peak to a value above one (as seen in Figure 2-7 in Chapter 2) that distinguishes the correlation in this case from that of the lattice as in Figure 3-11 persists for most values of δ. The correlation also tends to zero as in Figure 2-17, but the time scale depends on the size of δ. For smaller δ, the internal infections occur as an epidemic leaving some susceptibles uninfected, these are subsequently infected by the external source. This prolongs the extent of the correlation as has also been seen in the lattice, both in simulations (Figure 3-11) and the pairwise equation model (Figure 3-4). Eventually the correlation will tend to zero as the entire susceptible population is infected in this fashion. For larger values of δ, sufficient external infections occur alongside the internal infections that drive the epidemic, exhausting the susceptible population fast enough for the correlation to tend to zero on approximately the same time scale as the epidemic of internal infections.

Figure 3-15 shows the effect of the external infection δ and the loss of immunity rate ν on the proportion infected at equilibrium for the average of fifty realisations of the SIRS process on a scale-free network with an average degree $z = 6$. The level of infection at equilibrium is always smaller than for comparable parameter values on the lattice (Figure 3-12) where clustering and the homogeneous structure both play a part in maintaining the infection at equilibrium.

Whilst the effect of δ is similar in both figures 3-12 and 3-15, we can see that in comparison δ has a lesser effect on the outcome at equilibrium for the scale-free network

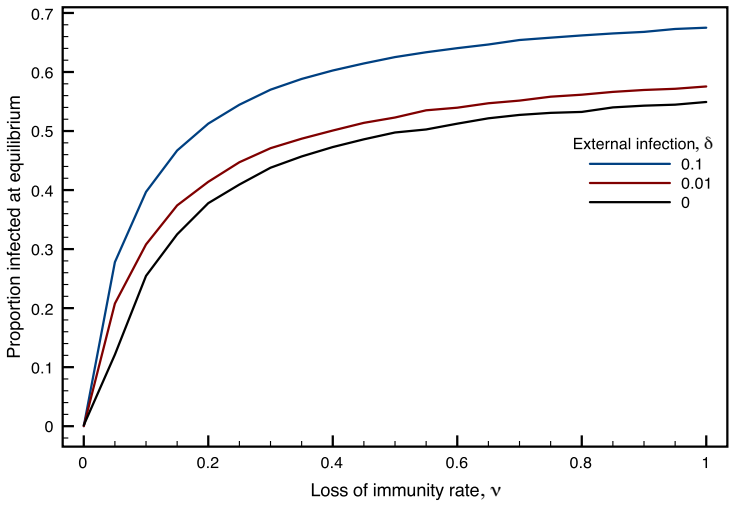

Figure 3-12: *The effect of increasing δ on an SIRS process simulated on a hexagonal lattice. The simulations were run for 150 time steps on a lattice comprising 10000 nodes. The parameters used were $\tau = 0.05$ and $\gamma = 0.1$. The results presented are the mean of 50 repetitions.*

than for the hexagonal lattice. As in the *SIR* model, this is most likely due to the topology of the network in the neighbourhoods of nodes affected by external infection. Whereas for the lattice these nodes are the same as the average, on the scale-free network these are most likely to have fewer neighbours than the mean.

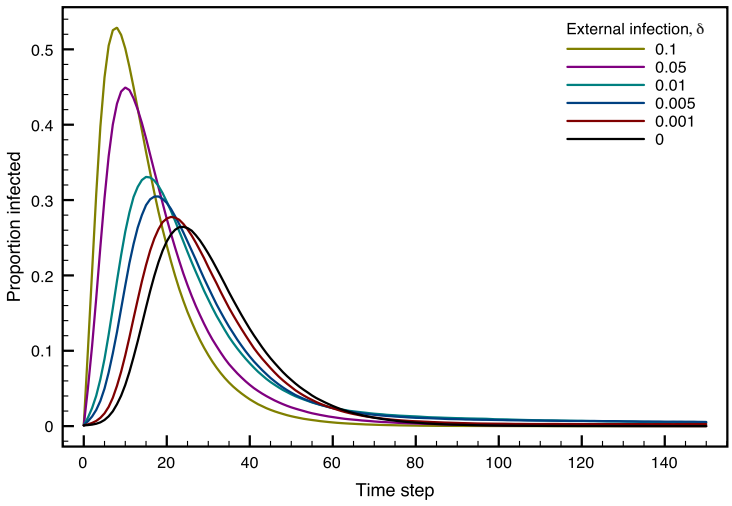

Figure 3-13: *The effect of increasing δ on an SIR process simulated on a scale-free network generated by the preferential attachment process, chosen so that the average degree is 6. The simulations were run for 150 time steps on a network comprising 10000 nodes. The parameters used were $\tau = 0.05$ and $\gamma = 0.1$. The results presented are the mean of 50 repetitions.*

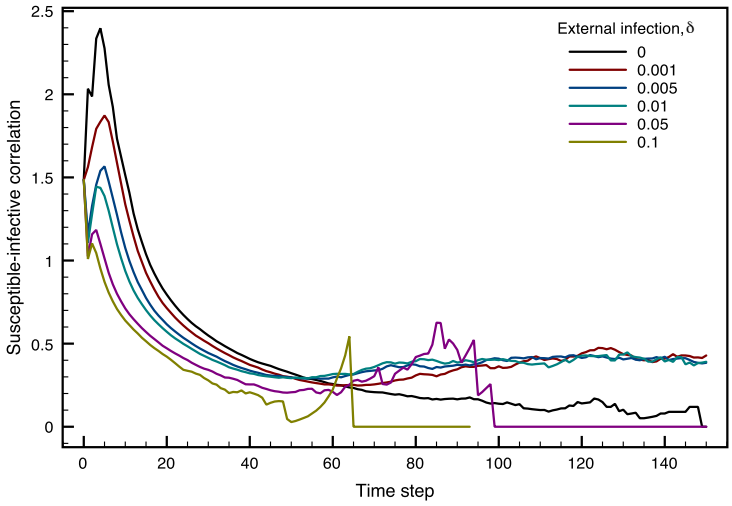

Figure 3-14: *The effect of increasing δ on the susceptible-infective correlation of an SIR process simulated on a scale-free network generated by the preferential attachment process, chosen so that the average degree is 6. The simulations were run for 150 time steps on a network comprising 10000 nodes. The parameters used were $\tau = 0.05$ and $\gamma = 0.1$. The results presented are the mean of 50 repetitions.*

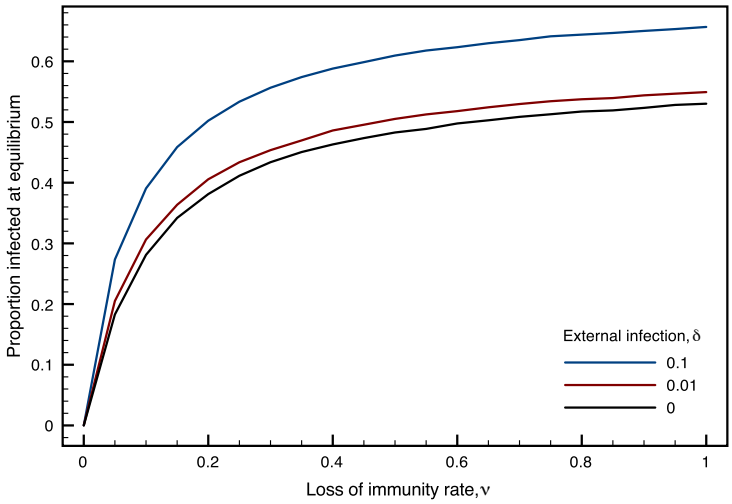

Figure 3-15: *The effect of increasing δ on an SIRS process simulated on a scale-free network generated by the preferential attachment process, chosen so that the average degree is 6. The simulations were run for 150 time steps on a network comprising 10000 nodes. The parameters used were $\tau = 0.05$ and $\gamma = 0.1$. The results presented are the mean of 50 repetitions.*

3.5 Discussion

In this chapter we have considered the impact of an external infection on a single group, whereby some susceptible individuals can become infected in a given time interval, irrespective of the states of their neighbours. The form of this external infection generally took the form of a constant δ, representing the maximum extent of the external infection, multiplied by a function f that is an ad hoc description of how the external infection might depend upon the state of the group.

For the mean field model (3.1), we considered the SIR and SIRS cases. For the SIR model, we investigated the effect of δ and f on a parameter-dependent threshold that determines, in the absence of external infection, whether an outbreak will occur. We showed that the addition of external infection increases the possible (β, γ) values for which an outbreak can occur. We also considered the effect of $\delta = 0$ on the final proportion susceptible by the end of the epidemic, S_∞.

For the SIRS model, we showed that for most forms of f, the unstable trivial equilibrium present for $\delta = 0$ will disappear in the presence of external infection. We showed that in the case of $f = 1$, the remaining positive equilibrium is unique and globally asymptotically stable via the techniques presented in [5] and reproduced in brief in Appendix A.

The disadvantage of the mean field models is that they incorporate none of the contact structure of the population. Core groups are by their very nature marked out from the remainder of the population by differences in behaviour, such as a high level of activity or shared contacts. Pairwise equations offer a means of incorporating this contact structure into models and furthermore, the parameters used to characterise network structure - group size, average degree and clustering coefficient - are extremely helpful when considering core groups. We incorporated the presence of external infection into the pairwise equation model exhibited previously in Chapter 2. For the SIR model, we see similar behaviour to the mean field model in that the epidemic threshold is lost and the final proportion susceptible is zero. Furthermore, the intuition provided by objects like the susceptible-infective correlation, concerning the placement of susceptible and infectives relative to one another, carries over into this setting. Change in the susceptible-infective correlation in response to increased external infection can explain how the new source of infection bypasses the spread within in clusters. This is also demonstrated in the SIRS model, where the effect of increasing the level of external infection is to allow for infection to persist on the highly clustered networks that would not support infection at equilibrium.

Finally we have conducted numerous computer simulations on both lattices and scale free networks, in order to validate our mathematical models and to explore the effects of contact structure on infection for networks that do not fit too well with the mean field or pairwise equation models. Happily, in the case of the SIR model there is good agreement between the solutions of the pairwise equation models and the averaged results of the computer simulations. There is also good agreement in the behaviour of the susceptible-infective correlation. In the case of the SIRS model, we see that the impact of external infection on the size of the equilibrium is modest. Simulations performed on scale-free networks show that the results for both the SIR and SIRS processes on these networks are similar in response to the presence of the external infection as those on the lattices. For the SIR process, which succeeds on a scale-free network if the infection reaches a hub, obviously thrives if one such hub is randomly switched to the infected state, even for a very low contact rate. In the case of the SIRS process, the effect of the external infection randomly turning highly connected nodes infective is mitigated by the heterogeneity of the network.

For the pairwise equations, we did not consider the effect of group infection state as we did for the mean field model. However, it is easy to see that though this would complicate the model, some valid assumptions could be made about which neighbourhoods would be more susceptible to an external infection. If we make the assumption that individuals will not seek external contacts if they are aware of infection amongst their neighbours, we could model this even with a constant external infection by incorporating a 'risk factor' in $[SS]$ pairs.

The pairwise equations could be further modified by incorporating degree and then allowing more highly connected nodes to have a greater probability of making external contacts, as seems reasonable.

Chapter 4

Multiple core groups

4.1 Motivation and Background

4.1.1 Chapter outline

This chapter builds upon the previous one by expanding the population structure to incorporate two or more subgroups that interact by externally influencing one another. We propose modifications to both mathematical models and computer simulations that allow a population comprising several subpopulations to be considered. As the mathematical models become more sophisticated, more features of each subpopulation can be manipulated, creating a better approximation to the real world population. We also use computer simulations to examine the differences between the spread of infection on distinct populations on one another. This is done with the aim of exploring the mathematical models, both in the context of their validation, and with a view to expansion into areas which cannot be mathematically modelled in a simple fashion.

4.1.2 Motivation

It is of interest, given a population comprising several 'at risk' groups, to ascertain whether an outbreak of an infection within one group will precipitate infection in any of the others. In this chapter we seek answers to the following questions:

(i) How do differences between groups affect the outcome of the disease spread?

(ii) How do the interactions between groups affect disease outcome?

(iii) For simulation purposes, when we can model almost any aspect of the subgroups

that comprise the population entire, what is the best way of capturing the difference between groups?

4.1.3 Background reading

The spread of disease within populations comprising several subgroups is a familiar extension of traditional epidemiological models. In the 'criss-cross' model for transmission of a sexually transmitted infection, the population is divided into male and female. With an entirely heterosexual population, each subpopulation can only acquire infection from the other. Modelling in this fashion, we have that the individuals in each subpopulation are infected entirely from without, with no infections occurring within the group. In what follows, our models will require that infection occurs within subgroups, as well as between them. However, by way of illustration, [35] constructs an SIS model.

$$\begin{array}{l} \frac{\mathrm{d}S_i}{\mathrm{d}t} = -\beta_i S_i I_j + \gamma_i I_i \\ \frac{\mathrm{d}I_i}{\mathrm{d}t} = \beta_i S_i I_j - \gamma_i I_i \end{array} \qquad i = 1, 2, \quad i \neq j, \tag{4.1}$$

where β_i, γ_i are the transmission and recovery rates specific to each group. After eliminating S_i, the steady states of the (I_1, I_2) phase plane are considered. There are two equilibria, the infection-free state $(0, 0)$, and a positive nontrivial steady state (I_1^*, I_2^*), with

$$I_i^* = \frac{N_1 N_2 - \frac{\gamma_1 \gamma_2}{\beta_1 \beta_2}}{N_j + \frac{\beta_i}{\gamma_i}}, \quad i = 1, 2, \quad i \neq j. \tag{4.2}$$

For determining the stability of each of the equilibria, there exists a threshold

$$\frac{\Pi \beta_i N_i}{\Pi \gamma_i} > 1. \tag{4.3}$$

If this holds, the trivial equilibrium becomes an unstable saddle, with stability conferred upon the positive nontrivial steady state. Otherwise, the trivial equilibrium is stable and the population remains infection-free.

This model is further developed to incorporate more detail by Lajmanovich and Yorke [27] (also discussed in [5] and [35]), who consider members of the population who are male/female, active/non-active, susceptible/infected, giving a total of eight classes. Again considering a heterosexual population, the interactions between the eight classes are given by the contact matrix L_{ij}. If the odd indices correspond to men and the even indices to women, then we have the further constraint on L:

$$L_{ij} = 0 \quad \text{if } i + j \text{ is even.} \tag{4.4}$$

A differential equation for the rate of the new infections is given by

$$\frac{\mathrm{d}N_iI_i}{\mathrm{d}t} = \sum_{j=1}^{8} L_{ij}(1-I_i)N_jI_j - \frac{N_iI_i}{D_i} \tag{4.5}$$

where I_i is the fraction of class i that is infected, D_i is the average duration in class i and N_i is the size of population i. The stability of positive equilibria are then examined as the parameters of the model are varied.

In [41], the idea of core and non-core individual is revisited, with emphasis placed on situations where the existence of core individuals is required to produce an epidemic within the whole population. The model takes the following form

$$\begin{aligned} \dot{u_1} =& \beta_1(1-p)u_1u_0 + \beta_2(1-p)u_2u_0 - u_1 \\ \dot{u_2} =& \beta_1 p u_1 u_0 + \beta_2 p u_2 u_0 - u_2. \end{aligned} \tag{4.6}$$

Here u_0 denotes the proportion susceptible, u_1 the proportion infected but non-core and u_2 the core infected. Non-core individuals infect susceptibles at rate β_1 and core individuals infect susceptibles at rate β_2. The parameter p dictates the proportion of the population in the core, so that p new infections are core and $(1-p)$ are non-core. Infectives are removed at rate 1.

The case $\beta_1 < 1 < \beta_2$ is considered, where infection cannot persist without core individuals (ie if $p = 0$) since $\beta_1 < 1$. Calculations yield that for the infection to persist, the proportion of the population in the core must be

$$p_c > \frac{(1-\beta_1)}{(\beta_2 - \beta_1)}. \tag{4.7}$$

A stochastic model is also considered, in which the states of nodes in the neighbourhood of an individual influence the infection process. In this situation, it is also found that a critical number of individuals have to be in the core in order for the infection to persist. The topology of the network considered is the d-dimensional lattice $\mathbb{Z}^d$ and even for $d = 1$ (each site has only two neighbours) the epidemic can persist, provided there are enough core individuals.

In [3], the spread of disease between population subgroups is considered in the context

of animal competition. The model for two such groups is given by

$$\begin{aligned}
\dot{S}_1 =& a(S_1 + I_1) - \beta S_1 I_1 - \eta q S_1 I_2 - \eta p (S_2 + I_2) S_1 - b S_1 \\
\dot{I}_1 =& \beta S_1 I_1 + \eta q S_1 I_2 - \eta p (S_2 + I_2) I_1 - c I_1 \\
\dot{S}_2 =& a(S_2 + I_2) - \beta S_2 I_2 - \eta q S_2 I_1 - \eta p (S_1 + I_1) S_2 - b S_2 \\
\dot{I}_2 =& \beta S_2 I_2 + \eta q S_2 I_1 - \eta p (S_1 + I_1) I_2 - c I_2
\end{aligned} \tag{4.8}$$

Here S_i and I_i denote the number infected in each group, $i = 1, 2$. The birth rate of new susceptibles is given by a, death rates for susceptible and infective individuals are given by b and c, with the assumption that $c > b$ so that infection confers a higher rate of mortality. The infection is spread both within and between groups. Within group infection is modelled as mass action, with spreading rate β. The spread of infection between groups occurs when individuals from each group meet, which is modelled by the constant rate η. Upon contact the individuals either die, with probability p; transmit infection, with probability q; or continue as before, with probability $1 - p - q$.

From our point of view, we are interested in the competition-free system with $p = 0$. This is analysed in [3] and it is found that there exists a threshold value for the interaction parameter η,

$$\eta < \frac{\beta}{q}. \tag{4.9}$$

Below this critical interaction value, neither group interacts sufficiently for the disease to significantly increase mortality. As a result, both groups co-exist. Above the threshold, one or both populations are driven to extinction.

Hyman and Li [19] consider a population in which individuals are heterogeneous with respect to either their susceptibility, their infectivity or both. Their model is an SIR-type model for AIDS transmission that makes the assumption of removal from the population upon contraction of full blown AIDS. The model is given by

$$\begin{aligned}
\dot{S} =& \mu(S^0 - S(t)) - \lambda(t) S(t) \\
\dot{I} =& \lambda(t) S(t) - (\mu + \nu) I(t) \\
\dot{R} =& \nu I(t) - \delta R(t)
\end{aligned} \tag{4.10}$$

with the spreading rate $\lambda(t)$ given by

$$\lambda(t) = \beta r \frac{I(t)}{S(t) + I(t)}, \tag{4.11}$$

where β the probability of transmission between individuals and r is the average number

of contacts per individual. The remaining parameters ν, μ and δ respectively represent the rate at which infected individuals develop full blown AIDS, the mortality rate from unrelated causes and δ is the mortality rate from AIDS.

Differential susceptibility is introduced by splitting the population into n groups, giving

$$\begin{aligned} \dot{S}_i &= \mu(S_i^0 - S_i(t)) - \lambda(t)S_i(t) \\ \dot{I} &= \sum_i \lambda_i(t)S(t) - (\mu + \nu)I(t) \\ \dot{R} &= \nu I(t) - \delta R(t) \end{aligned} \tag{4.12}$$

with individual spreading rates

$$\lambda_i(t) = \beta r \frac{I(t)}{N} \alpha_i, \tag{4.13}$$

where $N = \sum_i S_i + I$ and the parameters $\alpha_i > 0$ represent the differences in susceptibility between the different groups. Note that as with the previous criss-cross models (4.1), there is no modelling at the level of the interaction between subpopulations, only that of differences between individuals. [19] evaluates the effect of differential susceptibility on this form on R_0 and also for differential infectivity. The partition of the susceptible population is found to have greatest effect.

4.2 Mean-field models

We present a mean field model for multiple groups with the intention of using the simplified population structure to examine the effect of interaction strength on various features of the epidemic. We then proceed to investigate the effects of contact structure with a pairwise equation model in section 4.3.

4.2.1 Model Formulation

We assume the following about the disease and the population:

- Each subpopulation is of size $N_i \in \mathbb{N}$. Individuals are in one of three states: susceptible, infected or removed at time t. The number of individuals of the i^{th} population in the respective states at time t are denoted by $S_i(t)$, $I_i(t)$ and $R_i(t)$.
- An individual remains in the same subpopulation for all time, moving only between the states S_i, I_i and R_i.

- Within the i^{th} group, infection proceeds according to the law of mass action, so that the internal force of infection on the susceptibles of the i^{th} group is given by

$$g_i(I_i) = \beta_i I_i, i = 1, \ldots, k. \tag{4.14}$$

- Furthermore, each group is subject to an external infection which converts a fraction susceptibles of the i^{th} group to an infected state, depending on the state of the other groups. The external force of infection on the susceptibles of the i^{th} group is given generally by

$$h_i(I_1, \ldots, I_k) = \sum_{j=1}^{k} \delta_{ij} f_{ij}(I_j) \quad j = 1, \ldots, k, \quad j \neq i. \tag{4.15}$$

  Here δ_{ij} is the proportion of susceptibles in the i^{th} group that will be infected if the j^{th} group is wholly infected. The function $f_{ij} : [0, N_j] \to [0, N_i]$ is continuous and describes how the contribution of group j to the external infection on group i varies with the level of infection in the j^{th} group. We impose the restriction that $\sum_{j=1}^{k} \delta_{ij} < 1$.

- The recovery process is assumed to be a linear decay, occurring in the i^{th} group at a rate γ_i, $i = 1, \ldots, k$.

- Once recovered, an individual is deemed immune for a period. Like the recovery process, the loss of immunity is assumed to be a linear decay, with individuals moving from the R_i class to the S_i class at a rate ν_i.

This leads to the following set of equations for the SIRS model:

$$\begin{aligned} \frac{\mathrm{d}S_i}{\mathrm{d}t} &= -\beta_i S_i I_i - S_i \sum_{j \neq i} \delta_{ij} f_{ij}(I_j) + \nu_i (N_i - S_i - I_i) + \mu_i (N_i - S_i) \\ \frac{\mathrm{d}I_i}{\mathrm{d}t} &= \beta_i S_i I_i + S_i \sum_{j \neq i}^{k} \delta_{ij} f_{ij}(I_j) - (\gamma_i + \mu_i) I_i \end{aligned} \tag{4.16}$$

for $i = 1, \ldots, k$ and suitable initial conditions.

For the single group, we showed the existence of a unique globally asymptotically stable positive equilibrium using the framework in [5] and discussed in Appendix A. This demonstrated how the addition of external infection could push the population from an infection free state to a infected one, irrespective of the values of the epidemiological parameters that determine the spread of infection within the group.

For the same epidemiological model developed for multiple groups as in (4.16), it is no longer possible to cast the system into the form

$$\frac{\mathrm{d}z}{\mathrm{d}t} = \mathrm{diag}(z)(e + Az) + b(z), \tag{4.17}$$

because the functions f_{ij} will cause complications. Any cross terms of the form $S_i I_j$ as created by the external infection, even for the simple case of $f_{ij} = I_j/N_j$, produces negative entries in the matrix B in $b(z)$. See Appendix A for more details on the construction of this system. As a result, we will consider the SIRS model by more direct means subsequently.

4.2.2 SIS model

The method of Capasso et al [5] can however be applied to a similar model with SIS infection dynamics. The equations are as follows:

$$\frac{\mathrm{d}I_i}{\mathrm{d}t} = \beta_i S_i I_i + S_i \sum_{j \neq i}^{k} \delta_{ij} f_{ij}(I_j) - (\gamma_i + \mu_i) I_i. \tag{4.18}$$

Here β_i, γ_i, μ_i, δ_{ij} and f_{ij} have the same definitions as for the SIRS model (4.16).

It is helpful in this case to consider the proportion of each group that is infected. Using the appropriate substitutions, and the fact that $S_i + I_i = 1$, yields

$$\frac{\mathrm{d}I_i}{\mathrm{d}t} = \beta_i (1 - I_i) I_i + (1 - I_i) \sum_{j \neq i}^{k} \delta_{ij} I_j - (\mu_i + \gamma_i) I_i. \tag{4.19}$$

Putting the system in the form (4.17), we have

- $z := (I_1, \ldots, I_k)^{\mathrm{T}} \in \mathbb{R}^k$;
- $c := 0 \in \mathbb{R}^k$;
- $e := (\beta_1 - (\gamma_1 + \mu_1), \ldots, \beta_k - (\gamma_k + \mu_k))^{\mathrm{T}} \in \mathbb{R}^k$;
- $A_{ij} := \begin{cases} -\beta_i & : \quad i = j \\ -\delta_{ij} & : \quad i \neq j \end{cases}$;
- $B_{ij} := \begin{cases} 0 & : \quad i = j \\ \delta_{ij} & : \quad i \neq j \end{cases}$.

For simplicity we consider the case of two groups. For the above this gives

$$\tilde{A} = \begin{pmatrix} -\beta_1 & \frac{\delta_{12}}{I_1^*}(1-I_1^*) \\ \frac{\delta_{21}}{I_2^*}(1-I_2^*) & -\beta_2 \end{pmatrix}. \tag{4.20}$$

In this case, we cannot show the matrix $\tilde{A}$ is W-skew symmetric as in the previous chapter. However, if we can show that the matrix

$$V := \tilde{A} + \mathrm{diag}(-\delta_{12}\frac{I_2}{I_1^* I_1}, -\delta_{21}\frac{I_1}{I_2^* I_2}) \tag{4.21}$$

is negative definite then the positive equilibrium $z^* = (I_1^*, I_2^*)$ is globally asymptotically stable. The proof of this result is given in Appendix A.

Let $W := \mathrm{diag}(w_1, w_2)$ be a positive diagonal matrix. Then

$$\begin{aligned} WV &= \begin{pmatrix} w_1(-\beta_1 - \frac{\delta_{12}I_2}{I_1^* I_1}) & w_1\delta_{12}\frac{1-I_1^*}{I_1^*} \\ w_2\delta_{21}\frac{1-I_2^*}{I_2^*} & w_2(-\beta_2 - \frac{\delta_{21}I_1}{I_2^* I_2}) \end{pmatrix} \\ &= \begin{pmatrix} -w_1\frac{\delta_{12}I_2}{I_1^* I_1} & w_1\delta_{12}\frac{1-I_1^*}{I_1^*} \\ w_2\delta_{21}\frac{1-I_2^*}{I_2^*} & -w_2\frac{\delta_{21}I_1}{I_2^* I_2} \end{pmatrix} + \begin{pmatrix} -\beta_1 w_1 & 0 \\ 0 & -\beta_2 w_2 \end{pmatrix} \end{aligned} \tag{4.22}$$

The first matrix on the right hand side of equation (4.22) is symmetric provided we choose

$$w_1 > 0 \quad \text{and} \quad w_2 = \frac{I_2^*}{1-I_2^*}\frac{1-I_1^*}{I_1^*}w_1. \tag{4.23}$$

We note that the trace of WV is negative and that the determinant

$$\beta_1\beta_2 w_1 w_2 + \delta_{12}\delta_{21}w_1 w_2\left(\frac{1-(1-I_1^*)(1-I_2^*)}{I_1^* I_2^*}\right) \tag{4.24}$$

is positive since $0 < I_i < 1$ for $i = 1, 2$. Therefore WV is symmetric and has negative eigenvalues. As a result V is negative definite and this is sufficient to show that if a positive equilibrium z^* exists, it is unique and globally asymptotically stable.

4.2.3 The SIRS model for two groups

We will now consider the SIRS model (4.16) for the case of two groups and the group interaction form $f_{ij} = I_j$. If we set $\bar{S}_i = S_i/N_i$, $\bar{I}_i = I_i/N_i$ and $\beta_i = \beta N_i$, then we have

the following set of equations for the proportion of each group susceptible and infected:

$$\begin{aligned}
\frac{\mathrm{d}S_1}{\mathrm{d}t} &= -\beta_1 S_1 I_1 - \delta_{12} I_2 S_1 + \nu(1 - S_1 - I_1) + \mu(1 - S_1) \\
\frac{\mathrm{d}I_1}{\mathrm{d}t} &= \beta_1 S_1 I_1 + \delta_{12} I_2 S_1 - (\gamma + \mu) I_1 \\
\frac{\mathrm{d}S_2}{\mathrm{d}t} &= -\beta_2 S_2 I_2 - \delta_{21} I_1 S_2 + \nu(1 - S_2 - I_2) + \mu(1 - S_2) \\
\frac{\mathrm{d}I_2}{\mathrm{d}t} &= \beta_2 S_2 I_2 + \delta_{21} I_1 S_2 - (\gamma + \mu) I_2.
\end{aligned} \tag{4.25}$$

Here we have assumed that the parameters β, γ, μ and ν are the same for each group, and we have reverted to using S_i etc in place of $\bar{S}_i$ for ease of notation. Note that if each group is the same size, then $\beta_1 = \beta_2$ and because we are most interested in the group interaction parameters δ_{ij}, we assume this is the case from here on.

System (4.25) has the following Jacobian

$$\mathcal{J} = \begin{pmatrix}
-\beta I_1 - \delta_{12} I_2 - \nu - \mu & -\beta S_1 - \nu & 0 & -\delta_{12} S_1 \\
\beta I_1 + \delta_{12} I_2 & \beta S_1 - (\gamma + \mu) & 0 & \delta_{12} S_1 \\
0 & -\delta_{21} S_2 & -\beta I_2 - \delta_{21} I_1 - \nu - \mu & -\beta S_2 - \nu \\
0 & \delta_{21} S_2 & \beta I_2 + \delta_{21} I_2 & \beta S_2 - (\gamma + \mu)
\end{pmatrix}. \tag{4.26}$$

Evaluated at the trivial steady state, we have the following:

$$\mathcal{J}(1, 0, 1, 0) = \begin{pmatrix}
-\nu - \mu & -\beta - \nu & 0 & -\delta_{12} \\
0 & \beta - (\gamma + \mu) & 0 & \delta_{12} \\
0 & -\delta_{21} & -\nu - \mu & -\beta - \nu \\
0 & \delta_{21} & 0 & \beta - (\gamma + \mu)
\end{pmatrix}, \tag{4.27}$$

which has eigenvalues:

$$\begin{aligned}
\lambda_{1,2} &= -(\nu + \mu); \\
\lambda_{3,4} &= (\beta - \sigma) \pm \sqrt{\delta_{12}\delta_{21}},
\end{aligned}$$

where $\sigma := \gamma + \mu$. Therefore if $\beta > \sigma$, at least one of the eigenvalues is positive and the trivial equilibrium is unstable. If $\beta < \sigma$ and either of δ_{12} or δ_{21} are equal to zero, then all the eigenvalues are negative and the trivial equilibrium is stable. If both δ_{ij} are positive, then the following condition ensures that the trivial steady state is unstable:

$$\sqrt{\delta_{12}\delta_{21}} > \sigma - \beta. \tag{4.28}$$

In order to obtain the nontrivial equilbrium for this system, we shall consider the (I, R)

components of such an equilibrium. The equations are as follows

$$\begin{aligned}
\frac{\mathrm{d}I_1}{\mathrm{dt}} &= \beta_1 S_1 I_1 + \delta_{12} I_2 S_1 - (\gamma+\mu) I_1 \\
\frac{\mathrm{d}R_1}{\mathrm{dt}} &= \gamma I_1 - (\nu+\mu) R_1 \\
\frac{\mathrm{d}I_2}{\mathrm{dt}} &= \beta_2 S_2 I_2 + \delta_{21} I_1 S_2 - (\gamma+\mu) I_2 \\
\frac{\mathrm{d}R_2}{\mathrm{dt}} &= \gamma I_2 - (\nu+\mu) R_2,
\end{aligned} \tag{4.29}$$

from which it is easy to see that for each group

$$R_i^* = \frac{\gamma}{\nu+\mu} I^*, \quad i = 1, 2. \tag{4.30}$$

Thus I_1^* and I_2^* are the solutions of the equations

$$\begin{aligned}
g_1(I_1^*, I_2^*) &:= \beta(1 - (1 + \frac{\gamma}{\nu+\mu})I_1^*)I_1^* + \delta_{12}(1 - (1 + \frac{\gamma}{\nu+\mu})I_1^*)I_2^* - \sigma I_1^* = 0 \\
g_1(I_1^*, I_2^*) &:= \beta(1 - (1 + \frac{\gamma}{\nu+\mu})I_2^*)I_2^* + \delta_{21}(1 - (1 + \frac{\gamma}{\nu+\mu})I_2^*)I_1^* - \sigma I_2^* = 0,
\end{aligned} \tag{4.31}$$

namely the intersections of the two implicit curves $g_1(I_1, I_2) = 0$ and $g_2(I_1, I_2) = 0$. Figure 4-1 shows how this equilibrium varies with $\delta = \delta_{12} = \delta_{21}$. Meanwhile the Jacobian of (4.29) is

$$\mathcal{J} = \begin{pmatrix}
\beta(1 - I_1 - I_2) - \beta I_1 - \delta_{12} I_2 - \sigma & -\beta I_1 - \delta_{12} I_2 & \delta_{12}(1 - I_1 - R_1) & 0 \\
\gamma & \nu + \mu & 0 & 0 \\
\delta_{21}(1 - I_2 - R_2) & 0 & \beta(1 - I_2 - R_2) - \beta I_2 - \delta_{21} I_1 - \sigma & -\beta I_2 - \delta_{21} I_1 \\
0 & 0 & \gamma & \nu + \mu
\end{pmatrix}. \tag{4.32}$$

Figure 4-2 shows numerical results for how the eigenvalues of the Jacobian evaluated at the nontrivial equilibrium change as δ is increased. As we see, for all δ the eigenvalues are negative and the equilibrium is stable.

4.3 A pairwise equation model

We now propose a pairwise equation model that will allow for the incorporation of network structure using ordinary differential equations that describe how the states of edges in the network change with time.

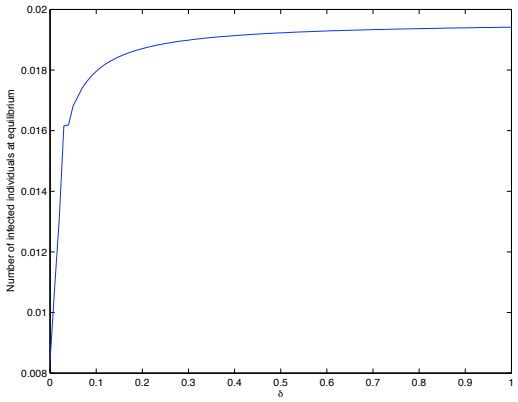

Figure 4-1: *The equilibrium of (4.29) as found from (4.31). Parameters used:* $\beta = 0.02$, $\gamma = 0.01$, $\mu = \nu = 10^{-4}$.

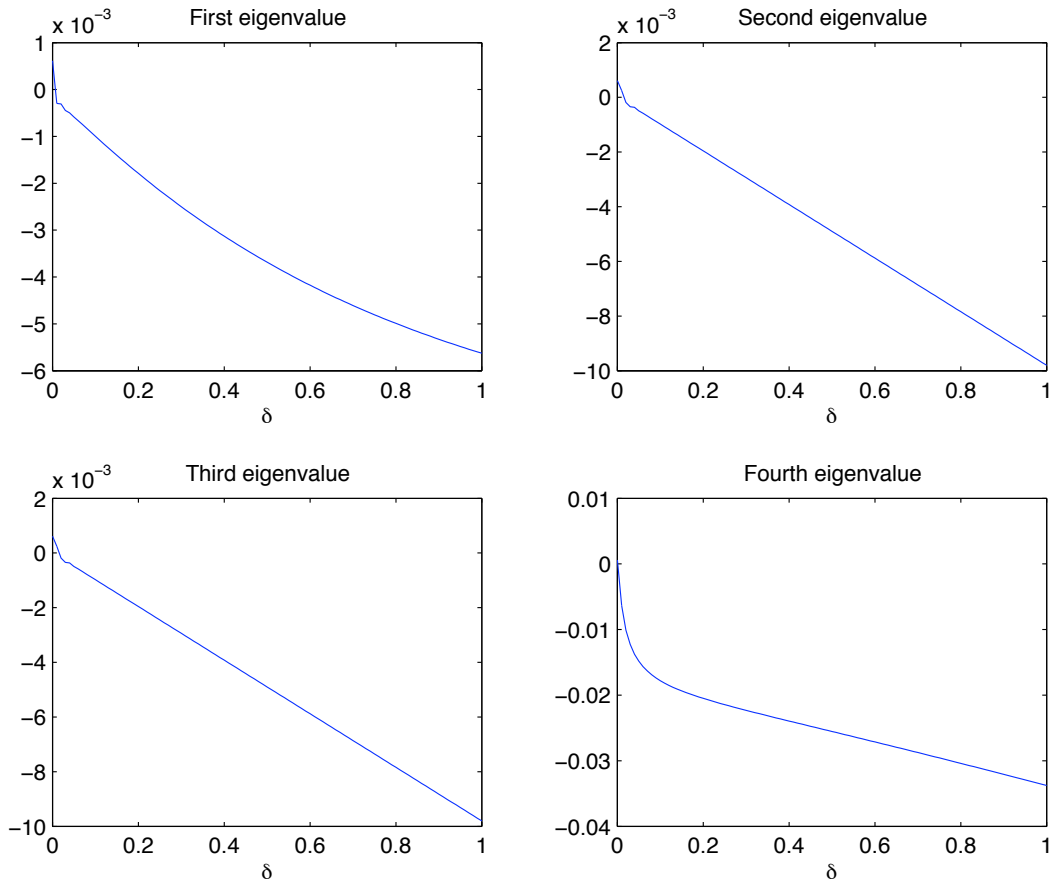

Figure 4-2: *Eigenvalues of the Jacobian (4.32) evaluated at the nontrivial equilibrium for increasing values of* δ. *Parameters used:* $\beta = 0.02$, $\gamma = 0.01$, $\mu = \nu = 10^{-4}$.

4.3.1 Model Formulation

We consider k groups, in which the number of individuals in state A in group i is denoted by $[A]_i$. Similarly, the number of edges involving connected individuals in states A and B in group i is denoted by $[AB]_i$, and the notation $[ABC]_i$ represents a similar construction for triples.

The contact structure of group i can be described by the following parameters: N_i, the number of individuals in the group; z_i, the number of neighbours of each member of the group; and ϕ_i, the clustering coefficient of each group. As with the mean field model, there is scope for epidemiological differences between the groups: τ_i is the rate at which infection is spread across pairs involving a susceptible and an infective within the group i; γ_i is the rate at which individuals within group i recover; and ν_i is the rate at which immunity is lost by immune individuals in group i.

As can be inferred from the notation, we do not explicitly model connections between individuals in different groups, so that quantities such as $[A_iB_j]$ are not considered. The influence of other groups $j \neq i$ on group i is instead given by an external influence function, naturally extending both the mean field model discussed above and the inclusion of external infection into the pairwise equation framework, as described in the previous chapter. Aside from the internal infection dynamics within each group, all pairs involving a susceptible can become infective due to contact with another group at the following rate:

$$\sum_{j \neq i} \delta_{ij} f_{ij}([I]_j) \tag{4.33}$$

where the constant parameters $\delta_{ij} \geq 0$ describe the maximum level of influence of group j on group i and qualitatively describe the relationships between groups. This enforces the restriction $\sum_j \delta_{ij} \leq 1$. The function f_{ij} describes in more detail how the level of infection in group j affects the number of susceptibles in group i becoming spontaneously infected. We impose the following conditions on f_{ij}:

(i) $f_{ij}(0) = 0$;

(ii) $f_{ij}([I]_j) \in [0, N_i] \quad \text{for all } 0 \leq [I]_j \leq N_j, \quad j = 1 \ldots k.$

As in prior pairwise equation models, the number of infectives at any given time is constructed from the number of pairs containing an infective, as in equation (2.4).

We have the following set of equations for the spread of a infection following a SIRS

model, within group i:

$$\begin{aligned}
[\dot{SS}]_i =& -2\tau_i[SSI]_i - 2\sum_{j\neq i}\delta_{ij}f_{ij}([I]_j)[SS]_i + 2\nu_i[SR]_i \\
[\dot{SI}]_i =& \tau_i[SSI]_i + \sum_{j\neq i}\delta_{ij}f_{ij}([I]_j)[SS]_i - \tau_i[ISI]_i - (\tau_i+\gamma_i)[SI]_i \\
& - \sum_{j\neq i}\delta_{ij}f_{ij}([I]_j)[SI]_i + \nu_i[IR]_i \\
[\dot{SR}]_i =& \gamma_i[SI]_i - \sum_{j\neq i}\delta_{ij}f_{ij}([I]_j)[SR]_i - \tau_i[ISR]_+\nu_i[RR]_i \\
[\dot{II}]_i =& 2\tau_i[SI] + 2\tau_i[ISI]_i + 2\sum_{j\neq i}\delta_{ij}f_{ij}([I]_j)[SI]_i - 2\gamma_i[II]_i \\
[\dot{IR}]_i =& \sum_{j\neq i}\delta_{ij}f_{ij}([I]_j)[SR]_i + \tau_i[ISR]_i + \gamma_i[II]_i - (\gamma_i+\nu_i)[IR]_i \\
[\dot{RR}]_i =& 2\gamma_i[IR]_i - 2\nu_i[RR]_i
\end{aligned} \tag{4.34}$$

where triples such as $[SSI]_i$ are to be approximated in terms of pairs.

Since we do not physically model the interactions between subgroups, we can approximate triples using the following formulation that assumes all nodes of a triple reside in the same group:

$$[SSI]_i \approx \xi_i \frac{[SS]_i[SI]_i}{[S]_i}((1-\phi_i)+\phi_i\mathcal{C}^i_{SI}), \tag{4.35}$$

where $\xi_i = \frac{(z_i-1)}{z_i}$ and $\mathcal{C}^i_{SI}$ is the notationally challenged susceptible infective correlation for the i^{th} group, defined entirely analogously to (2.12), using the appropriate subscripts.

This formulation for the triples demonstrates the advantage of not physically modelling the interactions between the groups, in that we do not have to worry about whether a triple comprises three nodes from the same group, or comprises two from one group and one from another. At the same time, the parameters δ_{ij} and the functions f_{ij} give a reasonable mechanism for how the groups interact. Moreover, the formulation of the equations themselves, together with the parameters z_i and ϕ_i, lead to a model that describes the interaction of multiple groups and allows for the structure of those groups to influence the interactions. Later on in this Chapter and in Chapter 6, we will use computer simulations to further investigate whether the physical connection between groups are accurately described by parameters such as δ_{ij}.

4.3.2 Results of numerical solutions

SIRS model We consider the effects of the structural parameters on the final infected equilibrium for a pairwise SIRS model on a population comprised of two subgroups. We first examine the effect of interactions between groups and then effects of structure within the subgroups on the outcome of the disease. Throughout we assume that $f_{ij}([I]_j) = [I]_j$.

Figure 4-3 shows the effect of varying the two interaction strengths δ_{12}, the effect of group two on group one, and δ_{21}, the effect of group one on group two. The remaining parameters are the same for each group, with the same initial conditions in each of the groups. The proportion infected at equilibrium in each group is plotted for particular values of δ_{12} and δ_{21}. The plots for each group reflect that if the values of δ_{12} and δ_{12} are exchanged, then the outcomes for each group are also exchanged. As a consequence of this symmetry, we need only discuss the outcomes for the first group.

For the first group, if $\delta_{12} = 0$ then there is no input into group one from group two. As a result the equilibrium value remains constant for all values of δ_{21}. For fixed δ_{21}, the level of infection in group one increases with δ_{12}, as we have seen for a single group in Figure 3-11. Furthermore, for a fixed non-zero value of δ_{12}, the infected equilibrium also increases with δ_{21} due to positive feedback - the increased effect of group one on group two leading to a larger effect of group two on group one.

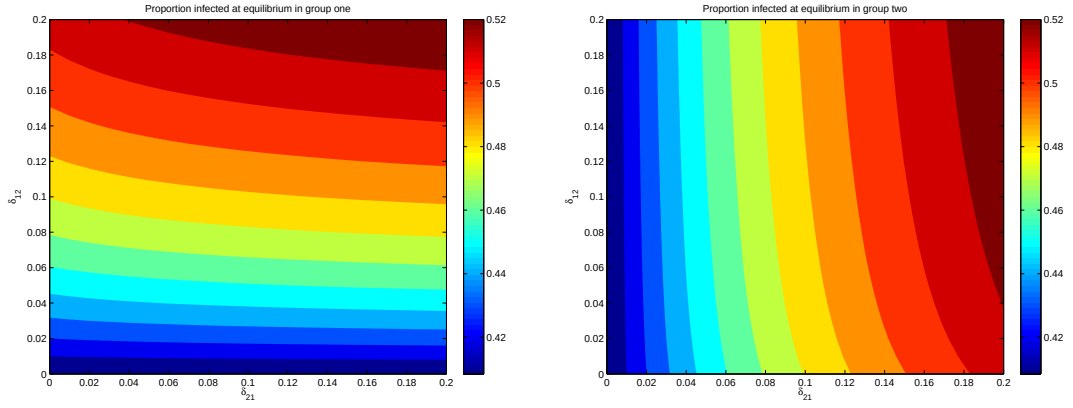

Figure 4-3: *The pairwise equations (4.34) are solved numerically for two groups, with* $N_i = 10000$, $z_i = 6$, $\phi_i = 0$, $\tau_i = 0.05$, $\gamma_i = 0.1$, $\nu = 0.01$, $i = 1, 2$. *The two interaction strengths* δ_{12} *and* δ_{21} *are varied between 0 and 0.2, and the proportion infected at equilibrium is plotted against these* δ *values.*

On examining the impact of structural features of the subgroups, we notice similar effects. Figures 4-4 and 4-5 respectively examine the impact of clustering ϕ_i and average

neighbourhood size z_i on the proportion infected at equilibrium. We consider two cases: one of symmetric influence, choosing equal values of δ_{12} and δ_{21}; and another where the influence exerted between groups is stronger in one direction than the other.

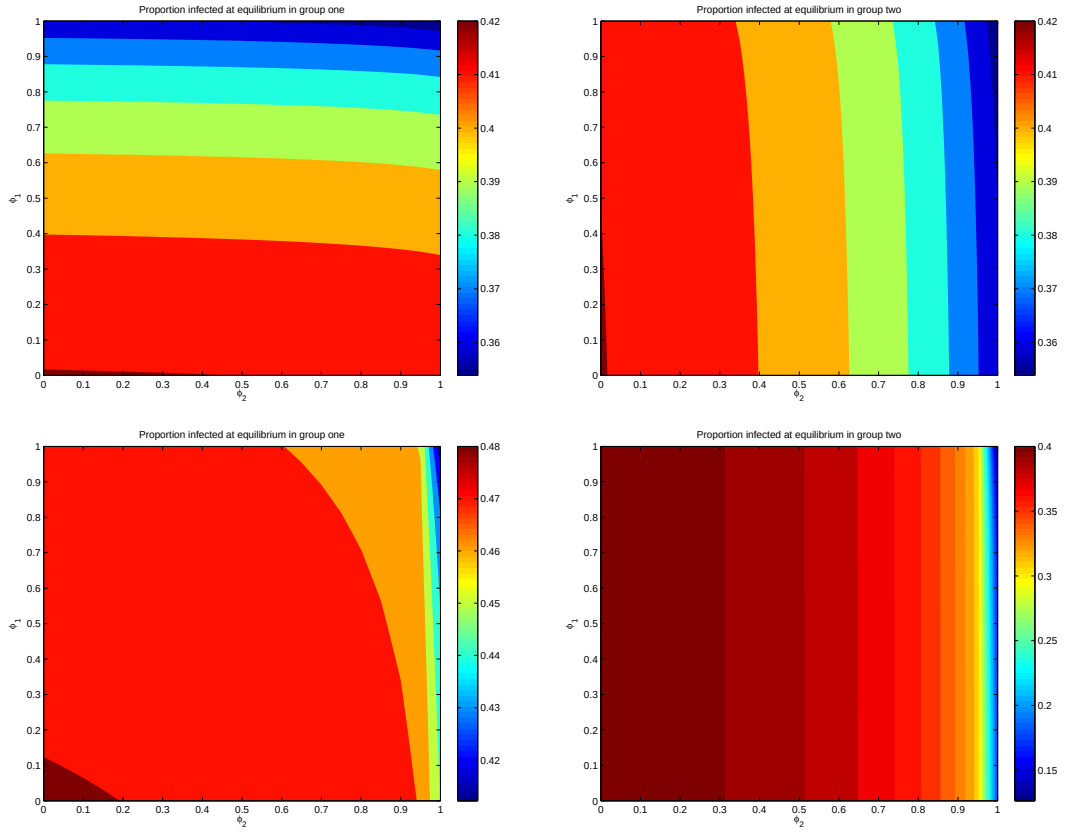

Figure 4-4: *The pairwise equations (4.34) are solved numerically for two groups, with* $N_i = 10000$, $z_i = 6$, $\tau_i = 0.05$, $\gamma_i = 0.1$, $\nu = 0.01$, $i = 1, 2$. *The clustering coefficient* ϕ_i *of each group is varied between 0 and 1, and the proportion infected at equilibrium is plotted for each combination of these values. The upper two figures are for the symmetric case with* $\delta_{12} = \delta_{21} = 0.01$ *and the lower two figures are for the asymmetric case in which* $\delta_{12} = 0.01$ *and* $\delta_{21} = 0.001$.

In the symmetric case, we only have to consider the case of group one. If the clustering coefficient ϕ_1 of group one is increased, the proportion infected at equilibrium will decrease as in Figure 3-9 for the single group. Furthermore, the effect of increasing ϕ_1 also decreases the effect of the first group upon the second. This explains why, for fixed values of ϕ_1, increasing ϕ_2 reduces the proportion infected at equilibrium.

In the asymmetric case, we have $\delta_{12} > \delta_{21}$ and the effect of group two on group one being greater than that of group one on group two. In fact changing the clustering coefficient of the first group has no impact upon the proportion infected at equilibrium

in the second group in this case. However in the first group, the effects of varying either parameter ϕ_1 or ϕ_2 has little effect on the size of the infected equilibrium.

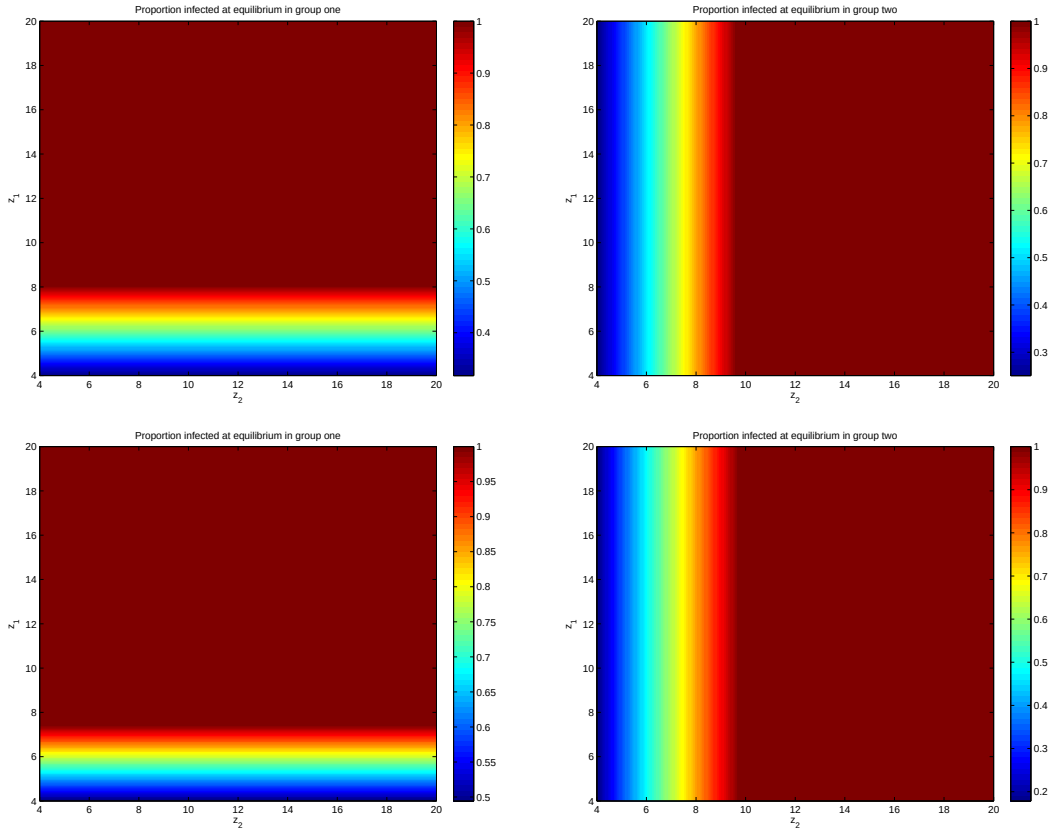

Figure 4-5: *The pairwise equations (4.34) are solved numerically for two groups, with* $N_i = 10000$, $z_i = 6$, $\tau_i = 0.05$, $\gamma_i = 0.1$, $\nu = 0.01$, $i = 1, 2$. *The neighbourhood size* z_i *of each group is varied, and the proportion infected at equilibrium is plotted for each combination of these values. The upper two figures are for the symmetric case with* $\delta_{12} = \delta_{21} = 0.01$ *and the lower two figures are for the asymmetric case in which* $\delta_{12} = 0.01$ *and* $\delta_{21} = 0.001$.

The situation is similar in Figure 4-5, where z_i the average number of neighbours per site is varied for each group. However, the size of the infected equilibrium in one group is independent of the neighbourhood size of the other. The difference between cases of symmetric and asymmetric influences is that for group one the equilibrium takes a smaller range of values and for group two a larger of range of values in the asymmetric case. This is another demonstration of how greater influence between groups can lead to homogenisation of outcomes with respect to parameters that describe internal features of subgroups.

SIR model Setting $\nu = 0$, we have an SIR model which will produce a single large epidemic. We investigate the effect of altering the interaction strength between groups on the spread of infection. We see a peak in infection for each group as demonstrated in Figure 4-6a. Provided there is sufficient connection between the groups and that R_0 for each group exceeds one, an outbreak will occur in each group. In Figure 4-6b we plot the time to the peak of infection in the first for various values of the interaction parameters, which demonstrates the feedback effect of both δ_{12} and δ_{21} being positive. If $\delta_{12} = 0$, that is, if the second group has no effect on the first, then increasing δ_{21} has no influence on the time taken for the epidemic in the first group to reach its peak. Obviously as δ_{21} is increased, the additional infection from the second group reduces the time taken to reach this peak. If we fix a positive value of δ_{21}, then increasing δ_{12} also decreases the time to reach the peak, since more infectives in group two produce more spontaneous infections in the first group.

Figure 4-6c shows the difference in time between the peaks of infection in each group (4-6d shows that the first peak is in group one if $\delta_{12} > \delta_{21}$ and vice versa, with coincidence if $\delta_{12} = \delta_{21}$. If we follow lines such as $\delta_{21} = 2\delta_{12}$ we see that the difference between peaks decreases as the extent of the interaction between groups increases, even if the relationship between δ_{12} and δ_{21} remains the same.

4.4 Simulating interactions between groups

In this section we use computer simulations to address the following issues:

(i) How reasonable is it to abandon the links between groups and replace them with parameters representing the influence of groups upon one another?

(ii) How do groups of more heterogeneous populations interact with one another in this setting?

Computer simulations facilitate the consideration of large scale systems with full contact structures in place, so that diseases can be simulated upon networks obtained from real world data or a random realisation of a member of an ensemble of graphs, perhaps representing a model of social network formation.

Whilst data acquisition may focus upon a particular demographic (or be biased towards one), in the case of a large data set of a random population community seeking algorithms may be run and groups may be isolated within the population - or the data maybe be sufficiently labelled for a natural subdivision of the network into subpopulations to take place. In either case, what results is a network comprised of k

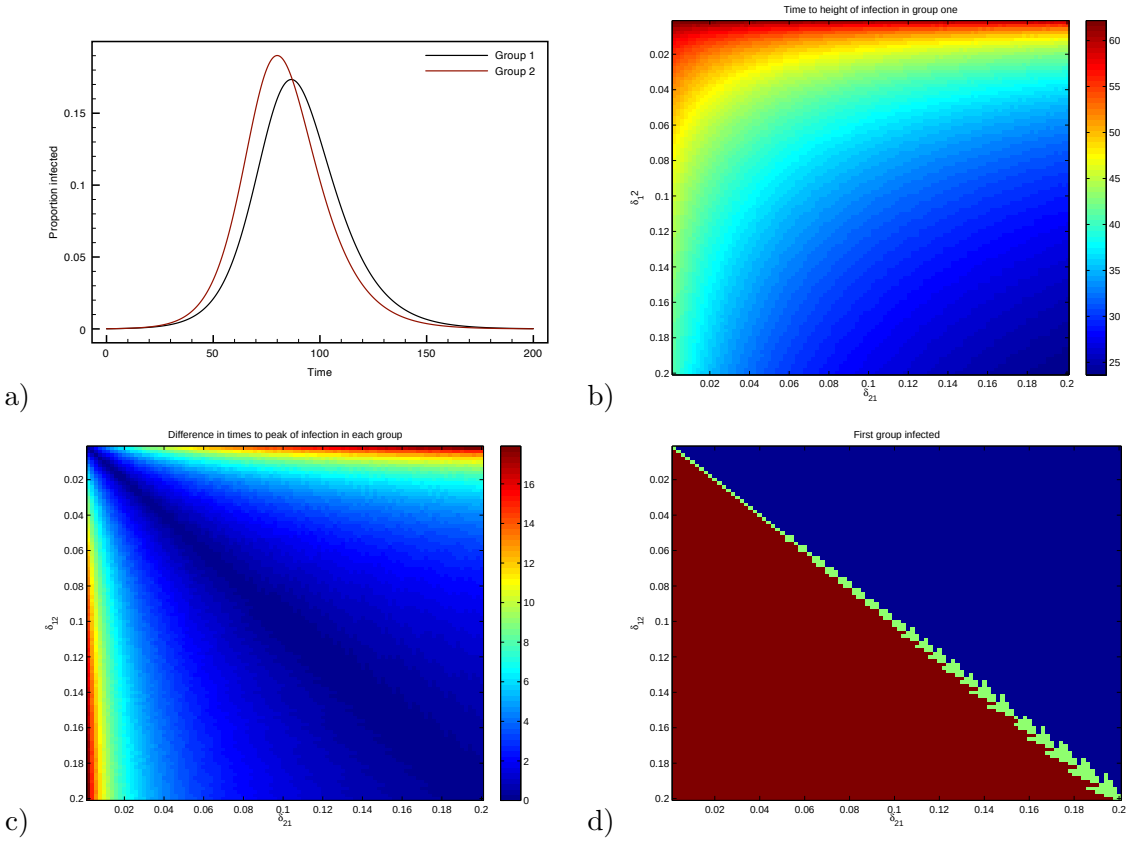

Figure 4-6: *The pairwise equations (4.34) are solved numerically for two groups, with* $N_i = 10000$, $\phi_i = 0$, $z_i = 6$, $\tau_i = 0.05$, $\gamma_i = 0.1$, $\nu_i = 0$, $i = 1, 2$. *a) The epidemic curves for each group are plotted for the values* $\delta_{12} = 10^{-4}$ *and* $\delta_{21} = 10^{-2}$. *b) As* δ_{12} *and* δ_{21} *are varied, we plot the time of the epidemic peak in group one. c) The difference in time between the peaks of the epidemics in each group as* δ_{12} *and* δ_{21} *are varied. d) In the red region the epidemic peaks first in group one and in the blue region, the epidemic peaks first in the second group.*

subpopulations. The edges between nodes in this network are either internal to a subgroup, where the nodes on each end of a link are in the same group, or they are bridges between groups when the two nodes comprising the edge are in different subpopulations.

For the mathematical models of this chapter, we have ignored the bridging links, using the parameters δ_{ij} and the functions f_{ij} to describe them implicitly. This is done in order to simplify the model, which would have been greatly complicated by considerations of triples that included bridges, not to mention the additional variables required to describe such quantities.

Simulations, however, afford us the opportunity to run realisations of full disease process and capture the local effects of having the possibility of spreading the disease

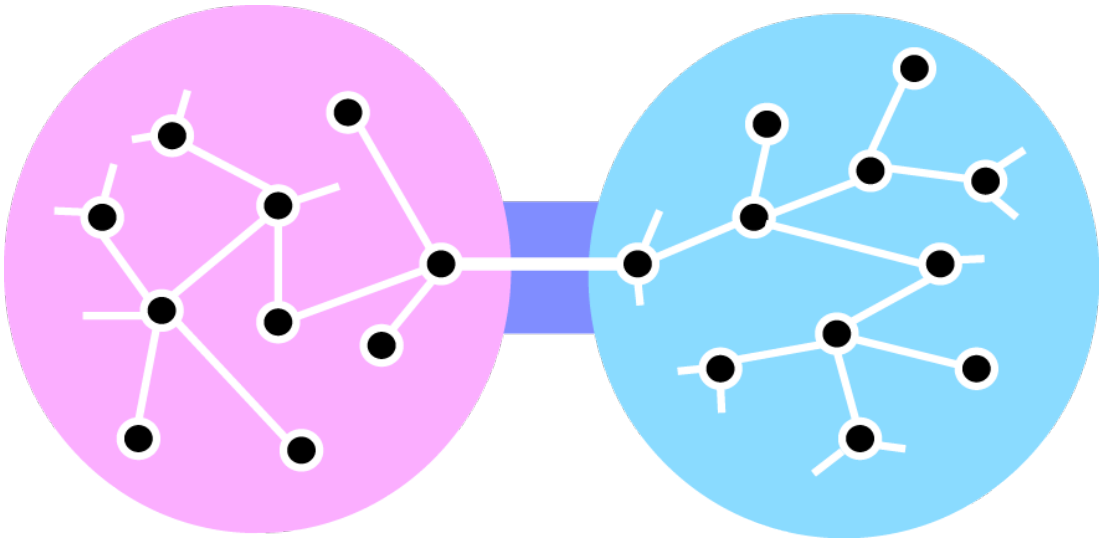

Figure 4-7: *Example of a bridging link between two subgroups.*

between different subpopulations confined to specific bridging links between particular individuals.

Furthermore, we can test how good an approximation of the full network is given to us by modelling the connections between subgroups in this implicit fashion. Since δ_{ij} represents the proportion of susceptibles spontaneously infected in group i when group j is fully infected, this gives us a crude relationship between δ_{ij} and the number of physical connection in the full network between groups i and j. For example, if group j consists of 1000 nodes and there are 10 connections between group j and group i, we can choose $\delta_{ij} = 0.01$.

For both experiments, we produced a network comprised of two groups, where either both of the groups were a hexagonal lattice, or both were scale-free networks chosen so that the average degree is the same as that of said lattice. In each case, one group had 1% of nodes infected ab initio, while the second remained infection free. We then ran simulations of an SIRS process multiple times on the composite network, modelling the interaction between the groups in the two ways detailed above.

The upper two subfigures of Figure 4-8 show the effects of increasing the number of physical links between the two groups, while the lower subfigures show the effect of increasing the parameter designed to replicate the addition of links. In each case, we show the number of infected individuals after 500 time steps in the initially infection-free second group. This is a steady state for each simulation. We see that when the groups are isolated, no infection occurs within the second group. However, when the

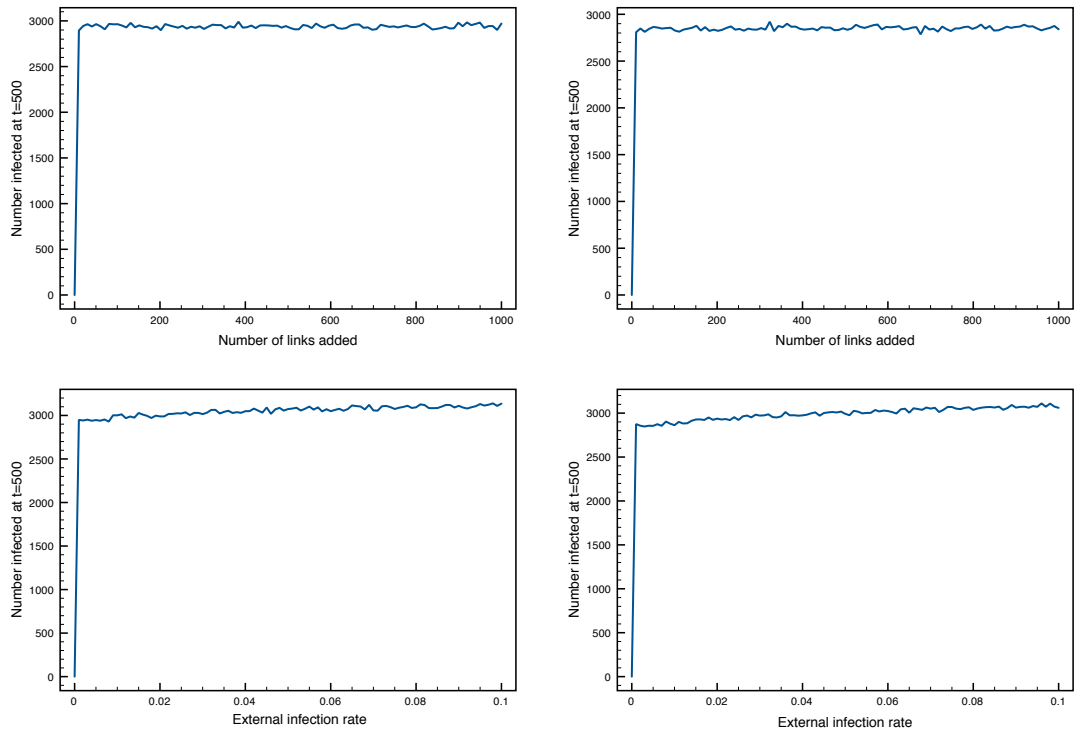

Figure 4-8: *The number of infectives at 500 time steps for different levels of physical (top) or parameter-based (bottom) interaction between two groups of hexagonal lattices (left) or scale-free networks (right). Each plot is for the second group, which is wholly susceptible at the start of each simulation. The subgroups consist of 10000 nodes each and the scale-free networks are chosen to have average degree $z = 6$. The epidemiological parameters were $\tau = 0.05$, $\gamma = 0.02$ and $\nu = 0.01$. Results are the average of ten repetitions.*

groups are connected by either means, the outcome is a large number of infections maintained within the second group. We note that whilst this equilibrium remains approximately constant as additional physical links are added, the effect of increasing the equivalent parameter has a more incremental effect on equilibrium size.

The physical links between the two subgroups are placed at random and so the effect of adding them is not necessarily incremental, particularly for small numbers. The spatial effects of the spreading process - particularly on the lattice (see Figure 2-4) - means that not all new links will confer the means for improved spread of infection. However, every increase of the parameter δ does increase the possibility of intra-group infection because each individual in the network has the possibility of being infected externally.

However, despite the similarity in equilibrium values throughout these experiments, the differences come to light when the arrival at equilibrium is examined. Figure 4-9 shows

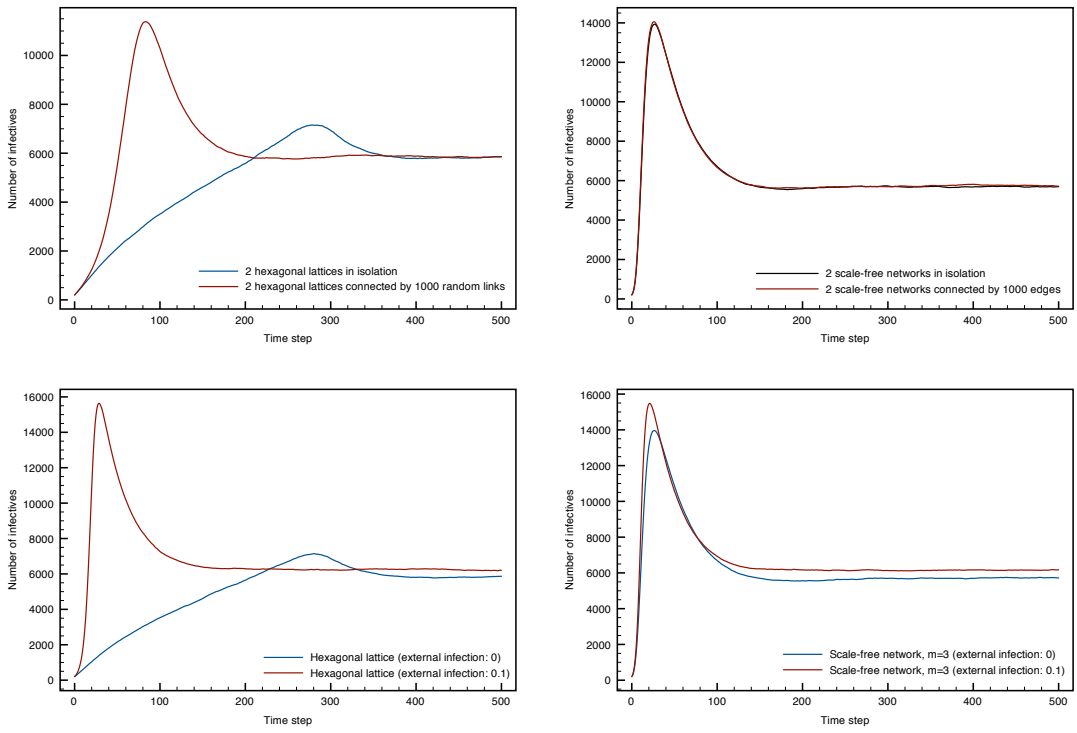

Figure 4-9: *The number of infectives versus time step for different levels of physical (top) or parameter-based (bottom) interaction between two groups of hexagonal lattices (left) or scale-free networks (right). Each plot is for the whole population, of which 1% is infected at the start of each simulation. The subgroups consist of 10000 nodes each and the scale-free networks are chosen to have average degree* $z = 6$*. The epidemiogical parameters were* $\tau = 0.05$*,* $\gamma = 0.02$ *and* $\nu = 0.01$*. Results are the average of ten repetitions.*

the infection profile versus time step for the extremal values in each of the four cases presented in Figure 4-8. For this experiment, each group has 1% of nodes initially infected. We see that the situation is different in respect to topology, but broadly similar when comparing the effect of physical intra-group links and the parameter based interaction.

For the composite network consisting of two hexagonal lattices, the figures demonstrate how (as previously discussed) the slow spatial spreading process of the disease across the lattice is accelerated by both the addition of extra links between the groups, and the parameter δ being increased. This results in a larger peak occurring earlier in time and settling down into an equilibrium faster than without interaction between the groups. The peak is sharper and occurs earlier for the parameter-based interaction, since, as previously discussed, not all of the random links added between the groups in

the physical process may be advantageous to the spreading process.

For the composite of two scale-free networks, the profiles shown in Figure 4-9 are almost identical, which is due to the dominance of the hubs in determining the outcome of the disease. Local to each node, the addition of random links does not change the overall structure a great deal - a hub is still a hub and a node of low degree is still likely to be connected to a hub - so the infection proceeds almost identically as in the case of two isolated groups.

The parameter-based interaction adds its own effects, as in the case of the network composed of hexagonal lattices. For $\delta > 0$, the number of infectives at equilibrium in isolation (the case $\delta = 0$) is augmented by the infectives generated by the external infection process, which is proportional to δ. The time profile of the spread of infection shows greater similarity than in the case of the lattice, indicating that, as with the physical links, the role of network structure in each of the groups is playing a greater role in determining the outcome of infection than the interaction between groups.

From these experiments we can draw the conclusion that modelling the interaction using the parameter δ may overestimate the effects of adding random links, and that the effect of groups upon one another may be less pronounced for more heterogeneous networks.

4.5 Discussion

In this chapter we have considered the case of multiple groups representing particular sectors of population, their interaction, and the spread of disease upon them. Using a mean field model as a platform, we have also incorporated the contact structure of each group into models. Finally a comparison was made with simulations, which allows for both the evaluation of the mathematical models presented and for expansion into contact structures that are more problematic to incorporate within said mathematical models.

Our mean field model was a straightforward expansion of the model for a single group (3.1) presented in Chapter 3. The external infection function for each group is recast to allow the infection state of other groups to influence the state of infection for that group. Our results focus on two groups, in which the external function is given a linear form.

For the SIS model, we find that if a positive equilibrium exists then it is globally asymptotically stable. We show numerically the effect of increasing the external infection on

the size of the equilibrium.

For the SIRS model, we show that for $\beta < \gamma$, parameter values which would usually render the disease free equilibrium stable, the introduction of mutual external influence above the threshold (4.28) changes the stability of this equilibrium, creating a saddle. As a result, if the two groups mutually influence each other, that is if δ_{12} and δ_{21} are both positive, the disease will persist if a small perturbation is made from the disease free state. We also showed the stability of the nontrivial steady state by calculating numerically the eigenvalues of the Jacobian for the system.

By formulating a similar system in terms of pairwise equations, the contact structure within the groups is emulated. Each group can be characterised by its size N_i, the average number of neighbours per site z_i and the degree to which those neighbourhoods of each site are interconnected, given by the clustering coefficient ϕ_i.

For the SIRS model, we investigate the effect on the level of infection at equilibrium that arises from varying the influences δ_{12} and δ_{21}, the clustering coefficient ϕ_i and the neighbourhood size z_i. We find a positive feedback occurs through the connection for the influences δ_{ij}, which is replicated for the clustering coefficient in the sense that if the value of ϕ_i is decreased for each group, the infection level increases more than either of the single directions. We show that this effect can disappear if the interaction between groups is sufficiently asymmetric. For neighbourhood size z_i, there is no positive feedback effect, in the sense that increasing the neighbourhood size of the second group z_2 has no effect on the number infected at equilibrium in the first group. The effects of increasing neighbourhood size are not transmitted through the connection between groups.

For the SIR model, we have an epidemic occurring in each group and it concerns us to know whether, for identical groups, the infection will be larger and quicker in a given group for varying values of the interaction parameters δ_{ij}. We find that this is indeed the case and that there is a similar feedback effect, so that it is the strength of both interactions and the difference between them that determine infection outcomes.

We then proceeded to computer simulations, concerning ourselves with two aspects, that of the nature of the interaction between groups, and that of contact structure beyond the scope of the parameters of the pairwise equations. It is found that the parameter δ may overestimate the effect of linkages between groups if the links between groups are random. We find that for more heterogeneous structures, the addition of random links has little impact on the outcome of infection profile. This is because random links do not alter the local structure as profoundly as in the case of homogeneous network such as a lattice.

As more of the contact structure of the subgroups that comprise the population are included within a mathematical model, the greater the complexity of the model and the greater the computational power required to solve it or to perform analogous simulations. In the following chapters, we shall seek to derive a simpler mathematical model that describes the spread of infection on particular contact structures, obtained from numerical simulations. We shall also attempt to estimate a nonlinear form for the external infection function f.

Part II

Simplifying contact structure

Chapter 5

Nonlinear Incidence Models

5.1 Motivation and Background

5.1.1 Chapter Outline

In this chapter we present a connection between the spread of disease on discrete network structures and a mathematical model that features a nonlinear incidence term. Being observed from simulations, this connection is empirical; however, it is certainly possible to identify potential avenues for the establishment of a true theoretical connection. These arguments are put forward in the discussion and in Chapter 8.

We begin by reviewing the use of nonlinear incidence models of this nature throughout the literature, pointing out the observations that have been made concerning how these mechanisms might arise. We pay close attention to the model presented by Liu, Hethcote and Levin [31] and exhibit the consequences of the nonlinear incidence term for the long term dynamics of a disease.

The connection between network structure and nonlinear incidence is then established by estimating the parameters of nonlinear incidence models from computer simulations. This is done with the aim of incorporating contact structure into mathematical models in subsequent chapters.

5.1.2 Motivation

In previous chapters we have sought to incorporate contact structure into mathematical models for the spread of disease using the technique of pairwise equations. This is a direct technique, which works well for homogeneous structures such as the lattice.

However, when faced with a heterogeneous degree distribution or a dense degree-degree matrix, this technique produces large systems of ordinary differential equations, which require large computational resources in order to solve them, as seen in Chapter 2. Furthermore, scaling up the number of disease states increases the number of pair types dramatically, as does subdividing the population into smaller groups and producing multi-group pairwise equation models, as seen in Chapter 4.

Faced with problems such as these, we can revert to performing computer simulations of these processes. This is not necessarily the ideal solution, since these simulations will require multiple realisations to average out stochastic fluctuations. Therefore exploring the effect of varying parameters of interest within a model may also take too much time and computational resources.

This chapter aims for a compromise between mathematical modelling and computer simulation. By using the data generated by computer simulations to estimate the parameters of the nonlinear incidence models discussed here, we hope to establish a connection between the contact structure and the values of the parameters. Since the use of nonlinear incidence has proved controversial due to the lack of a mechanistic derivation, we hope that this work will also present a case for the use of nonlinear incidence in future models of disease spread.

5.1.3 Background Reading

Introducing nonlinear incidence The traditional epidemic model, in the lineage of Kermack and McKendrick (examples of which are discussed in [16], [35] and [2] among others), makes the assumption that infectives mix freely among susceptibles according to the law of mass action, meaning that the force of infection is linearly proportional to the infected population:

$$g(I) = \beta I \tag{5.1}$$

where β is a parameter that captures epidemiological and sociological information about transmission such as the average number of contacts per individual and the probability of the transmission of infection from one infective to one susceptible.

Severo in [42] was among the first to generalise the force of infection, considering a stochastic model in which the probability of producing a new infective in a given time interval of width Δt was given by:

$$\beta I^a S^{1-b} \Delta t \tag{5.2}$$

together with a removal rate that scales to a power of the number of individuals infected: γI^{1+c}. Solutions are presented for a simple epidemic with $\gamma = 0$ and a general epidemic with $\gamma \neq 0$. However, the outcomes of solutions for different values of the parameters are not discussed. Nevertheless, some consideration is given to the motivation for each of the exponents. The parameters $a > 0$, $0 < b < 1$ and $c > 0$ are respectively referred to as the infection power, the safety-in-numbers power and the removal power. For a slow spreading epidemic, the rate of infection may be considered independent of the number of infected individuals, and so a value of the infection power a close to zero could be considered. Likewise, for a faster moving epidemic, if a k-fold increase in the number of infected individuals results in many more than k times the number of subsequent infections, a value of a greater than one could be considered.

Severo also argues that the exponent of S can represent the effect of an increased number of susceptibles. For some diseases, an increased number of susceptibles results in a slower rate of infection, for example if infection depends on the concentration of some infective material. In this case, a value of b close to zero would be appropriate. However, in circumstances where the addition of susceptibles does not decrease the likelihood of infections, for example when safety in numbers is not present, a value of b close to one would render the infection virtually independent of the number of susceptibles. Further environmental or treatment effects can be reflected within the recovery exponent c.

An SIRS model featuring nonlinear incidence A system of ODEs with a nonlinear incidence rate similar to that of (5.2) is presented in [32]. The model is similar to that considered in Chapter 3, (3.1). In the notation of that chapter, the model given is:

$$\begin{aligned} \frac{\mathrm{d}S}{\mathrm{d}t} &= -\beta I^p S^q + \mu(N - S) + \nu R \\ \frac{\mathrm{d}I}{\mathrm{d}t} &= \beta I^p S^q - (\gamma + \mu) I \\ \frac{\mathrm{d}R}{\mathrm{d}t} &= \gamma I - (\nu + \mu) R, \end{aligned} \tag{5.3}$$

where the number of individuals N is considered to be constant, and p and q are positive.

Reducing to the two dimensional system

$$\begin{aligned} \frac{\mathrm{d}I}{\mathrm{d}t} &= \beta I^p (N - I - R)^q - (\gamma + \mu) I \\ \frac{\mathrm{d}R}{\mathrm{d}t} &= \gamma I - (\nu + \mu) R, \end{aligned} \tag{5.4}$$

we can set

$$a = \frac{\beta}{\mu+\gamma}, \quad r = \frac{\gamma}{\mu+\gamma}, \quad h = \frac{\gamma}{\mu+\nu}, \tag{5.5}$$

and rewrite (5.4) as the following system

$$\begin{aligned} \frac{\mathrm{d}I}{\mathrm{d}T} =& aI^p(N-I-R)^q - I \\ \frac{\mathrm{d}R}{\mathrm{d}T} =& r(I - \frac{R}{h}), \end{aligned} \tag{5.6}$$

so that with $T = (\mu+\gamma)t$, time has been rescaled so that the average duration of infection is one time unit. For this system, the trivial equilibrium $(I, R) = (0, 0)$ corresponding to a disease free steady state exists, alongside any solutions to

$$\begin{aligned} aI^{p-1}(N-I-R)^q &= 1 \\ R &= hI, \end{aligned} \tag{5.7}$$

which correspond to nontrivial equilibria. Hence we have

$$aI^{p-1}(N-(1+h)I)^q = 1.$$

Taking the qth root and letting $z = \frac{p-1}{q}$, we have

$$a^{\frac{1}{q}} I^z N = 1 + a^{\frac{1}{q}} I^z (1+h)I,$$

and multiplying by $a^{-\frac{1}{q}} I^{-z}$ gives

$$N = a^{-\frac{1}{q}} I^{-z} + (1+h)I.$$

Therefore, if we define

$$f(I) = a^{-\frac{1}{q}} I^{-z} + (1+h)I \tag{5.8}$$

then the positive roots I^* of

$$f(I^*) = N \tag{5.9}$$

will correspond to the nontrivial equilibria of (5.6). The number of roots of (5.9) depends on the exponent p. For $p < 1$, we have $z < 0$, which results in $f(I)$ being monotonically increasing. Since $f(0) = 0$ and $f(I) \to \infty$ as $I \to \infty$, we have that for some unique I^*, we solve (5.9). This ensures a unique nontrivial equilibrium when $p < 1$. For $p = 1$, we have $z = 0$. Again, f is monotonically increasing but with $f(0) = a^{-\frac{1}{q}}$, we now have have a threshold population size for the existence of the nontrivial equilibrium. If $N > a^{-\frac{1}{q}}$, then there is a unique nontrivial equilibrium,

otherwise, there is none.

For $z > 0$, corresponding to $p > 1$, we have that $f(I)$ tends to infinity as $I \to 0$ and as $I \to \infty$. Thus, if the minimum of f is greater than, equal to, or less than N, there will be, respectively, 0, 1 or 2 nontrivial equilibria.

Regarding stability in each of these cases, in the case of $p < 1$, the single nontrivial equilibrium is globally asymptotically stable. In the case of $p = 1$, the nontrivial equilibrium is globally asymptotically stable if it exists. For $p > 1$, we have either 0, 1 or 2 nontrivial equilibria. In the first situation, the trivial equilibrium is globally asymptotically stable. When there are two nontrivial equilibria, the equilibrium consisting of smaller (I, R) values is an unstable saddle and the larger equilibrium is a locally asymptotically stable node. In this situation, the trivial equilibrium is also locally asymptotically stable. If N is allowed to decrease starting from a value for which there are two equilibria, these will coalesce into one stable equilibrium. As p is increased, there are circumstances under which more complicated behaviour can occur, giving rise to stable periodic orbits. Figure 5-1 shows some trajectories of the solutions to (5.3) for some of these scenarios.

Liu, Levin and Isawa, [32], also briefly discuss other forms of nonlinear incidence, in particular that of

$$S^q g(I) \tag{5.10}$$

where $g(I)$ takes a more general form than I^p. One form posited is

$$g(I) = \frac{\beta I^{p-1}}{1 + mI^{p-1}}, \quad m > 0, p > 1. \tag{5.11}$$

The motivation for a nonlinear incidence of this form is that for large values of I, the incidence rate is approximately the mean-field form $(\beta/m)IS$, whereas for smaller values of I, we will have an approximation of the form I^p considered above.

For this form of nonlinear incidence, the analysis proceeds as above and it can be shown that there are either 0, 1 or 2 nontrivial equilibria.

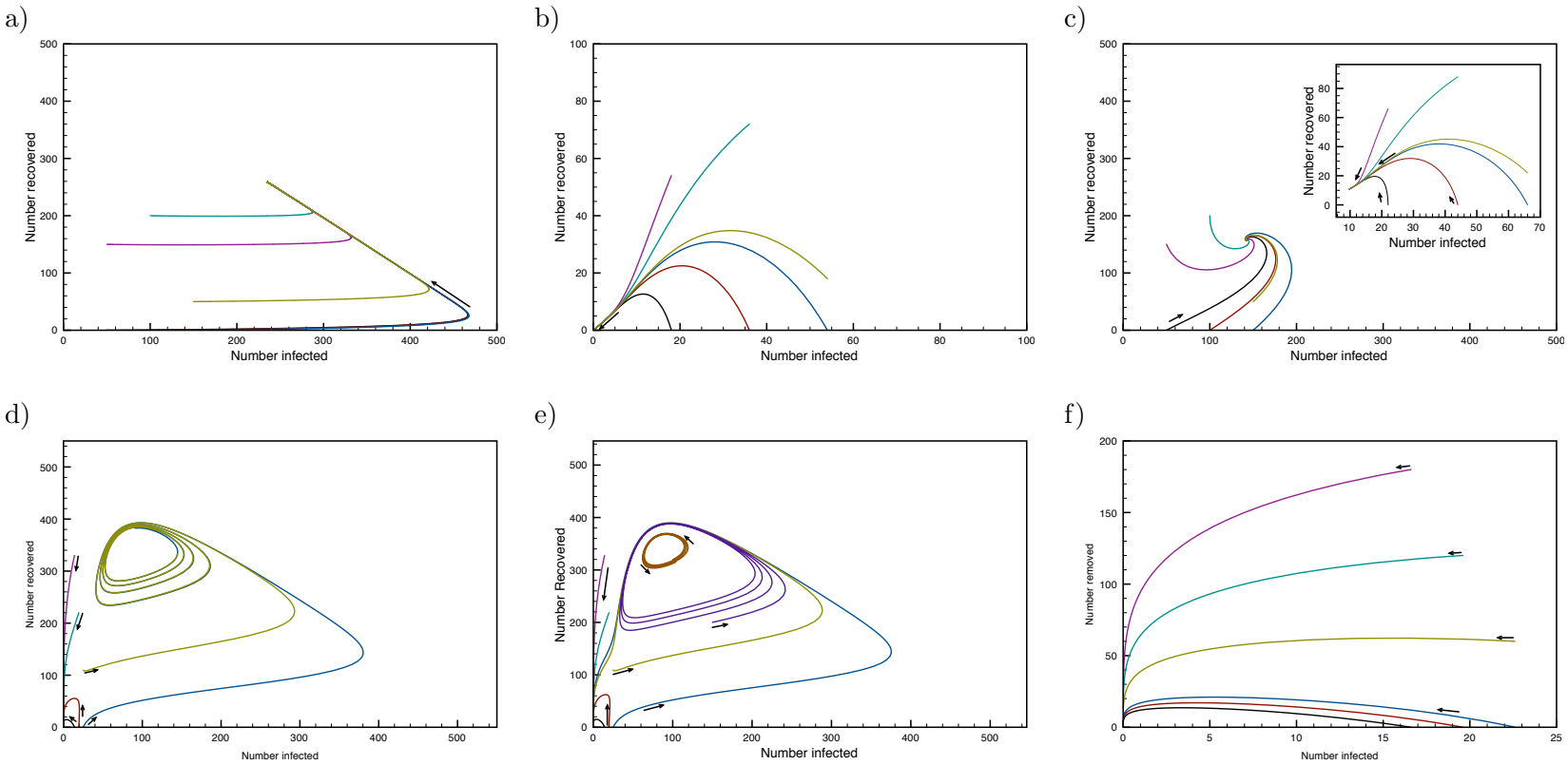

Figure 5-1: *Solutions of (5.3). a) A stable focus for* $p < 1$. *Parameters values:* $p = 0.8$; $a = 0.5$; $r = 0.997$; $h = 1.1$ *and* $N = 500$. *b) Globally stable trivial equilibrium for* $p = 1$ *and* $N < N^*$. *Parameter values:* $p = 1$; $a = 0.005$; $r = 0.997$; $h = 1.1$ *and* $N = 180$. *c) Globally stable nontrivial equilibrium for* $p = 1$ *and* $N = 500 > N^*$. *Inset figure is for* $N = 220$, *closer to the critical value* $N^* = 200$. *Parameter values as for b), aside from* N. *Parameters used for d)-f):* $a = 10^{-4}$; $r = 0.997$ *and* $h = 4$. *As* N *decreases, nontrivial equilibria are lost. d) Initially, a saddle separates the trivial equilibrium and a stable node for* $p = 2$ *and* $N = 550$. *e) As the nontrivial equilibria coalesce, for* $N = 546$ *we see periodic orbits. The trivial equilibrium attracts the remaining trajectories. f) For* $N = 300$, *there are no nontrivial equilibria and the disease free steady state is globally stable.*

An SEIRS model In [31], the model (5.3) is expanded to accommodate a class of individuals E, who are infected but not yet infectious. Individuals in this class graduate to the infectious state at a rate ϵ. As before the incidence rate is given by $\beta I^p S^q$. The model is:

$$\begin{aligned} \frac{\mathrm{d}S}{\mathrm{d}t} &= -\beta I^p S^q + \mu(1-S) + \nu R, \\ \frac{\mathrm{d}E}{\mathrm{d}t} &= \beta I^p S^q - (\epsilon+\mu)E, \\ \frac{\mathrm{d}I}{\mathrm{d}t} &= \epsilon E - (\gamma+\mu)I, \\ \frac{\mathrm{d}R}{\mathrm{d}t} &= \gamma I - (\nu+\mu)R, \\ S+E+I+R &= 1. \end{aligned} \tag{5.12}$$

The compartments are scaled so that they represent the proportion of individuals in a given state. As a result, the existence and number of nontrivial equilibria now depend on parameter values rather than the population size N. The nontrivial equilibria satisfy:

$$E^* = \frac{\gamma+\mu}{\epsilon} I^*, \quad R^* = \frac{\gamma}{\nu+\mu} \tag{5.13}$$

and

$$\beta (I^*)^p (1-E^*-I^*-R^*)^q = (\epsilon+\mu)E^*. \tag{5.14}$$

Therefore, the number of nontrivial equilibria depend on the roots of the equation

$$f(I) = \frac{1}{\sigma} \tag{5.15}$$

where

$$f(I) = I^{p-1}\left(1 - \frac{I}{H}\right) \tag{5.16}$$

with

$$H = \frac{\epsilon(\nu+\mu)}{\gamma\epsilon + (\nu+\mu)(\epsilon+\gamma+\mu)} \quad \text{and} \quad \sigma = \frac{\beta\epsilon}{(\epsilon+\mu)(\gamma+\mu)}. \tag{5.17}$$

Here H represents the maximum possible value of I^* and σ is the basic reproductive ratio R_0. In this instance, we persist with the notation of [31].

The classification of nontrivial equilibria proceeds as for the SIRS case: for $p < 1$ there is a single nontrivial equilibrium that is stable; for $p = 1$ and $\sigma \geq 1$ there is a single, stable nontrivial equilibrium, with only a globally stable trivial equilibrium for $\sigma < 1$; and for $p > 1$, there can be either 0, 1 or 2 nontrivial equilibria depending on the value of p and the size of σ.

The behaviour of nontrivial equilibria is shown in Figure 5-2, which is reproduced

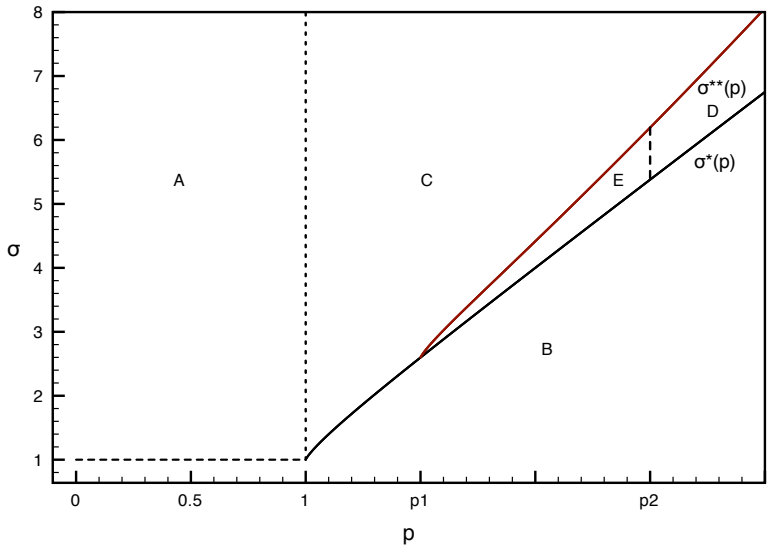

Figure 5-2: *Reproduction of a figure from [31], detailing long term behaviour of solutions to system (5.12). Each of the regions A to E corresponds to different behaviour of solutions, as discussed in main text.*

from [31]. In the (p, σ) plane, we have a single nontrivial equilibrium for $p < 1$, as in the region A. For $p > 1$, the number of nontrivial equilibria and their stability are determined by the two curves $\sigma^*(p)$ and $\sigma^{**}(p)$, along with two particular values p_1 and p_2. The curve $\sigma^*(p)$ determines whether the equation (5.15) has zero or two roots. Below this line in region B, there are no nontrivial equilibria. Above this line in region C, there are two nontrivial equilibria, the larger being a locally unstable node and the smaller an unstable saddle. Meanwhile, $\sigma^{**}(p)$ for $p > p_1$ represents the line on which Hopf bifurcations occur. For $p > p_2$, in region D, we lose the stability of the larger nontrivial equilibrium. For (p, σ) close to the line σ^{**}, locally asymptotically stable periodic orbits can occur. In region E, unstable limit cycles exist.

Setting $\nu = 0$ in (5.12) above gives the nonlinear SEIR model considered in [28]. The behaviour of solutions for $0 < p < 1$ and for $p = 1$ with $\sigma > 1$ is examined and it is found that in these cases there is a unique globally asymptotically stable nontrivial equilibrium. The behaviour of solutions for $p > 1$ is not studied.

Further generalisations of the incidence function In Hethcote and van den Driessche, [17], the system (5.12) is considered for a more general incidence rate:

$$\begin{aligned}\frac{\mathrm{d}E}{\mathrm{d}t} &= \beta g(I)(1-E-I-R) - (\epsilon+\mu)E,\\ \frac{\mathrm{d}I}{\mathrm{d}t} &= \epsilon E - (\gamma+\mu)I,\\ \frac{\mathrm{d}R}{\mathrm{d}t} &= \gamma I - (\nu+\mu)R,\end{aligned} \tag{5.18}$$

with the function g satisfying the properties:

(i) $g(0) = 0$;

(ii) $g(I) > 0$ for $I \in (0, 1]$;

(iii) $g \in C^3(0, 1]$.

Under these conditions, solutions to (5.18) exist and, together with the disease free equilibrium $(E, I, R) = (0, 0, 0)$, any possible nontrivial equilibria are solutions of

$$f(I) := \frac{g(I)}{I}\left(1 - \frac{I}{H}\right) = \frac{1}{\sigma}, \tag{5.19}$$

where H and σ are defined as in (5.17). The number of solutions depends on $f(0) = \lim_{I\to 0}\frac{g(I)}{I}$ and the the sign of $f'(I)$.

The authors then consider the particular form

$$g(I) = \frac{I^p}{1+\alpha I^q} \tag{5.20}$$

with $p, q > 0$ and $\alpha \geq 0$. This generalises (5.11) and encompasses a number of cases. For $\alpha = 0$ and $p = 1$, we have mass action, and more generally for $\alpha = 0$ we have the nonlinear case discussed in [31]. Taking $p = 1$ and $q = 1$ produces a saturated form of mass action. Figure 5-3 gives some examples of incidence functions that can be created using (5.20).

Further discussion is restricted to the cases $p = q$ (covered for the SIRS model in [32]) and $p = q - 1$. For $p = q$, the results are as in previous models. If $p < 1$, there is a single stable nontrivial equilibrium, for $p = 1$ there is a stable asymptotic equilibrium provided that $\sigma > 1$ and for $p = 1$, there are 0, 1 or 2 nontrivial equilibria, depending on the value of σ. As with prior cases, periodic behaviour can arise for particular values of p and σ. For $p = q - 1$ with $p < 1$, there is either no nontrivial equilibrium if $\sigma < \alpha$ or one globally asymptotically stable nontrivial equilibrium for $\sigma \geq \alpha$. For p=1, the

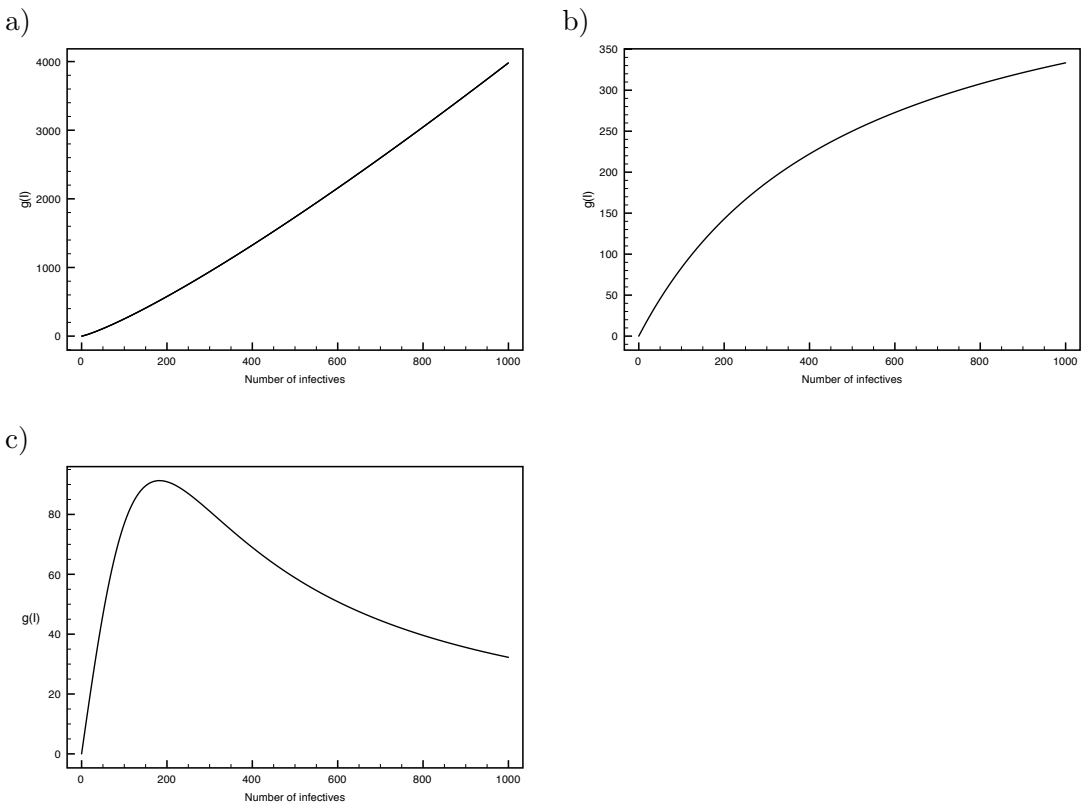

Figure 5-3: *Different nonlinear incidence functions produced by (5.20).*

nontrivial equilibrium exists if $\sigma > 1 + \alpha$ and is globally asymptotically stable in this case. Otherwise, the trivial equilibrium is stable. For $p > 1$, the number and stability of equilibria is the same as for $p = q$.

Moreover, Korobeinikov shows in [26] and [25] that for many models, results can be proved for yet more general incidence functions. In fact the incidence function $f(S, I)$ is only restricted by biological considerations. Generally this means that $f(S, I)$ should be positive and monotonically increasing for all $S, I \geq 0$ and that it should be zero if there are either no susceptibles or no infectives. Using Liapunov functions it is possible to show that the SIR, SIRS and SEIR model have globally asymptotically stable equilibria, which are endemic or disease-free depending on the size of R_0.

Obtaining nonlinear incidence from data Stroud et al [46] present the results of large scale simulations of the spread of diseases in representations of three American

cities. They attempt to fit their data to the model

$$\frac{\mathrm{d}S}{\mathrm{d}t} = -\left(\frac{R_0}{\tau_I}\right) I \left(\frac{S}{P}\right)^{\nu}, \tag{5.21}$$

which is another example of nonlinear incidence. The simulations used are highly detailed, incorporating such features as statistically accurate representations of the movements of individuals and the transport links between regions of work, leisure and residence. Topologies representing three major US cities are used, together with detailed data on population demography.

Having successfully determined values for their 'scaling parameter' ν, they discuss how the formulation leads to lower predictions of the final epidemic size for the SIR and SEIR models simulated. Taking our lead from this work, we consider the possibility of fitting data generated by more abstract simulations to the parameters of the incidence functions proposed by Liu, Hethcote and Levin, [31].

5.2 Estimating parameters of a nonlinear incidence model

We use the computer simulations presented in Chapter 2 to generate data from which the parameters of a nonlinear incidence function can be estimated using statistical methods.

Our primary aim is to investigate the effect of network structure on these parameter values. To this end, we consider three types of network: the lattice; the scale-free network and the random graph. Furthermore, we experiment on three realisations of each network type, chosen to have average degree $z = 4$, $z = 6$ and $z = 8$. Each network is comprised of 10000 nodes.

The lattices used are those illustrated in Figure 2-1. The scale-free networks are generated by preferential attachment, while the random graphs have tie probabilities that yield the requisite average number of contacts per site. The lattices are representative of homogeneous structures, which may yield nonlinear incidence functions due to clustering effects. As well as clustering, degree heterogeneity likely plays a large role in determining nonlinear incidence, so the heterogeneous structures - the scale-free network and the random graph - are considered. The former will have greater variation in degree distribution, being a network dominated by a few well-connected nodes. On the other hand, the degree distribution of a random graph will approximate a Poisson distribution (for a large number of nodes) and is centred on the average degree.

We seek to estimate the parameters $p, q > 0$ of the nonlinear incidence function proposed in [32] and [31]. Namely

$$f(S, I) = I^p S^q. \tag{5.22}$$

Estimation of the parameters p, q is made possible by considering a simple epidemic on each network, where the only process occurring is that of disease transmission.

In simulations on each of the networks detailed above, we run the infection from 100 initially infected sites for 1000 time steps, in which time the infection consumes the entirety of the network. As in Chapter 2, the infection process is modelled in discrete time and transmission occurs - across each edge that comprises one infective and one susceptible - with probability τ.

Consider the equation for the SI model

$$\frac{\mathrm{d}S}{\mathrm{d}t} = -\beta I^p S^{1+q} \tag{5.23}$$

where β represents the transmission at population level, which is to be estimated alongside the exponents p and q. The average of the simulations yields a time series, which we shall denote by (S_t, I_t). We wish to rewrite (5.23) in terms of this time series, so that the parameters β, p and q can be estimated.

Since $S + I = N$, we have

$$-\frac{1}{S}\frac{\mathrm{d}S}{\mathrm{d}t} = \beta I^p (N - I)^q. \tag{5.24}$$

We approximate the derivative $\frac{\mathrm{d}S}{\mathrm{d}t}$ from the data points by the simplest possible expression, that of the difference in the number of susceptibles between time steps:

$$\frac{\mathrm{d}S}{\mathrm{d}t} \approx S_{t+1} - S_t. \tag{5.25}$$

Hence we have the following approximation of (5.24) in terms of the data points

$$1 - \tfrac{S_{t+1}}{S_t} = \beta I_t^p (N - I_t)^q. \tag{5.26}$$

Defining $\sigma_t = 1 - \frac{S_{t+1}}{S_t}$ and taking logarithms throughout (5.26), we have

$$\ln \sigma_t = \ln \beta + p \ln I_t + q \ln(N - I_t). \tag{5.27}$$

Since (5.27) is linear in $\ln(N - I_t)$ and $\ln(I_t)$, we can use linear regression to estimate p, q and β. Table 5.1 shows the results of invoking the R procedure `glm` on the model (5.27) for each of the data sets.

Table 5.1: *Estimates for p and q from simulations averaged over 100 realisations. The value of $\ln(\beta)$ is given by the intercept. The residual deviance, RD, is the sum of the squared deviations between fit and data. The null deviance, ND, is the same quantity calculated for the null model consisting of just the intercept value. The Aikake Information Criterion, AIC, combines information about the number of parameters fitted together with the maximum likelihood estimate for the model. The value T in the right hand column gives the number of simulation time steps taken to reach 99.99% infection on the network (or the percentage given in brackets for the random graphs). This number of time steps is used by R to generate the parameter estimates.*

Network	Intercept	p estimate	q estimate	RD[a]	ND[b]	AIC[c]	T
$L4$	-7.6965	0.6611	0.8177	0.7761	188.00	-397.5	164
$L6$	-7.5855	0.6885	0.8373	0.7834	117.30	-193.1	102
$L8$	-7.3297	0.6938	0.8485	0.4117	78.00	-146.3	70
$SF4$	-8.6098	0.6765	1.0248	1.1360	39.22	-163.9	105
$SF6$	-8.4976	0.7019	1.0384	0.8325	28.48	-95.9	69
$SF8$	-8.2432	0.7036	1.0405	0.5115	21.75	-79.2	52
$RG4$	-14.6951	1.003	1.3983	0.2278	69.58	-175	67 (95%)
$RG6$	-12.5390	0.9872	1.2259	0.0611	51.3	-147.2	44 (98%)
$RG8$	-11.2505	0.9622	1.1373	0.004582	38.29	-156.6	30 (98%)

[a]Residual Deviance
[b]Null Deviance
[c]Aikake Information Criterion

We use only the data points up to the point of full infection, in order to avoid taking the logarithm at points where $N - I_t$ is equal to zero. As a standard, we cut off at the time when we reach 99.99% infection - for a single realisation this would be the time step at which a single susceptible remains. For random graphs, the situation is complicated by the fact that we cannot guarantee an entirely connected graph for the tie probabilities used. In this case we use the number of time steps taken to reach a smaller level of infection, as noted in Table 5.1. Due to the fact that the positions of the initially infected nodes are random for each realisation, we cannot simply restrict the value of N to the size of the largest connected component. Instead, it is felt that the propensity of random graphs to be disconnected may be a contributing factor in determining the values of p and q.

Table 5.1 shows the estimates for β, p and q produced by performing linear regression on the model (5.27). The values produced are similar within networks, indicating that structural properties of the network do indeed inform the parameter values. All parameter estimates were found to be statistically significant with P values less than 0.001.

For the lattices, we have $p < 1$ and $q < 1$, with both increasing towards one as the neighbourhood size increases. This sublinear rate of infections alludes to the increased clustering seen on a lattice as the number of infectives increases, with more infectives not necessarily producing more infectives as the 'wave front' of the infection (see Figure 2-2, for example) spreads through the network, leaving infectives with no individuals to infect.

For the scale-free networks, we have $p < 1$ and $q \approx 1$. As the neighbourhood size increases, p increases towards one and q increases away from one. The sublinear incidence rate for the infectives appears again, since once the hubs and their neighbours have been infected, the network is almost entirely infected. As a result, the infection rate begins to saturate for larger numbers of infectives. The exponent for the susceptibles seems to suggest that they decrease in number much faster as their numbers dwindle.

The random graphs yield $p \approx 1$ and $q > 1$, with q decreasing towards one as the size of the neighbourhood increases. It is plausible that the disconnected nature of the random graphs contributes to these parameter values. The superlinear dependence on the number of susceptibles favours infection when the number of susceptibles is large, with the infection rate decreasing quickly, perhaps due to the fact that below a certain number any remaining susceptibles are likely to be in small or isolated components of the graph.

Figure 5-4 shows the percentage error in the difference between the simulation data and solutions of the ODE

$$\frac{\mathrm{d}I}{\mathrm{d}t} = \beta S^q I^p, \tag{5.28}$$

for the parameter estimates given in Table 5.1. The lattices produce the most accurate solutions, with a minimum error of around 5% for $z = 4$, around 6.5% for $z = 6$ and approximately 8% for $z = 8$. The percentage error for the scale-free network can be as much as 50% initially, though for most time steps the error is much less than that for the lattices. The random graphs have maximum error around 20%, and above 5% for most of the time steps. Thus the fit between infection profiles is poorest for the random graphs.

Table 5.1 also contains statistical measures of the goodness of fit for the data and (5.23). We compare the residual deviance, the sum of squared deviations between fit and data, to the null deviance, the sum of squared deviations between a model fitted for $p = 0$ and $q = 1$ and the data. In all cases, we see that the full model is much closer to the data.

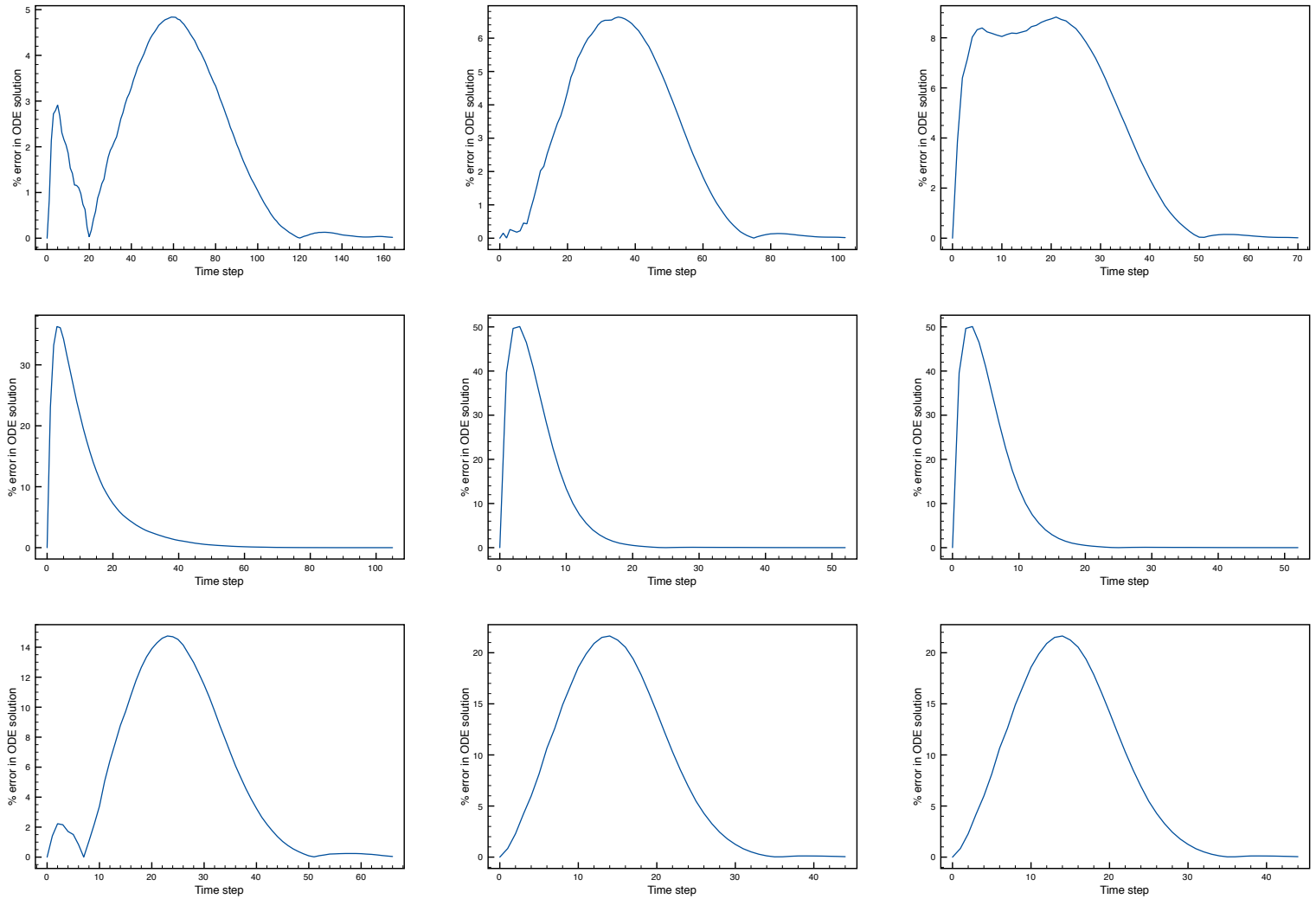

Figure 5-4: *Plots of solutions to (5.22) using the entries of Table 5.1 compared to original simulation data. Top: Lattice. Middle: Scale-free. Bottom: Random graph. Left:* $z = 4$. *Centre:* $z = 6$. *Right:* $z = 8$.

5.3 Validating parameter estimates

We wish to confirm the findings of the linear regression. In particular we seek consistency, that similar experiments produce similar results. One way in which this can be achieved is to vary the transmission rate τ whilst using the same network. Any resulting parameter estimates that exhibit little variation from our initial findings can be said to result from factors held fixed, such as the underlying contact structure.

Another validation of the method is to apply another process to the networks. We can formulate a means by which β, p and q can be estimated for the same incidence function for an SIS process, with data generated by experiments on the same networks as before.

We also seek the features of the contact structure that are responsible for particular parameter values. Using Watts-Strogatz networks, we compare the parameter estimates directly to structural features that change in a known and documented fashion as we interpolate between lattices and random graphs.

Finally, we can calculate the best fit to the mean field model for the data and compare these to the nonlinear incidence solutions we have calculated.

Varying τ For the experiments in which we vary τ, we concentrate on the hexagonal lattice and the scale-free network with average degree $z = 6$. We vary the transmission probability τ between 0.01 and 0.1 in increments of 0.01. As before, we use R to fit the parameters of (5.23) using linear regression. The results are shown in Table 5.2.

The two tables show that as τ in the simulations increases, the intercept representing β also increases, whilst the estimate for p decreases. This suggests that p, as well as β, is influenced by the transmission rate. When a Pearson Product Moment Correlation is performed for q and τ, we see a negative correlation for both the lattice and scale-free results but with P values of 0.807 and 0.165 respectively, it is not statistically significant in either case. We conclude that q is approximately constant. However, the same calculations for the p estimates show a strong statistically significant negative correlation with τ for both the lattice ($P = 0.002$) and the scale-free network ($P < 0.001$).

The decrease in p could be explained simply by the fact that increasing τ also increases the speed of the epidemic (note how the values of T decrease). Values of $p < 1$ tend to indicate that as infection levels get higher, the rate of new infections tends to slow down. Therefore as the infection spreads through the network quicker, the onset of this slowing down occurs earlier, leading to a better fit for a reduced value of p.

Nevertheless the similarity of the p and q values for both networks compared to the corresponding entries in Table 5.1 suggests that the network structure does determine the values of p and q.

The SIS process For the SIS model, in which infected individuals return to the susceptible state with probability γ, we have the following differential equation for the number of infectives:

$$\frac{\mathrm{d}I}{\mathrm{d}t} = \beta S^q I^{1+p} - \gamma I. \tag{5.29}$$

This yields

$$\frac{1}{I}\frac{\mathrm{d}I}{\mathrm{d}t} = \beta S^q I^p - \gamma, \tag{5.30}$$

and as before we estimate the derivative $\frac{\mathrm{d}I}{\mathrm{d}t}$ by quantities from the time series (S_t, I_t). Again we approximate this quantity as the difference in the number of infectives between time steps:

$$\frac{\mathrm{d}I}{\mathrm{d}t} \approx I_{t+1} - I_t. \tag{5.31}$$

Hence, in terms of the data points we have the following approximation of (5.29),

$$\frac{I_{t+1}}{I_t} - 1 = \beta {S_t}^q (N - S)^p - \gamma. \tag{5.32}$$

Rearranging (5.32) and taking logarithms throughout we have

$$\ln \sigma_t = \ln \beta + q \ln S_t + p \ln(N - S_t), \tag{5.33}$$

where we define $\sigma_t := \frac{I_{t+1}}{I_t} - (1 - \gamma)$. Therefore provided that $\sigma_t > 0$, we can use linear regression to estimate p, q and β as in the SI model. The values of σ_t are positive provided that

$$\frac{I_{t+1}}{I_t} > 1 - \gamma \tag{5.34}$$

which will be the case until equilibrium is attained. Therefore we perform linear regression on the time steps up to the point when the de facto equilibrium is reached, which for our purposes corresponds to the final point at which $\sigma_t > 0$.

Table 5.3 shows the R output for the SIS simulations on the nine chosen networks. Apart from the value of q for the lattices, the values are broadly similar to those for the SI process. Certainly, those values aside, the differences between types of network for each process are more marked than the differences between processes for each network.

The value of q for the lattices is perhaps explained by the fact that the SIS process

breaks up the clusters of infectives that form on the lattice as infection spreads. As infection increases, the lattice becomes percolated with recovered susceptibles which whether on the 'front' of infection or behind it, reduces the number of new infectives. In short, we see an increase in the number of susceptibles, whilst the number of new infectives decreases. This has been proposed by Severo [42] as mechanism through which a sublinear exponent for the number of susceptibles could be realised. Furthermore, it is the structure of the network that is contributing to this phenomenon.

On the scale-free network, recovering individuals have approximately the same neighbourhood composition of susceptibles and infectives as a 'first generation' susceptible would. Because scale-free networks consist of a few well-connected hubs with the remainder of the nodes at a short distance from them, each neighbourhoood either contains a hub, or with high probability is adjacent to one. As a result, since hubs quickly reacquire infection after recovery, most neighbourhoods maintain their composition of susceptibles and infectives despite the recovery process. This is a possible explanation as to why the values of p and q do not change so markedly between processes for the scale-free networks.

Table 5.2: *Estimates for p and q from simulations averaged over 100 realisations. The value of* $\ln(\beta)$ *is given by the intercept. The simulations were run on a hexagonal lattice and a scale-free network with* $z = 6$ *for different values of the transmission probability* τ*. The value T in the right hand column gives the number of simulation time steps taken to reach 99.99% infection on the network. This number of time steps is used by R to generate the parameter estimates.*

Hexagonal lattice

τ	Intercept	p estimate	q estimate	RD[a]	ND[b]	AIC[c]	T
0.01	-9.2473	0.7062	0.8334	6.977	602.9	-648.8	475
0.02	-8.4775	0.6984	0.8299	2.178	298	-436.6	239
0.03	-8.1101	0.6954	0.8356	1.638	197.6	-279.2	163
0.04	-7.8132	0.6929	0.8355	1.084	147.4	-225	123
0.05	-7.5423	0.6848	0.8354	0.7687	116.8	-195	100
0.06	-7.1659	0.6703	0.8238	0.4602	95.95	-198	83
0.07	-7.0618	0.6712	0.8277	0.4502	82.47	-153.1	72
0.08	-6.8714	0.6631	0.8268	0.2715	71.84	-160	64
0.09	-6.7700	0.6600	0.8301	0.2684	63.85	-139.2	58
0.1	-6.8070	0.6666	0.8394	0.3289	56.92	-111	53

Scale-free network, $z = 6$

τ	Intercept	p estimate	q estimate	RD	ND	AIC	T
0.01	-10.37869	0.73143	1.04576	15.95	153	-57.63	332
0.02	-9.71001	0.73152	1.04917	5.213	73.64	-98.66	168
0.03	-8.92652	0.70104	1.02976	1.74	47.78	-136	110
0.04	-8.49745	0.68690	1.02505	1.184	35.57	-109.2	83
0.05	-8.39610	0.69380	1.03405	0.5325	27.72	-125.8	67
0.06	-8.22974	0.69162	1.03755	0.5667	23.16	-90.3	56
0.07	-8.12591	0.69319	1.04107	0.3756	19.93	-88.6	48
0.08	-7.84210	0.67690	1.03776	0.3401	16.83	-75.09	42
0.09	-7.51770	0.66109	1.02739	0.2116	15.01	-78.06	37
0.1	-7.46658	0.66369	1.02947	0.2563	13.91	-61.69	34

[a] Residual Deviance
[b] Null Deviance
[c] Aikake Information Criterion

Table 5.3: *Estimates for p and q from simulations averaged over 100 realisations. The value of* $\ln(\beta)$ *is given by the intercept. Simulations of an SIS process were run on the nine chosen networks, with transmission probability* $\tau = 0.05$ *and recovery rate* $\gamma = 0.01$*. The value T in the right hand column gives the number of simulation time steps taken to reach a de facto equilibrium on the network, namely when the quantity* σ_t *first reaches zero. This number of time steps is used by R to generate the parameter estimates.*

Network	Intercept	p estimate	q estimate	RD[a]	ND[b]	AIC[c]	T
L4	-3.6514	0.6134	0.4115	0.03264	98.62	-857.7	155
L6	-4.0524	0.6112	0.5077	0.0348	84.2	-461.9	94
L8	-4.5202	0.6254	0.5903	0.0452	82.86	-291.1	68
SF4	-8.5475	0.7071	0.9940	0.3701	116.7	-198.6	82
SF6	-8.4910	0.7244	1.0220	0.4093	112.7	-124.2	62
SF8	-8.3080	0.7270	1.0314	0.2742	91.37	-80.96	42
RG4	-11.23542	0.92076	1.07638	0.1289	121.2	-388.1	104
RG6	-10.37732	0.92372	1.03308	0.09828	97.05	-202	60
RG8	-9.79977	0.91789	1.00873	0.1056	102.1	-158.1	51

[a] Residual Deviance
[b] Null Deviance
[c] Aikake Information Criterion

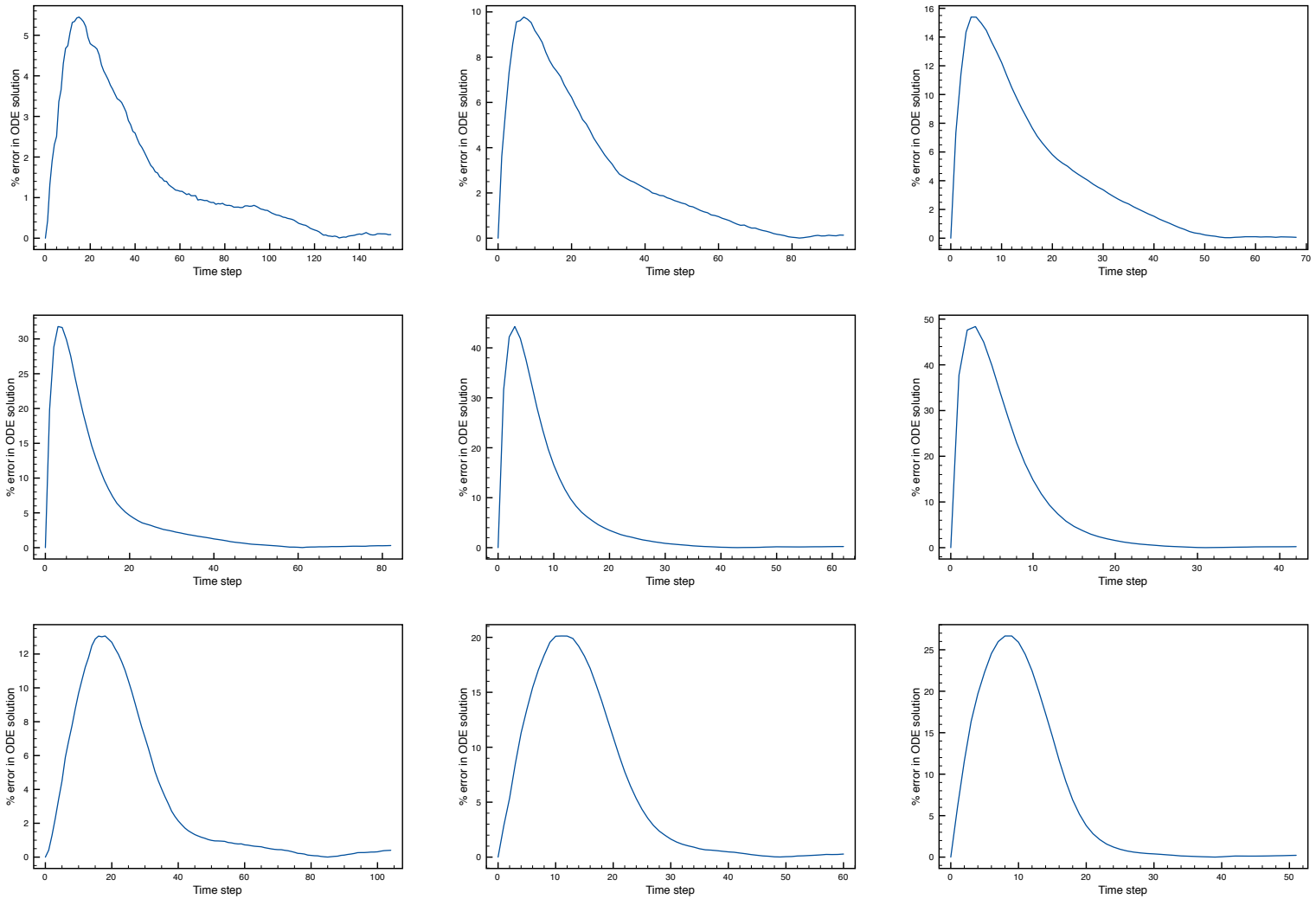

Figure 5-5: *Plots of solutions to (5.22) using the entries of Table 5.1 compared to original simulation data. Top: Lattice. Middle: Scale-free. Bottom: Random graph. Left:* $z = 4$*. Centre:* $z = 6$*. Right:* $z = 8$*.*

Figure 5-5 shows the percentage error in the number of infectives between the simulations and the solution of the ODE (5.29) for the estimated parameter values given in Table 5.3. The nature of the errors over time are the same as for the SI process in Figure 5-4, though the errors are all smaller in size. The residual and null deviances given in Table 5.3 again imply a good fit between the data and the model.

Watts-Strogatz networks Watts and Strogatz (as discussed in [10]), proposed a method for interpolating network structures between the order of a regular lattice and the disordered connection of a random graph. Each connection in the lattice is rewired with a fixed probability r, transforming it into a random graph as r tends to one. Watts and Strogatz then calculated the clustering coefficients $\phi(r)$ and the average shortest path lengths $\ell(r)$ for these networks as r varied.

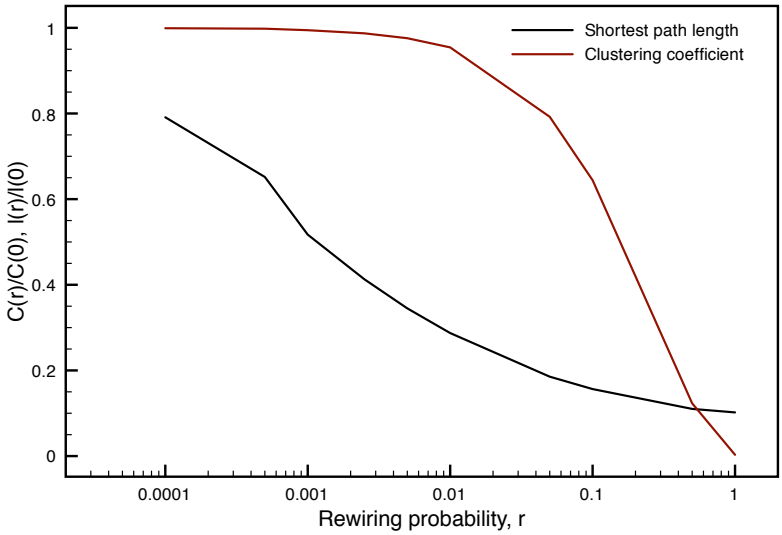

Figure 5-6: *Clustering and average shortest path lengths for Watts-Strogatz networks used in our experiments.*

Plotting the ratio of $\phi(r)$ to $\phi(0)$ and $\ell(r)$ to $\ell(0)$, they produced results similar to those seen in Figure 5-6, where we have plotted the same quantities for the networks used in our experiments. The primary feature of such plots is that they confirm intuition about what happens to networks as edges are rewired. As we can see from Figure 5-6, the average shortest path length is quickly reduced after a small proportion of the edges are rewired in this fashion, but there exist values of r for which the clustering remains high. These are referred to in the literature as 'small world' networks, because any given node retains a 'local' neighbourhood together with 'global' connections that

make for a short distance between it and any other node in the network.

Table 5.4: *Estimates for p and q from simulations on lattices with rewiring probability r varied.*

r[a]	Intercept	p estimate	q estimate	RD[b]	ND[c]	AIC[d]	T
0	-4.0623	0.6133	0.5071	0.02163	80.84	-493.1	90
0.0001	-4.0906	0.6147	0.5093	0.02873	84.66	-479.7	92
0.0005	-4.1016	0.6178	0.5081	0.02545	85.26	-491	92
0.001	-4.1460	0.6189	0.5128	0.02634	98.41	-538.8	100
0.0025	-4.3118	0.6307	0.5229	0.01833	91.22	-534.9	94
0.005	-4.5812	0.65	0.5403	0.01099	85.75	-540.4	88
0.01	-4.9469	0.6755	0.5637	0.02086	83.93	-457.4	84
0.05	-6.8623	0.7966	0.6994	0.06901	72.3	-257.7	65
0.1	-7.9005	0.8514	0.7826	0.05858	88.83	-273.7	66
0.5	-9.86703	0.91605	0.97785	0.05125	90.31	-230	56
1	-10.51225	0.93378	1.0385	0.1216	107.6	-215.8	64

[a]Rewiring probability
[b]Residual Deviance
[c]Null Deviance
[d]Aikake Information Criterion

Our interest in the Watts-Strogatz network is in whether the path lengths or clustering within the underlying contact structure are responsible for the estimates of p and q. We generated 10 networks for various values of r and ran the SIS process one hundred times upon each of them, and used (5.33) as the basis for linear regression on the average of those realisations. The results are tabulated in Table 5.4, and the estimates for p and q are plotted against the rewiring probability r in Figure 5-7. We see that both p and q increase quickly at the point in Figure 5-6 where the clustering value drops quickly. This is highly suggestive that the clustering maybe a predominant feature of contact structure that determines the exponents p and q.

Mean field model Finally, we can force the linear regression used for both the SI and SIS processes to estimate the value of β given that both p and q are equal to one. This yields the best possible mean field fit to the data we have generated. These are plotted in Figure 5-8 for the SI process, and in Figure 5-9 for the SIS process.

5.4 Discussion

In this chapter we have reviewed various models in the literature that incorporate non-linear incidence rates for the spread of infection. These extend the possible behaviours

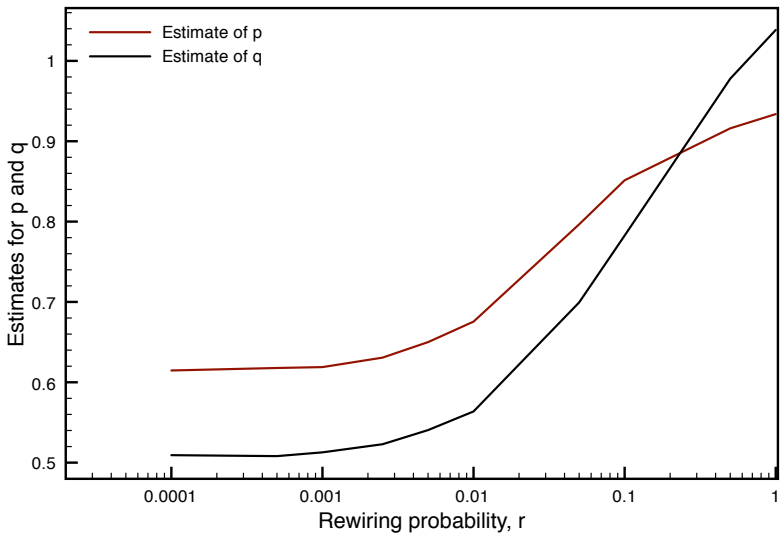

Figure 5-7: *Estimates of p and q for Watts-Strogatz networks used in our experiments.*

of epidemic systems to incorporate such features as periodic solutions and the possibility of maintaining a epidemic without the infection rate exceeding the recovery rate.

The need to simplify mathematical models of diseases spreading on particular contact structures has been established in prior chapters through the use of pairwise equations. Here, we have sought to find the parameters of the incidence function (5.22) by manipulating a simple SI model (5.23) and an SIS model (5.29) into forms upon which regression can be performed, using data points from simulations on nine particular networks. These networks consisted of three structural types that have appeared throughout previous chapters, and for each three, three average neighbourhood sizes were considered.

The results of the parameter estimates (SI process: Table 5.1, SIS process: Table 5.3) are consistent within network types for each process, with the estimate for β increasing as the neighbourhood size increases. However, across processes there are some significant variations in the parameter estimates for the lattices. These show a large variation for the estimate for q, dropping from around 0.84 (SI process) to 0.5 (SIS process). This suggests that the disordering effect of allowing nodes to recover may be playing a role. While the SI process respects the homogeneity of the lattice, the recovery of infected nodes during the SIS process produces a percolated network, where the neighbourhood of a susceptible is essentially a random combination of infectives and susceptibles. However, the estimates for the scale-free networks do not vary a great

deal between the two processes, suggesting that the heterogeneity introduced to the lattice by the SIS process is responsible for the drastic change in values of q.

Throughout our other experiments the contact structure seems to be genuinely responsible for the parameter values of the nonlinear incidence function. In experiments where we varied the transmission rate, only the intercept - which estimates β - was affected, though for the scale-free network the estimate for p did decrease a little. This was explained in terms of the increased speed with which the disease spread throughout the network in these instances.

We also demonstrated a potential connection between the parameter estimates for p and q, and the clustering coefficient of the underlying contact structure. As a lattice is rewired, the clustering decreases quickly once a critical probability has been exceeded. Our parameter estimates increase quickly at the same probability, as can be seen by comparing Figures 5-6 and 5-7.

Finally, we were able to produce optimal values of β for the mean field model and plot the corresponding ODE solutions alongside those of the nonlinear equations, together with the original simulations. It is clear that the nonlinear model represents a great improvement upon the mean field model.

This chapter shows that contact structure need not necessarily be directly incorporated within a mathematical model, but can instead be simplified and distilled into the parameters of simple (though nonlinear) model. Obviously no direct connection between the structure and the parameters exist, though we have suggested some contributory factors through which an explicit connection could be investigated.

In the following chapters, we shall use this technique to revisit models presented in Chapters 3 and 4 in an attempt to simplify them and better understand their results. In addition, we present models which could not previously be attempted with techniques such as pairwise equations.

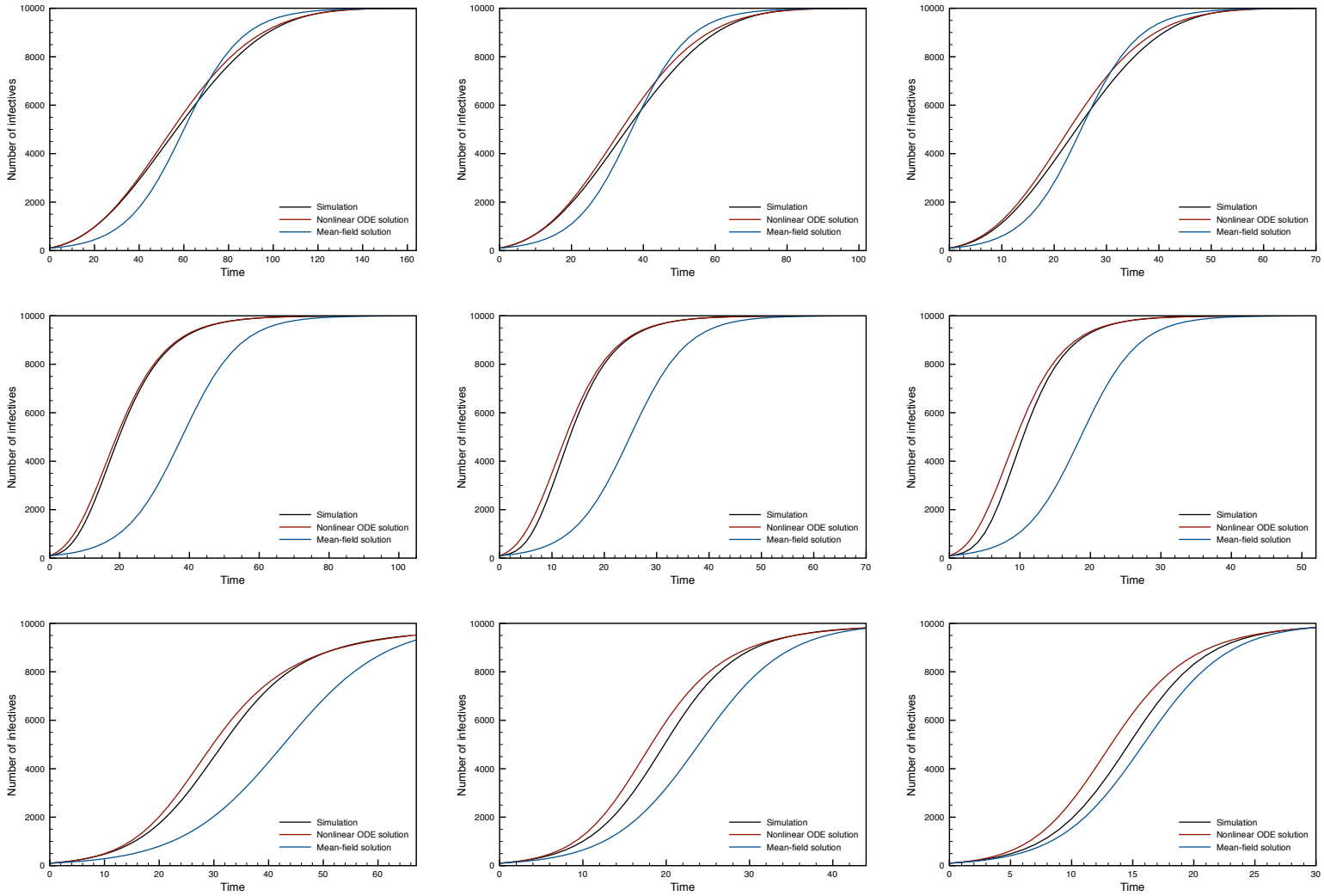

Figure 5-8: *The number of infectives versus time for the SI process. We include simulations, the solutions to the ODE (5.23), and the equivalent best mean field solution.*
Top: Lattice. Middle: Scale-free. Bottom: Random graph. Left: $z = 4$. *Centre:* $z = 6$. *Right:* $z = 8$.

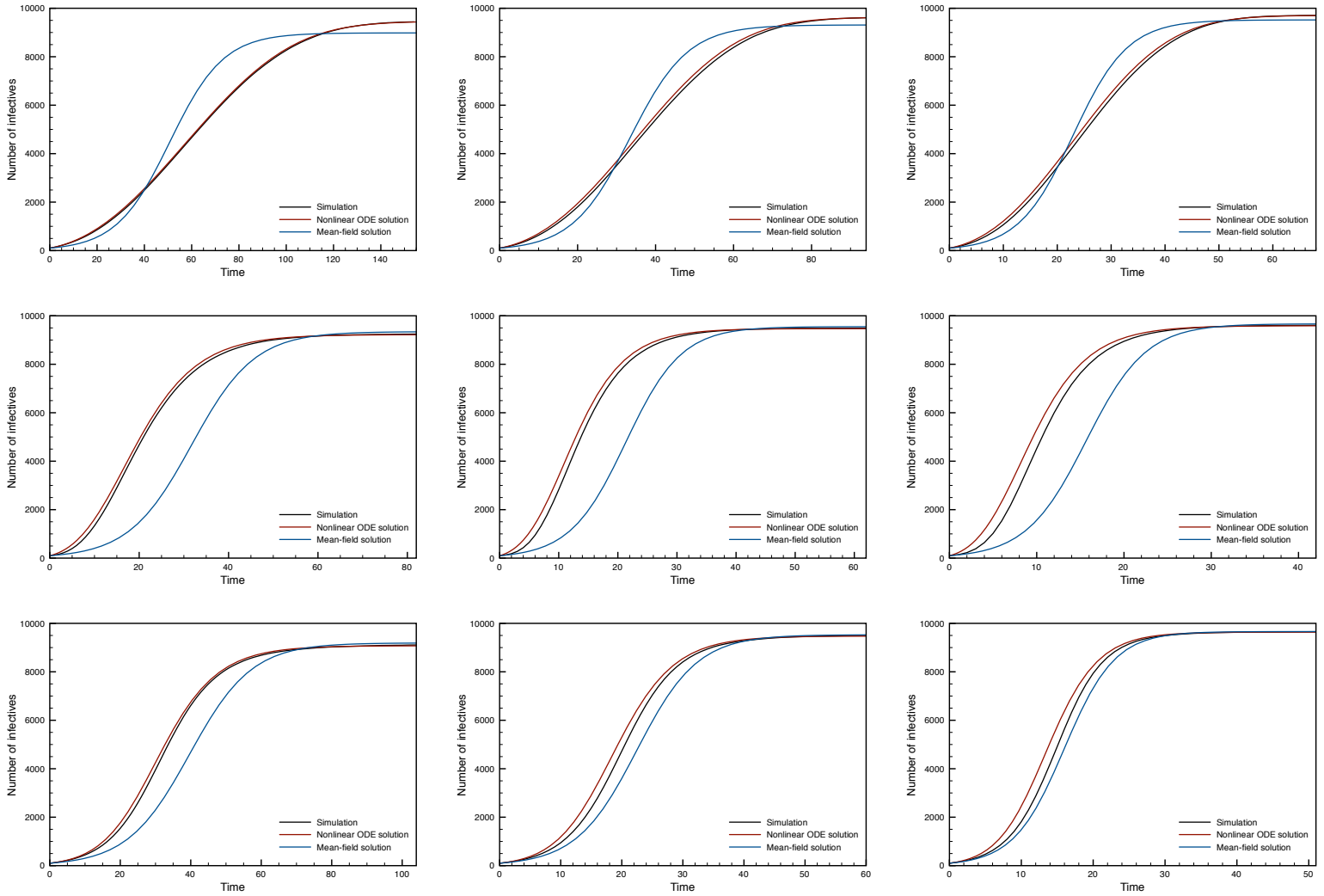

Figure 5-9: *The number of infectives versus time for the SIS process. We include simulations, the solutions to the ODE (5.29), and the equivalent best mean field solution.*
Top: Lattice. Middle: Scale-free. Bottom: Random graph. Left: $z = 4$. *Centre:* $z = 6$. *Right:* $z = 8$.

Chapter 6

Multiple Core Groups Redux

6.1 Motivation and Background

6.1.1 Chapter Outline

In the previous chapter, we provided estimates for the parameters of a nonlinear model and determined how those parameter values changed for different network structures. Prior to this, we had investigated techniques for incorporating network structure into mathematical models that divide the population into subgroups, be it along demographic or behavioural lines. This chapter takes these two ideas forward in tandem.

Initially we incorporate the synthesis of the network structure facilitated by the nonlinear model and explore the effects of allowing different network structures to interact with one another. Comparisons and evaluations are made based on simulations of similar scenarios.

Furthermore, we consider the method for modelling the linkage between groups. In previous chapters, we have alluded to the fact that the linkage function f, which determines the response of one group to infection in another, may not be linear. As in the previous chapter, we use simulations and statistical techniques to estimate the parameters of a nonlinear interaction model.

6.1.2 Motivation

In Chapter 4 we found that whilst it is relatively straightforward to analyse a mathematical model featuring mass action that describes the interaction of two identical groups, it is far more labourious to incorporate a physical realisation of the contact

structure within those groups. The resulting pairwise equations only allow for the representation of homogeneous lattice-like structures, as any further attempts to incorporate structure produce a model sufficiently complex to render simulation preferable. Furthermore, simulations then showed that the mechanism employed to model the transfer of infections between groups tended to overestimate the effects of interaction when compared to the addition of physical links between groups.

One way to incorporate structure is to use a nonlinear incidence model, such as those developed in Chapter 5. We demonstrated a relationship between the underlying contact structure of the population and the parameter estimates of a nonlinear model. We use this development to motivate a caricature system of interacting subpopulations that will allow us to investigate the effects of combining core groups with differing contact structures on the outcome of infection.

Furthermore, we require a more sophisticated model for the interaction of the core groups. In this case we utilise another technique exhibited in Chapter 5, that of estimating the parameters of mathematical models from data generated by simulations. Our previous assumption of linear influence of the external group was motivated by the need for simplicity, although other forms were briefly discussed in Chapter 3. Here we present the case for the interaction function to take a nonlinear form.

6.2 A two group SIRS model with nonlinear incidence

We consider the SIRS model for two groups of constant size N_i, $i = 1, 2$. The incidence function for the spread of disease within the i^{th} group is nonlinear, with

$$g(I, S) = I^p S^q, \tag{6.1}$$

as specified in [32]. The groups interact by mutual influence as in Chapter 4, with the influence of the infectives of the j^{th} on the susceptibles of the i^{th} group assumed to be linear, as given by

$$f_{ij} = \delta_{ij} I_j. \tag{6.2}$$

The full system of equations is then given by

$$\begin{aligned}
\frac{\mathrm{d}S_i}{\mathrm{d}t} =& -\beta {I_i}^{p_i} {S_i}^{q_i} - \delta_{ij} S_i I_j + \mu(N_i - S_i) + \nu R_i \\
\frac{\mathrm{d}I_i}{\mathrm{d}t} =& \beta {I_i}^{p_i} {S_i}^{q_i} + \delta_{ij} S_i I_j - (\gamma + \mu) I_i \\
\frac{\mathrm{d}R_i}{\mathrm{d}t} =& \gamma I_i - (\nu + \mu) R_i \\
N_i =& S_i + I_i + R_i, \quad i \neq j, \quad i = 1, 2.
\end{aligned} \tag{6.3}$$

Here β, γ, μ and ν represent respectively the transmission, recovery, mortality and loss of immunity rates, as they have done in previous models. We make the assumption here that these quantities are innate to the disease rather than the particular subpopulation, so they are assumed to be the same for each group. The quantities δ_{ij} represent the strength of the effect of group j on group i. The exponents p_i and q_i are to be thought of as representing the structure of the i^{th} group, following the results of Chapter 5.

The number of equations for each group can be reduced, and those that remain can be simplified, by considering the infective and recovered individuals in each group; while simultaneously we rescale time with $T = (\mu + \gamma)t$ so that the average duration of each infection is one unit of time. This leads to the reduced equations

$$\begin{aligned}
\frac{\mathrm{d}I_i}{\mathrm{d}T} =& a {I_i}^{p_i} (N - I_i - R_i)^{q_i} + d_{ij} I_j (N_i - I_i - R_i) - I_i \\
\frac{\mathrm{d}R_i}{\mathrm{d}T} =& r \left(I_i - \frac{R_i}{h} \right) \\
i =& 1, 2, \quad i \neq j,
\end{aligned} \tag{6.4}$$

where we define the rescaled parameters as follows:

$$a = \frac{\beta}{\mu + \gamma}, \quad r = \frac{\gamma}{\mu + \gamma}, \quad h = \frac{\gamma}{\mu + \nu}, \quad d_{ij} = \frac{\delta_{ij}}{\mu + \gamma}. \tag{6.5}$$

From here we wish to determine how the interaction between groups affects the equilibria reached within each group in isolation. As seen in Chapter 5, the nonlinear SIRS process produces a variety of outcomes. We will present numerical solutions for how the interaction between groups affects these outcomes.

Returning to system (6.4), we examine the equilibria of the full system. We have the

trivial equilibrium $(I_1, R_1, I_2, R_2) = (0, 0, 0, 0)$, together with any positive solutions of

$$\begin{aligned} aI_1{}^{p_1-1}(N_1 - I_1 - R_1)^{q_1} + d_{12}(N_1 - I_1 - R_1)\frac{I_2}{I_1} &= 1, & (6.6)\\ aI_2{}^{p_2-1}(N_2 - I_2 - R_2)^{q_2} + d_{21}(N_2 - I_2 - R_2)\frac{I_1}{I_2} &= 1, & (6.7)\\ R_1 &= hI_1, & (6.8)\\ R_2 &= hI_2. & (6.9) \end{aligned}$$

Despite the apparent complications presented by the interaction of the two groups, the analysis proceeds as for the case of a single group. Extracting a factor ${S_1}^{q_1}$ from the left hand side of (6.6) gives

$$(N_1 - (1+h)I_1)^{q_1}(aI_1{}^{p_1-1} + d_{12}\tfrac{I_2}{I_1}(N_1 - (1+h)I_1)^{\frac{1}{q_1}}) = 1, \qquad (6.10)$$

and taking the q_1^{th} root yields:

$$(N_1 - (1+h)I_1)(aI_1{}^{p_1-1} + d_{12}\tfrac{I_2}{I_1}(N_1 - (1+h)I_1)^{\frac{1}{q_1}})^{\frac{1}{q_1}} = 1. \qquad (6.11)$$

Multiplying out the first set of brackets and rearranging yields

$$N_1(aI_1{}^{p_1-1}+d_{12}\tfrac{I_2}{I_1}(N_1-(1+h)I_1)^{\frac{1}{q_1}})^{\frac{1}{q_1}} = 1+(1+h)I_1(aI_1{}^{p_1-1}+d_{12}\tfrac{I_2}{I_1}(N_1-(1+h)I_1)^{\frac{1}{q_1}})^{\frac{1}{q_1}}, \qquad (6.12)$$

and subsequent multiplication through by $(aI_1{}^{p_1-1}+d_{12}\frac{I_2}{I_1}(N_1-(I+h)I_1)^{\frac{1}{q_1}})^{-\frac{1}{q_1}}$ gives:

$$N_1 = (aI_1{}^{p_1-1} + d_{12}\tfrac{I_2}{I_1}(N_1 - (I+h)I_1)^{\frac{1}{q_1}})^{-\frac{1}{q_1}} + (1+h)I_1. \qquad (6.13)$$

Note that setting $d_{12} = 0$ in (6.13) eliminates I_2 and yields the function $f(I)$ that determined the number of nontrivial equilibria for a single group. Meanwhile, similar calculations on (6.7) yield the following

$$N_2 = (aI_2{}^{p_2-1} + d_{21}\tfrac{I_1}{I_2}(N_2 - (I+h)I_2)^{\frac{1}{q_2}})^{-\frac{1}{q_2}} + (1+h)I_2. \qquad (6.14)$$

We now see that whereas in the case of a single group the number of nontrivial equilibria is determined by the roots of a single function $f(I) = 0$; for the case of two groups, the number of nontrivial equilibria is determined by the intersection of two curves $f_1(I_1, I_2) = N_1$ and $f_2(I_1, I_2) = N_2$. We resort to this graphical description, as no closed form exists to describe I_1^* and I_2^* as solutions of (6.13) and (6.14).

In the single group case, the number of nontrivial equilibria is determined by p and

the population size N. In the case of two groups, the scenario is more complex - there are two population sizes N_i, two exponents p_i; and the strengths of the interactions between the groups, d_{12} and d_{21}, also play a role.

We proceed by solving (6.13) and (6.14) numerically, and by plotting the corresponding numerical solutions of system (6.4). We are particularly interested in cases where one or both groups are allowed to interact. As such, we classify the initial configurations of groups as trivial-trivial, trivial-positive and positive-positive. For simplicity, we begin by discussing each of these cases in the context of a symmetric interaction between the groups.

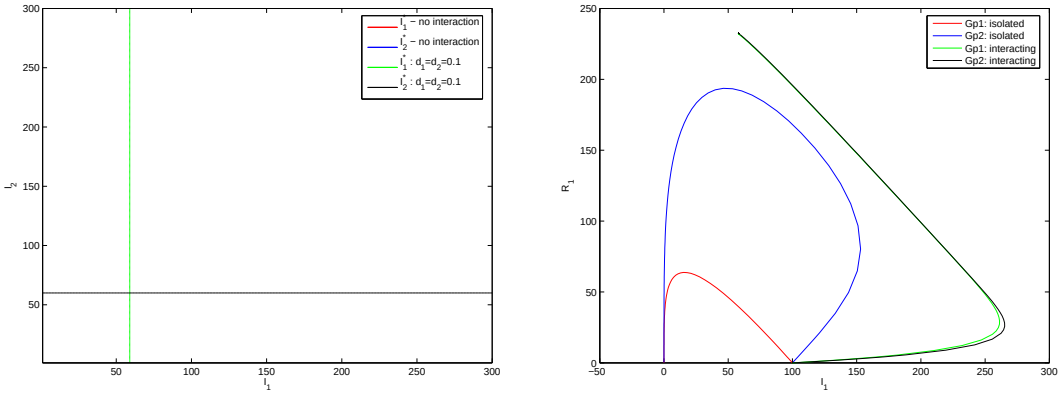

Figure 6-1: *Effect of interaction on two groups that reach a trivial equilibrium in isolation. The first group has exponent $p_1 = 1$, the second group $p_2 = 2$, with $q_i = 1$, $i = 1, 2$. Parameters used were $a = 10^{-1}$, $r = 0.997$, $h = 4$ and $N_i = 300$. The left hand figure shows the solution of (6.13) and (6.14) for the two cases $d_i = 0$ and $d_i = 0.1$. The right hand figure shows trajectories in the (I_i, R_i) phase plane for each group in isolation and for interaction with $d_i = 0.1$.*

In the case of two groups in which system (6.4) tends to a trivial equilibrium in each group, we see the emergence of a nontrivial equilibrium once the interaction is introduced between the groups. Figure 6-1 shows the case of $p_1 = 1$ and $p_2 = 2$ for parameter values that produce trivial equilibria in each group in isolation. The first figure shows the curves corresponding to (6.13) and (6.14), whose intersections correspond to nontrivial equilibria, for the two cases $d_{21} = d_{12} = 0$ and $d_{21} = d_{12} = 0.1$. No solution exists in the former case, whereas we see that the interaction produces a nontrivial equilibrium in each group. This can also be seen in the second figure, which plots the trajectories of solutions to (6.4) in the (I_i, R_i) plane, $i = 1, 2$. For both the isolated and interacting cases, the system starts with 100 infectives in each group. In isolation, the number of infectives diminishes to zero in both groups. However, when

the groups interact, solutions tend to a positive non-trivial equilibrium.

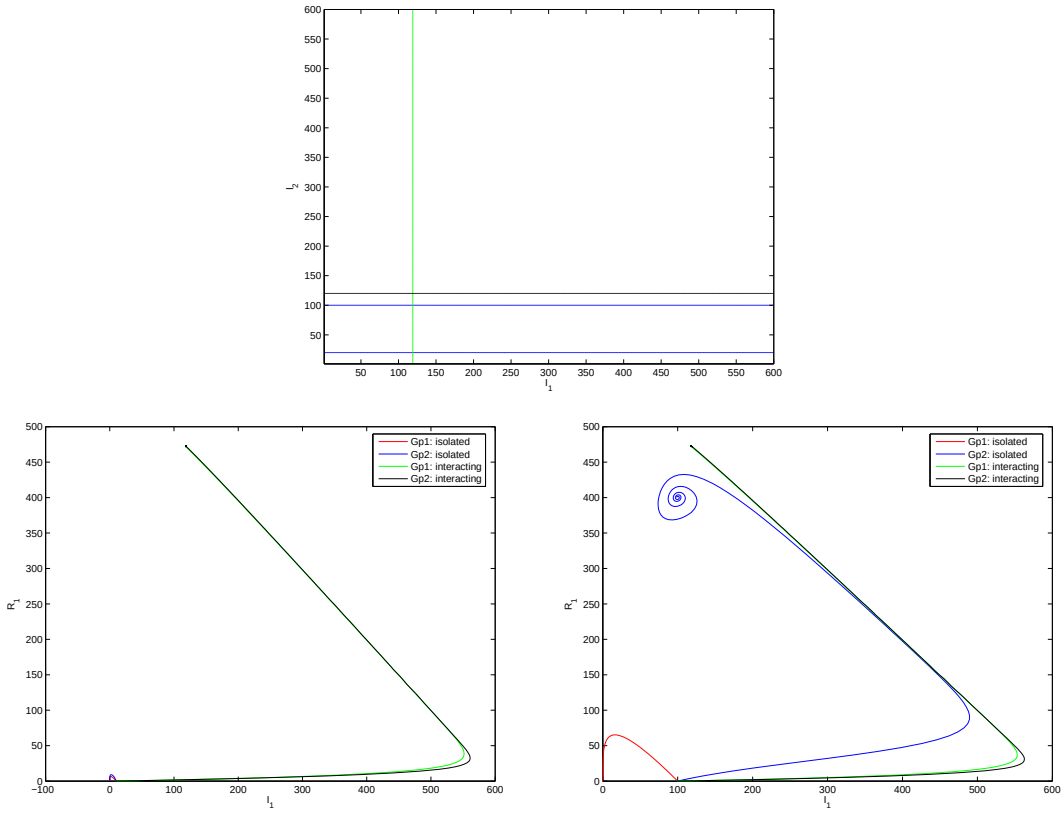

Figure 6-2: *Effect of interaction on two groups where one group reaches a trivial equilibrium in isolation. The first group has exponent* $p_1 = 1$*, the second group* $p_2 = 2$*, with* $q_i = 1$*,* $i = 1, 2$*. Parameters used were* $a = 10^{-1}$*,* $r = 0.997$*,* $h = 4$*. We use group sizes* $N_i = 600$*, so that the second group can achieve an equilibrium in isolation, provided that a threshold initial infection is exceeded. The upper plot shows the solution of equations (6.13) and (6.14) for the two cases* $d_i = 0$ *and* $d_i = 0.1$*. The lower plots show the* (I_i, R_i) *phase plane solutions starting below the threshold initial infection (left) and above it (right).*

In the trivial-positive case, we see similar behaviour. Figure 6-2 shows the case of $p_1 = 1$ and $p_2 = 2$ for a larger population size, which results in two nontrivial equilibria in the second group when system (6.4) is solved for the two groups in isolation - as seen in the uppermost figure, which shows the solutions of (6.13) and (6.14). As discussed in Chapter 5, one of these nontrivial equilibria is an unstable saddle, whilst the other is a stable node. This leads to dependence on initial conditions in the case of two isolated groups. We see that this is removed when the groups are allowed to interact. The solutions plotted in the (I_i, R_i) plane in the remaining figures also demonstrate this. The lower left hand figure shows the system starting from below the unstable

node in the second group. As a consequence, there is a trivial equilibrium reached in each group for the isolated system. These are supplanted by positive equilibria in the case of interacting groups. The lower right hand figure shows solutions of system (6.4) starting from values above the threshold. We note that the interacting system reaches the same equilibrium point in each group as for the sub-saddle case.

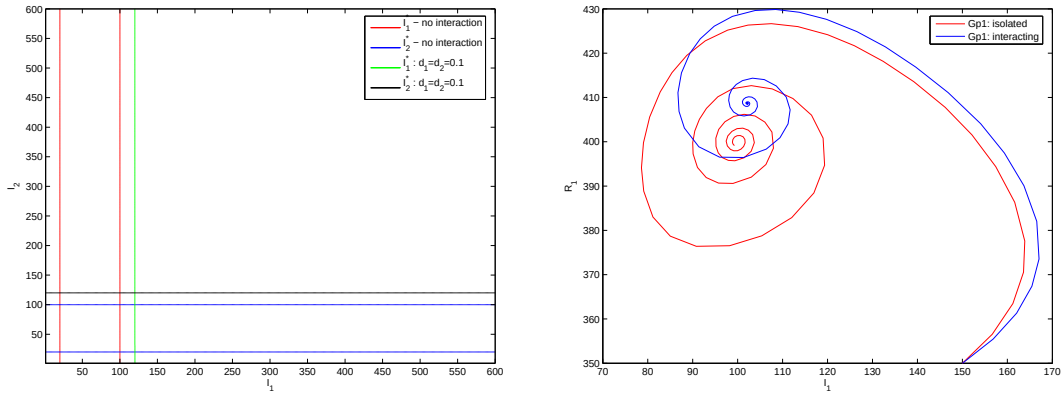

Figure 6-3: *Effect of interaction on two groups that each reach a positive infected equilibrium in isolation. Parameters used were* $a = 10^{-1}$, $r = 0.997$, $h = 4$. *Each group has exponents* $p_i = 2$ *and* $q_i = 1$, *with* $N_i = 600$. *Provided there are sufficient infectives ab initio, each group can sustain infection at equilibrium in isolation. The left hand plot shows the solutions of (6.13) and (6.14) for the two cases* $d_i = 0$ *and* $d_i = 0.1$ *The right hand plot shows solutions in the* (I_1, R_1) *plane, where we have plotted the first group only as solutions are identical for each group.*

In the positive-positive case, we present two scenarios for consideration. The first is that of $p_1 = 2$ and $p_2 = 2$ so that both groups in isolation develop nontrivial equilibria, provided the infection level exceeds the saddle point. Figure 6-3 shows that affairs proceed as expected, the interaction producing a single globally attractive nontrivial equilibrium. The equilibrium reached in the interacting case is larger than that achieved in isolation.

However, for the case of $p_i = 0.8$, $i = 1, 2$ shown in Figure 6-4, we see that the equilibrium reached in the interacting case is not much larger than that achieved in isolation. This can also be seen in the Figure 6-5, where we plot the number of infectives in the first group at equilibrium versus the interaction parameter d_i. The first plot details larger values of the interaction parameter in a system sustaining infection in isolation and the second for small values of the same parameter in the case where infection cannot be sustained without the interaction. A symmetric interaction used in both cases. In the first figure, we see that for systems sustaining positive equilibria in isolation, the effect of interaction is not that large (the entire y axis represents one

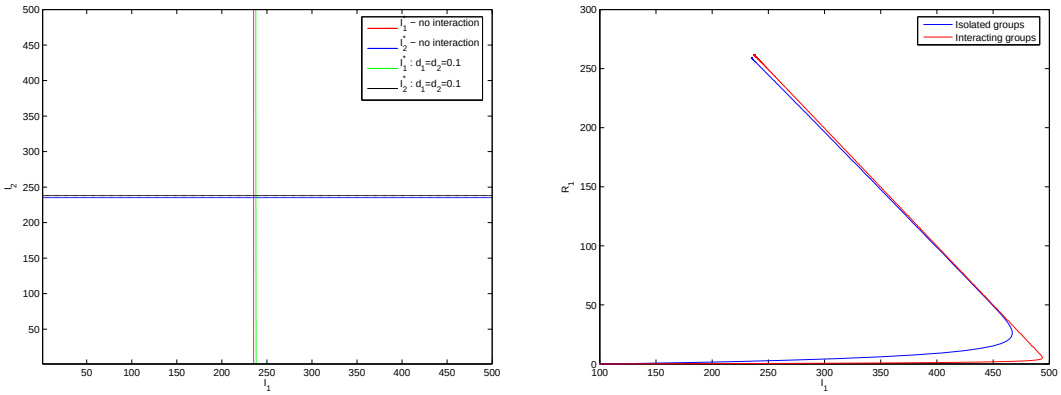

Figure 6-4: *Effect of interaction on two groups that each reach a positive infective equilibrium in isolation. Parameters used were* $a = 0.5$, $r = 0.997$, $h = 1.1$. *Each group has exponents* $p_i = 0.8$ *and* $q_i = 1$, *with* $N_i = 600$. *Under more favourable conditions, the effect of interaction is smaller. Left: Solutions of (6.13) and (6.14). Right:* (I_1, R_1) *phase plane trajectories for first group.*

individual!). We have that there is a larger increase for values of p_i smaller than one, which is due to the linear form of the interaction function. The greater the strength of the interaction, the more the linear source of infection dominates the sublinear incidence rate within the groups, pushing the level of equilibrium up faster in this case.

The right hand plot of Figure 6-5 shows that for situations in which the interaction is required in order for there to be a nontrivial level of infection at equilibrium, there is a threshold for the value of d_i, above which the positive equilibrium emerges and that this threshold is not necessarily zero. This kind of behaviour has been seen for the mean field model in Chapter 4, so there is a consistency to seeing it repeated here. We can also see that the value of p_i affects the nature of this transition. For $p_i \leq 1$, the transition is smoother than for $p > 1$, which is characterised by a sharp jump at the threshold value.

Figure 6-6 demonstrates the effects of asymmetric influence on the level of infection at equilibrium in the first group. The interaction parameters d_i are varied with the values of I_1^* represented chromatically. The gestalt figure also examines the effect of the exponents p_i on the nature of this interaction. For $p \leq 1$, we have a feedback effect occurring within the groups, as seen in the uppermost and bottom left figures. That is to say that increasing the effect of group one on group two also has an effect on group one. This can be seen by examining horizontal lines on these plots. However, it is increasing the effect of group two on group one that naturally has more direct consequences for the size of the equilibrium. This can be observed in tracking vertical

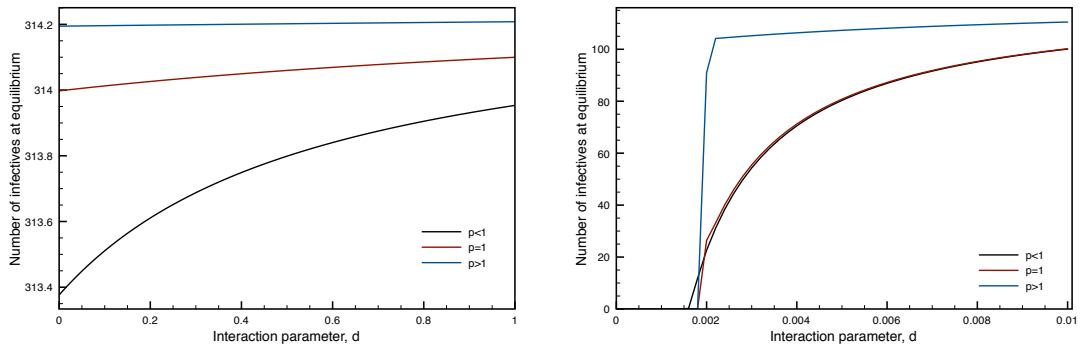

Figure 6-5: *Effect of increasing interaction parameters d_i on level of infection at equilibrium in group one. Left: Parameters represent a case when isolated groups sustain infection: $N_i = 600$, $a = 0.5$, $r = 0.997$, $h = 1.1$. Right: Small values of d_i for parameters that result in trivial equilibria in isolation: $a = 10^{-4}$, $r = 0.997$, $h = 4$, $N_i = 600$, $I_i(0) = 80$.*

lines on these plots.

For $p_i > 1$, there is no such feedback effect and far less variation in equilibrium size. Again, this is mainly due to the fact that the isolated groups for these parameter values are able to sustain infection at equilibrium. As a result, the effects of interaction are diminished, presumably to the point of masking any feedback infection between groups.

Since the exponents p and q serve to account for population contact structure within these models, it is of interest to know how the differences between groups affect the disease outcome, together with how the interaction itself affects the effects of these asymmetries in structure. Figure 6-7 explores this. The infection exponents of each group, p_1 and p_2, are varied and, as previously, the infection level at equilibrium in the first group is plotted chromatically. This is done for different levels of the interaction. The uppermost figure considers the two groups in isolation and replicates the results of chapter 5 for each of the groups. That is to say that for $p_1 < 1$, $I_1^* > 0$ (though $I_1^* \to 0$ as $p_1 \to 1$) and for $p_1 \geq 1$, $I_1^* = 0$.

The lower left figure is for a small amount of interaction between the groups, with $d_i = 10^{-3}$, $i = 1, 2$. This is akin to the values in Figure 6-5 where the interaction can have little or no impact on the outcome of infection. Here we see that for values of $p_1 < 1$, particularly smaller values, we have a larger value of I_1^*. Furthermore, for fixed values of p_1, the effect of increasing p_2 is to decrease I_1^*. This is because as $p_2 \to 1$ and so the effects of the interaction are mitigated against. The interaction also allows for $I_1^* > 0$ for $p_1 \geq 1$, provided p_2 is small enough for I_2^* to be sufficiently large in order that infection can be sustained in the first group. It should of course be noted that in

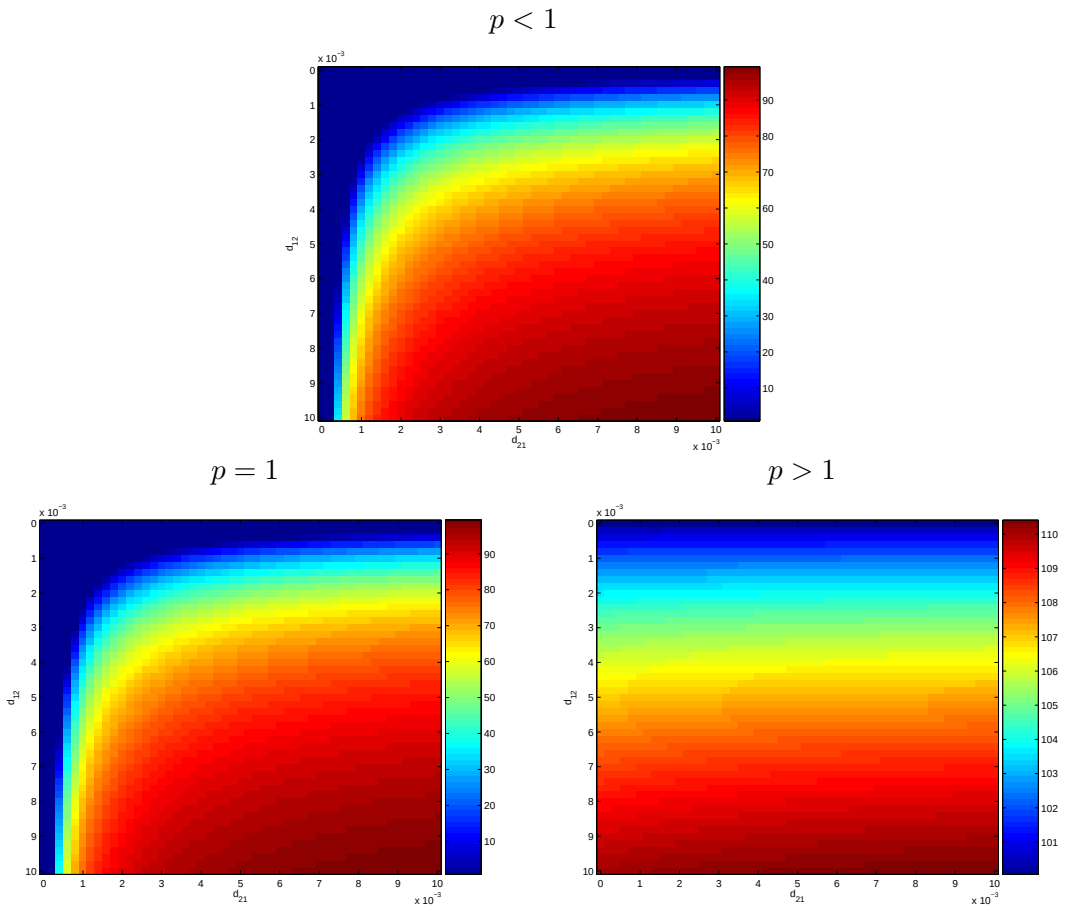

Figure 6-6: *Effect of asymmetric interaction between groups. The interaction parameters d_1 and d_2 are varied on the axes, with the value of I_1^* represented chromatically as per the colour bars to the right of each figure. In each figure the exponents p_i vary, with the following parameters fixed: $q_i = 1$; $a = 10^{-4}$; $r = 0.997$; $h = 4$ and $N_i = 600$. Top: $p_i = 0.8$. Lower left: $p_i = 1$. Lower right: $p_i = 2$.*

this figure, the values of I_1^* are very small.

In the third plot at the bottom right of Figure 6-7, we consider a stronger interaction between the two groups, with $d_i = 10^{-2}$. This stronger interaction dampens the effects of structural asymmetry. All (p_1, p_2) pairs produce a positive level of infection at equilibrium in the first group and as p_1 increases, the previously observed effects of increasing p_2 are lost.

Taken as a whole, Figure 6-7 serves to show that as the interaction between the groups is increased, the structural differences between them has less impact on disease outcome. This is an important point, which we shall return to in the discussion.

6.3 Simulations

We now consider the use of simulations to ascertain the form of the interaction between multiple groups. Up to this point, we have assumed that this interaction takes a similar form to that traditionally expressed in mathematical models for the spread of disease in multiple groups - that the probability of transmission between infectives in group i and the susceptibles of group $j \neq i$ depends linearly on said infectives. Our subpopulations have internal contact structure however, and this contact structure has been shown to contribute to the parameters of a nonlinear incidence function insofar as transmission within a single group is concerned. Naturally, it now concerns us as to whether the interaction between groups may be nonlinear in nature.

The simulations herein proceed as for the previous chapters, with the results for a given set of parameter values represented by the average of 100 realisations of the process. All simulations are run for two groups that are linked physically by a number of randomly inserted edges inserted between them. Each node in the first group is connected to a randomly selected node in the second group with a fixed probability r.

We consider two variants of the simulations, the first is as in Chapter 4 with undirected links between groups and the initial infections distributed randomly throughout the groups. The second is a reduced form in which all connections between the two groups directed one way, from the first into the second. In all of these simulations, the initial infection is concentrated entirely within the first group. This ensures that all outbreaks of infection are initiated by infectives within the first. Furthermore, even if infections within the second group are subsequently sustained without recourse to external infection, the directed nature of the links between groups prevents feedback of infection.

Throughout all of our experiments, we note when a susceptible is infected by a member of another group. This gives us a time series of external infections, which we shall denote by σ_t. We shall attempt to fit this data to the form

$$\sigma_t \sim \delta_{ij} S_i^{p_{ij}} I_j^{q_{ij}}, \tag{6.15}$$

where δ_{ij}, p_{ij} and q_{ij} are to be estimated using linear regression. It should be noted that this method can be used irrespective of the process, be it SI, SIS or SIRS and so on. We shall concentrate on the SIS process initially, and provide discussion of similar results for other processes.

The data is generated on 45 different networks consisting of two subpopulations. We

use three general types of contact structure: the hexagonal lattice; a scale-free network generated by preferential attachment so that the average neighbourhood size z is equal to 6; and a random graph with tie probability chosen so that $z = 6$. Since connections between the groups are directed in the reduced case, this gives nine possible combinations of these three structures. We then very the number of links between each of these combinations, using linkage probabilities of 0.1 to 0.5 in increments of 0.1 and the method of connecting the groups described above. For all of these networks, there are 2500 nodes in each subpopulation.

When examining these numerous combinations, we should see a number of features within the parameter estimates. For each of the five variations on the structural pairings, we should see an increase in the estimate for the value of the intercept as r increases, since this correlates with the interaction strength between the groups δ_{ij}. Furthermore, we might expect that if they are dependent only upon the contact structure, the exponents p_{ij} and q_{ij} will be constant as r increases, for each pair of structures.

We present the results grouped by the structure of the source network. The results of experiments with the hexagonal lattice as the source of infection are presented in Table 6.1, those with the scale-free network and the random graph as the source of infection are given in Table 6.2 and Table 6.3 respectively.

Before discussing the content of the tables, we can see from Figure 6-8 why we consider (6.15) as the form of the interaction. In this figure we plot the number of external infections versus the number of infectives in the source group. As with the tables, these plots are grouped by the source network, which in this case has the greater role in shaping the outcome. We can see that for small levels of infection in the source group, the number of external infections grows linearly with the number of infectives in the source group. However, the number of external infections is low when the number of infectives in the source group is very high, this is presumably because at that point, all nodes in the destination group into which the links between groups terminated have been infected. When the lattice is the source of infection, the number of external infections is at its peak for lower levels of source infection than is the case when both the scale-free network and the random graph are the source of infection. An obvious distinction here is the heterogeneity of the degree distribution, which likely plays a role in determining the nature of the interaction. It is also to be noted that a greater number of external infections occur when the lattice is the destination network. This is because the disease will spread more slowly on the lattice, emanating from cores of initial infection across local links and clustered, shared neighbourhoods; and as a result, the links across which external infections occur are more likely to terminate in susceptibles, especially for low

levels of infection in the source network.

Returning to Table 6.1, where the results of the linear regression are presented for the networks with a hexagonal lattice as the source of infection. For each receptive network, we see an increase in the estimate for δ_{21} as r is increased, barring some statistical fluctuations. Meanwhile, the exponents p and q are larger if the receptive group is heterogeneous. In order to make this comparison, we have averaged the five estimates for p and q obtained as r is increased.

Table 6.1: *Results of linear regression for data sets with a hexagonal lattice as source network. r is the probability that a node in the source group is connected to a node in the receptive group. The residual deviance, RD, is the sum of the squared deviations between fit and data. The null deviance, ND, is the same quantity calculated for the null model, ie a constant level of external infection. The Aikake Information Criterion, AIC, combines information about the number of parameters fitted together with the maximum likelihood estimate for the model. Smaller values are best. The residual degrees of freedom, rdof, are also listed as means of noting the number of data points used. A data point is eliminated if one or more of σ_t, S_t^2 or I_t^1 is equal to zero.*

Receptive group	r	Intercept	q_{est}	p_{est}	RD	ND	AIC	rdof
Hexagonal lattice	0.1	-10.5986	0.7941	0.7603	12.39	127.9	-32.56	246
	0.2	-8.5981	0.7643	0.6309	3.878	81.09	-321.7	246
	0.3	-9.4828	0.7876	0.7769	3.292	71.28	-362.5	246
	0.4	-9.1340	0.7916	0.7680	2.379	60.55	-443.4	246
	0.5	-9.2217	0.8094	0.7964	2.259	54.82	-456.3	246
Scale-free	0.1	-11.3271	0.7970	0.8683	6.73	26.66	-148.5	246
	0.2	-12.1134	0.9367	0.9688	3.561	23.54	-342.9	246
	0.3	-10.8300	0.8768	0.9015	2.792	17.37	-403.6	246
	0.4	-9.711	0.8204	0.8229	1.927	13.48	-495.9	246
	0.5	-9.6695	0.8876	0.8325	1.634	12.46	-536.9	246
Random graph	0.1	-13.2599	0.9223	1.0318	8.511	69.67	-124.5	245
	0.2	-10.6650	0.8615	0.8276	3.436	41.62	-351.8	246
	0.3	-10.7610	0.8729	0.8755	3.698	37.87	-333.6	246
	0.4	-11.1180	0.9233	0.9395	1.863	35.02	-504.3	246
	0.5	-9.2221	0.8178	0.7859	1.983	25.53	-494.4	246

Similar observations can be made for a scale-free source in Table 6.2 and for a random graph source in Table 6.3. However, for a random graph source it is no longer the case that the intercept estimate varies in the expected fashion. This is likely due to the fact that the random graphs can consist of multiple disconnected components, so adding random links between the groups does not necessarily guarantee more connections from the entirety of the source network.

Table 6.2: *Results of linear regression for data sets with a scale-free network as source group. Refer to Table 6.1 for more details on the quantities displayed.*

Receptive group	r	Intercept	q_{est}	p_{est}	RD	ND	AIC	rdof
Hexagonal lattice	0.1	-11.1427	0.8352	0.8144	12.94	174.1	-21.72	246
	0.2	-10.0321	0.8586	0.7536	6.731	141.1	-198.1	246
	0.3	-9.8424	0.8723	0.7754	3.655	124.5	-336.5	246
	0.4	-9.8111	0.8782	0.8039	2.847	113.2	-398.7	246
	0.5	-9.9816	0.8964	0.8458	2.338	106.8	-447.7	246
Scale-free	0.1	-12.9378	0.9396	0.9862	8.159	98.6	-136.5	246
	0.2	-11.7551	0.9335	0.9266	3.932	80.8	-318.3	246
	0.3	-10.9313	0.9365	0.8727	3.081	74.7	-379	246
	0.4	-10.2158	0.9183	0.8284	2.132	63.41	-470.7	246
	0.5	-10.3716	0.9278	0.8708	1.738	64.62	-521.6	246
Random graph	0.1	-12.299	0.9133	0.9127	7.945	131.6	-143.2	246
	0.2	-11.4222	0.9243	0.8780	5.477	112	-235.8	246
	0.3	-10.9973	0.9440	0.8609	3.61	101.4	-339.6	246
	0.4	-10.9244	0.9401	0.9010	2.878	91.77	-396	246
	0.5	-10.7097	0.9356	0.9050	2.387	88.23	-442.5	246

In fact, the most consistent results for the intercept value are for when the scale-free network is the source group. This is because our random links will either emanate from or close to a hub, thus guaranteeing a source of external infection, as hub are reinfected quickly if they recover. Thus to increase r is to increase the number of such links, and in turn the number of external infection events in the receptive group. Therefore there is a clear connection between r and δ_{21} in this case. This effect for scale-free networks has also been discussed in Chapter 4.

Table 6.3: *Results of linear regression for data sets with a random graph as source group. Refer to Table 6.1 for more details on the quantities displayed.*

Receptive group	r	Intercept	q_{est}	p_{est}	RD	ND	AIC	rdof
Hexagonal lattice	0.1	-10.7701	0.8205	0.7716	14.61	165.4	8.583	246
	0.2	-10.0145	0.8419	0.7643	5.701	128.6	-225.8	246
	0.3	-10.1601	0.8633	0.8077	4.727	120.8	-272.5	246
	0.4	-9.677	0.872	0.790	2.718	103.9	-410.3	246
	0.5	-10.1554	0.8956	0.8708	2.35	97.78	-446.4	246
Scale-free	0.1	-10.7135	0.8694	0.7315	6.627	63.11	-188.3	246
	0.2	-11.533	0.933	0.890	3.169	59.98	-372	246
	0.3	-11.3895	0.9433	0.9216	2.49	53.32	-432	246
	0.4	-11.4790	0.9567	0.9731	2.175	49.65	-465.7	246
	0.5	-10.4794	0.9215	0.8893	1.507	39.69	-557.1	246
Random graph	0.1	-11.4733	0.8936	0.8234	8.549	107	-124.9	246
	0.2	-11.9761	0.9451	0.9443	4.721	97.29	-272.7	246
	0.3	-10.5559	0.9113	0.8310	3.054	75.09	-381.2	246
	0.4	-11.3399	0.9498	0.9482	2.413	76.87	-439.8	246
	0.5	-10.8287	0.9391	0.9183	1.62	68.66	-539.1	246

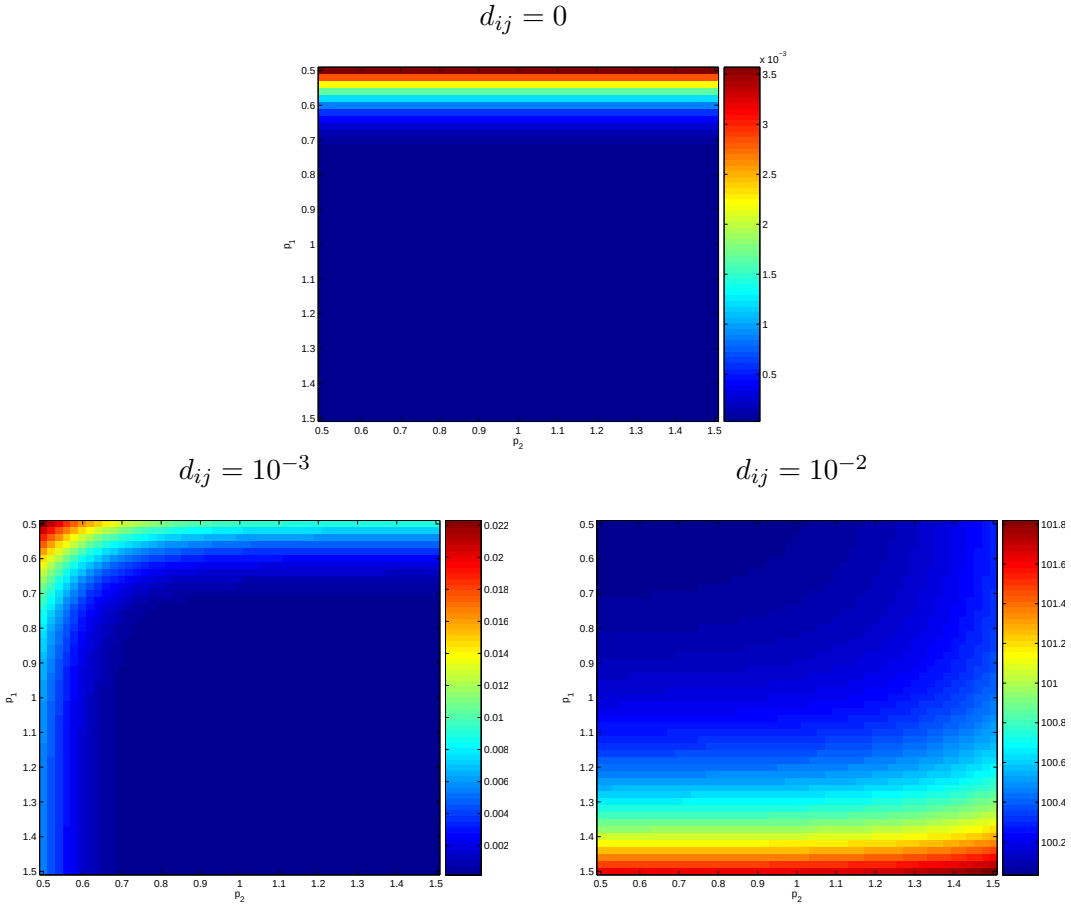

Figure 6-7: *Effect of asymmetric group structure (represented by proxy by the exponents p_i). The exponents p_i are varied between 0.5 and 1.5, with the value of I_1^* represented chromatically as per the colour bars to the right of each figure. In each figure the interaction strengths d_i vary, with the following parameters fixed: $q_i = 1$; $a = 10^{-4}$; $r = 0.997$; $h = 4$ and $N_i = 600$. Top: Two isolated groups, $d_i = 0$. Lower left: Low level of interaction, $d_i = 10^{-3}$ (refer also to Figure 6-5). Lower right: Stronger interaction, with $d_i = 10^{-2}$.*

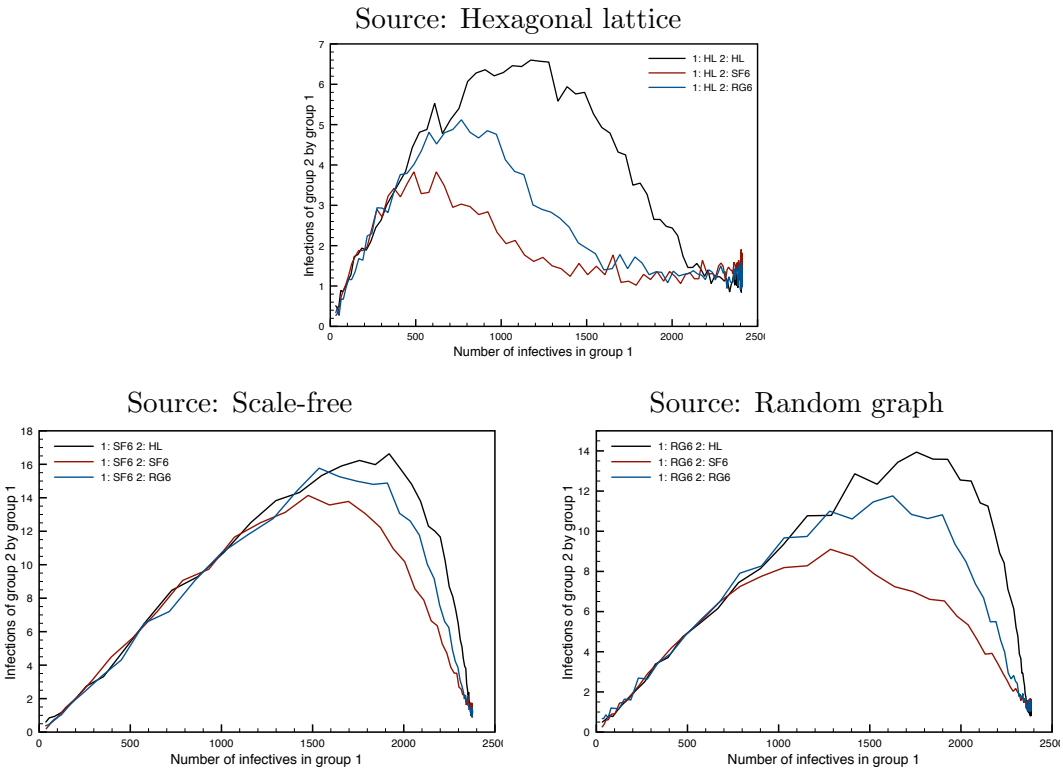

Figure 6-8: *Number of external infections by level of infection in source group.*

The residual and null deviances given in each of these tables indicate that these parameter estimates are a good fit. In Table 6.4, we present parameter estimates for the following models, alongside existing calculations for (6.15):

- $\sigma \sim 1$ This is the null model, equivalent to assuming constant external infection between groups.
- $\sigma \sim {S_2}^q$ This model assumes that the interaction depends only on the structure of the receptive group.
- $\sigma \sim {I_1}^p$ This model assumes that the interaction depends only on the structure of the source group.
- $\sigma \sim {I_1}^p S$, $q = 1$ Here we assume the form (6.15) with $q = 1$. If the estimate of p is close to one, our existing model (6.3) suffices.

We reduce further the number of networks considered, using just the hexagonal lattice and the scale-free network as base structures, yielding four combinations. We consider only the results for $r = 3$.

Table 6.4 shows that model (6.15) is the best fit of the models considered. As a way of reducing the number of parameters that would have to be considered in the mathematical model, the estimates for $q = 1$ are also quite a good fit. The remaining models fit the data quite poorly, especially those that do not incorporate the number of susceptibles in the receptive group. The fit for the model based on the infectives provides inadmissible exponents; though, as discussed previously in reference to Figure 6-8, for small levels of infection in the source group external infections are linearly proportional to the number of external infections.

We noted that it is possible to estimate the parameters of (6.15) for any process occurring between two groups, since we only have to track the number of susceptibles, infectives and external infections. The format of Table 6.4 is repeated across Tables 6.5 and 6.6, for the SI and SIRS processes respectively. The experiments used were the same, and were performed on the same networks. Throughout both of these tables we again see that model (6.15) is the best fit in each case.

Finally, we consider an experiment in which two groups mutually influence each other, with undirected links constructed between the two groups. Figure 6-9 shows the number of external infections between groups versus the number of infectives in the source group. The left hand figure shows the influence of the first group on the second, and the right hand figure, vice versa. We note the similarity between these profiles in both

Table 6.4: *Parameter estimates for different models of group interaction: SIS model.*

Hexagonal lattice into hexagonal lattice.

Model	Intercept	p_{est}	q_{est}	Deviance	AIC
NULL	0.3569	-	-	71.28	399.2
$\sigma \sim {S_2}^q$	-1.3895	-	0.3407	31.56	198.3
$\sigma \sim {I_1}^p$	1.7882	-0.1916	-	65.4	379.7
$\sigma \sim {I_1}^p S$, $q = 1$	-12.552	1.038	1	7.808	-149.5
(6.15)	-9.4828	0.7769	0.7876	3.292	-362.5

Hexagonal lattice into scale-free network.

Model	Intercept	p_{est}	q_{est}	Deviance	AIC
NULL	0.4229	-	-	17.37	47.61
$\sigma \sim {S_2}^q$	-0.1242	-	0.1062	15.18	16.01
$\sigma \sim {I_1}^p$	0.60852	-0.02484	-	17.27	48.21
$\sigma \sim {I_1}^p S$, $q = 1$	-12.437	1.032	1	3.078	-381.3
(6.15)	-10.8300	0.9015	0.8768	2.792	-403.6

Scale-free network into hexagonal lattice.

Model	Intercept	p_{est}	q_{est}	Deviance	AIC
NULL	0.4131	-	-	124.5	537.9
$\sigma \sim {S_2}^q$	-2.6024	-	0.6079	28.6	173.8
$\sigma \sim {I_1}^p$	2.7170	-0.3013	-	117.9	526.6
$\sigma \sim {I_1}^p S$, $q = 1$	-11.681	0.9833	1	6.104	-210.8
(6.15)	-9.8424	0.7754	0.8723	3.655	-336.5

Scale-free network into scale-free network.

Model	Intercept	p_{est}	q_{est}	Deviance	AIC
NULL	0.5292	-	-	74.7	410.9
$\sigma \sim {S_2}^q$	-2.2001	-	0.5345	26.04	150.5
$\sigma \sim {I_1}^p$	2.3334	-0.2358	-	71.02	400.3
$\sigma \sim {I_1}^p S$, $q = 1$	-11.8305	0.9479	1	3.393	-357
(6.15)	-10.9313	0.8727	0.9365	3.081	-379

Table 6.5: *Parameter estimates for different models of group interaction: SI model.*

Hexagonal lattice into hexagonal lattice.

Model	Intercept	p_{est}	q_{est}	Deviance	AIC
NULL	0.382	-	-	161	252.9
$\sigma \sim {S_2}^q$	-4.004	-	0.684	58.18	186.7
$\sigma \sim {I_1}^p$	1.2138	-0.1245	-	159.5	254.3
$\sigma \sim {I_1}^p S$, $q = 1$	-11.7796	0.8588	1	10.55	72.27
(6.15)	-12.812	0.937	1.079	9.736	68.91

Hexagonal lattice into scale-free network.

Model	Intercept	p_{est}	q_{est}	Deviance	AIC
NULL	-0.8161	-	-	210.6	255.8
$\sigma \sim {S_2}^q$	-4.3519	-	0.6879	24.45	124.3
$\sigma \sim {I_1}^p$	5.4323	-0.9466	-	131.9	228.7
$\sigma \sim {I_1}^p S$, $q = 1$	-11.1199	0.7822	1	9.03	62.5
(6.15)	-10.6135	0.7293	0.9694	8.907	63.65

Scale-free network into hexagonal lattice.

Model	Intercept	p_{est}	q_{est}	Deviance	AIC
NULL	0.5648	-	-	236	233.6
$\sigma \sim {S_2}^q$	-5.439	-	0.983	37.96	138.7
$\sigma \sim {I_1}^p$	2.3575	-0.2478	-	232.5	234.8
$\sigma \sim {I_1}^p S$, $q = 1$	-10.3550	0.6652	1	12.77	80.98
(6.15)	-12.8744	0.8462	1.1982	6.591	47.92

Scale-free network into scale-free network.

Model	Intercept	p_{est}	q_{est}	Deviance	AIC
NULL	-0.1739	-	-	276.2	245.4
$\sigma \sim {S_2}^q$	-5.4368	-	0.9691	39.95	143
$\sigma \sim {I_1}^p$	4.498	-0.644	-	253.1	242.7
$\sigma \sim {I_1}^p S$, $q = 1$	-10.0502	0.6128	1	19.24	103.5
(6.15)	-13.1827	0.8834	1.2153	11.67	78.5

Table 6.6: *Parameter estimates for different models of group interaction: SIRS model.*

Hexagonal lattice into hexagonal lattice.

Model	Intercept	p_{est}	q_{est}	Deviance	AIC
NULL	-0.5382	-	-	186.2	927.1
$\sigma \sim {S_2}^q$	-3.3088	-	0.5766	41.74	184
$\sigma \sim {I_1}^p$	3.2272	-0.5339	-	154.3	836.5
$\sigma \sim {I_1}^p S$, $q = 1$	-12.1551	0.9659	1	15.36	-315
(6.15)	-10.3206	0.7852	0.8796	12.7	-407.7

Hexagonal lattice into scale-free network.

Model	Intercept	p_{est}	q_{est}	Deviance	AIC
NULL	-0.4222	-	-	64.87	402
$\sigma \sim {S_2}^q$	-2.5468	-	0.4225	22.14	-132.4
$\sigma \sim {I_1}^p$	2.5979	-0.4283	-	44.11	211.5
$\sigma \sim {I_1}^p S$, $q = 1$	-11.7677	0.8958	1	11.13	-475.7
(6.15)	-10.3768	0.7676	0.9032	10.74	-491.2

Scale-free network into hexagonal lattice.

Model	Intercept	p_{est}	q_{est}	Deviance	AIC
NULL	-0.51	-	-	265.6	1105
$\sigma \sim {S_2}^q$	-4.2071	-	0.7843	52	293.7
$\sigma \sim {I_1}^p$	0.4261	-0.1318	-	264.5	1105
$\sigma \sim {I_1}^p S$, $q = 1$	-11.245	0.848	1	20.26	-176.8
(6.15)	-10.4397	0.7804	0.9310	18.91	-209.2

Scale-free network into scale-free network.

Model	Intercept	p_{est}	q_{est}	Deviance	AIC
NULL	-0.3688	-	-	170.8	885.1
$\sigma \sim {S_2}^q$	-4.0570	-	0.7369	45.66	228.8
$\sigma \sim {I_1}^p$	1.2405	-0.2266	-	167.4	877
$\sigma \sim {I_1}^p S$, $q = 1$	-11.4931	0.8618	1	12.18	-430.8
(6.15)	-11.6450	0.8748	1.0119	12.15	-429.7

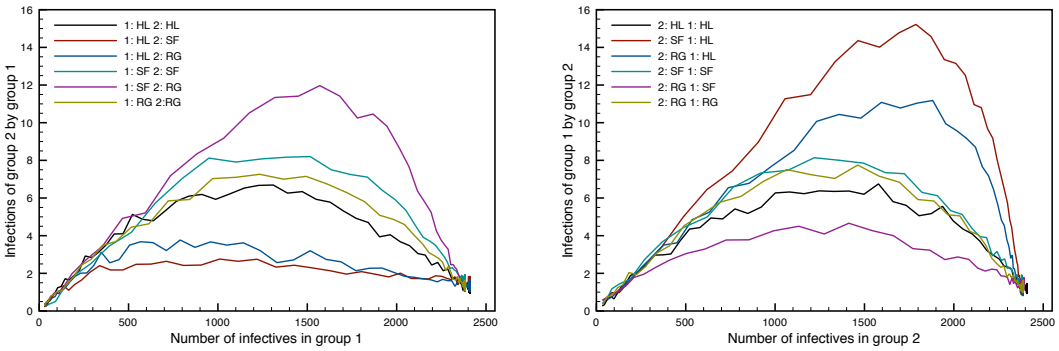

Figure 6-9: *Number of external infections versus level of infection in source group. Two subpopulations are connected by undirected random links, so infection can flow between groups. Results are for an SIS process with* $\tau = 0.05$ *and* $\gamma = 0.01$.

r	Interaction	Intercept	p_{est}	q_{est}	RD	ND	AIC
0.1	1 on 2	-11.3451	0.8430	0.8292	8.624	66.37	-122.7
	2 on 1	-10.8702	0.7819	0.8248	8.093	80.78	-138.5
0.2	1 on 2	-12.0626	0.9939	0.9074	4.335	68.41	-294
	2 on 1	-9.7324	0.7440	0.8135	3.954	65.61	-316.9
0.3	1 on 2	-11.1203	0.9253	0.9053	2.626	61.82	-418.8
	2 on 1	-10.4787	0.8807	0.8342	3.076	63.12	-379.5
0.4	1 on 2	-10.6282	0.8976	0.9116	1.977	59.69	-439.5
	2 on 1	-10.0805	0.8669	0.8336	2.156	59.24	-467.9
0.5	1 on 2	-11.0453	0.9686	0.9255	1.781	60.29	-515.6
	2 on 1	-9.4288	0.8074	0.8328	1.685	57.05	-529.3

Table 6.7: *Parameter estimates for interaction as in 6.15, where two hexagonal lattices influence one another under an SIS process with* $\tau = 0.05$ *and* $\gamma = 0.01$.

figures when source and destination network are the same. We provide the parameter estimates for the model (6.15) for an SIS process occurring on a network consisting of two subgroups that are hexagonal lattices in Table 6.7. The estimates are given for each interaction as r is increased.

There is the same trend in goodness of fit as for the reduced experiments, so that the fit improves as r increases. The estimates for p and q for each interaction pair should be approximately the same since source and receptive group have the same contact structure. However p can vary by as much as 0.16 and q by as much as 0.09. Individual measures for the standard error of each parameter estimate are around 0.01, and never more than 0.02, so the variation cannot be explained solely in terms of errors in the regression. There are many additional contributing factors, including the

random placement of the links between the groups, the random placement of the initial infectives, and feedback in the external infections.

In comparison with the results of the reduced model in Table 6.1, we see that the estimates for p and q in the full model are closer to one, but that the interaction strengths are generally smaller.

6.4 Discussion

In this chapter we have continued to investigate models for the spread of disease between multiple subpopulations. From the point of view of mathematical models, we examined the effects of the nonlinear incidence functions introduced in Chapter 5 on the outcomes of infection. Meanwhile, we continued to develop the model by estimating the parameters of a nonlinear interaction from the results of computer simulations.

In the mathematical model, we introduced interaction to systems consisting of groups that would evolve to known equilibria in isolation and investigated the outcomes for each group. From the results of [32] as discussed in Chapter 5, it was possible to know how a particular system would evolve in isolation. We demonstrated that in general, systems that evolve to trivial equilibria in isolation can sustain infection in each group when they are allowed to interact. In some cases, a threshold can exist such that if the initial level of infection is insufficient, a group may not sustain infection. However, once groups are allowed to interact and the interaction is sufficiently strong, such thresholds are eliminated and the resulting nontrivial equilibria are globally stable. In contrast, introducing the interaction to groups that can sustain infection in isolation does not change the position of that equilibrium by a large amount.

Upon closer investigation of the relationship between interaction strength and group structure - as represented via the exponents of the nonlinear incidence function - we find that the interaction has a far more profound effect when $p < 1$. This is because the assumed linear interaction dominates over sublinear internal incidence rates. Because Chapter 5 revealed that incidence rates on the structures on which we have simulated are indeed sublinear, this is an interesting feature.

We also see that as we consider asymmetries in structure, the differences in outcome that result for different (p_1, p_2) pairs diminish as the interaction strength increases. As a result, we can say that it is only worth considering separate groups interacting in this fashion if the connection between them is very weak. In the cases considered for example, this would be if approximately less than one percent of individuals in a given

group are connected to another group. This suggests a practical threshold for which models of this nature are applicable.

There is some sense that the addition of contact structure via the exponents p and q is merely adding greater complication to an already complicated model. For some situations it may be possible to regard the entire population as one contiguous network from which one set of parameters p and q as in Chapter 5. However, there are many modelling scenarios in which making a distinction between core groups is desirable; for example, the recovery and loss of immunity processes in (6.3) could easily be modified so that we are considering the efficacy of two different treatment regimes. In this case, it may be necessary to know how the underlying contact structure of each population affects the outcomes of treatment practice. This will be discussed further in Chapter 8.

A potential flaw in the model (6.3) is the assumption of linear dependence on the number of infectives in the external group. If contact structure can affect the course of infection throughout a group, it is perhaps reasonable to assume that the contact structure of that group can also have an effect on transmission between it and another group.

This was estimated from simulations in which we measured the number of infections occurring with the infective in one group and the susceptible in another, and fitted to the model (6.15). Due to the inherent variability of the links between the groups (which were added at random), the results of the ensuing linear regression have some variability within them too. Nevertheless, the results are consistent when grouped according to source and destination contact structure. There is also a strong demarcation between the parameter estimates for situations in which the homogeneous structure of the lattice is the source network, and when the source network is more heterogeneous.

We also considered a number of other potential nonlinear forms for the interactions, but of these (6.15) emerges as the most statistically accurate and credible. Whilst we concentrated in the main on the results of SIS processes, we also found this to be the best model for SI and SIRS processes. We found that while parameter estimates varied for a given network from process to process, there was a consistency to the differences between the networks for each process.

This flexibility suggests a mechanism by which the exponents of a nonlinear incidence function for processes other than those of SI and SIS could be estimated for a single group. We could take a network and randomly select sites to be in one of two groups, then by measuring the number of infections between groups we could fit the interactions to (6.15), as above. If we can divide our population so that the resulting network is bipartite, then all infections happen in this manner and we capture all transmis-

sions occurring on the network in this fashion. For example, it is possible to generate scale-free networks that are bipartite through a modified version of the preferential attachment process, as discussed in the paper by Ergun [14]. However, in general we will not know the structure of the two networks we create by this method, meaning that the ability to infer parameter values from structure without recourse to simulation and regression will be difficult. Of course, we could simply consider the source and receptive subgroup to both be the entire network. Nevertheless, we consider the prospects for this technique, and some variations, in Chapter 8.

Chapter 7

Co-infection in heterogeneous populations

7.1 Motivation and Background

7.1.1 Chapter Outline

In this chapter we continue to utilise the connection between nonlinear incidence and network structure in order to discuss the effects of co-infection on the spread of two diseases throughout a heterogeneous population. The co-infection effect is that of one disease increasing the susceptibility of individuals to another infection that is spreading contemporaneously. Whilst the mechanism of co-infection confers advantage to the disease, it is of interest whether contact structure plays any role in determining disease outcome in these situations.

To this end, we formulate a nonlinear model that incorporates both this co-infection effect and the underlying population structure. We explore the impact of these two features on the outcome of the spread of the diseases and the number of co-infected individuals over time.

We exhibit the results of simulations of the same process, comparing the outcomes on different contact structures to the results for the mathematical model. We also demonstrate the effects of co-infection within a population comprised of two subgroups using a more developed simulation and validate the outcomes utilising the results of this chapter and those of Chapter 6.

7.1.2 Motivation

The co-infection relationship is seen between many sexually transmitted infections. In [7] it is reported that the presence of anal warts due to HPV infection can increase the probability of HIV transmission by up to as much as five times, whilst patients infected with HIV will often experience larger and more numerous warts. This synergy is largely due to the fact that a sexually transmitted infection often produce tissues more susceptible to other bacterial infections generally, such as warts and sores.

For practitioners concerned with treating sexually transmitted infections, co-infection is a worry. The presence of two sexually transmitted infections within an individual may lead to ineffective treatment being pursued, particularly if one of the diseases is asymptomatic. Due to the effect on the immune system, the acquisition of other sexually transmitted infections can seriously affect HIV positive individuals, decreasing the quality of life for the patient and increasing the severity of the concurrent infection, [40].

7.1.3 Background Reading

One model for two infections acting in concert is given in [9], which considers the impact of a minor infection at equilibrium on the invasion of a major infection. The major disease is denoted D and the minor disease d.

The model for the major disease is a simple epidemic:

$$\frac{\mathrm{d}I}{\mathrm{d}t} = \beta\frac{SI}{N} - (\mu + \sigma)I. \tag{7.1}$$

Here β represents transmission, as is usual, and N the size of the population. The two mortality rates are μ and σ, with the latter being due to the disease. The transmission rate is considered to be split into two factors,

$$\beta = p\rho, \tag{7.2}$$

where p is the probability that D-transmission is successful on contact and ρ is the number of new contacts per unit time. If R_0^D is defined to be the basic reproduction ratio for the invasion of D into a homogeneous population, then we have

$$R_0^D = \frac{p\rho}{\mu + \sigma}. \tag{7.3}$$

The authors then assume that the minor infection d is in an endemic steady state and

proceed to calculate the basic reproduction ratio R_0 for the heterogeneous population in which individuals with d are ν times more susceptible to the major infection D. It is determined that

$$R_0 = KR_0^D, \tag{7.4}$$

where K is a multiplicative factor dependent upon ν and a number of other parameters such as the transmission and recovery rates of the minor infection d, and the increased transmission rate of D when individuals are infected by both infections.

By discussing how the multiplicative factor K depends upon these parameters, the authors are able to draw conclusions about how (for example) the increased effectiveness of treating the minor disease d can affect the prospects for the invading major disease D.

In this chapter, we shall develop similar models and present similar arguments, using mathematical models similar to those considered in earlier chapters. We shall also take into account the underlying contact structure of the population using the connection to nonlinear incidence models developed in Chapters 5 and 6.

7.2 Mathematical models for co-infection

We approach the description of two synergistic diseases spreading within a population by examining two factors that might account for their synergy, that of one infection by one disease causing greater susceptibility to the other and the prolonged recovery time for co-infected individuals. We also require a model that allows us to consider the underlying contact structure of the population.

We begin by formulating a model for two SIS diseases spreading in this manner. This simple model facilitates a straightforward incorporation of the co-infection effects. We begin with a model that assumes homogeneous mixing and study co-infection independently of contact structure. We do this by examining the perturbations that occur as the second infection is introduced to a population in which the first infection has reached equilibrium.

Contact structure is then introduced using the nonlinear incidence functions discussed in Chapter 5. For this model we examine how the number of co-infected individuals at equilibrium varies in response to changes in the parameters that describe the nature of the co-infection and those that are a proxy representation of contact structure.

Subsequently, we demonstrate how two SIRS processes may be considered together, producing a complicated model that depends on a number of parameters. We begin

our investigation of this particular model by referring back to parameter values that produced periodic orbits for a single nonlinear SIRS process in Chapter 5. In this scenario, we investigate how the co-infection parameters affect the long term behaviour of solutions. We conclude our discussion of this model by investigating what happens to the number of co-infected individuals at equilibrium as the three parameters central to the model are varied continuously.

7.2.1 A basic co-infection model

Modelling preliminaries We present a model for the spread of two diseases in tandem within a population. Each disease in isolation follows an SIS process so that individuals susceptible to a particular disease are infected and then recover back to a susceptible state. In addition to this, individuals can be co-infected with both diseases. Figure 7-1 details the processes by which individuals move between the compartments F, I_1, I_2 and C as described in Table 7.1.

We use F rather than S to denote individuals entirely free from infection, since individuals in the I_1 class (as an example) remain susceptible to the second disease. Moreover, this notation prevents confusion when nomenclature such as SIS or SIRS are used to describe individual disease processes.

We pay particular attention to the effect of being infected by one disease on the likelihood of acquiring the second, and the effect of co-infection on the recovery rate of either (or both) infections.

We model the effect of superinfection, the transitions $I_1 \to C$ and $I_2 \to C$ of Figure 7-1, with the parameter $\epsilon \geq 1$. This parameter represents how much more infective the first disease becomes to a recipient who already has the second disease, and vice versa. In the absence of the first disease, individuals transmit the second disease with probability β_2; however, in the presence of the first infection, the second disease is transmitted with probability $\epsilon\beta_2$.

We model the effect of co-infection on recovery rate using the parameter ρ. Whereas individuals infected with only the first infection will recover at rate γ_1, individuals with both infections will recover from the first infection at a rate $\rho\gamma_1$. Naturally we assume that the same thing happens for the second disease. Since we are assuming that co-infection diminishes the ability of individuals to recover from either disease, we would expect that $\rho \leq 1$.

In Figure 7-1, we have also annotated where simultaneous infection with and recovery from both infections can occur, in the $F \to C$ and $C \to F$ transitions respectively. We

Table 7.1: *Summary of states, parameters and processes featuring in the SIS co-infection model (7.5).*

State	Description
F	Individuals susceptible to both infections.
I_1	Infected with disease 1, susceptible to disease 2.
I_2	Infected with disease 2, susceptible to disease 1.
C	Infected with both diseases ('Co-infected').

Parameter	Description
β_i	Transmission rate of disease i, $i = 1, 2$.
β_*	Transmission of both infections from co-infected individuals.
γ_i	Rate of recovery from disease i per unit time, $i = 1, 2$.
γ_*	Rate of recovery from both diseases by co-infected individuals.
ϵ	Multiplying factor increasing transmission rate of infection i in presence of infection $j \neq i$.
ρ	Retardation of recovery rate from a single infection when co-infected.

Process	Description of label in Figure 7-1
$\bullet$	Transmission of single infection.
$\bullet\bullet$	Simultaneous transmission of both infections.
$\circ$	Transmission influenced by increased susceptibility due to extant infection.
$\square$	Recovery from a single infection.
$\square\square$	Simultaneous recovery from two infections.
$\Diamond$	Recovery from a single infection hampered by co-infection.

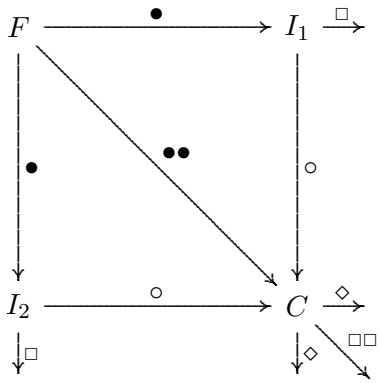

Figure 7-1: *Scheme showing transition between states for a population infected by two interacting SIS processes. All transitions to the right involve the first disease and all downward transitions involve the second. The edges should be thought of as being identified. The labels and transitions for the states are described in Table 7.1*

make the assumption that co-infected individuals will transmit both infections upon contact with individuals with no infection. The single disease is transmitted at rate β_i for $i = 1, 2$ and both are transmitted at a rate β_*. Very little is known about what β_* is likely to be - a case of simultaneous transmission of Syphilis and HIV is given in [33] but there is no mention of what the transmission probabilities might be. Similar difficulties abound concerning whether individuals recover simultaneously from both infections at once or not. Since our definition of recovery does not preclude treatment and because sexually transmitted infections that often occur together can be treated effectively with antibiotics (for example, Chlamydia and Gonnorhoea), we choose to investigate scanarios in which $\gamma_* > 0$.

Initially assuming that transmission between individuals occurs according to the law of mass action, these processes can be summarised in the following set of ordinary differential equations:

$$\begin{aligned}
\frac{\mathrm{d}F}{\mathrm{d}t} &= -\beta_1 I_1 F - \beta_2 I_2 F - \beta_* C F + \gamma_1 I_1 + \gamma_2 I_2 + \gamma_* C \\
\frac{\mathrm{d}I_1}{\mathrm{d}t} &= \beta_1 I_1 F - \epsilon\beta_2 I_2 I_1 - \epsilon\beta_2 C I_1 + \rho\gamma_2 C - \gamma_1 I_1 \\
\frac{\mathrm{d}I_2}{\mathrm{d}t} &= \beta_2 I_2 F - \epsilon\beta_1 I_1 I_2 - \epsilon\beta_1 C I_2 + \rho\gamma_1 C - \gamma_2 I_2 \\
\frac{\mathrm{d}C}{\mathrm{d}t} &= \beta_* C F + \epsilon(\beta_1 + \beta_2) I_1 I_2 + \epsilon\beta_2 C I_1 + \epsilon\beta_1 C I_2 - \rho(\gamma_1 + \gamma_2) C - \gamma_* C,
\end{aligned} \tag{7.5}$$

where Table 7.1 summarises the states, parameters and processes occurring within.

We use this linear version of the model to investigate the effects of the co-infection parameters ϵ and ρ. The Jacobian for (7.5) is

$$\mathcal{J} = \begin{bmatrix} -\beta_1 I_1 - \beta_2 I_2 - \beta_* C & -\beta_1 F + \gamma_1 & -\beta_2 F + \gamma_2 & -\beta_* F + \gamma_* \\ \beta_1 I_1 & \beta_1 F - \epsilon\beta_2(I_1 + C) - \gamma_1 & -\epsilon\beta_2 I_1 & -\epsilon\beta_2 I_1 + \rho\gamma_2 \\ \beta_2 I_2 & -\epsilon\beta_1 I_2^e & \beta_2 F - \epsilon\beta_1(I_2 + C) - \gamma_2 & -\epsilon\beta_1 I_2 + \rho\gamma_1 \\ \beta_* C & \epsilon(\beta_1 + \beta_2) I_2 - \epsilon\beta_2 C & \epsilon(\beta_1 + \beta_2) I_1 - \epsilon\beta_1 C & -a_{14} - a_{24} - a_{34} \end{bmatrix}. \tag{7.6}$$

Let us consider the equilibrium $(\frac{\gamma_1}{\beta_1}, N - \frac{\gamma_1}{\beta_1}, 0, 0)$ that represents a persistent single infection. In Figure **??**, we see that by numerically computing the eigenvalues of the Jacobian (7.6) as evaluated at this equilibrium for increasing values of ϵ, it is unstable. That is to say that the introduction of small number of infectives with the second disease will lead to the system departing from this equilibrium.

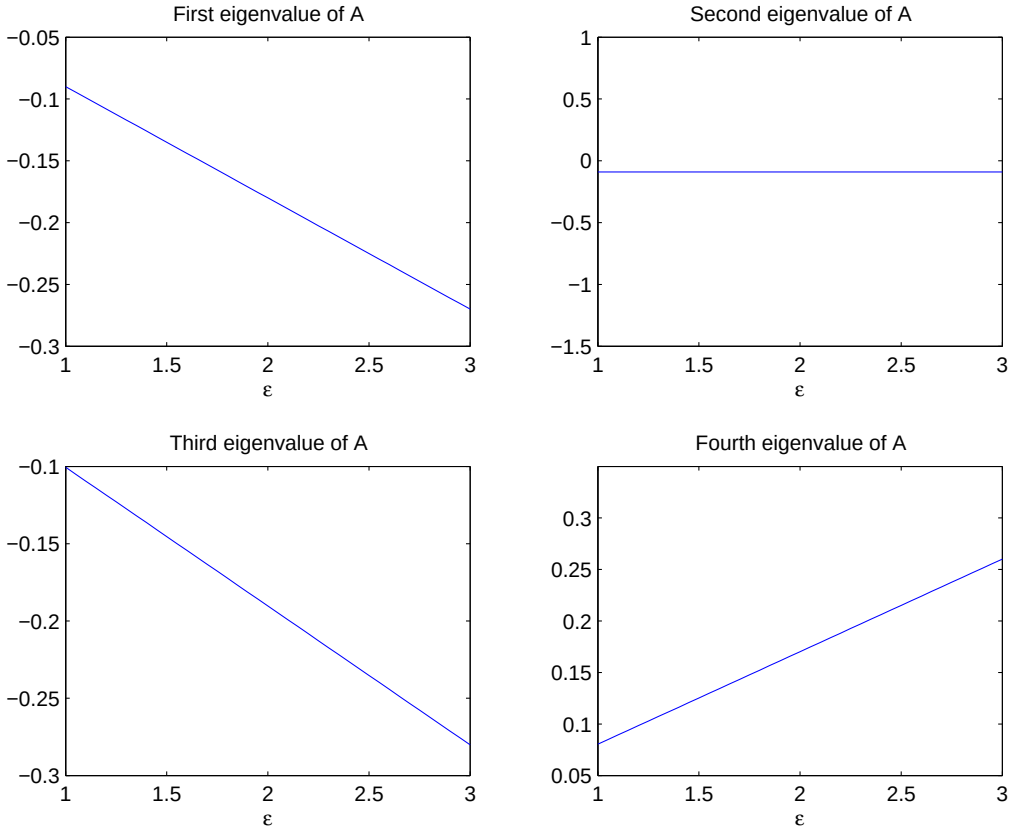

Figure 7-2: *Eigenvalues of the Jacobian matrix $\mathcal{J}$ for equations (7.5), for an equilibrium with respect to the first disease. Parameters used: $\beta_1 = \beta_2 = 10^{-5}$; $\gamma_1 = \gamma_2 = 0.01$; $\epsilon = 1.1$; $\rho = 1$; $N = 10000$; $F^* = \frac{\gamma_1}{\beta_1}$; $I_1^* = N - \frac{\gamma_1}{\beta_1}$ and $I_2^* = C^* = 0$. For β_* and γ_*, we assume $\beta_* = \beta_1\beta_2$ and $\gamma_* = \gamma_1\gamma_2$.*

7.2.2 Adding contact structure

We now incorporate a nonlinear incidence function into the model, a means of introducing contact structure by proxy, as discussed in Chapters 5 and 6. We have seen from the homogeneous mixing model that the second disease can enter a population where the first persists. We are now interested in whether such contact structure can impede or assist the co-infection process.

We use the nonlinear incidence functions introduced in Chapter 5, namely

$$H(X,Y) = X^p Y, \tag{7.7}$$

where X is the source of infection and Y the target population for that infection. We generalise in this fashion since there are multiple source and target compartments throughout this model, as detailed in Figure 7-1. Numerical results have suggested that using

$$H(X,Y) = X^p Y^q \tag{7.8}$$

may also be desirable for some networks, but for many structures $q \approx 1$ is sufficient. Furthermore, in the analysis of such systems, it is found that q plays only a supplementary role as the exponents are varied.

As such, taking into account the incidence function (7.7), the equations are now:

$$\begin{aligned}
\frac{\mathrm{d}F}{\mathrm{d}t} &= -\beta_1 I_1^p F - \beta_2 I_2^p F - \beta_* C^p F + \gamma_1 I_1 + \gamma_2 I_2 + \gamma_* C \\
\frac{\mathrm{d}I_1}{\mathrm{d}t} &= \beta_1 I_1^p F - \epsilon\beta_2 I_2^p I_1 - \epsilon\beta_2 C^p I_1 + \rho\gamma_2 C - \gamma_1 I_1 \\
\frac{\mathrm{d}I_2}{\mathrm{d}t} &= \beta_2 I_2^p F - \epsilon\beta_1 I_1^p I_2 - \epsilon\beta_1 C^p I_2 + \rho\gamma_1 C - \gamma_2 I_2 \\
\frac{\mathrm{d}C}{\mathrm{d}t} &= \beta_* C^p F + \epsilon\beta_1 I_1^p I_2 + \epsilon\beta_2 I_2^p I_1 + \epsilon\beta_2 C^p I_1 + \epsilon\beta_1 C^p I_2 \\
&\quad - \rho(\gamma_1 + \gamma_2) C - \gamma_* C.
\end{aligned} \tag{7.9}$$

Unfortunately, (7.9) is not amenable to analysis for $p \neq 1$, so we proceed with numerical solutions in order to determine the impact of p, ϵ and ρ on the outcome of the diseases. Figure 7-3 shows the solutions of (7.9) for the case of two identical infections and for two dissimilar infections (a minor and a major infection). We assume a larger number of infectives for the first infection, so that the solutions for I_1 and I_2 can be distinguished when the diseases are the same.

For the identical infections, we have co-infection arising as the individual infections

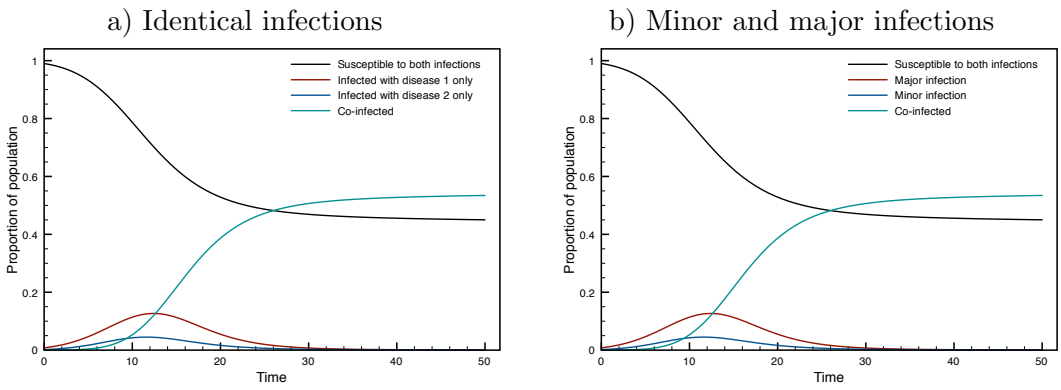

Figure 7-3: *Solutions of (7.9) for two scenarios relating to the difference in transmission rates for each infection rate. Parameters used: a)* $N = 10000$*;* $p = 0.8$*;* $\epsilon = 4$*;* $\rho = 0.8$*;* $\beta_1 = \beta_2 = 0.00011$*;* $\beta_* = \beta_1\beta_2$*;* $\gamma_1 = \gamma_2 = 0.0001$*;* $\gamma_* = \gamma_1\gamma_2$*. b) As a), with* $\beta_1 = 0.00011$*;* $\beta_2 = 0.00017$*;* $\gamma_1 = 0.0001$ *and* $\gamma_2 = 0.00018$*. In both cases there were initially* 80 *individuals with disease* 1 *and* 20 *with disease* 2*.*

take hold within the population. Eventually, the individual infections are suppressed and nearly all infected individuals are co-infected by the time equilibrium is reached. In the case of a minor and major infection the result is similar. The minor infection is quickly overtaken by the major infection allowing co-infection to take hold. As a result, a far larger proportion of the population is co-infected at equilibrium.

We now concentrate on two identical infections and examine the effect of the parameter ϵ on the number of co-infected individuals at equilibrium. Within this, we study three values of p in order to ascertain the effect of contact structure. Figure 7-4 shows the number of co-infected individuals at equilibrium in solutions of (7.9) when ϵ is increased. We consider the outcomes for different parameter values in the left and right hand figures.

We can see from Figure 7-4 that contact structure does indeed play a role in determining the number of co-infected individuals at equilibrium. Whilst for all values of p increasing ϵ increases the number of such individuals, the same effect is suppressed for larger values of p. As we have seen in Chapter 5, most contact structures examined therein produce a value of $p < 1$, suggesting that on true contact structures the effect of co-infection may be greater than that purported by a mean field model.

There is not a great deal of difference in outcome between the subfigures of Figure 7-4, though there are larger equilibrium values for the more aggressive co-transmission rates. Furthermore, there is a slight 'decrease' in the number of co-infected individuals at equilibrium for values of p greater than one in the first subfigure. This is due to

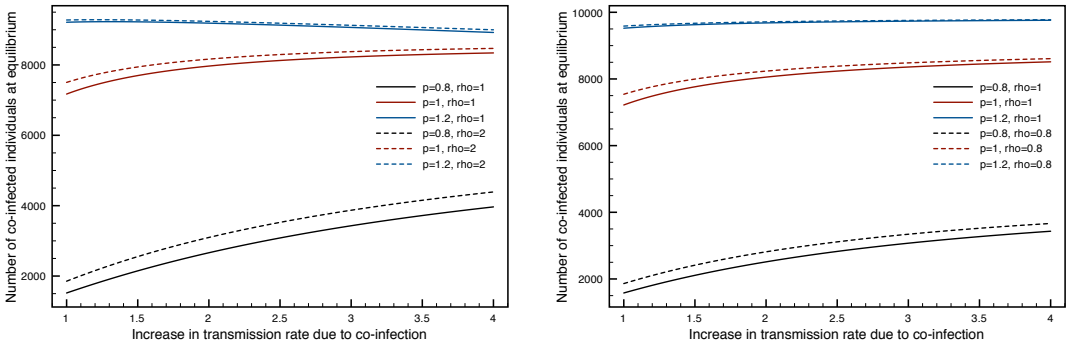

a) b)

Figure 7-4: *The number of co-infected individuals at equilibrium from numerical solutions of (7.9) are plotted against the increase in transmission probability in the case of superinfection, as given by* ϵ*. Parameters used: On both subfigures we use* $N = 10000$*;* $\beta_1 = \beta_2 = 10^{-5}$*;* $\gamma_1 = \gamma_2 = 0.01$*. On a) we have* $\beta_* = 10^{-10}$ *and* $\gamma_* = 10^{-4}$ *and on b) we have* $\beta_* = \beta_1$ *and* $\gamma_* = \gamma_1$*. Values of* p *and* ρ *are as stated on each subfigure.*

the system (7.9) tending towards a state in which wholly susceptible and co-infected individuals dominate the population. In this setting, the low transmission and recovery rates imposed for simultaneous infection and recovery ensure a slower progression to equilibrium. Figure 7-4a) therefore does not show the true equilibrium values for $p = 1.2$ as the system has yet to attain this state. Nevertheless we present these results alongside the true equilibria attained when $p = 0.8$ and $p = 1$ in order to highlight this phenomenon, which we shall refer to as the slow phase from now on.

In Figure 7-4 we also plot the effects of a decrease in ρ to demonstrate the effect this parameter has in varying the number of co-infected individuals at equilibrium. Figure 7-5 shows this in more detail, plotting the number of such individuals as ρ is varied between 0 and 1. Obviously in this setting the case of $\rho = 0$ is effectively a different model, in which all co-infected individuals never recover from a single infection, only from both simultaneously. The case of a small co-recovery rate is even more prescriptive, since the simultaneous recovery rate also depends on ρ and as a result, co-infected individuals remain so permanently. This accounts for much of the differences between the two subfigures of Figure 7-5. In the left hand subfigure, the smooth increase in the number of co-infected individuals at equilibrium is disrupted as ρ approaches zero. At a value of ρ close to zero the number of such individuals begins to decline, which is more significant and occurs for larger values of ρ at larger values of p. This is again due to the accelerated transition to the slow regime of a largely F and C population. Evidence of this is the earlier onset of this phenomenon as ρ decreases for

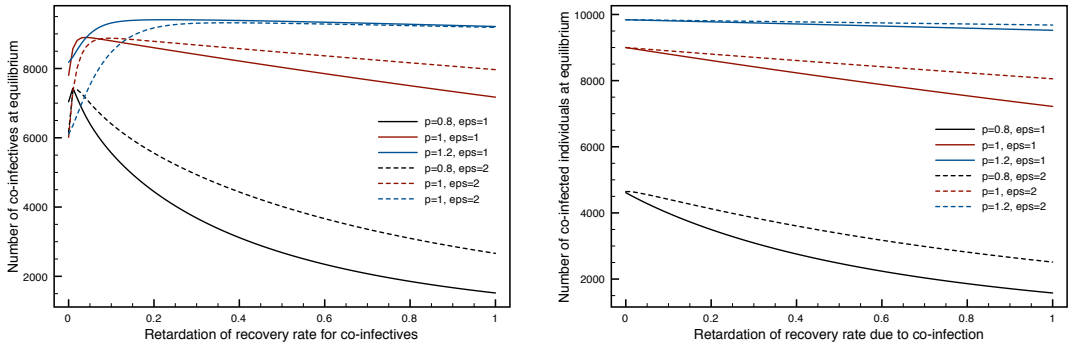

a) b)

Figure 7-5: *The number of co-infected individuals at equilibrium from numerical solutions of (7.9) are plotted against the retardation of the recovery rate for co-infected individuals, as given by ρ. Parameters used: On both subfigures we use $N = 10000$; $\beta_1 = \beta_2 = 10^{-5}$; $\gamma_1 = \gamma_2 = 0.01$. On a) we have $\beta_* = 10^{-10}$ and $\gamma_* = 10^{-4}$ and on b) we have $\beta_* = \beta_1$ and $\gamma_* = \gamma_1$. Values of p and ϵ are as stated on each subfigure.*

the larger value of ϵ shown.

In subfigure 7-5b) the situation is more straightforward and it is easier to discern the effects of increasing p, which is again to increase the number of co-infected individuals as ρ decreases. This is alongside the greater effect of ϵ for lower values of p, commensurate with overcoming the retardation of the infection rate caused by the sublinear exponent.

In Figure 7-6 we plot the number of co-infected individuals at equilibrium for increasing values of p. These figures highlight both the 'slow phase' alluded to previously and the existence of scenarios in which contact structure may aid or inhibit the spread of infection to such an extent that the co-infection parameter ϵ plays no role in determining the outcome.

The variation in the number of co-infected individuals towards equilibrium with p seen in Figure 7-6a) shows the existence of the slow phase and the fact that it occurs earlier and with larger extent for increased values of ϵ. By extending the time interval supplied to the numerical integrator, we can produce a figure that would be more like Figure 7-6b), one that features the smooth increase with p in the number of co-infected individuals at the the final time step. However, the time spans required to achieve the true equilibrium are far longer than those required for the second subfigure. In both subfigures, values of $p < 0.6$ and $p > 1.8$ produce little or no variation in outcome for different values of ϵ. In these cases the infection rate is either retarded ($p < 0.6$) or augmented ($p > 1.8$) by the exponent p to such an extent that the variation with ϵ is proportionately very small.

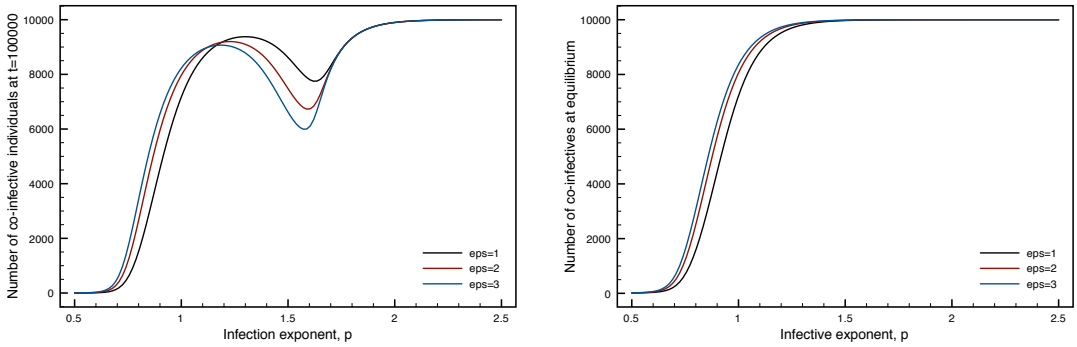

a) b)

Figure 7-6: *The number of co-infected individuals at equilibrium (*100000 *time steps) from numerical solutions of (7.9) are plotted against the infective exponent* p*. Parameters used: On both subfigures we use* $N = 10000$*;* $\rho = 1$*;* $\beta_1 = \beta_2 = 10^{-5}$*;* $\gamma_1 = \gamma_2 = 0.01$*. On a) we have* $\beta_* = 10^{-10}$ *and* $\gamma_* = 10^{-4}$ *and on b) we have* $\beta_* = \beta_1$ *and* $\gamma_* = \gamma_1$*. Values of* p *and* ϵ *are as stated on each subfigure.*

In summary, we see from this triumvirate of figures exploring the effects of varying the co-infection parameters ϵ and ρ, along with the contact structure through the infection exponent p, that the co-infection effects are increased when $p < 1$, a situation corresponding to values of p derived for both lattices and scale-free networks in Chapter 5.

7.2.3 Two SIRS processes

Model formulation We now consider two diseases that follow an SIRS process spreading throughout a population, with the same co-infection effects on transmission and recovery. We assume that loss of immunity to either of the infections is not affected by the other, thus we do not introduce another parameter akin to ϵ and ρ. Our model now has nine states, which are described, along with attendant parameters and processes, within Table 7.2. Transition between the states is described in Figure 7-7.

Table 7.2: *Summary of states, parameters and processes featuring in the SIRS co-infection model (7.10).*

State	Description
F	Individuals susceptible to both infections.
I_1	Infected with disease 1, susceptible to disease 2.
I_2	Infected with disease 2, susceptible to disease 1.
C	Infected with both diseases ('Co-infected').
T_1	Recovered from disease 1, susceptible to disease 2.
T_2	Recovered from disease 2, susceptible to disease 1.
P_1	Recovered from disease 1, infected with disease 2.
P_2	Recovered from disease 2, infected with disease 1.
A	Recovered from both diseases.

Parameter	Description
p	Infection exponent, represents contact structure.
β_i	Transmission rate of disease i, $i = 1, 2$.
β_*	Transmission of both infections from co-infected individuals.
γ_i	Rate of recovery from disease i per unit time, $i = 1, 2$.
γ_*	Rate of recovery from both diseases by co-infected individuals.
ν_i	Rate at which immunity to infection i is lost.
ν_*	Rate at which immunity to both infections is lost simultaneously.
ϵ	Multiplying factor increasing transmission rate of infection i in presence of infection $j \neq i$.
ρ	Retardation of recovery rate from a single infection when co-infected.

Process	Description of label in Figure 7-7
$\bullet$	Transmission of single infection.
$\bullet\bullet$	Simultaneous transmission of both infections.
$\circ$	Transmission influenced by increased susceptibility due to extant infection.
$\square$	Recovery to from a single infection.
$\square\square$	Simultaneous recovery from two infections.
$\Diamond$	Recovery from a single infection hampered by co-infection.
$-$	Loss of immunity from a single disease.
$--$	Simultaneous loss of immunity to both diseases.

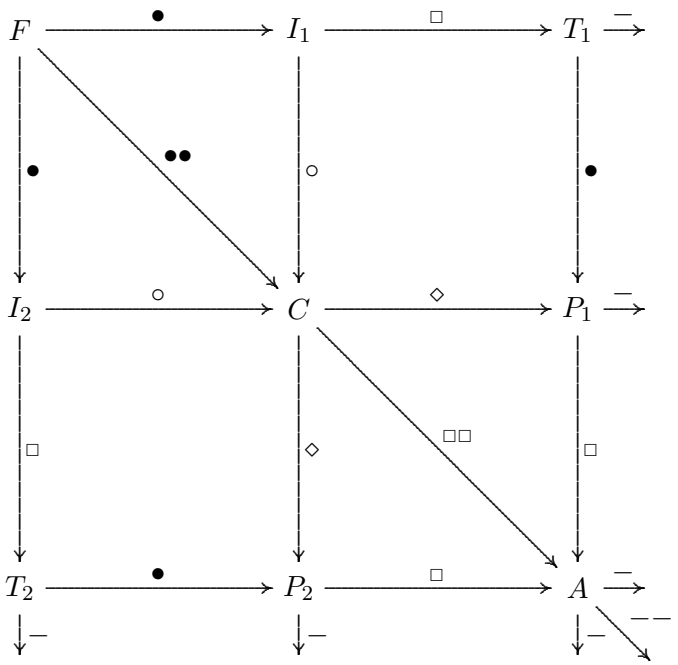

Figure 7-7: *Scheme showing transition between states for a population infected by two interacting SIRS processes. All transitions to the right involve the first disease and all downward transitions involve the second. The edges should be thought of as being identified. The labels for the transitions and the states are described in Table 7.2.*

These processes can be encapsulated in the following set of differential equations:

$$
\begin{aligned}
\frac{\mathrm{d}F}{\mathrm{d}t} &= -\beta_1 I_1^p F - \beta_2 I_2^p F - \beta_* C^p F - \beta_2 P_1^p F - \beta_1 P_2^p F \\
&\quad + \nu_1 T_1 + \nu_2 T_2 + \nu_* A \\
\frac{\mathrm{d}I_1}{\mathrm{d}t} &= -\epsilon\beta_2 I_2^p I_1 - \epsilon\beta_2 C^p I_1 + \beta_1 I_1^p F + \beta_1 P_2^p F + \nu_2 P_2 - \gamma_1 I_1 \\
\frac{\mathrm{d}I_2}{\mathrm{d}t} &= -\epsilon\beta_1 I_1^p I_2 - \epsilon\beta_1 C^p I_2 + \beta_2 I_2^p F + \beta_2 P_1^p F + \nu_1 P_1 - \gamma_2 I_2 \\
\frac{\mathrm{d}C}{\mathrm{d}t} &= \beta_* C^p F + \epsilon\beta_2 C^p I_1 + \epsilon\beta_1 C^p I_2 + \epsilon\beta_2 I_2^p I_1 + \epsilon\beta_1 I_1^p I_2 - \rho(\gamma_1+\gamma_2)C - \gamma_* C \\
\frac{\mathrm{d}T_1}{\mathrm{d}t} &= -\beta_2 I_2^p T_1 - \beta_2 C^p T_1 - \beta_2 P_1^p T_1 - \nu_1 T_1 + \nu_2 A + \gamma_1 I_1 \\
\frac{\mathrm{d}T_2}{\mathrm{d}t} &= -\beta_1 I_1^p T_2 - \beta_1 C^p T_2 - \beta_1 P_2^p T_2 - \nu_2 T_2 + \nu_1 A + \gamma_2 I_2 \\
\frac{\mathrm{d}P_1}{\mathrm{d}t} &= \beta_2 P_1^p T_1 + \beta_2 I_2^p T_1 + \beta_2 C^p T_1 - \nu_1 P_1 - \gamma_1 P_1 + \rho\gamma_1 C \\
\frac{\mathrm{d}P_2}{\mathrm{d}t} &= \beta_1 P_2^p T_2 + \beta_1 I_1^p T_2 + \beta_1 C^p T_2 - \nu_2 P_2 - \gamma_2 P_2 + \rho\gamma_2 C \\
\frac{\mathrm{d}A}{\mathrm{d}t} &= \gamma_1 P_1 + \gamma_2 P_2 + \gamma_* C - (\nu_1 + \nu_2 + \nu_*) A
\end{aligned}
\tag{7.10}
$$

From the nine states we can construct summary variables corresponding to the number of individuals infected with and recovered from each disease. D_i denotes those infected with disease i and R_i those recovered from disease i, for $i = 1, 2$. These are constructed as follows:

$$\begin{aligned} D_1(t) &= I_1(t) + C(t) + P_2(t) \\ D_2(t) &= I_2(t) + C(t) + P_1(t) \\ R_1(t) &= T_1(t) + A(t) + P_1(t) \\ R_2(t) &= T_2(t) + A(t) + P_2(t). \end{aligned} \tag{7.11}$$

We also have a new parameter ν_* describing the rate at which immunity is lost for both infections simultaneously. We assume throughout that

$$\nu_* = \nu_1 \nu_2. \tag{7.12}$$

A specific example In Chapter 5, it was shown that the system of equations (5.3) detailing an SIRS process with nonlinear incidence rate (7.7) can support periodic orbits. We begin our discussion of solutions to (7.10) by investigating what happens to such periodic solutions as infectives with the second disease are introduced and when the co-infection effect is varied.

Figure 7-8 shows what happens to such a periodic orbit as individuals with a second infection are introduced. Throughout this figure, we suppress the effects of co-infection, taking $\epsilon = 1$ and $\rho = 1$. We see that if a small number of individuals with the second infection are introduced, the second disease quickly dies out whilst the first disease continues to persist. However, as the number of individuals with the second infection introduced to the population is increased, both diseases head for a trivial steady state. This is due to the assumption of low values for the transmission and recovery rates for co-infected individuals. These mean that once a solely co-infected population is established, infection cannot be maintained.

Figure 7-9 shows the result of varying the co-infection effect. Expanding upon the scenario of introducing 46 individuals with the second infection as seen in Figure 7-8c); we see that increasing ϵ alone prolongs the existence of the second infection, but that both infections subsequently die out nonetheless. In the second subfigure, we see that as ρ is increased, thereby increasing infection time for co-infected individuals, the system is guided to a steady state. As ϵ is increased in this scenario, we seen that both infections equilibrate at a larger value.

Solving system (7.10) for similar parameter values, but instead assuming larger trans-

mission and recovery rates for co-infected individuals, together with

$$\nu_* = \nu_1, \tag{7.13}$$

we produce some interesting results. These are summarised in Figures 7-10 and 7-11. Figure 7-10 is an analogue of Figure 7-8, in which we increase the number of individuals with the second infection that we introduce. As before, if the number introduced is sufficiently small, the second disease dies out and the first disease continues in its periodic orbit. However, as further such infectives are introduced, we can see that we produce larger periodic cycles of the first infection (as seen in the third subfigure) until the saddle is broached and the first infection is driven toward the trivial equilibrium. As this happens, the second infection emerges and settles into a periodic orbit, replacing the first disease.

The supplantation of the first disease by the second occurs without conferring any co-infection effects to the model. Figure 7-11 shows some of what happens when ϵ and ρ are altered. The first subfigure shows the original system with the introduction of 146 individuals with the second infection, for both $\epsilon = 1$ and $\epsilon = 3$. In this situation, instead of the second disease replacing the first, both die out together. Thus in some situations, co-infection may not necessarily aid the establishment of the incoming infection.

The remaining subfigures all show the effect of increasing ϵ in the situation when the effect of co-infection on recovery time is increased. When $\epsilon = 10$, the introduction of the second infection has little impact and the periodic orbit is only slightly perturbed, as seen in subfigure b). However, in c) as ϵ is increased, we see that both infections are eradicated. Then in subfigure d), with ϵ increased still further, sufficient numbers of co-infected individuals are created and both diseases persist in a co-infected equilibrium.

This example shows that with systems of the nature of (7.10), there are always a large number of results to be obtained, even for the most specific of parameter values. We resorted to these particular examples because of their connection to the results of Figure 5-1 and subsequent work in Chapter 6; also, whilst we have focussed on explaining the effects of parameter changes on the long term behaviour of the system, the phase plane plots here also give a sense of how the system evolves in the intermediate time. However, we now resort to a more general analysis of the effects of contact structure and the co-infection parameters on the long term outcomes of the two diseases as these quantities are continuously varied.

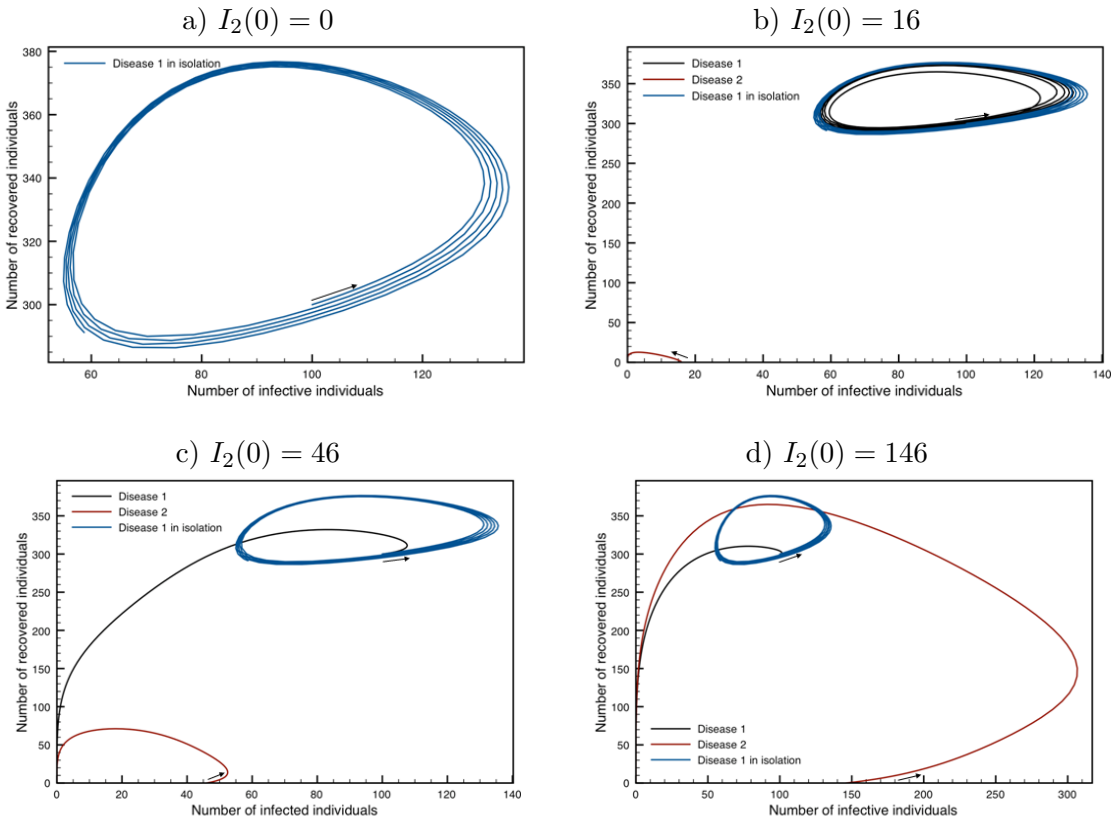

Figure 7-8: *Solutions of system (7.10) converted to the (I_i, R_i) phase plane using (7.11). a) As we have seen in Chapter 5, we can have periodic solutions for a SIRS-type infection with nonlinear incidence, as recreated here with $\beta_2 = \gamma_2 = \nu_2 = 0$. b)-d) For the remaining figures, we introduce increasing numbers of individuals with the second infection. For small values, we see that - as in b) - the second infection dies out, while the first persists in a periodic solution. For larger values, we see that both diseases are eliminated from the population. Parameters used: $N = 546$; $\beta_1 = \beta_2 = 10^{-5}$; $\beta_* = \beta_1\beta_2$; $\gamma_1 = \gamma_2 = 0.1$; $\gamma_* = \gamma_1\gamma_2$; $\nu_1 = \nu_2 = 0.025$; $\nu_* = \nu_1\nu_2$; $p = 2$; $\rho = 1$; $\epsilon = 1$.*

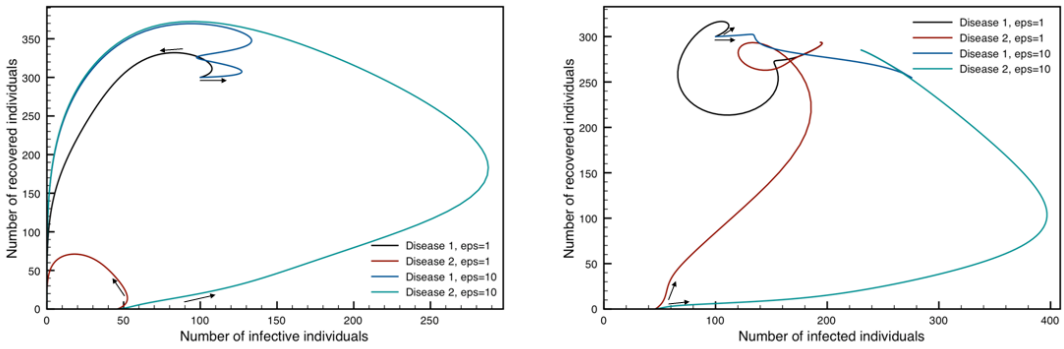

Figure 7-9: *Solutions of system (7.10) converted to the* (I_i, R_i) *phase plane using (7.11). Left: If we increase the probability of transmission for superinfection events by increasing the parameter* ϵ*, the two infections can be sustained for longer, with a larger outbreak of the second infection. However, the system still tends to a trivial steady state. Right: If we also decrease* ρ *so that co-infected individuals are infected for longer, we see that a positive equilibrium can be reached. In this situation increasing* ϵ *produces more infectives at equilibrium. Parameters used:* $N = 546$*;* $\beta_1 = \beta_2 = 10^{-5}$*;* $\beta_* = \beta_1\beta_2$*;* $\gamma_1 = \gamma_2 = 0.1$*;* $\gamma_* = \gamma_1\gamma_2$*;* $\nu_1 = \nu_2 = 0.025$*;* $\nu_* = \nu_1\nu_2$*;* $p = 2$*;* $\rho = 1$ *(left) and* $\rho = 0.1$ *(right);* ϵ *is as stated for each subfigure.*

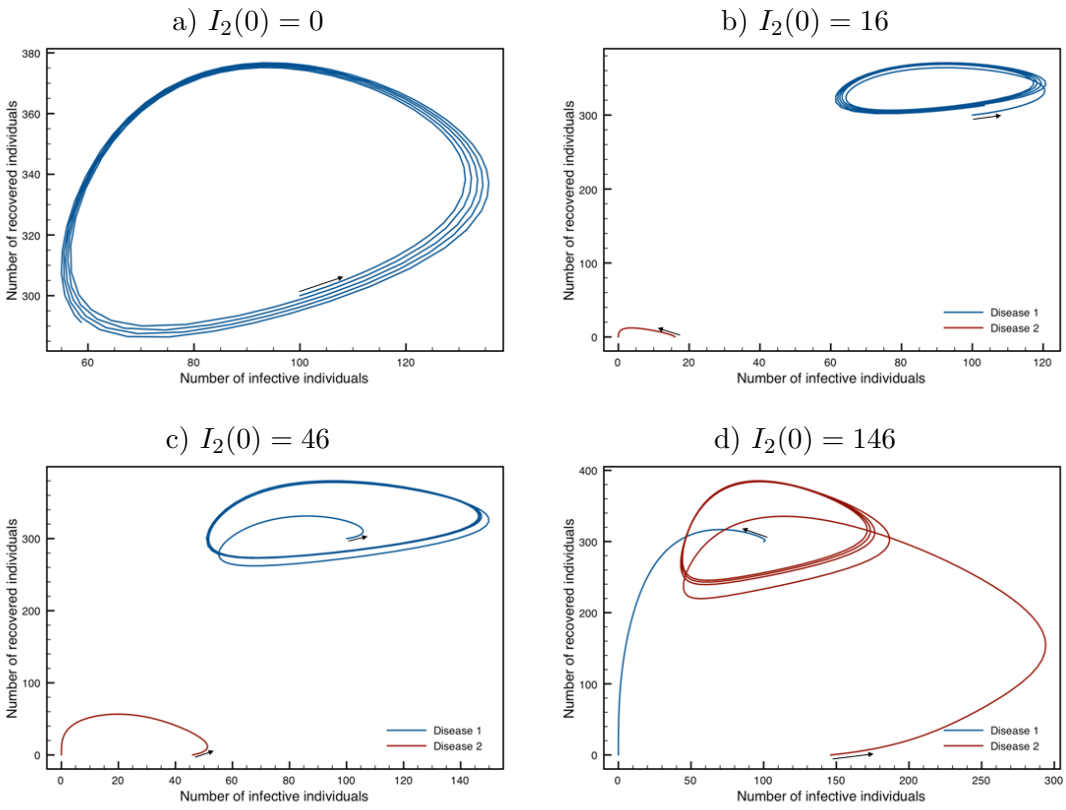

Figure 7-10: *Solutions of system (7.10) converted to the (I_i, R_i) phase plane using (7.11), with transmission, recovery and loss of immunity rates adjusted for co-infected individuals. a) As we have seen in Chapter 5, we can have periodic solutions for a SIRS-type infection with nonlinear incidence, as recreated here with $\beta_2 = \gamma_2 = \nu_2 = 0$. b)-d) For the remaining figures, we introduce increasing numbers of individuals with the second infection. For small values, we see that - as in b) - the second infection dies out, while the first persists in a periodic solution. As more individuals with the second infection are introduced, we see that the second disease enters a periodic orbit as the first is eliminated from the population. Parameters used: $N = 546$; $\beta_1 = \beta_2 = \beta_* = 10^{-5}$; $\gamma_1 = \gamma_2 = \gamma_* = 0.1$; $\nu_1 = \nu_2 = \nu_* = 0.025$; $p = 2$; $\rho = 1$; $\epsilon = 1$.*

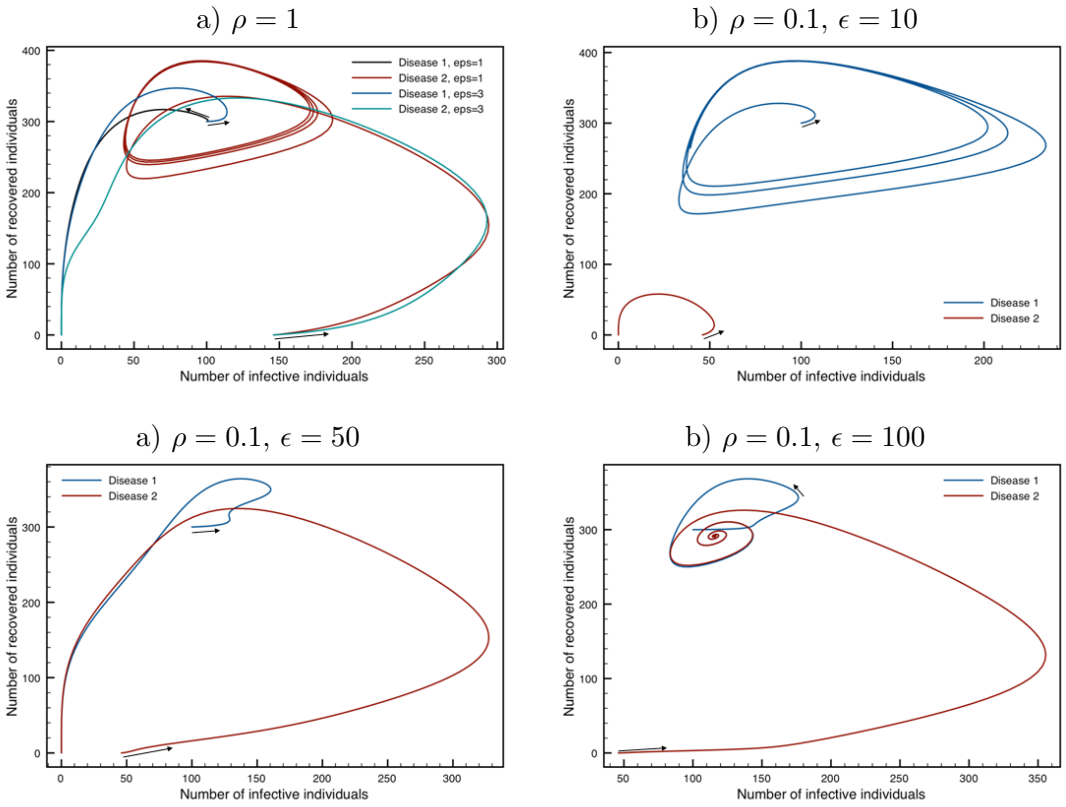

Figure 7-11: *Some solutions of (7.10) reconstructed for the phase plane using (7.11), with transmission, recovery and loss of immunity rates adjusted for co-infected individuals. In subfigure a) we show how increasing ϵ prevents the second disease from establishing itself. In this situation, both diseases die out. The remaining three subfigures show what happens as ϵ is increased for a smaller value of ρ and the introduction of 50 individuals with the second infection. In b), the first disease continues to persist and the second disease makes no impact, as when $\rho = 1$. In c), increasing ϵ by a small amount drives both diseases to a trivial equilibrium; meanwhile, in d), larger values of ϵ contribute to a nontrivial and co-infected equilibrium for both diseases. Parameters used: $N = 546$; $\beta_1 = \beta_2 = \beta_* = 10^{-5}$; $\gamma_1 = \gamma_2 = \gamma_* = 0.1$; $\nu_1 = \nu_2 = \nu_* = 0.025$; $p = 2$.*

General effect of structure on co-infection Moving on to more general scenarios, we explore the effect of contact structure on the response of two SIRS infections to variation in the co-infection effect. Figures 7-12, 7-13 and 7-14 are analogues of earlier figures produced for the dual SIS system. In the context of the dual SIRS model we solve system (7.10) and alongside the same simultaneous transmission and recovery rates β_* and γ_*, we use (7.12) for the left hand figures and (7.13) for right hand figures.

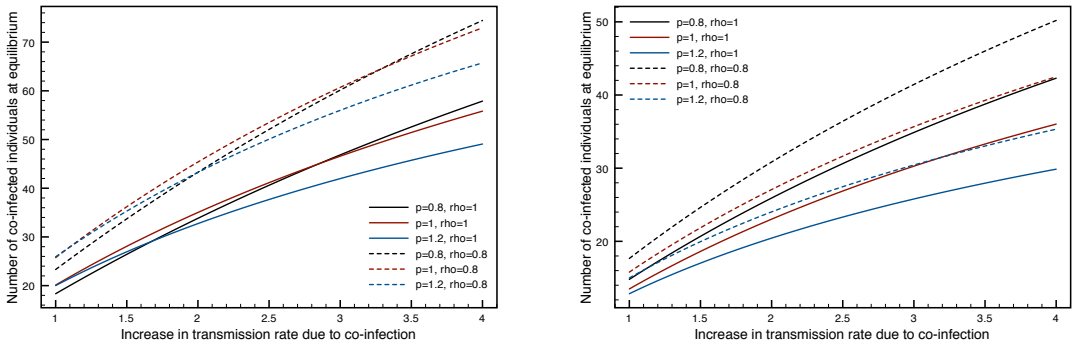

a) Using $\beta_* = \beta_1\beta_2$, $\gamma_* = \gamma_1\gamma_2$ and ν_* from (7.12)

b) Using $\beta_* = \max(\beta_1, \beta_2)$, $\gamma_* = \min(\gamma_1, \gamma_2)$ and $\nu_* = \nu_1$

Figure 7-12: *The number of co-infected individuals at or near to equilibrium from numerical solutions of (7.10), plotted against the increase in transmission probability in the case of superinfection, as given by* ϵ*. Parameters used:* $N = 10000$*;* $\beta_1 = \beta_2 = 10^{-5}$*;* $\gamma_1 = \gamma_2 = 0.01$*;* $\nu_1 = \nu_2 = 0.025$*; together with values of* p*,* ρ*,* β_**,* γ_* *and* ν_* *as stated on each subfigure.*

Figure 7-12 shows how the number of co-infected individuals at equilibrium varies with ϵ for different values of p and ρ. In the left hand subfigure, we see that there is a change in outcome with respect to p as ϵ increases. When there is no co-infection effect and $\epsilon = 1$, larger values of p favour co-infectives at equilibrium. However, as ϵ increases, the smaller values of $p < 1$ favour co-infectives at equilibrium. This behaviour does not change as ρ is decreased. In the right hand subfigure, things are more straightforward, the sublinear incidence rates always produce a greater number of co-infectives at equilibrium, whilst larger values of ϵ produce greater variations in the number of such individuals across values of p. Both subfigures therefore show that contact structure plays an important role in determining the outcomes of co-infection.

Figure 7-13 examines how the number of co-infected individuals at equilibrium varies with ρ for different values of p and ϵ. Here the left subfigure exhibits variations in outcome with respect to contact structure if $\rho < 0.5$. For $\rho > 0.5$ there is little or no variation in the number of co-infected individuals at equilibrium for the values of p considered. Increasing ϵ increases the size of the equilibrium and causes the appearance

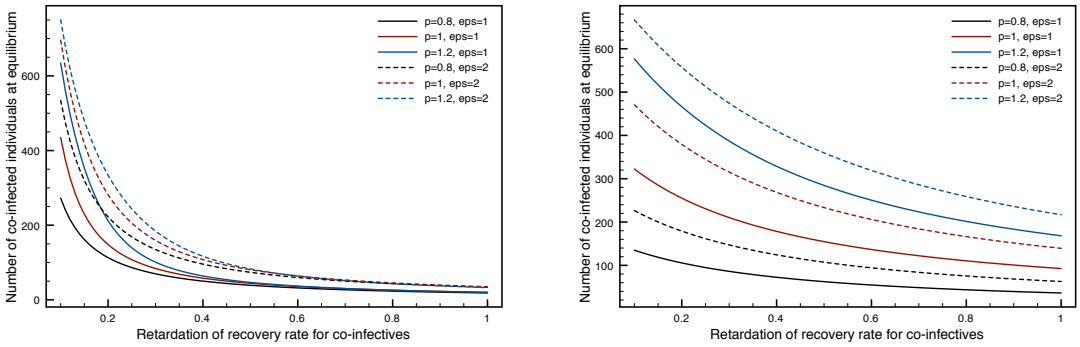

a) Using $\beta_* = \beta_1\beta_2$, $\gamma_* = \gamma_1\gamma_2$ and ν_* from (7.12)

b) Using $\beta_* = \max(\beta_1, \beta_2)$, $\gamma_* = \min(\gamma_1, \gamma_2)$ and $\nu_* = \nu_1$

Figure 7-13: *The number of co-infected individuals at or near to equilibrium from numerical solutions of (7.10), plotted against the retardation of the recovery rate for co-infected individuals, as given by ρ. Parameters used: $N = 10000$; $\beta_1 = \beta_2 = 10^{-5}$; $\gamma_1 = \gamma_2 = 0.01$; $\nu_1 = \nu_2 = 0.025$; together with values of p, ϵ, β_*, γ_* and ν_* as stated on each subfigure.*

of variation with respect to p to occur at a higher value of ρ.

As with the SIS model, $\rho = 0$ represents the special case of of preventing all recovery from the co-infected state in the case when the co-recovery rate is chosen to be the same as that for a single disease. Therefore as $\rho \to 0$, the number of co-infected individuals at equilibrium increases to this optimum level of co-infection. Note that we only plot values of ρ down to 0.1 in order to capture the detail of what is happening for intermediate values of ρ. In the case of $\rho = 0$, for all values of p and ϵ, we have the entire population co-infected at equilibrium.

In the right hand figure, we see variation across contact structure for all values of ρ. Because the assumption of a larger recovery rate permits simultaneous recovery from both infections even as $\rho \to 0$, we have that the sole effect of decreasing ρ in this fashion is to prolong the period of co-infection. As a result, more such individuals are found at equilibrium. Moreover, this explains why the larger values of the exponent p lead to larger numbers of co-infected individuals at equilibrium since this causes the recruitment of more co-infectives as the duration of co-infection is prolonged.

Figure 7-14 shows how the number of co-infected individuals towards equilibrium varies as the infection exponent p is increased. As with Figure 7-6 both the slow phase for intermediate values of p, and the lack variation in outcome with respect to the co-infection effect for extremal values of p, are again exhibited here. The slow phase because we have used transmission, recovery and loss of immunity rates that are unable

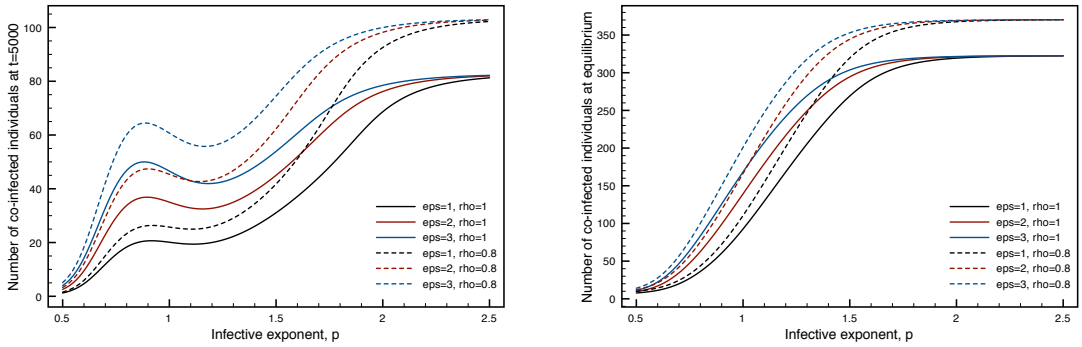

a) Using $\beta_* = \beta_1\beta_2$, $\gamma_* = \gamma_1\gamma_2$ and ν_* from (7.12)

b) Using $\beta_* = \max(\beta_1, \beta_2)$, $\gamma_* = \min(\gamma_1, \gamma_2)$ and $\nu_* = \nu_1$

Figure 7-14: *The number of co-infected individuals at or near to equilibrium from numerical solutions of (7.10), plotted as the infection exponent p is increased. Parameters used:* $N = 10000$*;* $\beta_1 = \beta_2 = 10^{-5}$*;* $\gamma_1 = \gamma_2 = 0.01$*;* $\nu_1 = \nu_2 = 0.025$*; together with values of* ϵ*,* β_**,* γ_* *and* ν_* *as stated on each subfigure.*

to sustain co-infected individuals in the absence of singly-infected individuals. The right hand figure shows a smooth increase in the number of co-infected individuals at equilibrium as p increases, with larger numbers as ϵ is increased and ρ is decreased. As was the case with the dual SIS system, we find that the number of time steps required to achieve a true equilibrium is many times greater for the first choice of the parameters β_*, γ_* and ν_* than for the second.

Overall these figures show that whilst co-infection is suppressed in the case of two SIRS processes when compared with the dual SIS process, the effect of the parameters that describe it have broadly similar effects on the outcome. However, the value of p plays a larger role in co-infection than in the case of the two SIS processes, as it would in a model of a single disease in a population. The nonlinear SIRS process produces a rich variety of behaviours when spreading alone, as has been seen in the results summarised in Chapter 5, so the fact that model (7.10) produces such an array of results is to be expected.

7.3 Computer simulations of co-infection

We use computer simulations to confirm the results of our mathematical models and to explore further the effects of contact structure. Beyond this, we investigate more complicated processes that can be more easily modelled with simulations than with sets of ordinary differential equations. This includes the incorporation of multiple core

groups into the model.

7.3.1 Comparison with the mathematical models

We simulate the spread of two infections on a network with the same co-infection effects as in the mathematical model. The transmission rate for the i^{th} disease is $\epsilon\beta_i$ with $\epsilon \geq 1$ in cases of superinfection, and the recovery rate from the i^{th} infection is $\rho\gamma_i$ with $\rho \leq 1$ for co-infected individuals.

Unlike in the mathematical model, we do not have to consider the simultaneous transmission of both diseases when a co-infected individual comes into contact with one entirely free from infection. Instead, we can allow the potential for two transmission events (one of each disease) to occur within a single time step. As a result, the experiments we perform place more emphasis on the roles of the co-infection parameters in determining the outcome, rather than the choice of the simultaneous transmission, recovery and (where applicable) loss of immunity rates β_*, γ_* and ν_*, which often entered into the discussion for the mathematical model.

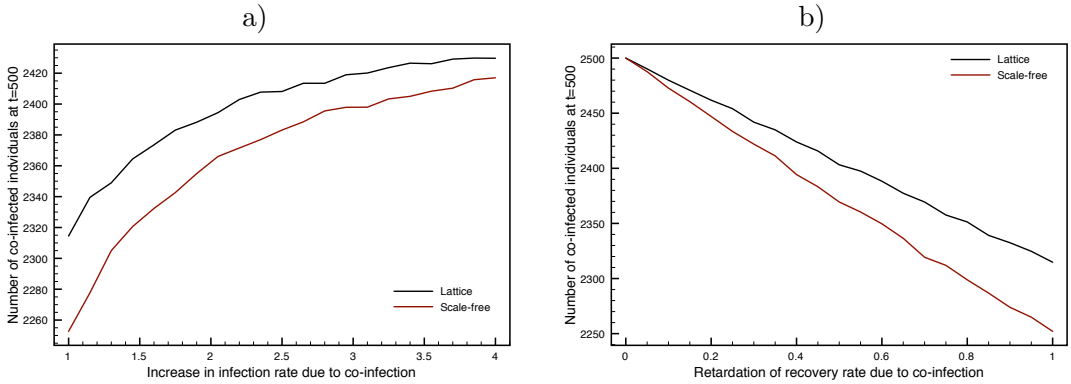

Figure 7-15: *Results of simulations of two SIS processes spreading on a network with co-infection effects. In the left hand figure, the number of co-infected individuals after five hundred time steps is plotted for increasing values of ϵ, the increase in transmission rate for superinfection. In the right hand figure, ϵ is fixed at 1 while ρ - the retardation of the recovery rate for co-infected individuals - is varied. A lattice and scale-free network were used, each having an average degree $z = 6$ and comprising 2500 nodes. Other parameters used: $\beta_1 = \beta_2 = 0.05$; $\gamma_1 = \gamma_2 = 0.01$. Results are the average of fifty repetitions.*

In Figure 7-15, we examine the effect of varying ϵ and ρ on the outcome of two SIS processes spreading on networks comprising 2500 sites. The topologies considered were that of a hexagonal lattice and a scale-free network with average degree $z = 6$. Running

each simulation of the co-infection process for 500 time steps, we take the average of fifty realisations for values of ϵ between 1 and 4. We see from Figure 7-15a) that as ϵ increases, we have more co-infected individuals at the observation time. For fixed ϵ, there are always more such individuals on the hexagonal lattice, though the difference between the networks decreases as ϵ increases.

Referring back to Figure 7-4, which is the analogue for the mathematical system (7.9), we can see a similarity between the simulation results and the solutions of the ODE system. The parameter values used for the simulations are more favourable to the spread of the two diseases, which may explain why so much more of the network is co-infected than one might expect from the predictions of the mathematical model.

In Figure 7-15b), we vary ρ between 0 and 1. With $\rho = 0$ we have the situation in which co-infected individuals never recover, so for both networks at the final time step we have the entire population co-infected. This did not happen in the mathematical model, where in spite of the value of ρ we had a fixed value for γ_*, always allowing for the simultaneous recovery from co-infection. Reading the remainder of the figure from right to left, as ρ decreases to zero from one, the duration of infection increases for co-infected individuals. As a result, the number of co-infected individuals at the de facto equilibrium increases all the while. The increase in the number of co-infectives at end time occurs faster for the scale-free network, as more co-infective hubs can reach a larger proportion of the population as the duration of co-infection is increased.

Figure 7-16 shows the same experiments carried out for two SIRS processes occurring on the same networks. There are fewer co-infectives at equilibrium than for the SIS model, though there are still more on the lattice than for the scale-free network. The left hand subfigure shows qualitatively the same variation in the number of co-infectives at end time as ϵ is varied as for the SIS, with slightly greater variation. In the right hand subfigure, we see very little difference between either network as ρ varies between zero and one. As before, $\rho = 0$ prevents co-infected individuals from ever recovering, so the entire network is again co-infected by the end time step.

7.3.2 Beyond the mathematical models

We now turn our attention to the possibilities afforded to us by computer simulations in the context of modelling co-infection. We consider the case of a population consisting of two equally sized subgroups which are connected with random links in the manner discussed in Chapter 4. With probability r an individual in one population is connected to an individual in the other population.

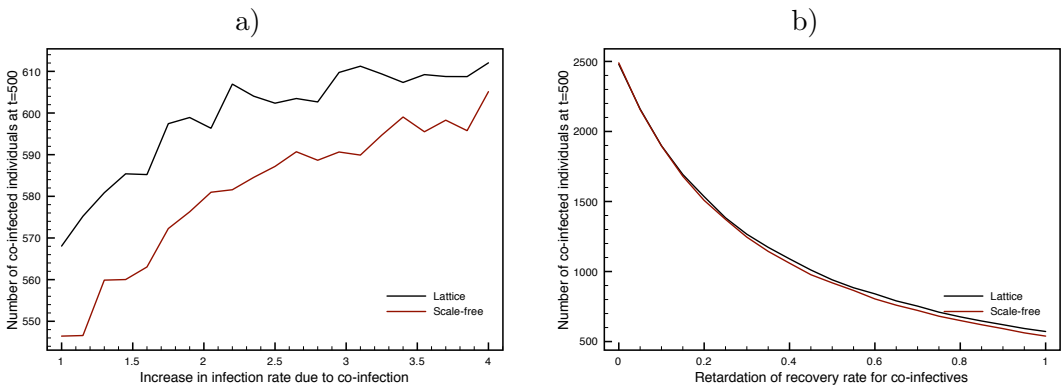

Figure 7-16: *Results of simulations of two SIRS processes spreading on a network with co-infection effects. In the left hand figure, the number of co-infected individuals after five hundred time steps is plotted for increasing values of ϵ, the increase in transmission rate for superinfection. In the right hand figure, ϵ is fixed at 1 while ρ - the retardation of the recovery rate for co-infected individuals - is varied. A lattice and scale-free network were used, each having an average degree $z = 6$ and comprising 2500 nodes. Other parameters used: $\beta_1 = \beta_2 = 0.05$; $\gamma_1 = \gamma_2 = 0.01$ and $\nu_1 = \nu_2 = 0.01$. Results are the average of fifty repetitions.*

We restrict ourselves to the discussion of the spread of two SIS infections and consider three population structures: one comprised of two hexagonal lattices; one composed of two scale-free networks; and one comprising a scale-free network and a hexagonal lattice. In all cases, each subgroup has an average degree of six.

We wish to investigate whether the number of links between subpopulations and the contact structure of the subpopulation affects the number of co-infectives in the population, and how this varies with the co-infection effect on superinfection. In this context, two initial configurations should be considered. First of all, if we regard the subpopulations as demographic core groups then it is logical to assume that both diseases are present in each subgroup initially. However, regarding the subpopulations as geographically distinct core groups may lead us to separate the two diseases into the two subpopulations initially, as different STIs have been seen to be localised, [7,15]. Of course, this separation of diseases can also be regarded in the demographic sense when particular STIs are regarded as being associated with different demographic groups within the population or the practice of risky behaviours, [15].

Figure 7-17 plots the number of co-infected individuals after one hundred and fifty time steps, averaged over fifty realisations, against the increase in transmission rate for superinfections, ϵ. These are repeated for the variation in structure and initial configurations of the diseases, as detailed above.

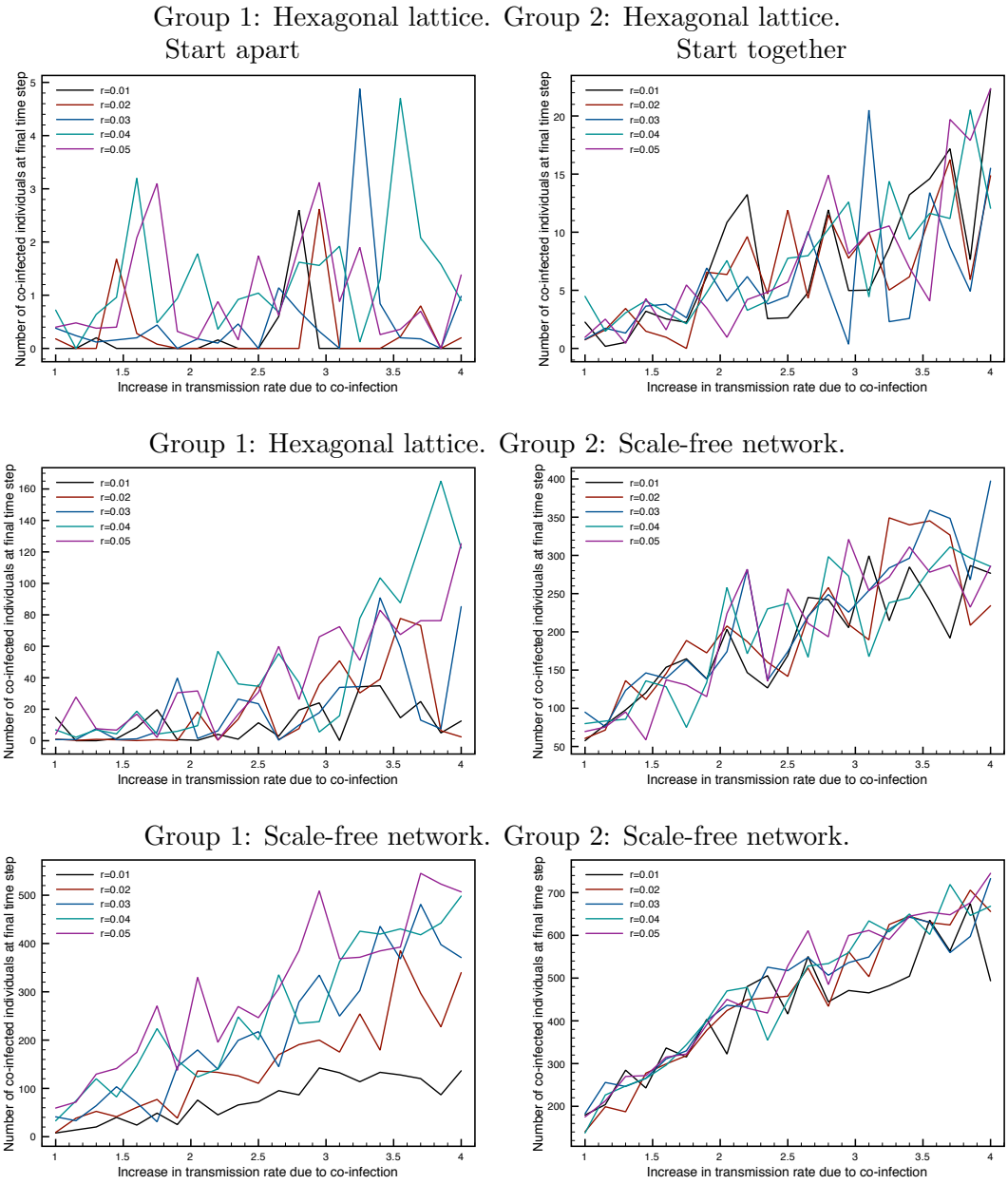

Figure 7-17: *Summary of simulations of SIS processes with co-infection effects, as performed on networks comprising two distinct subgroups. Vertically, the nature of the interacting groups is varied, with variation in the initial conditions occurring horizontally. The parameter r indicates the probability that a member of the population has a neighbour in the other subgroup. In each figure, we plot the number of co-infected individuals after one hundred and fifty time steps against the increase in transmission rate for superinfections. Other parameters used:* $N = 1250$*;* $\beta_1 = \beta_2 = 0.005$*;* $\gamma_1 = \gamma_2 = 0.01$*;* $\rho = 0.99$*. Results are the average of fifty repetitions.*

Starting with the network with two hexagonal lattice subpopulations, we see that if the infections are separated initially, there are practically no co-infectives present at the end of the time interval of the simulations. The two diseases do not intersect often enough for an outbreak of co-infection, even for the higher levels of interaction considered. When the diseases begin in each group, there is still quite a wide variation in outcomes perhaps indicative of the clustered structure of the lattice, nevertheless there is a trend toward larger numbers of co-infectives at end time as the parameter ϵ increases. However, there are still a very small number of such individuals which is indicative either of a smaller outbreak or a slower one.

The second case is for one of the subpopulations to be a scale-free network. In this situation and beginning with the two diseases starting in different groups, we see that there is a trend for the number of co-infected individuals to increase with ϵ and a separation of responses with respect to the group interaction parameter r. This is because on the scale-free subpopulation we have a fast successful outbreak of one infection that ensures the bridging links transmit that infection to the lattice population, on which each disease spreads much more slowly. Obviously, the more such links between subgroups there are, the faster the disease spreads among the lattice subpopulation. Naturally, once there are sufficient numbers of co-infected individuals present in the scale-free population they will spread throughout this group as well. It is perhaps not a surprise that co-infection is more established on this network when both infections begin in each group. The fact that the outbreaks are larger than for the first structure considered is most likely down to the heterogeneous structure of the scale-free subpopulation.

For the network composed of two scale-free subpopulations we see a nice separation in outcomes for different values of r. In this case, both infections spread quickly on each subgroup with the links between them provided opportunities for co-infection to develop. It is then simply the case that the more such links there are, the more co-infectives are produced to spread both diseases throughout the whole network. When both diseases start in each of the subgroups, we see a strong increase in the number of co-infected individuals as ϵ is increased and larger numbers of such individuals. Variation in the number of co-infected individuals between different values of r for a particular value of ϵ is quite large, though when taken proportionally it much smaller than for the lattice-lattice network.

These experiments show that it is possible to build upon simulations of the co-infection process to discuss co-infection in other scenarios of interest, such as on a multicore populations. It is also the case that the process involved here is simply an SIS but others, from SIRS and beyond, can be quickly incorporated into the simulation process.

This means that other features such as vaccination, contact tracing and waiting could easily be incorporated within this simulation framework.

7.4 Discussion

One worry for GUM practitioners is the effects of undiagnosed treatable infections contributing to more malevolent incoming infections such as HIV. A number of sexually transmitted infections can increase susceptibility to other incoming infections, these include vaginal and anal warts [15, 40], and the scarring to internal tissues caused by long term undiagnosed Chlamydia, [8]. We wished to investigate whether the underlying contact structure of the population can contribute to the spread of super-infection, and specifically whether altering the underlying contact structure can in turn change the action of any of the co-infection effects we model.

We considered the spread of two diseases in tandem within a population and model the effects of co-infection in two ways that have been observed in studies of multiple STI acquisition, [33]. First, we modelled the increase in susceptibility that results when an individual comes into contact with a second disease when already infected. This was done by increasing the transmission rate of superinfection by a multiplicative factor ϵ. This is a natural way to present this phenomenon, which is often reported in the literature in these terms: "Chlamydia can increase the probability of HIV acquisition by as much as five times", [8].

The second feature of co-infection modelled was the increased recovery time from either infection when an individual is co-infected. Since our models utilise recovery rates, the reciprocals of which can be regarded as the recovery time when recovery rates are exponentially distributed, we denote by $\rho \leq 1$ the positive scaling factor of the recovery rate for each disease when individuals are co-infected. The reciprocal of ρ can then be regarded as the multiplicative factor for the increase in recovery time.

In addition to these parameters, we also included incidence functions of the form (7.7) as a proxy for examining the effects of contact structure on the establishment, development and outcome of the two diseases. The connection between contact structure and the exponents p and q of the full incidence function (7.8) was developed and discussed in Chapter 5. We use the simplified form (7.7) as it is also shown in Chapter 5 that the exponent of the susceptible population q does not contribute significantly to the mathematical results, and the analysis of the system is aided by the assumption that $q = 1$.

Within this framework, we considered in two models (7.9) and (7.10), the spread of two SIS infections and of two SIRS infections throughout a population, with the co-infection effects represented by ϵ and ρ in place. A reduced form of the dual SIS model which assumed homogeneous mixing of the population was developed in order to explore how a system at equilibrium with respect to one disease evolved as the second disease was introduced, along with how the co-infection parameters impacted on this. This information was supplied by the eigenvalues of the Jacobian matrix (7.6), which showed that the introduction of the second infection destabilised the equilibrium with respect to the first disease.

In terms of the mathematical results, the main difference in these rates for simultaneous events is the creation of two time scales in the model when we choose small values for the co-transmission and co-recovery rates. Whenever co-infectives outnumber the mono-infectives the system approaches equilibrium much more slowly.

We considered the variation of ϵ and ρ and its effect on the number of co-infected individuals at equilibrium for different values of p. In general, the co-infection effects were stronger for $p < 1$. Given that the estimates for the infective exponents from simulations on different contact structures derived in Chapter 5 all produce $p < 1$, this suggests that the results of simulations should show greater response to the co-infection effects than predicted by a mean-field model.

There is of course considerable scope within model (7.10) for further investigation and extension. For example, we have only considered two identical diseases and usually the host population has been considered to be naïve of both infections, whereas in the reality of modelling HIV and Chlamydia say, the latter is clearly established and endemic. Furthermore, the SIS and SIRS processes are rather simplistic and restrictive models for infections that often involve complex diagnosis and treatment patterns, not to mention interventions such as contact tracing. The models could be made more useful by incorporating these features.

The use of the nonlinear incidence function to represent contact structure within the models presented here has been largely symbolic, even given the connection developed in Chapter 5. We have not provided a direct connection between SIRS process data and the corresponding nonlinear incidence model, for example. In the case of the co-infection we also have the additional aspect of there being two distinct diseases, which we have considered to be sufficiently alike that the exponent p is the same for each disease and so on. Even given this assumption, it is not necessarily true that the super-infection process would then have the same exponent p. Clearly, the very nature of this nonlinear model that we have presented deserve further investigation, a

programme for which we present in Chapter 8.

Returning to the co-infection process, we should also consider the fact that the parameters ϵ and ρ have been introduced pragmatically. One could make a case for different values of ϵ for each disease, since the fact that (for example) Chlamydia may well increase the chances of HIV acquisition by up to five times, [8], but there is no reason to suspect that the reverse might be true until confirmed by data. The lack of data about superinfection processes is also a factor here.

If we consider the alternatives to the nonlinear incidence model in constructing a mathematical model for co-infection that incorporates contact structure, we could consider a pairwise equation model. However, such a model would present numerous problems, the chief of which would be the formulation of closures for the system. Even considering just the four state system for two SIS diseases, writing down such triples as

$$[I_1FI_2] \approx f([I_1F], [FI_2], \ldots) \tag{7.14}$$

and attempting to represent the possible outcomes in terms of pairs is a complicated process that would involve presaging the interactions between the diseases - our very motivation for exploring co-infection to begin with!

It is the case then that direct computer simulation is the best alternative to our proposed models. They avoid the technical difficulties of describing any simultaneous events that may occur and allow us to see deeper into the effects of contact structure by the obvious virtue of being directly performed upon them. We ran computer simulation of dual SIS processes and SIRS processes in order to evaluate models (7.9) and (7.10), and to compare the response of different contact structures to the co-infection parameters ϵ and ρ. The results were favourably similar to those of the mathematical model, though parameter variation using simulations of this nature is a computationally intensive and time consuming process meaning that larger networks are difficult to obtain results for.

Nevertheless, the simulations can be quickly extended to take account of multiple subgroups and other variations, something that can complicate and obfuscate a mathematical model. We simulated the spread of the two diseases on a population composed of two subgroups; in this context, we were able to consider both the effects of varying the number of physical links between the groups and of varying the starting configurations of the two diseases. The results of these simulations show a connection to both the co-infection models of this chapter and the multiple subpopulation models of the one previous. This indicates that further models built upon the foundations provided in

this thesis should be consistent with the results herein.

This chapter represents the realisations of the aims stated within Chapter 1; to produce mathematical models that incorporate the contact structure of the population, whilst allowing for the discussion of epidemiological problems unique to sexually transmitted infections. The following chapter summarises the strengths of the project and identifies directions for improvement of the models and for future research.

Chapter 8

Summary and Discussion

8.1 Discussion

This thesis has considered the implications of contact structure for the spread of a disease throughout a population. The standard assumption of homogeneous mixing has been challenged throughout. In Chapter 2, we demonstrated how the outcomes of computer simulations on structures that have been identified with human social contact patterns differ from that predicted by the mean field model. Responses to the differences included the formulation of pairwise models, in which the structure of the network is partially incorporated through the consideration of the disease states of connections between individuals. This works well for lattices because there is a strong intuitive sense of where these connections should be. The model also requires closure in order to prevent an infinite iteration of the model into the use of successively larger combinations of individuals. Again, this process is easier for the lattice and in fact is only really possible on regular structures.

In the case of more heterogeneous networks such as those with a scale-free degree distribution, the pairwise equation models do not give such a good match to simulation data. A pairwise model incorporating degrees of nodes along with the degree states can be formulated but the model produced is large and unwieldy, and reliant upon the degree-degree distribution being reasonably sparse.

In the chapters that comprise the second half of the thesis, the direct incorporation of contact structure into the mathematical models was waived in favour of a more indirect approach. We considered the use of computer simulation to parameterise a nonlinear incidence model. Models such as these often prove controversial due to there being no mechanistic derivation to justify their existence, though in Chapter 5

an empirical connection is established that is consistent across multiple instances of different contact structures. Moreover, we were able to demonstrate that topological features of the underlying contact structure, such as the average shortest path length and the clustering coefficient, play a role in determining the parameters of the model.

This more indirect model for disease transmission means that structure can be considered by proxy. As a result, models for disease transmission can be formulated with one variable for each disease state. This is in contrast with pairwise equations, where n states results in T_n variables for undirected networks and n^2 variables on directed ones, where T_n is the nth triangular number. This is a boon when formulating models for the interaction of multiple core groups.

Prior to the consideration of the nonlinear incidence models, we had set forth a model for a population of multiple core groups utilising pairwise equations as a means of incorporating structure. These models were based on allowing the subgroups to mutually influence one another. In the main, this influence was assumed to be linear, so that the number of infections caused in the receptive subgroup was linearly proportional to the level of infection in the source group. An equivalent mean field model shows that for very small levels of interaction equilibria attained in each group in isolation will subsequently persist despite the interaction. However, in the pairwise equations and the simulations this is not seen, and the smallest of interactions produces a different outcome for each group. This is further evidence of how the homogeneous mixing assumption does not compare favourably with simulation data.

The sensitivity to interaction of equilibria achieved in isolation could not be analytically evaluated for the nonlinear model of Chapter 6, and numerical solutions of particular examples were required in order to investigate this. It was again found that even as small an interaction was introduced, the groups experienced different outcomes. Groups that in isolation exhibit a threshold below which infection cannot be established were found to be able to sustain infection once the interaction was introduced.

Another factor considered was the extent to which interaction between the groups affected the outcome for distinct groups. It was found that if the interaction between groups was sufficiently strong, the structural differences between the groups had no impact on disease outcome. This suggests a mechanism for deciding whether it is worth modelling particular subgroups distinctly.

Throughout the process of modelling multiple groups in this fashion, it was assumed that the influence of one group over another depended linearly on the extent of infection within the source group. However, the simulations performed in Chapter 4 demonstrated that when translating this assumption to the number of links between

groups, the act of physically adding links between the groups had a far more immediate effect than using the corresponding process assumed in the mathematical model. That is to say, on the discrete structure adding a small number of links has a far greater effect on the outcome than the equivalent parameter values for spontaneous infection of a proportion of the receptive population. In Chapter 6, we were motivated by this observation to find an alternative formulation for the interaction between the groups. This was done by creating time series of the number of infections between groups and fitting this to the number of infectives in the source group and the number of susceptibles in the receptive group. Out of this, the nonlinear incidence forms studied in Chapter 5 emerge as credible candidates.

Finally, we have also used nonlinear incidence models in Chapter 7 to investigate the impact of contact structure on the effects of co-infection when two diseases spread on a network. We found that the manner in which simultaneous transmission is modelled had an impact on the outcome. The co-infection effects studied were the advantage conferred to superinfections by individuals already infected by another disease and the extent to which recovery time was prolonged by co-infection. Both were found to contribute to larger numbers of co-infected individuals at equilibrium as their effect was increased. Across different contact structures, as represented by the infection exponent, the effects of co-infection were greater for the sublinear infection rates that we had observed for the contact structures simulated upon in Chapter 5. We were able to confirm the outcomes of the mathematical models using simulations.

In conclusion, we have used computer simulations of diseases spreading on discrete structures to confirm and inform mathematical models relevant to the specific case of sexually transmitted infections.

8.2 Future Work

With the establishment of the connection between simulations and nonlinear incidence models, a number of further developments are possible. Here we discuss examples of such extensions.

Improvement of simulations Throughout all simulations have been performed on static networks of fixed size. The explanation for this has been that we consider the underlying population to have reached an equilibrium with respect to contact structure. However, many studies show that the rate of turnover of partners is a crucial factor in driving the spread of diseases like STIs. Furthermore, it is the formation and

destruction of partnerships that facilitate onward transmission. By their very nature as illicit affairs or transitions between longer term monogamous relationships, concurrent partnerships tend to be transitory.

There is therefore a clear need to incorporate changes in structure into future simulations. Attempts have been made to model a more changeable contact structure in a pairwise equation setting, as in [12], though it may not be necessary to extend the changes in topology directly into mathematical models. Since topological features of contact structure appear to influence estimates for the exponents of the nonlinear incidence model in a consistent fashion, it would be worth investigating how the variation of parameters within simulations featuring dynamic network structure influence the exponents.

Further improvement of nonlinear incidence models Alongside improvement in the simulations from which the parameters of the nonlinear incidence model are estimated, it may be worth considering additional variations of the process as it is detailed in Chapters 5 and 6. There we consider one particular form for the incidence function, along with the SI and SIS models, because they were amenable to linear regression techniques. More sophisticated nonlinear regression techniques may allow estimation of parameters for more sophisticated incidence functions (perhaps ones with more intuitive formulation or less abstract parameterisation) and for more sophisticated epidemiological processes including the SIR and SIRS processes, and beyond.

One possible approach, alluded to in the discussion within Chapter 6, does not actually move beyond linear regression but instead is suggested by the creation of more simulation data. Because each transmission can be tracked within the simulations, we can produce a time series for the incidence that depends on the number of susceptibles and infectives but is not constructed from either. In Chapter 5, the time series for the incidence was inferred from either the number of susceptibles or infectives and the estimation carried out with the other, meaning that only models with two disease states could be considered. However, by constructing the time series of incidence data in this fashion, it can be fitted to both the time series $\{S_t\}$ and $\{I_t\}$, allowing parameter estimates to be performed for more disease processes.

In the co-infection model of Chapter 7, the exponent for the infection process was assumed to be the same throughout the model because the underlying contact structure of the population can be considered to be the same irrespective of which disease is being transmitted. However, for the process of superinfection that produces co-infected individuals, the underlying contact structure depends upon the infection states of members

of the population as well as whatever topology exists between them. For this reason, an attempt should be made to estimate the parameters of the superinfection process from relevant simulation data.

Further epidemiological scenarios Chapter 7 exists to demonstrate how the non-linear incidence models developed in Chapter 5 can be further extended to take account of more sophisticated epidemiological scenarios and used to examine the effect of contact structure.

There are a number of scenarios that could be modelled using the techniques presented in this thesis, such as the effect of waiting times for treatment and the results of interventions such as contact tracing. It is important to consider contact structure within these scenarios since it is possible to measure the effects of health care interventions on factors such as the propensity to take new partners and the number of partners using surveys of attitudes towards sexual behaviour conducted within the target population. The consequences of the resultant change in contact structures can then be evaluated and the financial investment required to bring about such changes can be assessed.

Appendix A

A general structure for epidemic systems

A general structure for epidemic systems is presented in [5], that has been the basis for many stability results for mean-field models in Chapters 3 and 4. In order to present the results from this framework in a clear and concise manner, we have presented them in this appendix. The proofs and further discussion can be found in [5] and the references cited therein.

The results concern solutions of ODEs of the form:

$$\frac{\mathrm{d}z}{\mathrm{dt}} = \mathrm{diag}(z)(e + Az) + (c + Bz), \tag{A.1}$$

where $z \in \mathbb{R}^n_+$ is a vector of the n disease states, A and B are $n \times n$ real constant matrices and c and e are constant n-vectors. The matrix B must satisfy the following conditions:

(i) $b_{ij} \geq 0$, $i, j = 1 \ldots n$,

(ii) $b_{ii} = 0$, $i = 1 \ldots n$,

and the vector c is non-negative.

Solutions to (A.1) are considered on the set $\Omega = \{z_i > 0, i = 1 \ldots n\}$, for which there is at least one positive equilibrium z^* guaranteed by fixed point theorems, provided that the right hand side of (A.1) is continuous. If this is indeed the case, it is helpful to define

$$z^{*-1} := \left(\tfrac{1}{z_1^*}, \ldots, \tfrac{1}{Z_n^*}\right)^{\mathrm{t}}, \tag{A.2}$$

from which a Liapunov function V can be constructed. The derivative of V along trajectories of (A.1) is found to depend on the structure of the following matrix:

$$\tilde{A} := A + \mathrm{diag}(z^{*-1})B. \tag{A.3}$$

The simplest case, resulting in $\dot{V}(z) \leq 0$ for all z with equality if and only if $z = z^*$, arises when

$$-\left[\tilde{A} + \mathrm{diag}\left(\frac{-b_1(z)}{z_1 z_1^*}, \ldots, \frac{-b_n(z)}{z_n z_n^*}\right)\right] \in S_W. \tag{A.4}$$

Here a matrix M belongs to the set of matrices S_W if there exists a positive diagonal real matrix W so that $WM + M^{\mathrm{t}}W$ is positive definite. In this situation, we have the following result:

Theorem A.1. *If system (A.1) admits a strictly positive equilibrium $z^* \in \Omega$, and condition (A.4) holds, then z^* is globally asymptotically stable within Ω. As a consequence of global asymptotic stability, z^* is unique.*

A simpler condition to check is whether $\tilde{A}$ is skew-symmetrisable. A real matrix M is skew-symmetric if $M^{\mathrm{t}} = -M$. A matrix is skew-symmetrisable if there exists a positive diagonal real matrix W such that WA is skew-symmetric.

If $\tilde{A}$ is skew-symmetrisable, then we have a set of zeroes D of the derivative of the Liapunov function V and so we must show that the largest invariant subset of D is a singleton set consisting of z^*. La Salle's invariance principle then guarantees the global asymptotic stability of the equilibrium.

We can ascertain the structure of invariant subsets of D using the following graph theoretic construction that associates a graph to the sign distribution of the matrix $\tilde{A}$:

(i) Each component of z is represented by vertex in the graph. Each of the n vertices is labelled as open or closed according to whether $b_i(z) = 0$ for all $z \in \Omega$. If $b_i(z)$ is constant and zero on Ω, the i^{th} vertex is labelled open, $\circ$, and otherwise closed, $\bullet$.

(ii) Edges are created between the vertices according the sign of elements of $\tilde{A}$. If $\tilde{a}_{ij}\tilde{a}_{ji} < 0$ then the vertices i and j are connected.

The following lemma associates the structure of this graph with the invariant subsets we require:

Lemma A.2. *If $\tilde{A}$ is skew-symmetrisable and the associated graph takes one of the following forms:*

(i) a tree with two of the $n-1$ end vertices that are closed;

(ii) a chain with two consecutive internal vertices that are closed;

(iii) a cycle featuring two consecutive closed vertices;

then the largest invariant subset of D is $\{z^*\}$.

This allows us to state the following analogue of Theorem A.1 for systems in which $\tilde{A}$ is skew-symmetrisable.

Theorem A.3. *If system (A.1) admits a strictly positive equilibrium $z^* \in \Omega$ and the matrix $\tilde{A}$ is skew-symmetrisable, with one of the conditions of Lemma A.2 holding for the associated graph, then z^* is globally asymptotically stable with Ω. As a consequence of global asymptotic stability, z^* is unique.*

The following corollary to Theorems A.1 and A.3 gives a sufficient condition for the existence of a nontrivial endemic equilibrium z^*:

Corollary A.4. *If the vector c in system (A.1) is strictly positive, then it admits a strictly positive equilibrium $z^* \in \Omega_+$. For either of the descriptions of $\tilde{A}$ given in Theorems A.1 and A.3, the positive equilibrium z^* is globally asymptotically stable (and therefore unique) within Ω_+.*

Bibliography

[1] R. Albert and A-L. Barabási. Statistical mechanics of complex networks. *Reviews of Modern Physics*, 74(1):47–97, January 2002.

[2] R.M. Anderson and R.M. May. *Infectious Diseases of Humans: Dynamics and Control*. Oxford University Press, 1991.

[3] I. Beardmore and K.A.J. White. Spreading disease through social groupings in competition. *J. theor. Biol.*, 212:253–269, 2001.

[4] M. Boguna, R. Pastor-Satorras, and A. Vespignani. *Statistical Mechanics of Complex Networks*, volume 625 of *Lecture Notes In Physics*, chapter "Epidemic spreading in complex networks with degree correlations", pages 127–147. Springer, 2003.

[5] V. Capasso. *Mathematical Structures of Epidemic Systems*. Number 83 in Lecture Notes in Biomathematics. Springer-Verlag, 1993.

[6] G. Casanova. *The Story of My Life*. Penguin Classics, 2002.

[7] CDC. HIV prevention through early detections and treatment of other sexually transmitted diseases – united states recommendations of the advisory committee for HIV and STD prevention. *MMWR*, 47(RR12):1–24, 1998.

[8] CDC. STD facts: Chlamydia. CDC website, October 2007. http://www.cdc.gov/std/chlamydia/STDFact-Chlamydia.htm.

[9] O. Diekmann and J. A. P. Heesterbeek. *Mathematical Modelling of Infectious Diseases*. Wiley Series in Mathematical and Computational Biology. Wiley, 2000.

[10] S.N. Dorogovtsev and J.F.F. Mendes. *Evolution of Networks: From Biological Nets to the Internet and WWW*. Oxford University Press, 2003.

[11] K.T.D. Eames and M.J. Keeling. Modeling dynamic and network heterogeneities in the spread of sexually transmitted diseases. *PNAS*, 99(20):13330–13335, 2002.

[12] K.T.D. Eames and M.J. Keeling. Contact tracing and disease control. *Proc. R. Soc. Lond. B*, 270:2565–2571, 2003.

[13] K.T.D. Eames and M.J. Keeling. Monogamous networks and the spread of sexually transmitted diseases. *Mathematical Biosciences*, 189:115–130, 2004.

[14] G. Ergün. Human sexual contact network as a bipartite graph. *Physica A*, 308(308):483–488, 2002.

[15] The UK Collaborative Group for HIV and STI Surveillance. A Complex Picture. HIV and other Sexually Transmitted Infections in the United Kingdom: 2006. Health Protection Agency, Centre for Infections, November 2006. Available on the internet at http://www.hpa.org.uk/publications/2006/hiv_sti_2006/contents.htm.

[16] H.W. Hethcote. The mathematics of infectious diseases. *SIAM Review*, 42(4):559–653, 2000.

[17] H.W. Hethcote and P. van den Driessche. Some epidemiological models with nonlinear incidence. *J. Math. Biol.*, 29(3):271–287, 1991.

[18] H.W. Hethcote and J.A. Yorke. *Gonorrhea Transmission Dynamics and Control*, volume 56 of *Lecture Notes in Biomathematics*. Springer-Verlag, 1984.

[19] J.M. Hyman and J. Li. An intuitive formulation for the reproductive number for the spread of diseases in heterogeneous populations. *Math. Biosci.*, 167(1):65–86, 2000.

[20] A.M. Johnson, C.H. Mercer, B. Erens, A.J. Copas, S. McManus, K. Wellings, K.A. Fenton, C. Korovessis, W. Macdowall, K. Nanchahal, S. Purdon, and J. Field. Sexual behaviour in Britain: partnerships, practices, and HIV risk behaviours. *The Lancet*, 358(9296):1835–42, 2001.

[21] M.J. Keeling. Correlation equations for endemic diseases: externally imposed and internally generated heterogeneity. *Proc. R. Soc. Lond. B*, 266:953–960, 1999.

[22] M.J. Keeling. The effects of local spatial structure on epidemiological invasions. *Proc. Roy. Soc. Lond. B*, 266:859–867, 1999.

[23] W.O. Kermack and A.G. McKendrick. Contributions to the mathematical theory of epidemics-i (reprint). *Bulletin of Mathematical Biology*, 53(1-2):33–55, 1991.

[24] I.Z. Kiss, D.M. Green, and R.R. Kao. Disease contact tracing in random and clustered networks. *Proc. Roy. Soc. B*, 272:1407–1414, 2005.

[25] A. Korobeinikov. Global properties of infectious disease models with nonlinear incidence. *Journal of Mathematical Biology*, 69:1871–1886, 2007.

[26] A. Korobeinikov and P.K. Maini. Non-linear incidence and the stability of infectious disease models. *Mathematical Medicine and Biology*, 22(2):113–128, 2005.

[27] A. Lajmanovich and J.A. Yorke. A deterministic model for gonorrhea in a nonhomogeneous population. *Mathematical Biosciences*, 28:221–236, 1976.

[28] M.Y. Li and J.S. Muldowney. Global Stability for the SEIR Model in Epidemiology. *Math. Biosci.*, 125:155–164, 1995.

[29] F. Liljeros, C.R. Edling, and L.A. Nunes Amaral. Sexual networks: implications for the transmission of sexually transmitted infections. *Microbes and Infection*, 5:189–196, 2003.

[30] F. Liljeros, C.R. Edling, L.A. Nunes Amaral, H.E. Stanley, and Y. Åberg. The web of human sexual contacts. *Nature*, 411:907–908, 2001.

[31] W-m. Liu, H.W. Hethcote, and S.A. Levin. Dynamical behaviour of epidemiological models with nonlinear incidence rates. *J. Math. Biol.*, 25(4):359–380, 1987.

[32] W. M. Liu, S. A. Levin, and Y. Iwasa. Influence of nonlinear incidence rates upon the behaviour of sirs epidemiological models. *J. Math. Biol.*, 23:187–204, 1986.

[33] D. Mabey. Interactions between HIV infection and other sexually transmitted diseases. *Tropical Medicine and International Health*, 5(7):A32–A36, July 2000.

[34] Y. Moreno, R. Pastor-Satorras, and A. Vespignani. Epidemic outbreaks in complex heterogeneous networks. *Eur. Phys. J. B*, 26:521–529, 2002.

[35] J.D. Murray. *Mathematical Biology I: An Introduction*. Interdisciplinary Applied Mathematics. Springer-Verlag, 3rd edition, 2003.

[36] NCSSG. New Frontiers: Annual Report of the National Chlamydia Screening Programme in England 2005/2006. Health Protection Agency, November 2006. Available on the internet at http://www.dh.gov.uk/.

[37] M.E.J. Newman. The structure and function of complex networks. *SIAM Review*, 45(2):167–256, 2003.

[38] M. O'Hara. Dangerous liaisons. *The Guardian*, November 17 2004.

[39] E. Ravasz, A.L. Somera, D.A. Mongru, Z.N. Oltvai, and A.-L. Barabási. Hierarchical Organization of Modularity in Metabolic Networks. *Science*, 297:1551–1555, August 2002.

[40] T. Rosen and J.H. Spedale. Relationships between sexually transmitted diseases and human immunodeficiency virus infection. *Current Problems in Dermatology*, 9(6):14–24, November/December 1997.

[41] R.B. Schinazi. On the importance of risky behaviour in the transmission of sexually transmitted diseases. *Mathematical Biosciences*, 173:25–33, 2001.

[42] N. Severo. Generalizations of some stochastic epidemic models. *Mathematical Biosciences*, 4:395–402, 1969.

[43] K.J. Sharkey, C. Fernandez, K.L Morgan, E. Peeler, M. Thrush, J.F. Turnbull, and R.G. Bowers. Pair-level approximations to the spatio-temporal dynamics of epidemics on asymmetric contact networks. *J. Math. Biol.*, 53:61–85, 2006.

[44] A.M.A. Smith, J. Grierson, D. Wain, M. Pitts, and P. Pattison. Associations between the sexual behaviour of men who have sex with men and the structure and composition of their social networks. *Sexually Transmitted Infections*, 80:455–458, 2004.

[45] D.K. Smith, L.A. Grohskopf, R.J. Black, J.D. Auerbach, F. Veronese, K.A. Struble, L. Cheever, M. Johnson, L.A. Paxton, I.M. Onorato, and A.E. Greenberg. Antiretroviral Postexposure Prophylaxis After Sexual, Injection-Drug Use, or Other Nonoccupational Exposure to HIV in the United States. *MMWR*, 54(RR02):1–20, 2005.

[46] P.D. Stroud, S.J. Sydoriak, J.M. Riese, J.P. Smith, S.M. Mniszewski, and P.R. Romero. Semi-empirical power-law scaling of new infection rate to model epidemic dynamics with inhomogeneous mixing. *Math. Biosci.*, 203:301–318, 2006.

[47] UNAIDS. AIDS epidemic update : December 2007. Joint United Nations Programme on HIV/AIDS (UNAIDS) and World Health Organization (WHO), December 2007. Available on the internet at http://data.unaids.org/pub/EPISlides/2007/2007_epiupdate_en.pdf.

[48] J.L. Wylie and A. Jolly. Patterns of Chlamydia and Gonorrhea Infection in Sexual Networks in Manitoba, Canada. *Sexually Transmitted Diseases*, 28(1):14–24, January 2001.